A STUDY OF THE INTRODUCTION OF IONS INTO THE REGION OF STRONG FIELDS WITHIN A QUADRUPOLE MASS SPECTROMETER

By
WILSON M. BRUBAKER

BELL & HOWELL RESEARCH CENTER
360 SIERRA MADRE VILLA
PASADENA, CALIFORNIA

CONTRACT NASW-1298

FINAL REPORT
for the period
17 AUGUST, 1965 THROUGH 17 OCTOBER, 1967

NATIONAL AERONAUTICS AND SPACE ADMINISTRATION
WASHINGTON, D. C.

A STUDY OF THE INTRODUCTION OF IONS INTO THE REGION OF STRONG FIELDS WITHIN A QUADRUPOLE MASS SPECTROMETER

by

Wilson M. Brubaker

ABSTRACT

Theoretical and experimental studies are made of the introduction of ions into the strong fields of a quadrupole mass filter, and of the advantages of using hyperbolic instead of round field-forming surfaces. As an ion traverses the fringing fields of a conventional quadrupole the working point moves through the y-unstable portion of the stability diagram. Under these circumstances, computer studies have shown that the ion receives a large impulse in the y-direction. Through the use of an additional set of four electrodes in the vicinity of the entrance to the mass filter, it is possible to cause the working point to remain within the stable portion of the stability diagram as the ion traverses the fringing fields. This is accomplished by lessening the ratio of the dc to the ac potentials applied to the auxiliary electrodes. This refinement increases the sensitivity of the quadrupole by factors of ten to one-hundred at no sacrifice in resolving power under favorable conditions. The perturbations in the electric fields which result from the use of round instead of hyperbolic rods have been evaluated with the help of a computer. They are surprisingly large. The influence of these perturbations on the trajectories is quite significant, particularly at the higher resolving powers. Carefully performed, comparative experiments show a distinct advantage of the quadrupole with hyperbolic field-forming surfaces over a similar quadrupole with round field-forming surfaces. At comparable sensitivities, the resolving power of a hyperbolic rod system is about two times that of a round rod system of comparable size, operated at equivalent potentials.

TABLE OF CONTENTS

Page

Page

LIST OF TABLES

LIST OF FIGURES

PART I

INTRODUCTION

Part I of this report relates to the work done during the first year of the contract. It is concerned with the introduction of ions into the region of strong fields within a quadrupole mass filter. Since it is usually impossible or impractical to form the ions within the strong field region of the mass filter, they are normally formed outside the filter, where the quadrupole fields are essentially zero. As the ions traverse the region of fringing fields (defined as the space which is bounded on one side by nearly zero quadrupole fields, and on the other by the full field of the mass filter), they are subjected to accelerations which grossly alter their trajectories. These alterations usually are very detrimental in that they greatly diminish the probability of the ion traversing the filter without striking the rods.

That the traversal of the fringing fields results in these undesirable consequences has been recognized for years; but without the services of a digital computer, it has been impossible to evaluate the effect. The use of a computer in these studies has dramatically shown the seriousness of this effect in the usual, conventional quadrupole geometry. It has also shown that a proposed solution to this problem is practical. This conclusion is confirmed by experimental data.

Part II of this report is concerned with the operation of quadrupoles with round and with hyperbolic rod surfaces. All of the theories of the quadrupole have assumed that the surfaces are hyperbolic, when in reality almost all quadrupoles have been constructed with round cylinders for the field-forming surfaces. Both theoretical and experimental investigations have been made. It is found that the performance of the hyperbolic system is significantly superior to that of the round system.

THEORY

GENERAL DISCUSSION

A schematic of a laboratory quadrupole, using round rods, and the manner of excitation is shown in Figure 1. When round rods are used, their radius is made slightly larger than the instrument radius, r_o, to better approximate the hyperbolic fields with circular-shaped electrodes.

The formal, classical, exact theory of the motion of the ions as they traverse the quadrupole is given by the Mathieu equation. It is revealed by the solutions of the Mathieu equation that the amplitudes of the trajectories are either stable, or unstable. That is, they oscillate between bounded limits, or they grow without limit with time. This portion of the Mathieu solution is applied directly, and simply to the problem.

The derivation of the actual trajectories from the Mathieu equation is a most laborious job, and is not attempted in this report. However, the solutions of the Mathieu equation are given, in their infinite series form, for identification.

A simplified, approximate theory of the y-component of the motion of the ions in the quadrupole field was presented at the meeting of the American Physical Society in 1961. The appropriate parts of this theory are presented in this report, as they are necessary to give a basis for the understanding of the physics of the ionic motions.

FORMAL THEORY

The formal theory of the quadrupole mass filter[1] is based upon the use of field-forming surfaces which are hyperbolic cylinders. For use of the quadrupole in the laboratory, it has been found that the compromise of using round rods instead of the hyperbolic cylinders is an expedient one to make.

When hyperbolic surfaces are used, the potential throughout the space between the field-forming surfaces is given by:

$$V = (V_{dc} + V_{ac} \cos \omega t)\ (x^2 - y^2)/r_o^2. \tag{1}$$

The gradients are given by:

$$E_x = (V_{dc} + V_{ac} \cos \omega t)\ (-2x/r_o^2), \tag{2}$$

and,

$$E_y = (V_{dc} + V_{ac} \cos \omega t)\ (+2y/r_o^2). \tag{3}$$

Note that the x-component of gradient is independent of the y-variable and vice versa. Because the x-component of motion is completely independent of the y-position, the motions in the x - z plane can be considered entirely independently of the motions in the y - z plane and vice versa.

The equations of motion of the ions are obtained by the integration of the force equations. In this case, the integration cannot be done directly or simply. The equations are:

$$M\ddot{x} = eE_x = -(2e/r_o^2)\ (V_{dc} + V_{ac} \cos \omega t)\ x, \tag{4}$$

$$M\ddot{y} = eE_y = +(2e/r_o^2)\ (V_{dc} + V_{ac} \cos \omega t)\ y. \tag{5}$$

Equations (4) and (5) are transformed to the standard Mathieu equation through the use of the dimensionless variables a, q and τ. The transformations which accomplish this are:

---

[1] Paul, W.; Reinhard, H. P.; and von Zahn, U.: Z. Physik, Vol. 152, 1958, p. 143.

$$a = 8eV_{dc}/Mr_o^2\omega^2,$$

$$q = 4eV_{ac}/Mr_o^2\omega^2,$$

$$\tau = \frac{\omega t}{2} .$$

The transformed equations are:

$$\frac{d^2x}{d\tau^2} + (a + 2q \cos 2\tau)\, x = 0, \tag{6}$$

$$\frac{d^2y}{d\tau^2} - (a + 2q \cos 2\tau)\, y = 0. \tag{7}$$

The solutions of the Mathieu equation are given in books by McLachlan[2] and by Meixner and Schafke.[3] They are characterized by regions of stability and regions of instability. The amplitude of the variable (x or y) remains bounded in the former case, and increases without limit in the latter. Whether the trajectory is stable or unstable is determined solely by the values of a and q. The a - q plane is divided into stable and unstable regions as shown in Figure 2. The region of interest for the mass filter is limited to values of a and q less than unity. An enlarged view of this portion is shown in Figure 3.

In order for ions which are incident upon the filter with random components of radial velocity to traverse the filter and reach the collector, their trajectories must be stable for both the x- and y-components of velocity. Further, their amplitudes must be less than r_o. Reference to Equations (6) and (7) shows that the only difference between the force equation for the x- and y-components of motion is the sign of the coefficients of a and q. By reflecting the stability criteria for the negative or y equation about the line a = 0, the stability criteria are superimposed. The results are shown in Figure 4.

For a given ratio of the dc voltage to the ac voltage, all values of a and q lie on the scan line which passes through the origin. Each point on this line corresponds to a value of mass-to-charge ratio (m/e) of the ion. The interval of this value, d(m/e), which lies within the stability diagram, corresponds to the range of masses whose trajectories are stable. If the ratio of the dc to the ac voltage is increased,

---

[2] McLachlan: Theory and Application of Mathieu Functions, (Oxford), 1947.

[3] Meixner, J.; and Schafke, F. W.: Mathieusche Funktionen und Spharioid-funktionen. (Berlin), 1954.

the slope of the scan line is increased, and it passes nearer to the apex of the stability diagram. This causes the ratio of dm/m to decrease and the resolving power m/dm to increase. By changing the ratio of $(V_{ac}$ and $V_{dc})/\omega^2$, ions of any chosen m/e ratio can be caused to have stable trajectories.

A mass scan is accomplished by varying the ratio of the applied voltages to the frequency. Usually the voltages are varied but mass spectrometers have been constructed in which the frequency is varied to produce a mass scan.

Reference to Figure 4 shows that the portions of the a, q diagram for which the solutions are stable are limited to values of β which lie between 0 and 1. The general solution which describes the amplitude of the trajectory as a function of time is given by McLachlan as

$$y(\tau) = A \sum_{r=-\infty}^{r=+\infty} c_{2r} \cos(2r+\beta)\tau + B \sum_{r=-\infty}^{r=+\infty} c_{2r} \sin(2r+\beta)\tau \qquad (8)$$

The coefficients of the terms of the infinite series are themselves continued fractions. Further, there is no simple relationship between the known variables a and q and the dependent variable β which appears in the above equation.

APPROXIMATE SOLUTIONS, BASED UPON PHYSICAL PRINCIPLES

Equations (4) and (5) for the x- and y-components of force differ only by a minus sign. For the steady state conditions, this has no significance for the ac term, as it merely represents a phase shift of 180°. Hence the difference between the motions in the x - z and y - z planes results solely from the influence of the dc term. In particular, when the dc component of the field is zero, strong focusing results. This is the principle upon which many modern particle accelerators operate. It is also denoted as alternating gradient focusing.

The influence of the dc field is to render the trajectories unstable. Reference to Figure 4 shows that relatively small amounts of dc potential, as contained in the dimensionless variable a, suffice to render the y-component of the trajectories unstable even in the presence of sizeable quantities of ac fields. In contrast, it is noted that the addition of small amounts of dc field superimposed upon large amounts of ac field have minor effects on the stability of the x-component of motion.

It is of interest to consider the mechanism whereby the dc gradient causes the trajectories to be unstable. Reference to Equation (4) shows that the x-component of motion is stable under the influence of dc potentials only. In the absence of ac potentials the ions execute simple harmonic motion at a resonant frequency. Energy can be stored in a resonant system and so the fact that the addition of the appropriate amounts of ac fields renders the trajectory unstable is not surprising. Reference to Equation (5) shows that under the influence of dc fields only, the y-component of motion is unstable; the acceleration is proportional to y and is directed away from the axis. The problem here is to show how the trajectories can be made stable in the presence of dc fields by the addition of much stronger ac fields.

APPROXIMATE SOLUTIONS, THE Y-COMPONENT OF MOTION

Equation (5) shows that the dc field accelerates a positive ion away from the axis. If stability is to be obtained, it must result from the interaction of the ion and the ac field. An analysis of the motion of the ion in response to the alternating electric field whose strength is proportional to the distance from the axis leads to an evaluation of this interaction. The boundary between the stable and the unstable portions of the stability diagram is characterized by a balance between the inwardly-directed acceleration due to this interaction and the outwardly-directed acceleration in the dc field. For other a, q values, these accelerations are not balanced. In the unstable portion the dc-derived acceleration dominates and the trajectory expands without limit. In the stable portion the ac-derived acceleration dominates, and the average position of the ion oscillates slowly with bounded amplitude about the x - z plane.

The acceleration in the dc field is obtained by setting q = 0 in Equation (5),

$$\ddot{y}_{dc} = (2eV_{dc}/Mr_o^2)\, y$$

$$= (a/4)\, \omega^2 y \ . \qquad (9)$$

The average acceleration owing to the interaction with the ac fields is obtained in an approximate manner. It is assumed that the ion is oscillating, in response to the ac field, at an average position $\bar{y}$. Any drift velocity is assumed to be negligible relative to the velocity of oscillation. As a first approximation, the space-dependence of the field is ignored. This gives sinusoidal motion. Setting a = 0 in Equation (5) and normalizing to the dimensionless variable q,

$$\frac{d^2y}{dt^2} = (1/2)\, q\omega^2\bar{y} \cos \omega t. \qquad (10)$$

Integrating and using the boundary conditions yields

$$y = \bar{y}\, [1 - (1/2)q \cos \omega t] \ . \qquad (11)$$

The value of q in the vicinity of the apex of the stability triangle is 0.7. For a, q values near the apex,

$$y = \bar{y}\, (1 - 0.35 \cos \omega t) \ . \qquad (12)$$

Reference to Figure 6 (a trajectory obtained with a digital computer) reveals that this is an excellent approximation.

The interaction of the ion with the ac field is evaluated by assuming that the ion moves as given by Equation (11) in the nonuniform electric field. The impulse which the ion receives during one radiofrequency cycle is found by integrating the force [Equation (5)] the ion experiences during the cycle. The acceleration is found through multiplication by the frequency, and division by the mass.

$$\frac{d(mv)}{\text{cycle}} = \int_{\omega t = 0}^{\omega t = 2\pi} F \, dt$$

$$= (1/2)q \, M \, \bar{y} \, \omega \int_{\omega t = 0}^{\omega t = 2\pi} [1 - (1/2)q \cos \omega t] \cos \omega t \, d\omega t$$

$$= -(1/4)q^2 \, M\omega \, \bar{y} \, \pi \tag{13}$$

The acceleration is:

$$\ddot{\bar{y}}_{ac} = -(1/8)\omega^2 q^2 \bar{y} \tag{14}$$

for any value of $\bar{y}$.

The net acceleration of the mean displacement of the ion, averaged over several cycles, is the sum of Equations (9) and (14).

$$\ddot{\bar{y}} = (1/4) \, [a - (1/2)q^2] \, \omega^2 \bar{y} \tag{15}$$

The boundary between the stable and the unstable regions of the stability diagram is predicted by this equation when $\ddot{\bar{y}}$ is zero. That is,

$$a = (1/2)q^2. \tag{16}$$

This is to be compared with the exact solution,

$$a = (1/2)q^2 \left[1 - (7/64)q^2 + (29/1152)q^4 \ldots\right] . \qquad (17)$$

At the apex, $q = 0.706$, and $a = 0.4755\ q^2$.

Thus, the above expressions for the accelerations are in error by less than 5% at the boundary. Applying this correction to Equation (15),

$$\ddot{\bar{y}} = 0.25\ (a - 0.4755\ q^2)\ \omega^2 \bar{y} \qquad (18)$$

This adjustment brings the approximate solution into agreement with the formal solution at the apex of the stability triangle. When it is realized that the a, q values of interest in mass spectrometry lie within a few percent of their values at the apex, the merit of the solution obtained by the approximate methods becomes apparent.

Equation (18) may be written as:

$$\ddot{\bar{y}} = 0.25\ (\Delta a)\ \omega^2 \bar{y} \qquad (19)$$

where Δa is the vertical distance from the working point to the y-stability limit, and is positive when the working point is above the stability limit. Within the stable portion of the diagram, Δa is negative, and the quantity $0.25\ (\Delta a)\ \omega^2$ bears a very close resemblance to a spring constant for an undamped, resonant system. Equation (19) is applicable to the y-component of the motion of the ions, for all values of a and q.

Along the scan line (Figure 4) the spring constant is zero by definition at the y-stability limit. As the working point moves to the right along the scan line, the spring constant increases, causing the ions to be more tightly bound to the y-axis. Concurrently, the spring constant for the x-component of motion weakens, becoming zero at the x-stability limit. Somewhere along the scan line, the spring constants for the x- and for the y-components of motion become equal. Under these conditions the amplitudes for ions which cross the axis with the same x- and y-components of velocities are equal. Paul[1] has postulated, and the calculated trajectories of Figures 5 and 6 indicate, that this happens when $\beta_x + \beta_y = 1$. The maximum transmission efficiency occurs at this point on the scan line. Let the point of maximum transmission be denoted as a_1, q_1.

PASSAGE OF IONS THROUGH THE FRINGING FIELDS

As the ions enter the quadrupole through the fringing fields, the intensity of the field varies from zero to the full value which corresponds to the working point, a_1, q_1, as in Figure 4. In the conventional quadrupole, where the potentials are applied to only one set of electrodes, the ratio of the dc to the ac fields in the fringing field region is the same as it is within the quadrupole. HENCE THE WORKING POINT MOVES ALONG THE SCAN LINE, FROM THE ORIGIN TO THE POINT a_1, q_1 AS THE IONS PASS THROUGH THE FRINGING FIELDS. Under conditions of high resolution, when the point a_1, q_1 lies close to the apex, the y-component of motion is unstable for all but a very small portion of this traversal. Further, the degree of instability is very great.

If it is assumed that the point a_1, q_1 lies near the apex and that the equation of the y-stability is that of the parabola expressed by Equation (16), the maximum value of Δa in the fringing field is readily calculated. It is found to be

$$\Delta a_{max} = a_o/4 = 0.237/4 = 0.05925 \qquad (20)$$

Comparison of Δa_{max} of Equation (20) with Δa of Equation (19) reveals that even at modest resolving power the positive acceleration in the radial direction, which the ion receives as it traverses the fringing field, is many times greater than the acceleration toward the axis within the filter.

When the filter is being used at high resolving power, it is essential that the transit time of the ions through the filter be equal to many periods of the applied ac voltage. This is achieved by using high frequency of excitation, by making a long filter, or by using a low injection energy for the ions. Since a low injection energy for the ions increases the time spent in traversing the fringing field, it increases the radially directed impulse which the ions receive as they traverse the fringing field. Thus it is seen that the loss of ions owing to traversal of the fringing field is most acute at high resolving powers.

PHASE ANGLE AT TIME OF ION ENTRANCE INTO FIELDS

As the quadrupole is normally used, ions enter the analyzer at all phases of the applied radiofrequency potential. For some time it has been realized that the trajectory of an ion is dependent upon the phase of the voltage at the time of ion entry. Further, it has been appreciated that the importance of phase angle decreases as the number of radio-frequency periods, which the ion spends in the fringing field, increases.

The mathematical treatment of the trajectory in the quadrupole field requires the help of a computer. However, if the space dependence of the electric field (quadrupole) is simplified to a uniform (parallel plate) field, the influence of phase angle is readily assessed.

In the mathematical treatment which follows it is assumed that the field is uniform in space, that the ion is formed in a region of full field (does not pass through a fringing field), and that it is at rest at the time of its formation.

Let the ambient field be given by:

$$E = E_o \cos (\omega t + \theta) \tag{21}$$

The force equation is:

$$m\ddot{y} = E_o e \cos (\omega t + \theta) \tag{22}$$

The first integration yields:

$$\dot{y} = \frac{E_o e}{m\omega} \sin (\omega t + \theta) + C_1 \tag{23}$$

The second integration gives:

$$y = -\frac{E_o e}{m\omega^2} \cos (\omega t + \theta) + C_1 t + C_2 \tag{24}$$

The constants of integration are evaluated by the boundary conditions that $y = \dot{y} = 0$ when $t = 0$. This results in:

$$\dot{y} = \frac{E_o e}{m\omega} \left\{ \sin (\omega t + \theta) - \sin \theta \right\} \tag{25}$$

and

$$y = - \frac{E_o e}{m\omega^2} \left\{ \cos (\omega t + \theta) + \omega t \sin \theta - \cos \theta \right\} \qquad (26)$$

The first term in Equation (25) represents the anticipated oscillatory velocity. The second term is zero only for $\theta = n\pi$. For all other phase angles, a constant drift velocity exists. This results from the momentum impulse which the ion receives during its starting transient. Since the magnitude of this impulse is proportional to the field intensity, E_o, it is suggested that if the ion were to enter the field gradually, this impulse would be reduced appreciably.

In the above mathematical derivation it has been assumed that the fields are uniform in space, and thus different from those of the quadrupole. However, since the phenomenon under investigation occurs within the first whole cycle of radiofrequency, the impulse given to the ions, as represented by the second term of Equation (25), is relatively independent of the field configuration (quadrupole or linear). Thus, the simplifying assumption of uniform field does not reduce the validity of the conclusions, as the ion would not move an appreciable distance and into fields of differing strength, in the time equal to one period of the applied voltage.

PART I

THE PROBLEM

In the conventional quadrupole the fields are produced by potentials applied to one set of four electrodes. In this case the ratio of the dc to the ac fields is the same in the fringing region as it is within the quadrupole. Thus, for an ion whose working point is near the apex of the stability diagram for the conditions of full field within the quadrupole, the working point corresponding to the weaker fields in the fringing region lies in the y-unstable portion of the stability diagram. As the ion traverses the fringing field its working point moves along the scan line, as shown in Figure 7.

All ions except those which enter the quadrupole very near the x - z plane, where the y-directed fields are zero, experience strong radial accelerations as they traverse the fringing field region. As a result, the radial impulse which an ion receives in this region causes it to have a high probability of striking one of the rods and being lost.

The problem, simply stated, is to improve the efficiency of transport of ions through the filter.

THE SOLUTION

Some time ago it was suggested[4] that the y-instability in the fringing field be eliminated by reducing the dc component of the electric field in the fringe region. When this is done, the working point remains under (beneath) the y-stability limit as the ion traverses this region. In Figure 7 the paths taken by the working point as the ion traverses the fringing field are shown for two cases. When one set of electrodes is used, the working point moves along the scan line, as the ratio of the dc to the ac field is everywhere constant. When an auxiliary set of electrodes is used in the vicinity of the entrance aperture, and they are energized with less or zero dc potential as compared to the rods, the working point can be made to follow a path such as that drawn below the y-stability limit. Such operation has been termed the "delayed dc ramp mode".

By causing the working point to move through the stable portion of the diagram, instead of through the y-unstable portion, the very undesirable impulse to the radial velocity is avoided. This is particularly important when the quadrupole is used at higher resolving powers, as the spring constant of Equation (19) becomes quite weak under these conditions. When this happens, any addition to the radial component of ionic velocity causes the amplitude of the trajectory to become very large. In practical quadrupoles, this means that the ions strike the rods and are not transmitted. It is anticipated that this phenomenon is largely responsible for the acute attenuation of the transmission of ions at high resolving powers (high ratio of dc/ac potentials), as shown by Brubaker and Tuul.[5] Figure 7 of that paper is included in this report as Figure 8. Note how rapidly the transmission falls as the ratio of dc to the ac voltages (a/q) increases. As would be expected, the attenuation is more acute for ions which enter farther from the axis, 1/4-inch aperture vs. 1/16-inch aperture.

---

[4] Brubaker, W. M.: Auxiliary Electrodes for Quadrupole Mass Filters. U. S. Patent 3,129,327, April 14, 1964.

[5] Brubaker, W. M.; and Tuul, J.: Performance Studies of a Quadrupole Mass Filter. RSI, Vol. 35, Aug. 1964, p. 1007.

COMPUTER STUDIES

Ion Entrance Considerations

A series of computations has been made of ionic trajectories under the influence of quadrupole electric fields. In the specification of the conditions for the calculations, the values of many parameters had to be chosen. First and most important is the locus of the working point in the a - q diagram. It was chosen to give comparable envelopes for the trajectories in both the x- and the y-directions. This is achieved by selecting a point such that $\beta_x + \beta_y = 1$. (See Figure 4.) The coordinates of the chosen working point are $a_1 = 0.23462$ and $q_1 = 0.70482$. This choice gives an anticipated resolving power of 100. Other variables which must be specified for the computations are: entrance position, entrance angle, phase of the applied ac potential at the time the ion enters the field, and the number of cycles the ion spends in traversing the fringing fields.

The entrance position was chosen as unity. In almost all cases the amplitude of the trajectory becomes larger than unity. Thus, the amplitude as observed in the trajectory plots tells how far the ion goes from the instrument axis. The units of this distance are the x- or y-distances at which the ions enter the quadrupole. It follows that the ion which enters the field at a distance greater than the distance to the rod, divided by the maximum amplitude of the trajectory, will strike the rod and be lost. The entrance angle was assumed to be zero. Not only is this near to reality in a well-designed ion source, but little new information would be gained by using different angles, since the ion velocity vector is frequently altered appreciably during the first few cycles, owing to the transient, radially directed momentum impulse which the ions receive as they travese the fringing fields. The phase of the ac potential at the time of the entrance of the ion into the field has been made a parameter in several of the series of runs. Special attention is given to the number of ac periods which occur during the passage of the ions through the fringing fields.

When the above variables have been specified, a normalized trajectory is achieved. That is, it is not a function of the instrument size, the magnitude and frequency of the applied voltage, or of the ionic mass.

The first step toward an understanding of this fact is made through reference to Equation (19). This equation, for constant values of Δa and ω^2, represents simple harmonic motion. Its solution is of the form:

$$y = A \sin \alpha t \tag{27}$$

where

$$\alpha = (- \Delta a)^{1/2} \omega \tag{28}$$

Thus it is seen that the ratio of α/ω is uniquely fixed by the variable Δa.

For all operating conditions the fixed ratio of α/ω determines the distance between successive crossings of the axis. Thus for the assumed conditions of the computations, the normalized trajectory is independent of the applied frequency.

For operating conditions in which the ions enter the filter with a radial component of velocity, the amplitude of the trajectory is frequency-dependent, since the negative accelerations which bring this outwardly-directed motion to a halt are proportional to the square of the frequency. The computed trajectories described in this report concern ions which enter the fields with zero component of radial velocity.

While the data obtained from the computed trajectories are most illuminating, and much is to be learned from them, the high cost of using the computer restricts its use to only the most pressing questions. Accordingly, the assumed conditions of operation were chosen with considerable care, in an endeavor to obtain maximum benefits from the computer program.

Four sets of computer runs were made, and the results are summarized in Figures 9, 10, and 11. The detailed trajectories are presented in the Appendix. (Figures A-1 through A-36)

The first set of runs was made under conditions which simulate the formation of ions within the quadrupole structure, where the fields are of full strength. This choice was made to form a base from which the influence of various manners of applying the fields gradually may be assessed. It accurately describes the situation in which ions are formed within the quadrupole either by a laser beam, or perhaps by an electron beam.

To reveal the influence of the phase of the ac potential at the time the ion is formed within the quadrupole, trajectories were computed for four different phase angles, namely, 0°, 90°, 180°, and 270°. In general, the computations bear out the predictions made by the consideration of linear field conditions. First, the amplitudes are all large for conditions in which large amplitudes are expected (θ = 90°, 270°) and second, in three of the instances in which small amplitudes are predicted (θ = 0°, 180°), they are confirmed. When θ = 180° the x-component has a large amplitude. This comes about because of the variation of the field with distance from the axis. Under this starting condition the force on the ion is directed outwardly for a quarter cycle. This impulse drives the

ion away from the axis, and while the field becomes small and reverses, the ion penetrates deeply into the region of stronger field. (The field is proportional to the distance from the axis.) The maximum amplitudes of the x- and y-trajectories for each of the four starting phase angles are displayed in Figure 9a.

The assumed conditions for the second and third sets of runs more nearly simulate those of the conventional quadrupole, with one set of four electrodes. Here the ac and the dc fields, in constant proportion, increase linearly with time from zero to full value as the ion traverses the fringing fields. These can be described graphically as coincident ramps. For convenience the lengths of the ramps are given in cycles of the applied ac potentials. Ramps of two and ten cycles were considered. The two-cycle ramp is as short as would be experienced in a practical instrument. The ten-cycle ramp is frequently used when analyzing higher masses. The maximum amplitudes of the trajectories (x and y) resulting from each of four starting phase angles are displayed in Figures 9b and 9c.

The y-amplitudes for the ten-cycle ramp are quite startling. As expected, the amplitudes of the x-components remain small in all cases. The working point for this motion is well removed from the stability limit, even in the fringe region, and the use of the ac ramp reduces the entrance transient. In the y-direction, the operation of the device with the working point in the unstable region for a longer time produces dramatic results. Regardless of the phase angle, the y-amplitude becomes greater than 1000! This fact undoubtedly has considerable bearing upon the data of Figure 8, which shows the severe attenuation of the transmission at increasing ratios of dc to ac potentials. As mentioned earlier, this result was anticipated.

Additional studies were made of the maximum y-amplitude for coincident ramps of different lengths, again for a resolving power of 100. These data, combined with those of previous calculations, are shown in Figure 12. The points fall very near to a straight line, whose equation is given by

$$A_{max} = 3.5 \times 10^{0.25n} \qquad (\text{for } n \geq 2) \qquad (29)$$

According to theory, the maximum amplitude is proportional to the square root of the resolving power. Since the above equation was calculated for a resolving power of 100, the general equation becomes

$$A_{max} = 0.34\ (\text{Resolving Power})^{1/2} \times 10^{0.25n} \qquad (30)$$

That the maximum amplitude should vary exponentially with time spent by the ion in the fringing fields could have been expected. Simple theory relates the acceleration experienced by the ions to the vertical distance between the working point and the stability limit. When the working point is above the stability limit, the acceleration is positive and the ions move into ever-increasing fields. Under this condition the trajectories increase exponentially with time. Since the distance between the working point and the stability limit changes continuously as the ions traverse the fringing field, the exponential relationship for the maximum amplitude was not apparent before the calculations were made.

The above data indicate the importance of minimizing the number of cycles spent by the ions in the fringing field of the conventional quadrupole.

Having demonstrated with the computer the great loss of ions by the passage of the working point through the y-unstable portion of the diagram, there was great interest in learning of the effectiveness of a previously proposed scheme for eliminating this loss by the use of an additional set (or sets) of electrodes near the entrance aperture. These electrodes are to be energized with lesser portions of dc to ac potentials, relative to the main electrodes (rods). Since the results of the previous calculations had shown the small dependence of the amplitudes upon the phase angle when a ramp is used, the phase angle was not changed during this series. Instead, the influence of different manners of applying the dc potentials was investigated. In each case the working point remained below the stability limit. For the fourth set of calculations, three normalized patterns with delayed dc ramps were assumed, and for each pattern the length of the ac ramp was made 12 and 24 cycles. The results of these investigations are shown in Figure 10. Interestingly, in four of the six pairs of trajectories the y-amplitude remained smaller than the x-amplitude.

The prime revelation of these data when compared with previous results (see Figure 11) is the fact that regardless of the detailed manner in which the dc/ac ratio is tailored, so long as y-stability is maintained by keeping the working point below the stability limit, both maximum x- and y-amplitudes remain quite small. And when it is recalled that the transport of ions is proportional to the square of the effective entrance aperture dimension, the importance of these data is further enhanced.

Ion Exit Considerations

Because of the large radial components of velocity which the ions acquire as they respond to the strong electric fields within the quadrupole, it is anticipated that they leave the end of the quadrupole with high velocities, randomly directed. This condition makes it virtually impossible to focus the emerging beam with electrostatic lenses, using convenient potentials.

It is important to learn what, if any, reduction can be made in the magnitude of the random velocities of the emerging ions by appropriately terminating the fields at the exit of the quadrupole. To this end, trajectories have been computed for a variety of field terminations. Computations show that, for an operating point which corresponds to a resolving power of about 400, the envelopes of the x- and y-trajectories reach maximum amplitudes when $\omega t = 140$.

In the studies of field terminations the fields are assumed to be of full value for $0 \leq \omega t \leq 140$ radians. The terminations begin when $\omega t = 140$, $140 + \pi/2$, and $140 + \pi$. The various phase angles at which the terminations begin were chosen because it was suspected that the phase of the ac potential has a considerable influence on the trajectories.

The first series of computations assumes a conventional quadrupole termination, in which the ratio of the dc to the ac potentials is everywhere the same. Three lengths of field ramp terminations are assumed: two, six, and ten cycles long. In the second series the dc field is assumed to decrease to zero before the ac. This is done in two different manners, but in each case all fields go to zero in an interval of ten cycles. In the first manner the dc field decays during five cycles, and then the ac decays during the following five cycles. In the second manner the dc is assumed to decay during two cycles, and the ac field, during the following eight cycles.

Figures 13 through 22 show the detailed trajectories, with the nearly sinusoidal response indicated by the envelopes drawn through points of reversal. The influence of the phase of the ac potentials at the time the field termination begins is apparent, but is not as dominant as anticipated. It is interesting to note that the conditions at the exit end of the quadrupole are similar to those at the entrance. That is, for the coincident ramp of the conventional quadrupole, an appreciable weakening of the fields makes the trajectory unstable in the y-direction. In the x-direction the stability is increased and the amplitudes of the trajectories, in general, become less.

Figures 23 through 27 are on a quite different scale, to show the relative magnitudes of the exit velocities of the ions under the different field terminations. In these figures the trajectories of the ions after they leave the fringe fields are shown. In each case the axial velocity of the ions is assumed to be constant, so that the z-distance increases linearly with time. Thus the ωt axis is completely analogous to the z axis of the instrument.

The normalized, dimensionless components of radial velocity are tablulated in Table I. The velocity is in terms of $(r/r_o)/(\omega t)$. These data, and the corresponding graphic display of the trajectories, indicate quite clearly the important conclusions which can be drawn from this investigation. They are:

1. When the field termination is abrupt the ions leave the quadrupole with radial velocities which are 30% to 40% as large as those with which they respond to the fields within the quadrupole.

2. If the termination is gradual, very large components of velocity are added to the y-component of motion.

3. The x-component of velocity is usually less than a third of the normal radial velocity within the quadrupole under almost all conditions of field terminations.

4. When the dc fields are attenuated ahead of the ac fields, the x- and the y-components of velocity become quite small, much less than their normal velocities within the quadrupole.

For circumstances in which it is desired to apply any kind of ion optics to direct the ions from the quadrupole to a remote detector, the use of the delayed ac ramp becomes of prime importance.

EXPERIMENTAL APPARATUS

Mechanical

The apparatus used for the experiments comparing the dc ramp mode of operation with that of the conventional mode consists of a series of components which are shown in block diagram form in Figure 28.

The Vacuum System

The heart of the vacuum system is a 100 liter per second DriVac triode ion pump. The quadrupole is separated from the pump by a baffled stainless steel tube and a mechanically operated gate valve. An ionization gauge and a three-inch quadrupole are used to monitor the pressures. A zeolite adsorption pump is used for rough pumping.

The Quadrupole

The quadrupole used in these experiments has stainless steel rods of 0.600 inches in diameter and 10-inches long. One insulated segment 0.600 inches in length is located at the entrance end of each rod.

Electrical

Radiofrequency Oscillator and Scanning Means

A self-excited, push-pull radiofrequency oscillator was used for this experiment. It operates at 1.6 MHz. when loaded with the capacity of the rods and segments of the quadrupole. The dc rod voltages are derived from rectified ac rod potentials.

Mass scanning is accomplished by varying all the potentials in proportion. The incremental potential variations required for the desired mass scan are controlled by the saw-toothed sweep voltage generated in the scanning power supply. This same saw-toothed sweep voltage is connected to the horizontal input of the x - y recorder. Thus, as in an oscilloscope display, the plotted peaks appear at predetermined points on the x-axis as a function of mass number. The mass spectrum is scanned at a rate of about once in 30 seconds.

Electrical Connections to Quadrupole

Figure 29 shows the manner in which the change from the conventional mode to the delayed dc ramp mode of operation is accomplished. The two 32-megohm resistors from the segment pairs allow the dc potential to remain at zero without disturbing the ac potential.

Secondary Emission Multiplier

A "Venetian-blind" type of secondary emission multiplier (C-70120E made by RCA) using beryllium-copper dynodes is used to amplify the current from the quadrupole. It has a measured gain of between 10^5 and 10^6 when supplied with -4000 volts.

Electrometer Amplifier and X - Y Recorder

The ion current detector, Figure 30, consists of a secondary emission multiplier with leads from the first and fourteenth dynodes brought through the vacuum wall to allow changes in external connection. The anode is likewise brought through the vacuum wall for this same purpose. Thus, the secondary emission multiplier can be made, by external connection, to function as a multiplier or it may be made to function in its entirety as a Faraday collector. These external connections also allow the gain of the secondary emission multiplier to be measured accurately by comparing the current in both modes. Ion current from the collector assembly is fed through an electrometer amplifier to the y-axis of the x - y recorder. Alternately, current from the multiplier anode may be applied directly to the input resistor of a cathode ray oscilloscope.

Partial Pressure Monitor

An independent three-inch quadrupole operating in the high pass mode, and responsive to the spectrum of krypton, is mounted on the same vacuum system. Current representing this partial pressure is displayed on a strip chart recorder to provide a continuous monitor of the partial pressure of krypton.

EXPERIMENTAL PROCEDURE

General

A comparison was made during each of the tests between the performance of the segmented rod quadrupole in the conventional and in the delayed dc ramp mode. All other operating conditions remained constant during the period of the testing.

The spectrum of krypton was used for all measurements. It presents two nearly equal-sized peaks at masses 82 and 83 and a dominant peak at mass 84. Further, the spectrum falls in the mass range in which there are no interfering background peaks.

Calibration

Krypton Monitor

The three-inch quadrupole was adjusted to operate in the high pass mode to respond to krypton. By admitting krypton into the vacuum system and observing the changes in the reading of the Bayard-Alpert gauge, and in the output from the krypton monitor quadrupole, the partial pressure of mass 84 was calculated and the calibration of the monitor quadrupole established. This was done while the valve was nearly closed to avoid ion pump interference. This process was repeated frequently providing corrected partial pressures of the mass 84 isotope from which the sensitivity of the quadrupole was established for each mode of operation.

Secondary Emission Multiplier

The gain of the secondary emission multiplier was determined by comparing the current for a flat-topped peak at low resolving power as detected with and without the multiplier. For most of the experiments the secondary emission multiplier was operated at a reduced voltage to provide a gain of about 1,500.

Data Reduction

The basic data were the ion currents of the resolved mass 84 peaks plotted by an x - y recorder as a function of the potentials on the rods. The independent axis corresponds to the rod potentials. Repeated scans

were made for different values of the ratio of the dc to the ac potentials. From these data in the form of plotted mass 84 peaks and the corresponding partial pressures of the mass 84 isotope, the sensitivity in amperes per torr was obtained as a function of the resolving power. This was done for both modes of operation. Resolving power is defined as (s/w)m, where s is the distance between adjacent peaks of one mass number apart, w is the width measured at 10% of the peak height, and m is the mass number in amu.

EXPERIMENTAL DATA

The comparative performance data of the quadrupole in the two modes of operation are shown in Figures 31, 32, and 33. Other operating conditions were used too, but these suffice to well illustrate the advantages which can be obtained through the use of the delayed dc ramp.

The parameter which was varied in these experiments is the energy of the incident ions. In Figure 31 the ion energy is 15 volts. In this case, the greatest advantage of using the delayed dc ramp occurs at the lower resolving powers. The advantage practically disappears at the higher resolving powers. This is to be expected, since the number of cycles which occur during the ion transit time limits the obtainable resolving power. (Since the analyzing portion of the quadrupole is shorter in the delayed dc ramp mode, it is not surprising that the advantage of the delayed ramp nearly disappears at high resolving power.)

In Figure 32 the ion energy is 8 volts. Here the advantages of the delayed ramp are quite apparent. At comparable resolving powers the sensitivity of the delayed mode exceeds that of the conventional by factors in excess of 100! At constant sensitivity the resolving power of the delayed is more than five times that of the conventional!

In Figure 33 the ion energy is 4 volts. At this low ion energy the sensitivity of the conventional quadrupole is extremely low, owing to the impulse which the ions receive as they traverse the fringe fields. Since in the delayed mode of operation the ions do not receive this undesired impulse as they traverse the fringe fields, the sensitivity remains high. Because the slower ions spend more time within the analyzer fields, considerably higher resolving power is obtainable with this particular set of operating conditions.

SOURCE STUDIES

Introduction

The most popular type of ion source for use with mass spectrometers forms ions by electron bombardment. For magnetic mass analyzers in which the velocity or the energy of the ions has a first order influence upon the trajectory, it is of the utmost importance that the energy of the emerging ions be homogeneous. For quadrupole mass spectrometers, the homogeneity is of less importance. However, as the ion injection energy is lowered, it is desirable that the spread in ion energy becomes small also.

Work done on this study contract has shown that it is advantageous to inject ions into the quadrupole mass analyzer at a low velocity. When ion sources are operated at low accelerating potentials, the influence of space charge on the trajectories of the ions becomes of increasing importance. This is because space-charge-induced potentials become larger fractions of the applied potentials.

Theory

In the theoretical analyses which follow, emphasis is placed upon the potential variation in the volume from which the ions are withdrawn. This, of course, is exactly equal to the spread in the energy of the emerging ions. The ionizing electrons are assumed to pass through the ionizing region with high velocity, and not to return. In the ionization process, electrons removed from the neutral molecules usually come off with very low energy, and these add to the space charge of the more energetic electrons. Their contribution is small, however. Also to be considered are the positive ions which are formed. In general, the energy of the newly made positive ions is the same as the thermal energy of the neutral molecules from which they were formed. This is a small fraction of an electron volt. It will be shown that in some cases the space charge of the electrons may form a potential well. When this happens, it is reasonable to assume that positive ions formed in this well will be trapped and tend to remain there until they have essentially neutralized the space charge depression caused by the electrons. When potentials are applied to electrodes to make a field to accelerate the ions in the desired direction, there may not be a potential well due to the electrons. Under these conditions the ions are removed from the ionizing volume as fast as they are formed, and their density is quite small relative to that of the ionizing electrons.

Calculation of Potential Variation Over Ionizing Volume

In this derivation, a worst-case situation is assumed in that the role played by the positive ions is assumed to be zero. The potential variation owing to the space charge of the electrons is obtained for two different electron density distributions within cylindrical volumes. In the first, the electron density is assumed to be constant throughout the ionizing volume. In the second, the electron density is assumed to vary inversely as the radius.

Case I, Uniform Electron Density

Since it is appropriate to inject ions into a quadrupole through an essentially round aperture, it is assumed that the ions are drawn from a cylinder whose axis coincides with that of the quadrupole. The direction in which the ionizing electrons traverse this volume is of no consequence, so far as their space charge effects are concerned. However, in order to evaluate the magnitude of the current represented by this flow of electrons, it is convenient to think of them as moving parallel to the instrument axis with a velocity v_z.

The derivation is made using rationalized MKS units. The charge density due to the electrons, coulombs per cubic meter, is given by:

$$\rho = n_e e \tag{31}$$

where n_e is the number of electrons per cubic meter. The resulting alteration of the space potential is obtained through the use of Poisson's equation:

$$\nabla^2 V = -(\rho/\epsilon_o)$$

$$= (1/r)(d/dr)(r\ dV/dr) \tag{32}$$

A first integration yields:

$$r\ dV/dr = -(\rho/\epsilon_o)(r^2/2) + C_1 \tag{33}$$

where C_1 is zero because when $r = 0$, dV/dr also is zero, from symmetry. A second integration gives:

$$V = -\rho r^2/4\epsilon_o + C_2 \tag{34}$$

where C_2 is zero if the potential on the axis is taken as reference.

The potential of (34) is due solely to the space charge of the electrons, and to distinguish it from other potentials, it is denoted as $V(\rho)$.

The electron current contained in a cylinder of radius r is:

$$i_- = \pi r^2 \rho v_z \tag{35}$$

The elimination of ρ through the combination of (34) and (35) results in:

$$i_- = -4 \pi v_z \epsilon_o V(\rho) \tag{36}$$

The negative sign in (36) is redundant, because it is obvious that the current is that of electrons, and negative. Besides, the positive direction of the vector quantity v_z is unspecified and irrelevant. The non-relativistic value of the velocity of an electron which has been accelerated through a potential difference of V_{e1} volts is:

$$v_z = 5.95 \times 10^5 \ (V_{e1})^{0.5} \text{ meters/sec.} \tag{37}$$

Combining Equations (36) and (37),

$$i_- = 6.6 \times 10^{-5} \ (V_{e1})^{0.5} V(\rho) \tag{38}$$

For electrons of a given energy, (38) relates the magnitude of the electron current and the potential difference between the axis and the periphery of the assumed cylindrical volume. When the charge density is uniform over the volume, as is assumed in this case, the integration of Poisson's equation leads directly to the result that the radial distribution of the potential is parabolic. Equation (38) shows that the total potential difference along a radius of the cylinder is independent of the radius, and proportional to the total electron current represented by the motion of the uniform density electrons.

Case II, Non-Uniform Electron Density

If an ion source of circular symmetry is used, and the electrons are injected into the active volume along radii, the electron density is a maximum in the vicinity of the axis. In this instance the distribution of the space charge owing to the presence of the electrons is given by:

$$\rho = \rho_o \ (r_o/r) \tag{39}$$

where ρ_o is the charge density at $r = r_o$, the assumed periphery of the ionizing cylindrical volume. Under these conditions, Poisson's equation becomes:

$$(1/r)(d/dr)(rdV/dr) = -(\rho_o/\epsilon_o)(r_o/r) \tag{40}$$

As before, the constants of integration are zero because of symmetry. A double integration leads to:

$$V(\rho) = -(\rho_o/\epsilon_o)\, r_o r \tag{41}$$

Since the electron density is no longer uniform, it is necessary to do an integration to find the magnitude of current contained within a cylindrical tube of radius r. The differential equation is:

$$di_- = v_z\, \rho_o\, (r_o/r)\, 2\pi\, r\, dr \tag{42}$$

When integrated between the limits $r = 0$ and $r = r$,

$$i_- = 2\pi\, v_z\, \rho_o\, r_o\, r \tag{43}$$

The elimination of ρ_o by combining Equations (41) and (43) gives:

$$i_- = 2\pi\, v_z\, \epsilon_o\, V(\rho) \tag{44}$$

which, with the help of (37) becomes:

$$i_- = 3.3 \times 10^{-5}\, (V_{e1})^{0.5} \tag{45}$$

Discussion of Calculated Potential Distributions

The first and most obvious difference in the two cases is the fact that the potential difference for a given ionizing current is twice as large when the electron density is non-uniform. This follows directly from the laws of electrostatics, as a larger portion of the electrons are to be found at a large distance from the periphery, namely near the axis.

$V(\rho)$, the potential variation in the ionizing volume owing to the space charge of the electrons, is always small relative to the potential difference through which the ionizing electrons are accelerated. Hence, it is appropriate to ignore any change in the velocity of the electrons as they traverse the ionizing region.

It is interesting to note the magnitude of the axial electron current required to produce a potential difference of one volt. If the energy

of the electrons is assumed to be 100 volts, Equation (38) gives the value of 660 microamperes. From Equation (45) the corresponding current for the non-uniform distribution of Case II is 330 microamperes.

These conclusions may seem to be somewhat restrictive. However, with the sole exception of the alleviating role that may be played by positive ions, here neglected, it is basic. The presence of electrode surfaces external to the cylindrical volume can in no manner alter the above conclusions.

Ion Production

The ion current which is represented by the ion production rate is obtained from the equation:

$$i_+ = S\ P\ L\ i_- \tag{46}$$

where S is the probability of an electron making an ionizing collision in a gas at a pressure of one torr, in a distance of one centimeter. S is proportional to the ionization cross-section which is a function of the gas and of the electron energy. P is the gas pressure in torr, and L is the length in centimeters of the ionizing electron path from which the ions are drawn. S has a maximum value of about ten for many gases for electrons of energy near 100 volts.

When 100-volt electrons traverse an ionizing volume one centimeter long filled with a gas for which S is 10, the resulting ion current from this volume is equal to 10 P times the electron current. For Case I, this is:

$$i_+ = 6.6 \times 10^{-3}\ P \tag{47}$$

and for Case II, it is:

$$i_+ = 3.3 \times 10^{-3}\ P \tag{48}$$

Equations (47) and (48) set an upper limit for the ion current which can be drawn from a cylindrical volume one centimeter long under the assumed potential variation of one volt when the space charge of the positive ions is ignored. This is an upper limit because the electrons are assumed to traverse the volume at constant velocity, and nearly optimum energy to maximize the ionization cross-section. In some ion sources the electrons are reflected and tend to reverse their paths. When this happens the electrons lose kinetic energy and slow down. This reduces

the ionization cross-section and increases the space charge depression of the potentials, because each electron spends more time in the ionizing region (and makes fewer ions).

Practical Ion Sources

The laws of physics state that any energetic electron moving through molecules will ionize some of them. Thus the production of ions is readily obtained. This is a necessary, but not a sufficient condition for achieving an efficient ion source for a mass spectrometer. After the ions are made they must be formed into a beam which is as nearly parallel as is possible. For introduction into a quadrupole mass filter, they should be in a beam of small diameter. Thus the ionizing region cannot be devoid of fields other than those induced by the presence of the electrons. In steady state conditions the ions leave the ionizing region at the same rate as they are formed. The potentials will adjust themselves to bring this condition into being. In particular, the potentials cause a gradient to accelerate the ions from their place of formation. In the design of a practical ion source the gradients should accelerate the ions to form them into a beam. The gradients to which the ions respond are those which result from all sources. These include the potentials applied to the field-forming surfaces, space charge of electrons and ions, and charges trapped on surfaces. The latter result from the continued ion or electron bombardment of surfaces on which an insulating layer is formed. Ideally, the fields which result from applied potentials dominate the situation. This condition is approached when high potentials are applied. However, the results of these quadrupole investigations encourage the use of low energy ions. Under these conditions, care must be used in the design of the ion source to minimize the influence of space and surface charges upon the trajectories of the ions as they leave the source.

Experimental

Improved Ion Source

Guided by experience, we had previously designed an ion source of nearly circular symmetry. This is a very good source, and when used on a ten-inch quadrupole with a secondary emission multiplier permits the display of peaks at a partial pressure of 2×10^{-14} torr. The data of the earlier experiments indicate that the sensitivity of the source, amperes per torr, is somewhat lower than that claimed for sources of other designs. However, it should be kept in mind that the more significant figure-of-merit is the signal-to-noise ratio of the system, not the amperes per torr. The former figure alone determines the lowest molecular density to which the system is responsive.

"Noise" signal in a system with a secondary emission multiplier can be the result of photons striking the elements of the multiplier. Photons in an ion source originate at the electrodes when struck by the electrons at the ends of their paths. This source has been designed so that there is no line-of-sight path between the multiplier and any surface that can be struck by an electron. This consideration has been found to be of extreme importance in keeping the signal-to-noise ratio at a maximum value.

New Ion Source

Since the improved source, hereafter referred to as the old source, could not be made to produce an ion beam of large diameter, a new one was designed and built. The dimensions of the new source provide an aperture whose diameter is half that of the rods. The aperture can be readily reduced by the application of a mask when a smaller one is desired. The sources are similar in that the filament nearly surrounds the ionizing region. The radial flow of electrons results in a maximum electron density near the axis of the source, causing the ion production rate to be large near the axis.

The old source used several electrodes to bound the ionizing region. This is shown in Figure 34. It was found that optimum operation was obtained when the potentials on most of the electrodes which enclose the ionizing region are quite similar. Hence, in the new design, Figure 35, the outer periphery of the ionizing region is made of a wire mesh screen of high transparency, forming a unipotential surface. As in the earlier source, the ionizing electrons converge toward the axis of the instrument, making their density a maximum in the vicinity of the axis.

The gradient which urges the ions toward the quadrupole is provided by leakage fields from the ends. The field at the end remote from the quadrupole results from a small potential on the repeller. The field at the exit end of the quadrupole results from a larger (negative) potential placed on the ion focusing electrode. The combination of these two fields provides the necessary gradient to direct the ions into the quadrupole.

Ion Source Data

Data with the new source has been obtained using a 4-volt ion accelerating potential. Two aperture sizes have been used, namely 0.100 and 0.300 inch. The sensitivity as a function of the resolving power for each aperture is shown in Figure 36. For comparison, the data obtained previously with the old source with a 0.030-inch aperture are repeated on the same scale. It can be seen that the sensitivity of the new ion source with the 100-mil aperture is about three times that of the old ion source with a 30-mil aperture at resolving powers greater than 200. At resolving powers below 200, the advantage of the new ion source becomes even greater.

The performance of the instrument with the 300-mil aperture is outstanding at the lower resolving powers. However, the sensitivity falls rapidly with increasing resolving power. For resolving powers above about 300, the sensitivity is less than with either of the other two.

While the performance of the new ion source is superior to that of the old ion source at the higher resolving powers, it is comparable to the performance which is obtainable with the old ion source if optimum potentials are provided for all electrodes.

One of the advantages of the new ion source is the absence of any critical potential adjustments. Reproducible results are readily obtained.

PART II

STATEMENT OF THE PROBLEM

The theory upon which the operation of the quadrupole is based assumes hyperbolic field-forming surfaces. Experience has shown that excellent performance is obtained when round rods are used instead of the more expensive hyperbolic ones. There are no known published data on a direct comparison of the operation of quadrupoles with round and hyperbolic field-forming surfaces. Therefore, it seemed expedient to make such a test.

There are reasons to believe that there should be a significant difference in the operation of the two types of instruments. Obviously, the fields formed by round rods differ significantly from those formed by hyperbolic surfaces. These differences are perturbations. Particularly as the resolving power is increased, the influence of these perturbations on the mass resolving capabilities of the quadrupole would be expected to become of importance.

Any symmetrical four-pole array of linear, parallel electrodes, when energized with appropriate potentials, produces in the immediate vicinity of the axis of symmetry a field which departs only slightly from the desired hyperbolic nature. In general, it is reasonable to assume that the perturbations increase with distance from the axis.

As ions proceed through a quadrupole they are subjected to two very strong but oppositely directed radial accelerations. A relatively small perturbation in the fields would be expected to have a very pronounced influence upon the ionic trajectories. Thus, ions which reach a critical radius in the presence of the perturbations may proceed to the rods and not return, whereas in the unperturbed hyperbolic fields they would return to the vicinity of the instrument axis. If these conditions do exist, then a set of hyperbolic rods spaced closer together will give the same performance as round rods spaced farther apart. For operation at constant fields, the power required to excite the field-forming surfaces varies as the geometrical factor to the fourth power! Thus even a modest change in the scale factor of the instrument makes a most significant change in the power required to operate it. For spectrometers to be used in space probes, this potential saving in power which may be obtained through the use of hyperbolic instead of round rods may be of much greater significance than the extra cost of the hyperbolic surfaces.

COMPUTER STUDIES

This portion of the program started with a computer study, first of the perturbations in the fields which result from the use of the round rods, and second with an exploration of the influence of the perturbations on the ionic trajectories. To determine the magnitude of the perturbations, it was first necessary to obtain the values of the potentials over the plane transverse to the instrument axis. From this knowledge of the potentials, the x- and y-components of the gradients were determined.

Derivation of Potentials and Fields, Round Electrodes

The computer has been used to determine the potentials in the quadrupole when the field-forming surfaces are round rods. In particular, it has been used to determine the fields for the case of rod radius equal to 1.16 times the instrument radius, r_o. This is the compromise rod radius which has been most commonly used. Lines representing contours of the round and the hyperbolic surfaces touch in three places for each electrode: on the axis, and at symmetrical points which lie at the intersections of the circle and radii at angles of about 32.5° relative to the x- or y-axis. This particular compromise causes the fields near the instrument axis to be very similar for equal excitation potentials on the round and hyperbolic electrodes.

The computer calculations were done by our consultant, Tom Harris, of Optical Research Associates. His description of the method used to determine the potentials and fields follows.

* *

STUDY OF QUADRUPOLE DETERIORATION DUE TO THE USE OF ROUND, RATHER THAN HYPERBOLIC, FIELD-FORMING SURFACES

This computer study is to determine the effect of using round rods instead of the theoretically desirable hyperbolic surfaces.

I. Representation of the Perturbation

With hyperbolic surfaces the potential throughout the space between the field-forming surfaces is given by the equation,

$$V = (V_{dc} + V_{ac} \cos \omega t)(x^2 - y^2)/r_o^2$$

This has been converted to the equations for ion motion:

$$\ddot{x} = \frac{e}{M} E_x = \frac{-e}{M} \frac{\partial V}{\partial x}$$

$$\ddot{y} = \frac{e}{M} E_y = \frac{-e}{M} \frac{\partial V}{\partial y}$$

which lead to,

$$\ddot{x} = \frac{-e}{M} \left(V_{dc} + V_{ac} \cos \omega t\right)\left(\frac{2x}{r_o^2}\right)$$

$$\ddot{y} = \frac{-e}{M} \left(V_{dc} + V_{ac} \cos \omega t\right)\left(\frac{-2y}{r_o^2}\right)$$

These equations can be converted to the standard Mathieu Equation as has been done in Equations 6 and 7.* To give the trajectories included in Figures A1 through A36 in the Appendix, these two equations were integrated numerically; note the independence of the x- and y-variables.

The introduction of circular rods instead of hyperbolic surfaces perturbs the hyperbolic potential distribution. The form of this perturbation conceivably could be a power series and, if suitable in form, could be used to trace trajectories through the perturbed fields. The conditions which such a potential function should have are the following:

1. Symmetrical in x (even order).
2. Symmetrical in y (even order).
3. When $x = \pm y$, $V = 0$ and, ideally:
4. $\frac{\partial V}{\partial x}$ independent of y.
5. $\frac{\partial V}{\partial y}$ independent of x.

One such equation would be:

$$V = \frac{(V_{dc} + V_{ac} \cos \omega t)}{r_o^2} \left[(x^2 - y^2) + a(x^4 - y^4) + b(x^6 - y^6) + c(x^8 - y^8)...\right]$$

Once the perturbation coefficients a, b, c, ... are known, the resulting differential equations of motion:

* Page 4.

$$\ddot{x} = \frac{-e}{M} \frac{(V_{dc} + V_{ac} \cos \omega t)}{r_o^2} \left[2x + 4ax^3 + 6bx^5 + 8cx^7 + \ldots\right]$$

$$\ddot{y} = \frac{e}{M} \frac{(V_{dc} + V_{ac} \cos \omega t)}{r_o^2} \left[2y + 4ay^3 + 6by^5 + 8cy^7 + \ldots\right]$$

can be numerically integrated, as before, to give the required trajectories.

The principal remaining problem is to find the coefficients a, b, c, ...; this is to be done by a two-step process. First a representation of the true potential distribution must be found; second, the chosen potential function such as the one above must be fitted to this true potential distribution, determing a, b, c, ... to give the best fit.

II. Finding the True Potential Distribution

There are a number of analogs of an electrostatic potential distribution which satisfy the Laplace Equation:

$$\frac{\partial^2 V}{\partial x^2} + \frac{\partial^2 V}{\partial y^2} = 0;$$

this equation must be satisfied by any process which is used to obtain the potential distribution. Two of the analogs which have been used in experimental work are the rubber-dam model and the electrolytic plotting tank. Analogs such as these give insufficient accuracy for determination of perturbations. Therefore, a computational analog, the Liebmann Method* will be used on a digital computer.

A. The Liebmann Procedure - Definition of Boundaries. - This consists of overlaying a computational model of the electrode structure with a grid of discrete points at which the potential values are to be adjusted repeatedly until no significant change takes place. The values of potential thereby obtained will satisfy the Laplace Equation. The finer the grid, the more accurate will be the final curve fitting; however, the computing cost will be increased also. It is, therefore, important to recognize that there is an eightfold symmetry in the electrode structure which requires that the computation be carried out only over the area shown in Figure 37, enclosed by the solid lines. The computational processes can be set up to recognize the fact that the potential distribution in the -y direction is only a reflection of that in the +y direction. However, the

---

* Zworykin, V. K. et al.: Electron Optics and the Electron Microscopes, John Wiley & Sons, Inc., pp. 386-388.

open end along the line $x = x_{max}$ presents a problem. Either a particular distribution along this line must be assumed or a particular value of $E_x \left(\frac{\partial V}{\partial x}\right)$ must be assumed. The latter is less restrictive on the accuracy of the process and has been used in the ensuing program.

In the region near the origin the equipotential lines will be nearly the hyperbolic surfaces required by the quadrupole theory. As we move out toward any rods, the equipotential line shape will be dominated by the nearest rods. We could, therefore, assume that, for the region shown as the open end, the values of $\frac{\partial V}{\partial x}$ are similar to those for a circular conductor; however, the equipotential lines for such a conductor are concentric circles -- a form which obviously would match the distribution very poorly near the grounded plane. The grounded plane should be a member of the set of equipotential lines. Fortunately, there is a better approximation which satisfies this condition and which can be put in analytic form. This is for the potential distribution associated with two parallel cylindrical conductors; the equipotential lines are circles with displaced centers and include one of infite radius coinciding with the grounded plane. The equation for potential* is, when translated to the coordinates under consideration, the following:

$$V = \left[\frac{V_o}{2 \ln\left(\frac{x_c + b}{\sqrt{2}\, R}\right)}\right] \ln\left[\frac{(x - y - b)^2 + (x + y - x_c)^2}{(x - y + b)^2 + (x + y - x_c)^2}\right]$$

where V_o = potential of the conducting rod
R = radius of the conducting rod
x_c = X coordinate of the center of the conducting rod
$b = \sqrt{X_c^2 - 2R^2}$

As mentioned before, to assume this distribution as a boundary condition would introduce a possibly inaccurate assumption. Instead, only the slope of this distribution will be assumed and only for the X-direction. This is given by,

$$\frac{dV}{dx} = \frac{V_o}{\ln\left(\frac{x_c + b}{\sqrt{2R}}\right)} \left[\frac{(x - b) + (x - x_c)}{(x - y - b)^2 + (x + y - x_c)^2} - \frac{(x + b) + (x - x_c)}{(x - y + b)^2 + (x + y - x_c)^2}\right]$$

* Ramo, S.; and Whinnery, J. R.: Fields and Waves in Modern Radio, John Wiley & Sons, Inc., pp. 138-140.

Using this to represent the desired slope, in the X-direction at the open end will allow the slope in the Y-direction to be determined without imposing any artificial conditions. With the open end, defined, one of the requirements of the Liebmann procedure has been met -- namely that it must be applied over a closed region.

B. Starting Potential Distribution. - A second requirement is that an initial potential distribution must be provided. The closer this distribution is to the final distribution, the shorter the computation time will be. It is, therefore, important that the starting distribution be reasonable. Several have been considered, as follows:

1. Hyperbolic Form. Since the quadrupole theory says that hyperbolic equipotential surfaces are required, it is natural to try:

$$V = \frac{V_o}{r_o^2} (x^2 - y^2)$$

Although this matches what the final distribution is expected to be near the grounded plane, it matches poorly near the conducting rod. In fact, in the shaded area of Figure 37, V is greater than V_o, the potential of the rod; this is obviously impossible.

2. Hyperbolic Form with Plateau. An easy improvement over the hyperbolic form would be all values of V greater than V_o be set equal to V_o. In other words, the shaded region of Figure 37 would have its potential set to V_o. This still leaves a significant change to be made by the Liebmann procedure.

3. Hyperbolic Form with Parabolic Fall-off from Cylinder Edge. A cross section with x = c in the region between the cylinder and the origin shows that:

$$V = K - \frac{V_o}{r_o^2} y^2;$$

thus there is a parabolic fall-off in the y-direction. This suggests that a parabolic fall-off from the edge of the cylinder would be an improved representation. Although this is true, this implies that there is no sharp edge to the distribution in the y-direction at the edge of the conductor -- that is, the slope of V is 0 in the y-direction at the edge of the conductor; this is not consistent with a physical understanding of what the final distribution ought to be.

4. Hyperbolic Form with Parabolic Fall-off from X-Axis. This last objection can be removed by centering the parabolas about the x-axis so that the skirt of the parabola describes the fall-off. In other words, from the origin out to the cylinder ($x = x_c - R$) the hyperbolic distribution is used:

$$V = \frac{V_o}{r_o^2} (x^2 - y^2)$$

From the edge of the cylinder:

$$V = V_o \left[\frac{Y_{max}^2 - y^2}{Y_{max}^2 - Y_{min}^2} \right]$$

where Y_{max} = the y value of the grounded plane ($= x$),
Y_{min} = the y value of the cylinder edge ($= \sqrt{R^2 - (x - x_c)^2}$);
or

$$V = V_o \left[\frac{x^2 - y^2}{x^2 - R^2 + (x - x_c)^2} \right]$$

This can readily be shown to be continuous with the hyperbolic distribution. Thus, a reasonable starting distribution has been obtained.

III. Fitting the Polynomial to the Distribution

Once the potential distribution has been determined, it could be used to trace trajectories directly by integration processes. However, this would be quite expensive and inaccurate. For this reason, it is best to fit a function such as the polynomial previously discussed. This is done with the least-squares method using an equation such as,

$$A_{1i}z_1 + A_{2i}z_2 + A_{3i}z_3 + A_{4i}z_4 = V_i$$

where z_1, z_2, z_3 ... are the coefficients a, b, c, ... of the chosen polynomial -- the values of which must be determined. For each point (i) in the grid, there is an associated value of V_i as well as the coordinates x_i and y_i. The value of A_{1i} is the function of V_o, r_o, x_i, and y_i which multiplies the coefficient a in the chosen polynomial; the other terms (A_{2i}, A_{3i} ...) are the corresponding multipliers of b, c, ...

If these equations are set up for all the points in the grid, a matrix equation can be formed:

$$Az = V$$

which includes all equations. If then this is premultiplied by the transpose of A, we get:

$$A^T Az = A^T V$$

which is a problem consisting of four equations in four unknowns (for the above example) which, when solved, will give a least-squares fit of the coefficients to the potential distribution. With the large number of equations available to form A, the fit should be very smooth.

* *

Field Perturbations

The data of the perturbation of the fields as a function of position in the plane perpendicular to the instrument axis are presented in Figures 38 and 39 and in Table II. From symmetry, x and y are interchangeable.

The data presented relate the fields to positions in the x - y plane. This field variation is equivalent to a variation in the a - q values over the x - y plane, as is shown below:

$$V = (V_{dc} + V_{ac} \cos \omega t)\ (x^2 - y^2)/r_o^2 \tag{49}$$

$$E_x = (-2x/r_o^2)\ (V_{dc} + V_{ac} \cos \omega t) \tag{50}$$

$$= (-m\omega^2/4e)\ (a + 2q \cos \omega t)\ x$$

Similarly,

$$E_y = (m\omega^2/4e)\ (a + 2q \cos \omega t)\ y. \tag{51}$$

Since these fields are supported by potentials on a single set of electrodes, the ratio of a/q is constant over the entire x - y plane. Thus, a variation of the fields as a function of position in the x - y plane is equivalent to a proportionate variation in a and q.

Ion Trajectories in Perturbed Fields

General Comments

When the fields in the quadrupole are the result of potentials applied to hyperbolic surfaces, the equipotential surfaces throughout the instrument

are themselves hyperbolic. However, when round rods are used in the place of hyperbolic surfaces, the equipotentials depart slightly from hyperbolae. It is the purpose of this investigation to evaluate these departures. The departures are described as fractional variations (perturbations) of the fields from those which result from the use of hyperbolic rod surfaces.

The trajectories computed in this present study were made under conditions quite different from those previously discussed where attention was focused on the passage of ions through the fringing field at the entrance to the quadrupole. Here the entrance to the quadrupole is completely ignored; the ions are assumed to be within the quadrupole where the fields have full strength. The velocity vector is entirely radial, so the ions never enter or leave the quadrupole. In many of the computations the initial radial velocity is the independent parameter of a family of curves.

In the computation of the ionic trajectories the previously obtained information of the field perturbations was used. The independent variable is the velocity with which the ions enter the radial fields. The instrument radius, r_o is normalized to unity. The initial velocity of the ions is given in units of r_o per microsecond, and the time axis is in radians of the applied ac potentials. The specification of the a - q values sets the ratio of the applied dc and ac potentials, but does not determine their absolute values.

Consistent with obtaining the maximum amount of information in the least time and expense, the computer was asked to print out only the envelopes of the trajectories. In many instances, the computations were interrupted when it was obvious that the maximum amplitude of the envelope had been passed.

As is so well shown by the solutions of the Mathieu Equation, in which the a - q diagram is divided into regions of stability and those of instability, the nature of the ionic trajectories is determined by the a - q values of the working point. Since the working point lies very close to the stability limits when the quadrupole is being used at high resolving powers, very small changes in the a - q values can have a profound effect upon the trajectories.

The description of the dependence of the trajectory upon the position of the working point usually assumes that the locus of the working point is the same for all values of x and y. When the locus of the working point becomes x- and y-dependent, the situation becomes very complicated, because the ions execute rapid excursions over large portions of the

x - y plane. Obviously, the envelope of the trajectories is influenced by the integrated effect of the forces as the ions move over the x - y plane and experience regions of varying a - q values. However, even when the x- and y-components of the fields, or their equivalent a - q values are known over the x - y plane, it is not easy to predict the nature of the resulting ionic trajectories. In later sections of this report an attempt is made to correlate the distortion of the usual trajectory envelopes with the calculated field perturbations.

A glance at the plot of the field perturbations (Figures 38 and 39) reveals that there is no such thing as a typical trajectory which can be considered for the purposes of comparing the operation of round and hyperbolic rod quadrupoles. In the round rod case the y-component of field is dependent not only upon the y-position, but also upon the x-position. In the hyperbolic case the y-component of field is completely independent of the x-position, and the "y-trajectories" are the same for all values of x.

The general characteristics of the y-trajectories are well understood without resort to the solutions of Mathieu's Equation, as described earlier in this report. However, the x-trajectories are not similarly appreciated. Thus it follows that it is easier to interpret the influence of the field perturbation for the y-trajectories than it is for the x-trajectories.

The conditions under which the trajectories were calculated are such that the fields near the instrument axis are the same for both shapes of field-forming surfaces. Hence, for amplitudes which lie near the instrument axis there is negligible difference between the trajectories in the two cases. Because the fields near the axis are quite small (zero on the axis) they do not have as great an influence on the trajectories as do the fields remote from the axis. In general, the perturbations in the fields produced by the round rods increase rapidly with the distance from the axis. Since ions spend more time at positions remote from the axis than at positions close to the axis, the importance of the perturbations becomes apparent. The perturbations on the x- and y-axes increase slowly from zero on the instrument axis to a maximum value at the rods. In other planes the perturbations vary with position in a much more complicated manner.

If the incremental change in the a - q values occurred all over the x - y plane, the influence on the trajectories would be apparent. Weakening of the fields is equivalent to a motion of the working point in the stability diagram toward the origin. To the extent that the effect of this decrease in the a - q values can be simply interpreted, a weakening of the fields corresponds to an increase in the stability of the x-component of motion, and a lessening of the stability of the y-component.

The case under consideration is not as simple as that just discussed, because the ions oscillate in response to the applied field, and thus are not responsive uniquely to the values of the fields at a particular point. Rather, the ions travel over a considerable portion of the x - y plane. Further, as far as the y-component of motion is concerned, any weakening of the fields at the maximum excursion of the ionic position during any ac cycle appreciably weakens the average acceleration of the ion toward the instrument axis. Similarly, any strengthening of the fields at the outer excursion of the trajectory tends to increase the acceleration of the ion toward the axis. Our present understanding of the x-component of motion permits interpretation of the influence of the perturbations only in terms of the position of the working point in the stability diagram. That is, a weakening of the field increases the stability, and vice versa.

Regardless of the detailed nature of the x- and y-trajectories, the envelopes to the traces are sine waves for the hyperbolic rod quadrupole. The particular working points in the stability diagram used for computations were chosen to make the periods and amplitudes of the envelopes nearly identical for the x- and y-components of motion. Through an observation of the distortion of the envelopes from their normal sinusoidal form an estimate of the influence of the field perturbations may be obtained.

Y-Trajectories in the Perturbed Field

In its response to the y-component of electric field, the ion oscillates in near synchronism with the applied ac field, with a peak-to-peak amplitude which is half the maximum excursion from the x - z plane. For the hyperbolic case the value of the maximum amplitude (envelope) varies sinusoidally with time. This characteristic is displayed in the normal hyperbolic trajectory of Figure 40. When the excursion of the trajectory penetrates to regions where the field perturbation becomes appreciable, the nature of the trajectory is changed. This change is noted first as a variation in the period of the trajectory envelope.

The y-component of motion of the ions is characterized by a near balance between two large, oppositely-directed accelerations. The field which results from the dc potential applied to the rods accelerates the ions toward the rods, away from the axis. Except that the opposing acceleration which results from the motion of the ions in non-uniform fields exceeds that due to the dc field, the ions continue their radial

y-directed motion and strike the rods. The restoring influence of the motion of the ions in the ac field results from the larger magnitude of the field at greater y-distances.

One potentially effective manner of evaluating the distortion of the envelope is to calculate the acceleration from its curvature. For the hyperbolic case, where the envelope is a sine wave, the acceleration is proportional to the displacement. The constant of proportionality is logically termed the "acceleration constant", in a manner similar to that of the "spring constants" of force equations. When the contour of the envelope is not sinusoidal, the "acceleration constant" is no longer constant, but it becomes a function of the displacement. The differential equation of the envelope then becomes

$$\ddot{y} = -k(y)\, y \tag{52}$$

If this equation is solved for k(y),

$$k(y) = -d(v_y)/(ydt) \tag{53}$$

k(y) can be evaluated from the envelope contour data by observing the change in the velocity at a given displacement in a small interval of time.

The data from the computer contain the maxima of the high frequency excursions of the ions. These form points on the trajectory envelope, and can be used to calculate k(y) as described above.

Y-trajectories were computed at two resolving powers: 100 and 400. In the data for the lower resolving power the critical value of the injection velocity which causes ions to strike the rods was well determined. In Figure 40 it is seen how a very small change in the initial velocity of the ion causes its trajectory to change abruptly from one of bounded amplitude to one of an ever-expanding amplitude. This change occurs at a normalized radial distance of 0.82 r_o. As discussed above, k(y) becomes zero at this value of y, and reverses sign for values of y larger than 0.82 r_o.

Similar trajectory envelopes for the y-component of motion at a higher resolving power of 400 (and for x = 0) are shown in Figure 41. Most impressive is the observation that the ion trajectory becomes unstable at a y-value of only 0.67 r_o, instead of 0.82 r_o as it was for the lower resolving power case. Values of the normalized acceleration, k(y), were calculated from these data. The results are presented in Figure 42.

For small values of y, the computed values of k(y) scatter about the constant value of the hyperbolic case. For values of y greater than 0.67, it is seen that k(y) becomes strongly positive, indicating that the ion is being accelerated outward at a high rate. If the values of a and q were nearly constant over the interval in y represented by the peak-to-peak values of y, then the perturbation of the trajectory envelope could be well correlated with a shift of the working point in the stability diagram. Unfortunately, this is not the case. The shift in the locus of the working point during one cycle of the applied potential is in many cases sufficient to carry it outside the stability diagram. When such large excursions occur, it is necessary to consider the accelerations which the ions receive during the entire cycle of applied voltage. Because the perturbations depend upon the x - y position in such a peculiar way, and because the complex motions of the ions carry them over the entire x - y plane in a manner which is highly dependent upon the exact position of the working point in the stability diagram (along the scan line), it is not possible to correlate the trajectory envelopes with the details of the field perturbations in a very precise manner.

The trajectory envelopes of Figure 41 were computed for a - q values which would give resolving powers of about 400. It is interesting to observe the perturbations of the E_y field for x = 0, as they relate to this situation. Were the incremental change in the a - q values the same all over the x - y plane, it would need to be of the order of dm/(2m) to scan a half peak width, as is required to go from the peak to the valley. This is a value of 0.00125. Surprisingly, the trajectory becomes unstable when only the outermost excursion of it, as given by the envelope, reaches a region where the perturbation is 0.0011. When the ion is at its maximum excursion of 0.67 r_o, its associated minimum excursion is about 0.34 r_o. At this value of y the perturbation is 0.00023. Thus it is seen that over the space reached by the ion in one cycle of its motion the perturbation is very much less than that required to render the trajectory unstable if the perturbation were everywhere the same.

That the relatively small average perturbation of the fields renders the trajectory unstable results from the nature of the dependence of the perturbation upon the position of the ion. When the ac field at maximum excursion is reduced by the perturbation, this weakens the acceleration toward the axis. It follows that the stability of the trajectory in the perturbed field is influenced not only by the magnitude of the perturbation, but also by the slope of the perturbation as a function of position from the median plane. (Instrument axis for x = 0.)

An example of the dominance of the slope of the perturbation vs. position curve over the value of the perturbation is seen in the y-trajectories in the plane $x = r_o$. Trajectories calculated for different initial velocities are shown in Figure 43. The best measure of the influence of the perturbation is to be found in the time required for a half-period of the trajectory envelope. As reference, for the hyperbolic case the time required for a half-period is 138 radians. For an ion injected at a modest radial velocity of 0.0236 $r_o/\mu sec$, the half-period is 25 radians. An initial velocity of 0.0574 results in a half-period of 16 radians, and a velocity of 0.1 results in a half-period of 14.5 radians. Compared to operation with hyperbolic rods, the time required for the half-period is reduced by a factor approaching ten and the maximum amplitudes of the trajectories are similarly reduced. As is seen in Figure 39 the perturbation in the y-field for small values of y is very large, and the slope is quite steep. The fact that the ion is so strongly focused toward the axis when the working point lies so far outside the stability limit for the major portion of the trajectory clearly demonstrates the dominance of the slope of the perturbation vs. position over the location of the working point.

The above discussion emphasizes the virtual impossibility of predicting in any detail the nature of the trajectories as a function of the field perturbations. While emphasis has been placed upon the nature of the y-trajectories, similar behavior was seen for the x-trajectories. If the dependence of the trajectories upon the perturbations were all as simple as those for y at $x = 0$, some rather definite predictions could be made. Here it is seen that the ions cannot be made to approach the round electrode on trajectories which return them to the axis. If the trajectory reaches a value of y which is only (2/3) r_o the ion is lost to the rod (for a resolving power of 400). If this were true for most of the trajectories, the advantages of the hyperbolic rods over the round ones would be apparent, and the savings of power through the use of the hyperbolic rods would be very appreciable, since the power increases as the instrument radius to the fourth power.

In some cases, as a function of the trajectory excursion, the perturbations seem to either increase or decrease the stability of the trajectory. In order to predict from computed trajectories the influence of the perturbations, many more trajectories would need to be analyzed than can be accomplished within the available time on this project.

It can be concluded that this study of the trajectory perturbations introduced by the use of round rods reveals disturbing departures from the normal trajectories of the hyperbolic quadrupole. Thus it was anticipated that the laboratory tests of the round and hyperbolic instruments would reveal a real superiority of the hyperbolic quadrupole over the round one.

EXPERIMENTAL APPARATUS

Mechanical

The apparatus used for the comparison of round and hyperbolic rod quadrupoles consists of two quadrupole assemblies, each with its own ion source and detector (Figure 44). These independent systems are mounted parallel and closely adjacent to each other on a common ion-pumped vacuum system (Figure 45). Except for the contours of the field-forming surfaces of the rods (Figures 46 and 47), the two quadrupoles are identical. Rods, ion sources, and secondary emission multipliers are all interchangeable.

The hyperbolic rods are forged from billet stock of 304 stainless steel. They are annealed after forging and between the stages of rough and finish machining. The insulated segment at the ion source end of each rod is held in place by a ceramic bushing. Figure 47 clearly shows the segments, ceramic bushing and the rod ends.

The hyperbolic contours were generated first on a scale 50 times larger than the desired rod surfaces. This hyperbola was used as a master on a pantograph to control the formation of a highly precise positive hyperbola on a tungsten carbide wheel. This wheel was used to "crush-form" a negative hyperbola on a carborundum grinding wheel which in turn was used in "form-grinding" the stainless steel rods. To insure contour stability, the grinding wheel was "touched-up" periodically by contact with the tungsten carbide master which was mounted directly on the grinding machine.

The hyperbolic rods have a cross section of about 0.6-inch x 1.25-inches. The rod side opposite the hyperbolic surface, and an adjacent side were ground square to within 10^{-4} radians. These are the rod-positioning surfaces. During the grinding operation the rods were supported by a special fixture. The rod-positioning surfaces on this fixture were ground in place on the same machine which was used to grind the hyperbolic surfaces of the rods. This procedure resulted in rods with surfaces of high contour accuracy.

Electrical

The apparatus for the control and excitation of the round and hyperbolic rod quadrupoles consists of several discrete sections which are depicted in Figures 45 and 48. Figure 49 shows a front view of the

apparatus. All controls and information readout devices concerned with the actual data collection are readily accessible to the operator. The crystal oscillator, amplitude modulator, and rf power amplifier are located on a short rack section in the rear and are not shown. Essential details of each major section are described.

Design Goals

The principal goal is to provide an apparatus of sufficient refinement to enable a critical comparison to be made of the performance of the quadrupoles with round and with hyperbolic field-forming surfaces. In other words, the mass resolving power is not to be limited by the electronic components.

Since the scanning of one mass peak is accomplished in less than 30 seconds, the gradual changes in electrical parameters due to temperature changes, and/or component aging, are insignificant. Therefore, the emphasis is placed on maximum stability during a comparatively short time.

A feeling for the permissible tolerances in the operating parameters of voltage and frequency is obtained by reference to the dimensionless variables a and q. Logarithmic differentiation of the defining equations for a and q relates variations in the above mentioned variables and the mass of the ion. In the apparatus under consideration the dc potentials are caused to be proportional to the ac potentials through the use of negative feedback amplifiers. This limits the motion of the working point, during a mass can, to a line through the origin of the stability diagram. Under these conditions it is not necessary to consider separately the variations of the dc potentials. Differentiation of the defining equation for q yields:

$$dq/q = dV_{ac}/V_{ac} - dm/m - 2\, dr_o/r_o - 2\, df/f \qquad (54)$$

Assuming that dq is zero and limiting our attention to the electrical quantities,

$$dm/m = dV_{ac}/V_{ac} - 2\, df/f \qquad (55)$$

Experience has shown that if the sum of the possible variations of Equation (55) are less than about 1×10^{-4} the resolving power will not be limited significantly by these variations. Accordingly, such a goal is attempted in the design and assembly of this apparatus.

Crystal Oscillator

The crystal oscillator circuit is designed to operate at seven frequencies from 0.5 through 4.0 MHz. differing by factors of $2^{1/2}$. For these experiments only the frequencies 0.707, 1.0 and 1.414 MHz. were used. The frequency of the crystal oscillator varies with temperature less than one part in 10^6 per degree Celsius. This constitutes the major long-term drift. The oscillator is electrostatically shielded from the other modules and is capacitance coupled to the input of the modulator.

Amplitude Modulator and RF Power Amplifier

The constant amplitude rf voltage from the crystal oscillator is amplified by varying amounts to achieve the desired excitation levels for the quadrupoles. The level to which the rf voltage is amplified is determined by the dc scanning voltage. The maximum power available from the plate-tuned power amplifier is about 90 watts. Two plug-in rf transformers (tank coils) are required to cover the entire frequency range. One coil was built for the three frequencies used in these experiments. The output is link-coupled to a 52-ohm coaxial transmission line. Since the transmission loss at 4 MHz. is only 0.4 db per 100 ft., the location of the quadrupole with respect to the rf amplifier is of little practical importance.

Quadrupole Excitation Tank Coil

A second plug-in rf transformer (tank coil) is located in the immediate vicinity of the quadrupoles. (See Figure 45.) Its function is to provide the necessary impedance match between the transmission line and the resonant circuit of which the rod and segment capacitances are a major part. Four of these plug-in coils are required to cover the entire range of frequencies. One such coil was built to cover the three frequencies used. Corresponding electrode terminals of each quadrupole are connected in parallel so that the same potentials are simultaneously applied to both.

High Frequency Rectifiers

Two independent dc feedback voltages for the control unit are provided by two full wave shunt rectifiers capacitance coupled to the tank coil. One controls the modulator to keep the ac potential stable and proportional to the scanning control voltage. The other is used as a reference for stabilizing the dc/ac ratio. In each case the negative feedback voltage is compared with its respective control voltage at the input of a high gain operational amplifier. The open loop gain of these stabilizing circuits is sufficient to enable these portions of the apparatus to achieve the design goals.

EXPERIMENTAL PROCEDURE

General

Two sets of operating conditions were used. In one, an attempt was made to maintain constant the number of periods of the excitation potential which occur during the transit time of the ions, while the excitation frequency is varied. Under these conditions all applied potentials vary as the square of the excitation frequency. When this is done the trajectories and the resolving power should be independent of the excitation frequency.

In the second set of conditions the ion energy was held constant while the excitation frequency was varied. Under these conditions higher resolving power is expected at the higher frequency, since the number of cycles which occur during ion transit is higher.

While every effort was made to duplicate operating conditions in the two quadrupoles, there remained some differences in the ion output of the two sources. These small differences were evaluated and used to normalize the comparative data from the two quadrupole units.

During these tests a careful control of the partial pressure of krypton was maintained. A strip chart recorder with a retransmitting slide wire displayed the current from the calibrated monitor quadrupole and controlled the speed of the ion pump so that the partial pressure remained constant. Different partial pressures of the mass 84 peak varied from 1.5×10^{-8} to 5.0×10^{-7} torr. To assure the validity of the partial pressure measurements the monitor quadrupole was calibrated daily. Ion current from the quadrupole under test was divided by the known partial pressure to give the sensitivity in amperes per torr.

Calibration

Krypton Monitor

An auxiliary three-inch quadrupole mounted symmetrically with respect to the round and hyperbolic quadrupoles is adjusted in the high pass mode to respond to the spectrum of krypton. By admitting this gas into the vacuum system and observing the change in the pressure determined by a Bayard-Alpert gauge and the change in the pressure of krypton from the monitor quadrupole while no ion pumping was in process, the partial

pressure of mass 84 was calculated and the calibration of the monitor quadrupole established. This process was repeated daily, and the calibration of the monitor remained fixed with only a ± 10% deviation during a month of operation. From the daily calibration a corrected partial pressure of mass 84 was used in establishing the absolute sensitivity of each quadrupole.

Ion Sources

The two ion sources were also calibrated. This was accomplished by dividing the current resulting from 100% transmission of ions for a flat-topped peak at low resolving power by the partial pressure of the mass 84 isotope of krypton. This measurement was made for the three ion injection energies used in the experiments and is shown in Figure 50. The ion source used in the quadrupole with the hyperbolic rods was slightly more sensitive and was therefore chosen as the reference. The absolute sensitivities of the quadrupoles when operating at 100% transmission are assumed to be the same as the sensitivity of the reference ion source for each of the ion injection energies.

Secondary Emission Multipliers

The gain of each of the two secondary emission multipliers was determined by comparing the current for a flat-topped peak at low resolving power as detected with and without the multiplier. For most of the experiments, the secondary emission multiplier was operated at reduced voltage to provide a gain of about 150.

Data Reduction

The basic data from these comparisons were in the form of ion current from the quadrupole for the resolved mass 84 peak mechanically plotted as a function of the potentials on the rods. Repeated scans were made for different values of the ratio of the dc to the ac potentials. From these basic data, in the form of plotted mass 84 peaks and the corresponding partial pressures of the mass 84 isotope, the sensitivity in amperes per torr was obtained as a function of the resolving power. Resolving power is defined as $(s/w)m$, where s is the distance between the adjacent peaks of one mass number apart, w is the width measured at 10% of the peak height, and m is the mass number in amu.

EXPERIMENTAL DATA

The initial data comparing the operation of the round and hyperbolic quadrupoles indicated a very decided superiority of the hyperbolic unit. The outstanding difference was quite impressive. To demonstrate that this difference was indeed due to the contours of the field-forming surfaces, and not to any other cause, the following "operation" was performed on the two units. They were taken apart and reassembled with the rods interchanged between the two units. Sources, detectors, and all other components remained as before. The excellent performance remained with the hyperbolic rods! The data which are reported were obtained after the interchange of the rods.

Considerably more data were obtained than is reported here. In particular, some data were obtained with a larger entrance aperture, namely, 0.100 inches instead of 0.050 inches. The main difference observed is in sensitivity; the larger aperture gives the expected two-fold increases. The expected increase is proportional to the diameter, not the area of the entrance aperture because of the nonuniform radial distribution of the electrons.

In the first set of experiments, all applied voltages were varied as the frequency squared. Frequencies of 0.707, 1.0, and 1.414 MHz. were used. The corresponding ion accelerating potentials were 1, 2 and 4 volts. Figure 51 shows the sensitivity of the round and hyperbolic quadrupoles as functions of resolving power for operation at 1.414 MHz.

At low resolving power, where essentially 100 percent transmission is obtained, the sensitivities of the two instruments appear to be identical, as they should. However, as the resolving power is increased, the attenuation of the sensitivity is much greater for the unit with the round rods. In the sensitivity interval between approximately 50 and 10% of the maximum, the resolving power of the hyperbolic unit is about twice that of the round!

Figures 52 and 53 show data similar to that of Figure 51. The differences are the excitation frequencies. At the lower frequencies (and voltages) the sensitivities are lower. Reference to Figure 50 reveals that the changes in sensitivity are due almost entirely to reduced output of the ion sources at the lower ion accelerating potentials. It is most worthy to note that the resolving powers attainable at the lower excitation frequencies are essentially the same as at the higher frequencies.

In Figure 54, the data of Figures 51 and 53 are combined for direct comparison. These show that the main disadvantage in the operation at the lower frequency is that of instrument sensitivity, which has been shown to be due to the ion source characteristics. The attainable resolving power is quite similar for the two cases, even though the power required to supply the ac excitation differs by a factor of 32! These conclusions may seem to be at variance with the data reported earlier by Brubaker and Tuul. However, the conditions here are quite different, in that the energy of the ions was varied proportionally with the square of the excitation frequency, while in the earlier experiment the ion energy remained constant. This is the factor which makes the difference.

Figures 55 and 56 show the performance of the round and hyperbolic quadrupoles when the energy of the ions is maintained low and frequency of excitation is varied. Under these conditions, which are similar to those of the earlier experiments of Brubaker and Tuul, an increase in the excitation frequency has a pronounced influence on the attainable resolving power. This is fully anticipated by the theory.

In Figure 57, the data for the round and the hyperbolic units, from Figures 55 and 56, are combined. These are combined to make a direct comparison of the performance of the round and the hyperbolic rods when they are excited at widely different power levels. Here it is seen that the sensitivity and the resolving power of the hyperbolic unit are comparable to those of the round unit when the excitation frequency varies by a factor of two!

Figure 58 reveals the operation of the hyperbolic quadrupole under the most favorable conditions. Delayed dc ramp mode of operation is used, the ion energy is low, and the excitation frequency is high. The portion of the krypton spectrum includes only masses 83 and 84. Repetitive scans over these two peaks were made using an x - y recorder. The parameter which was varied between scans is the resolving power, as influenced by the ratio of the applied dc to ac potentials. Note that as the resolving power is increased from low values to about 400, the height of the peaks remains quite constant. At a resolving power of 1000, the peaks are still 20% of the maximum. Note also the slope of the sides of the peaks as they are attenuated by an approach to the x- or y-stability limits. In the conventional quadrupole, the attenuation on the y-limit (low mass side) is much more gradual than on the high mass side. In the delayed dc ramp mode the slope appears steeper on the low mass side. This comes about through the alteration in the manner in which the working point crosses the y-stability limit in the delayed dc ramp mode.

When a quadrupole is used to transmit ions of a given m/e ratio, the excitation power is proportional to f^5C/Q, where f is the excitation frequency, C the capacitance of the two terminal quadrupole, and Q the dissipation factor, $\omega L/R$. First order, Q is frequency independent, so it changes very little as the frequency is varied by a factor of two. Owing to their larger cross-section, the capacitance of the hyperbolic assembly is greater than that of the round. The magnitude of this difference depends upon the design of the hyperbolic rods. In this laboratory experiment, the hyperbolic rods were of considerably larger cross-section than would normally be required. Even so, the capacitance of this unit was only 1.5 times that of the round. In this experiment the ratio of the excitation powers is $(0.5)^5 \times 1.5$, or 0.047. Thus it is seen that the performance of the hyperbolic quadrupole equals that of the round when the excitation power of the hyperbolic is only 5% that of the round!

CONCLUSIONS

Theoretical computations and laboratory experiments have shown that the sensitivity of a quadrupole mass filter may be increased by factors of ten to one hundred by appropriately altering the ratio of the dc to the ac fields in the vicinity of the entrance aperture. This is accomplished without the loss of resolving power or any other desirable characteristic. This refinement gives peaks with flat tops to much higher resolving power than is obtainable in a conventional mass filter. This circumstance greatly increases the analytical accuracy of the instrument, as it renders the peak height less dependent on the ratio of the dc to ac potentials applied to the rods. The improved performance is obtained with only moderate increase in the complexity of the apparatus.

Computer investigations have been made of the perturbations produced in the contours of the equipotential surfaces by the substitution of round instead of hyperbolic field-forming electrodes. These perturbations are surprisingly large, in view of the excellent performance experienced with the round rods in practice. However, laboratory experiments with a quadrupole with hyperbolic field-forming surfaces indicate a decided superiority as compared to the performance of a conventional quadrupole of similar size. In particular, it has been found that comparable performance from round and hyperbolic units is obtained when the excitation frequency of the hyperbolic is only half that of the round. Under these conditions, the power required to excite the quadrupoles differs by about 20 times. This is of prime importance in space applications!

ABSTRACTS OF PAPERS PRESENTED DURING THE FORCE OF CONTRACT NASW-1298

On the following pages are copies of Abstracts and Extended Abstracts of papers presented at Technical Society Meetings during the performance of this contract. The manuscript submitted for presentation at the International Mass Spectrometry Conference and for publication in "Advances in Mass Spectrometry," Volume 4, is included in its entirety.

ABSTRACT OF A PAPER PRESENTED AT
THIRTEENTH NATIONAL SYMPOSIUM OF THE AMERICAN VACUUM SOCIETY
OCTOBER 26-28, 1966
SAN FRANCISCO, CALIFORNIA

IMPROVED QUADRUPOLE MASS FILTER*

by

Wilson M. Brubaker

The transmission of ions through a conventional quadrupole mass filter is severely attenuated by the impulses which the ions receive as they traverse the fringing field. A computer study has been made to evaluate this phenomenon. Serious losses are indicated. The computer was also used to explore the effectiveness of a proposed scheme for eliminating these undesired radially directed impulses. The results of the computer study were encouraging, and an experimental apparatus was built to evaluate the scheme in the laboratory. Preliminary results indicate that, at the higher resolving powers, the transmission of ions through the quadrupole is increased by factors of ten to one-hundred by the use of this refinement. This increased transmission is obtained without loss of resolving power.

---

* This research was supported in whole or in part by the National Aeronautics and Space Administration under Contract No. NASW-1298, monitored by Dr. Donald P. Easter.

ABSTRACT OF A PAPER PRESENTED AT
FIFTEENTH ANNUAL CONFERENCE ON MASS SPECTROMETRY AND ALLIED TOPICS
MAY 14-19, 1967
DENVER, COLORADO

THE EFFICIENT INTRODUCTION OF IONS INTO A QUADRUPOLE MASS SPECTROMETER*

by

Wilson M. Brubaker

The efficiency with which ions are introduced into a quadrupole mass filter is increased by several powers of ten by the appropriate control of the fields at the entrance to the filter. This is accomplished by using an additional set of four electrodes. The potentials applied to these additional electrodes have a smaller ratio of dc to ac values than the potentials applied to the quadrupole. Computer studies reveal the high vulnerability of the entering ions to the impulses which they receive as they traverse the fringe fields of the conventional quadrupole. Further studies with the computer reveal the effectiveness of the altered fields in eliminating these undesired impulses. Experimental data compare the operation of the quadrupole with and without use of the additional electrodes. It is found that the sensitivity of the instrument can be increased by powers of ten without degrading the resolving power through the use of these auxiliary electrodes.

* * * * * * * * * * *

It has long been recognized that there is a direct relationship between the resolving power of the quadrupole and the number of cycles spent by the ions in traversing the device. Increasing the frequency of excitation and decreasing the axial velocity both increase the transit time in periods of the ac excitation. The former is accomplished only at a great expense in power, and the latter with a decrease in sensitivity. The severe attenuation of the transmission of ions through the quadrupole which results from directing ions toward the instrument at low velocity occurs because the ions receive a large component of radial velocity as they traverse the fringing fields.

---

* This research was supported in whole or in part by the National Aeronautics and Space Administration under Contract No. NASW-1298, monitored by Dr. Donald P. Easter.

Through an alteration of the relative strengths of the dc and the ac fields at the entrance to the quadrupole it is possible to avoid the severe loss of low velocity ions. This alteration of the fields is accomplished through the use of an additional set of four electrodes in the vicinity of the entrance aperture.[1] This refinement in the quadrupole significantly decreases the size of the instrument and the required power for a given resolving power. These considerations are particularly important for space applications.

The usual use of the stability diagram is to indicate the manner in which the mass spectrum is produced. In this discussion it is used to help understand what happens to an ion as it passes through the fringe fields while entering the quadrupole. As an ion enters the quadrupole on a path which is parallel to the instrument axis, the values of both a and q vary from zero to full value. For ions which are transmitted through the quadrupole at high resolving power the locus of the working point lies very close to the apex of the stability diagram while the ion is within the quadrupole. During almost all of the transit of the ion through the fringe fields, the working point lies far above the y-stability limit. Here the acceleration is directed away from the instrument axis.

If the path of the working point as the ion enters the quadrupole can be made to lie within the stable portion of the stability diagram, the undesired y-directed impulse can be avoided. This desired situation can be achieved if the working point moves first along the q-axis as it leaves the origin. Such motion is obtained if the field-forming surfaces adjacent the entrance aperture are excited with ac potentials only. These additional electrodes lie between the entrance aperture and the usual quadrupole rods which are excited with their normal amounts of ac and dc potentials. Because the dc fields are delayed (along the instrument axis), this mode of operation has been termed "delayed dc ramp".

Experiments were made in which eight-volt ions were injected into a ten-inch quadrupole operating at 1.6 MHz. Direct comparison of the operation in the conventional and the delayed dc ramp modes were made. At the modest resolving power of 100 the sensitivity of the delayed dc ramp mode was 50 times that of the conventional. At a resolving power of 400 this difference becomes 250.

In the conventional quadrupole, as has just been shown, the use of low injection energy increases the number of cycles spent by the ions in traversing the fringe fields and causes severe attenuation of the transmission efficiency. Conversely, if high transmission efficiency is obtained by using higher ion injection energies, then the upper limit of the resolving power is reduced.

In the improved quadrupole, operating in the delayed dc ramp mode, ions can be introduced at low energies without causing the transmission efficiency to be low. Thus high resolving power at high sensitivity can be achieved.

REFERENCES

[1]W. M. Brubaker, "Auxiliary Electrodes of Quadrupole Mass Filters," U. S. Patent 3,129,327.

A more detailed paper will be published in "Advances in Mass Spectrometry," Volume 4, (Proceedings of International Mass Spectrometry Conference, Berlin, September, 1967).

EXTENDED ABSTRACT OF A PAPER PRESENTED AT
FOURTEENTH NATIONAL AMERICAN VACUUM SYMPOSIUM
OCTOBER 24-27, 1967
KANSAS CITY, MISSOURI

COMPARISON OF QUADRUPOLE MASS SPECTROMETERS WITH ROUND AND HYPERBOLIC RODS*

by

Wilson M. Brubaker

The theory upon which the operation of the quadrupole is based assumes hyperbolic field-forming surfaces. Experience has shown that excellent operation is obtained when round rods are used instead of the more expensive hyperbolic ones. The perturbations of the fields which result from this substitution have been evaluated with the aid of a computer. Experimental data have been obtained which compare the performances of quadrupoles with round and with hyperbolic field-forming surfaces.

COMPUTER STUDIES

When hyperbolic field-forming surfaces are used, the x- and y-field components are proportional to the x- and y-displacements. Under these conditions the trajectories are readily computed, and are well known. When round rods are used, the resulting fields must be determined before the trajectories can be computed. As would be expected, the perturbations are small in the general vicinity of the axis, and become larger at large distances from the axis. It is not surprising that in some regions the perturbations are positive (indicating a stronger field) and in others they are negative.

The most disturbing factor, from the standpoint of predicting the performance of the quadrupole from a knowledge of the fields, is that the perturbations in the y-component of the field are functions not only of the y-position, but also of the x-position, and vice versa. Thus the y-trajectory for an ion in the plane $x = 0$ differs appreciably from that of an ion in the plane $x = r_o$. When it is realized that the x-component of motion is completely independent of the y-component (in the hyperbolic case) it becomes apparent that it is impossible to compute a "typical" trajectory. One of the less perturbed trajectories is that which starts on the instrument axis and remains in the plane $x = 0$. In this instance the perturbation is very small for the portions of the trajectory which are of small amplitude.

---

* This research was supported in whole or in part by the National Aeronautics and Space Administration under Contract No. NASW-1298, monitored by Dr. Donald P. Easter.

Figure 1 shows the results of computations made for an ion in the plane x = 0. The trajectory envelopes are plotted as a function of time. The ion is introduced on the axis at various y-directed velocities. It is found that at a critical injection velocity of 0.029714 r_o cm/μsec the ion reaches the maximum displacement from which it will return to the axis. At higher velocities, it hesitates at the 0.83 r_o position and then proceeds to strike the rod. For comparison, the trajectory of an ion injected into the unperturbed hyperbolic field is included. These data were calculated at a resolving power of approximately 100. Similar calculations at higher resolving powers show that the ion reaches a "point of no return" at amplitudes considerably less than 70% or r_o. Trajectories in other planes are more complicated than this one.

If ions which reach 70% of the distance to the round rods are lost to the rods, it follows that hyperbolic rods placed at 70% of the distance to corresponding round rods would produce very similar trajectories. The same fields would be produced by the hyperbolic rods with 49% of the voltage which is applied to the round rod unit. The power to energize the hyperbolic quadrupole would be less than a fourth that required to energize the round, and the performance would probably be superior! While this saving of power may be of limited importance in the laboratory, it is of paramount importance for instruments used in the space program!

EXPERIMENTAL STUDIES

An apparatus was assembled which consists of two ten-inch long quadrupoles with the same instrument radius, r_o. The field-forming surfaces in one are the familiar round rods, and in the other they are of hyperbolic cross section. These instruments are mounted symmetrically on an ion-pumped vacuum system. Corresponding electrodes are connected in parallel and energized from a common power supply. These quadrupoles are operated in the delayed dc ramp mode.[1,2] Their performances were compared by plotting their sensitivities as functions of their resolving powers. The initial results showed a marked superiority of the hyperbolic rods. To assure that this difference was indeed due to the rod contours and not to some other, unrecognized factor, the units were disassembled and then reassembled with the rods placed on the alternate support structures. That is, the rods from one vacuum envelope were placed in the other. Sources, rod support members, and multiplier-detectors were not interchanged. The data appeared to be unaffected by this maneuver.

As the instruments were operated, the resolving power of the hyperbolic exceeded that of the round by about a factor of two. Typical data are presented in Figure 2.

To indicate the excellent performance given by the hyperbolic system, operated in the delayed dc ramp mode, the spectra of the mass 83 and 84 isotopes of krypton are presented in Figure 3. Note that, as the resolving power is increased by an increase in the ratio of the dc to the ac applied potentials, the mass 84 peak remains flat-topped to a resolving power of about 400. At a resolving power of 1,000 the transmission efficiency, as given by the peak height, is 20%.

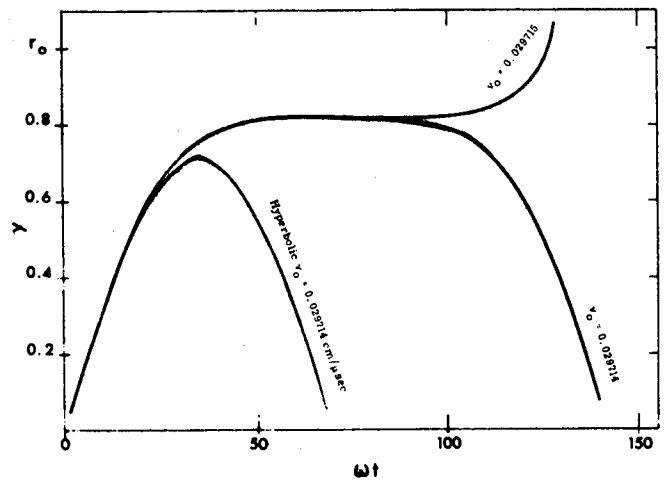

FIGURE 1.

Y-TRAJECTORIES FOR X=0, A=0.23462, Q=0.70482, M/DM ≈100

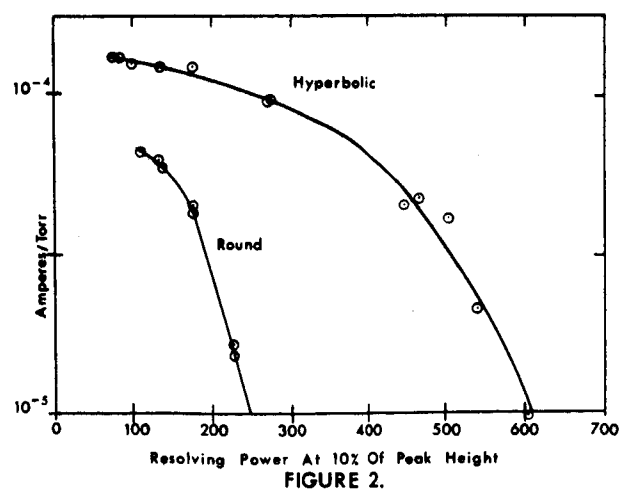

FIGURE 2.

SENSITIVITIES OF ROUND AND HYPERBOLIC QUADRUPOLES AS FUNCTIONS OF RESOLVING POWER. EXCITATION FREQUENCY 1.414 MHz, ION ENERGY 4 VOLTS.

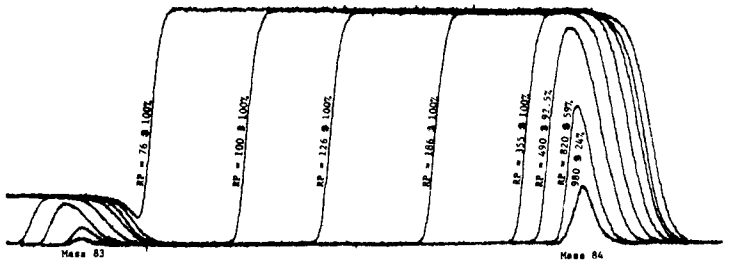

FIGURE 3.

MULTIPLE SCANS OF MASS 84 PEAK AT VARIOUS RESOLVING POWERS. EXCITATION FREQUENCY 1.414 MHz; ION ENERGY 1.0 VOLT.

REFERENCES

[1] "The Efficient Introduction of Ions into a Quadrupole Mass Spectrometer," presented at the ASTM Committee E-14 Meeting in Denver, May, 1967.

[2] "Improved Quadrupole," presented at the International Mass Spectrometry Conference in Berlin, September, 1967, and published in "Advances in Mass Spectrometry," Vol. 4.

MANUSCRIPT OF A PAPER PRESENTED AT
INTERNATIONAL MASS SPECTROMETRY CONFERENCE
SEPTEMBER 25-29, 1967
BERLIN, WEST GERMANY
AND FOR PUBLICATION IN "ADVANCES IN MASS SPECTROMETRY," VOLUME 4

IMPROVED QUADRUPOLE*

by

Wilson M. Brubaker

ABSTRACT

Experimental data reveal that the sensitivity of the conventional quadrupole can be increased by a factor of ten to one-hundred with no sacrifice in the resolving power. This is accomplished through the use of a set of four additional electrodes at the ion entrance end of the mass filter. As an ion traverses the fringe fields of a conventional quadrupole the working point moves through the y-unstable portion of the stability diagram. Under these circumstances, computer studies have shown that the ion receives a large impulse in the y-direction. By appropriately energizing the auxiliary electrodes of the improved quadrupole, it is possible to have the working point remain within the x- and y-stable portion, and thus to avoid the undesirable radial impulse. The results of computer studies and experimental data are presented.

INTRODUCTION

The quadrupole mass filter is uniquely different from most other mass analyzers. Its maximum dimension is along the axis, yet the fields within the structure have no component in this direction. Additional length of the instrument serves merely the purpose of increasing the time spent by the ions in traversing the analyzer. It has long been recognized[1] that there is a direct relationship between the resolving power of the quadrupole and the number of cycles spent by the ions in traversing the device. Increasing the frequency of excitation and decreasing the axial velocity both increase the transit time measured in periods of the ac excitation. The former is accomplished only at a great expense in driving power, and the latter results in a decrease in sensitivity. The severe attenuation of the transmission of ions through the quadrupole which results from

---

* This research was supported in whole or in part by the National Aeronautics and Space Administration under Contract No. NASW-1298, monitored by Dr. Donald P. Easter.

directing ions into the instrument at low velocity occurs because the ions receive a large component of radial velocity as they traverse the fringing fields.

Through an alteration of the relative strengths of the dc and the ac fields at the entrance to the quadrupole it is possible to avoid the severe loss of low velocity ions.[2] This alteration of the fields is accomplished through the use of an additional set of four electrodes in the vicinity of the entrance aperture. This refinement in the quadrupole significantly decreases the size of the instrument and the required driving power for a given resolution. These considerations are particularly important for space applications.

THEORY

General discussion of the theory of the quadrupole mass filter requires reference to the stability diagram, shown in Figure 1. The coordinates are the dimensionless numbers a and q. For a given ratio of the dc to the ac potentials, the "working point" for ions of all values of m/e fall on a straight line which passes through the origin. This is denoted as the "scan line".

The usual use of the stability diagram is to indicate the manner in which the mass spectrum is produced. In this discussion it is used to help understand what happens to an ion as it passes through the fringe fields while entering the quadrupole. First, it should be noted that the dimensionless variables a and q are proportional to the fields at a given position in the plane transverse to the instrument axis. Thus, as an ion enters the quadrupole on a path which is parallel to the instrument axis, the values of both a and q vary from zero to full value. For ions which are transmitted through the quadrupole at high resolving power the locus of the working point must lie very close to the apex of the stability diagram while the ion is within the quadrupole.

Theory previously developed[3] shows that the radial acceleration experienced by an ion as it responds to the combined dc and ac fields is proportional to the vertical distance between the y-stability limit and the working point. The working point in the quadrupole for a transmitted ion lies very near to the apex, just under the y-stability limit, and the net acceleration is directed toward the instrument axis. But during almost all of the transit of the ion through the fringe fields, the working point lies far above the y-stability limit. Here the acceleration is directed <u>away</u> from the instrument axis. Computations have shown that the magnitude of the y-directed momentum impulse which the ion receives as it traverses the fringe fields varies <u>exponentially</u> with the number of periods (cycles) of ac excitation which occur during

its transit. Thus it is seen that the number of cycles spent by the ions in the fringe fields must be kept quite small, unless there is to be an acute attenuation of the transmission of ions through the instrument.

If the path of the working point can be made to lie within the stable portion of the stability diagram while the ions are passing through the fringing fields, the undesired y-directed impulse can be avoided. This desired situation can be achieved if the working point moves first along the q-axis as it leaves the origin. Such motion is obtained if the field-forming surfaces adjacent the entrance aperture are excited with ac potentials only. These additional electrodes lie between the entrance aperture and the usual quadrupole rods which are excited with their normal amounts of ac and dc potentials. Because the dc fields are delayed (along the instrument axis), this mode of operation has been termed "delayed dc ramp". One of the many paths the working point may take through the stability diagram in the delayed dc ramp mode of operation is denoted as a "preferred path" in Figure 1.

COMPUTER STUDIES

The purpose of the computations was to evaluate the seriousness of permitting the working point to move through the y-unstable portion of the diagram as the ions traverse the fringe fields of the conventional quadrupole. Computations were made in which the ions were assumed to be formed within the quadrupole, to enter a conventional quadrupole with coincident (normalized) dc and ac ramps, and to enter the improved quadrupole, in the delayed dc ramp mode.

Computer studies differ from laboratory studies in that the trajectory is never terminated by the ions striking the rods. The amplitude is limited only by the number of digits in the computer. This was never a concern during these investigations.

The a, q values chosen for the uniform field region correspond to a resolving power of about 400. Further, the working point selected lies very close to the line $\beta_x + \beta_y = 1$, since the envelopes for the x and the y trajectories are nearly identical for this value.

In the first set of calculations the ions were assumed to be formed within the uniform field region, with zero radial velocity, and at the point $x = y = 1$. Since the x and the y forces are completely orthogonal and independent of each other, trajectories for both components of motion were obtained simultaneously. Trajectories were started at 90° phase intervals (of the applied ac potential).

The maximum amplitudes were in general similar for x and y motions, the largest at 90° and 270°, as expected. The amplitudes remained less than 25 times the initial displacement.

In the second set of computations the passage of the ions from regions of zero fields to those of full fields was simulated by causing the magnitudes of the fields (dc and ac) to increase together at a uniform rate from zero to their full values. Computations were again made at the four phase angles, and for ramp lengths of two and ten cycles. In all cases the maximum amplitude for the x-component of motion is less than ten times the initial position, but for the y-component at ten-cycle ramp the normalized amplitudes are all greater than 1000 times the initial displacement! The phase of the ac potential at the start of the computations has little influence on these extremely large amplitudes.

Further computations were made in which the independent variable is the number of cycles which occur while the ions traverse fringe fields. As might have been anticipated, the maximum amplitude varies exponentially with the ramp length, measured in cycles (periods) of ac excitation.

In the third set of computations the ions were assumed to enter the quadrupole in the delayed dc ramp mode. Several different "preferred paths" were used. In the steepest ramp case, the ac fields build up uniformly during the first twelve cycles, the dc field during the second set of six cycles, from the seventh to the twelfth cycle. In all cases, the normalized amplitudes are less than five times the initial displacement.

The results of these computations are summarized in Figure 2. It is seen that the magnitude of the "entrance transient" given the ions is greatly reduced through the use of the delayed dc ramp mode of operation.

EXPERIMENTAL

Apparatus

The additional set of four electrodes at the entrance of the quadrupole has been provided in the form of insulated rod segments, one on each rod. The rod assemblies of the improved quadrupole, and the method used for energizing them are shown schematically in Figure 3. By moving the switch from position A to B, the operation of the quadrupole is changed from conventional to delayed dc ramp modes. The diameter of the rods is 0.6 inches, their length 10 inches. The segments are 0.6 inches long. The excitation frequency was 1.6 MHz.

Results

Krypton gas was used for all observations made in this study. Resolving power measurements were made by observing the width of the mass 84 peak at 10% height and the separation of this peak from the mass 83 peak. Instrument sensitivities are plotted as functions of resolving power at different ion injection energies and for operation in the conventional and the delayed dc ramp modes.

The data obtained at 15-volt ion injection energy are presented in Figure 4. In this instance the resolving power is limited by the transit time of the ions. At this high injection energy the ions traverse the fringe fields in less than three cycles, and the resulting transmission loss is nominal. Even so, the sensitivity in the delayed mode is six times that of the conventional at low resolving powers.

At 8-volt ion injection energy the difference between the conventional and the delayed dc ramp modes of operation is more apparent, as shown in Figure 5. The increased time spent in the quadrupole raises the resolving power very appreciably. However, the greater time spent in the fringe fields of the conventional quadrupole causes a rather severe attenuation of the transmission efficiency. At a resolving power of 100 the instrument sensitivity of the delayed dc ramp mode is 50 times that of the conventional. At a resolving power of 400, this difference becomes a factor of 250!

Four-volt incident ions remain in the system during a large number of cycles of the ac voltage, and the nominal resolving power is high. However, in the conventional quadrupole the sensitivity is too low to be useful because the impulse given the ions in the fringe fields causes them to strike the rods, and be lost. In the dc ramp mode, useful sensitivity is achieved for resolving powers as high as 650. These data are shown in Figure 6.

CONCLUSIONS

In the conventional quadrupole, as has just been shown, the use of low injection energy increases the number of cycles spent by the ions in traversing the fringe fields and causes severe attenuation of the transmission efficiency. Conversely, if high transmission efficiency is obtained by using higher ion injection energies, then the upper limit of the resolving power is reduced.

In the improved quadrupole, operating in the delayed dc ramp mode, ions can be introduced at low energies without causing the transmission efficiency to be low. Thus high resolving power at high sensitivity can be achieved.

REFERENCES

[1]W. Paul, H. P. Reinhard und U. von Zahn, "Das Elektrische Massenfilter als Massenspektrometer und Isotopentrenner," Zeitschrift fur Physik, Bd. 152, S. 143-182 (1958).

[2]W. M. Brubaker, "Auxiliary Electrodes of Quadrupole Mass Filters," U. S. Patent 3,129,327.

[3]W. M. Brubaker, "The Quadrupole Mass Filter," Paper presented at IX Colloquium Spectroscopicum Internationale, Juin, 1961, Lyon, France. "Study and Development of the Paul-type Mass Spectrometer," Contract No. AF 19(604)-5911, April, 1963.

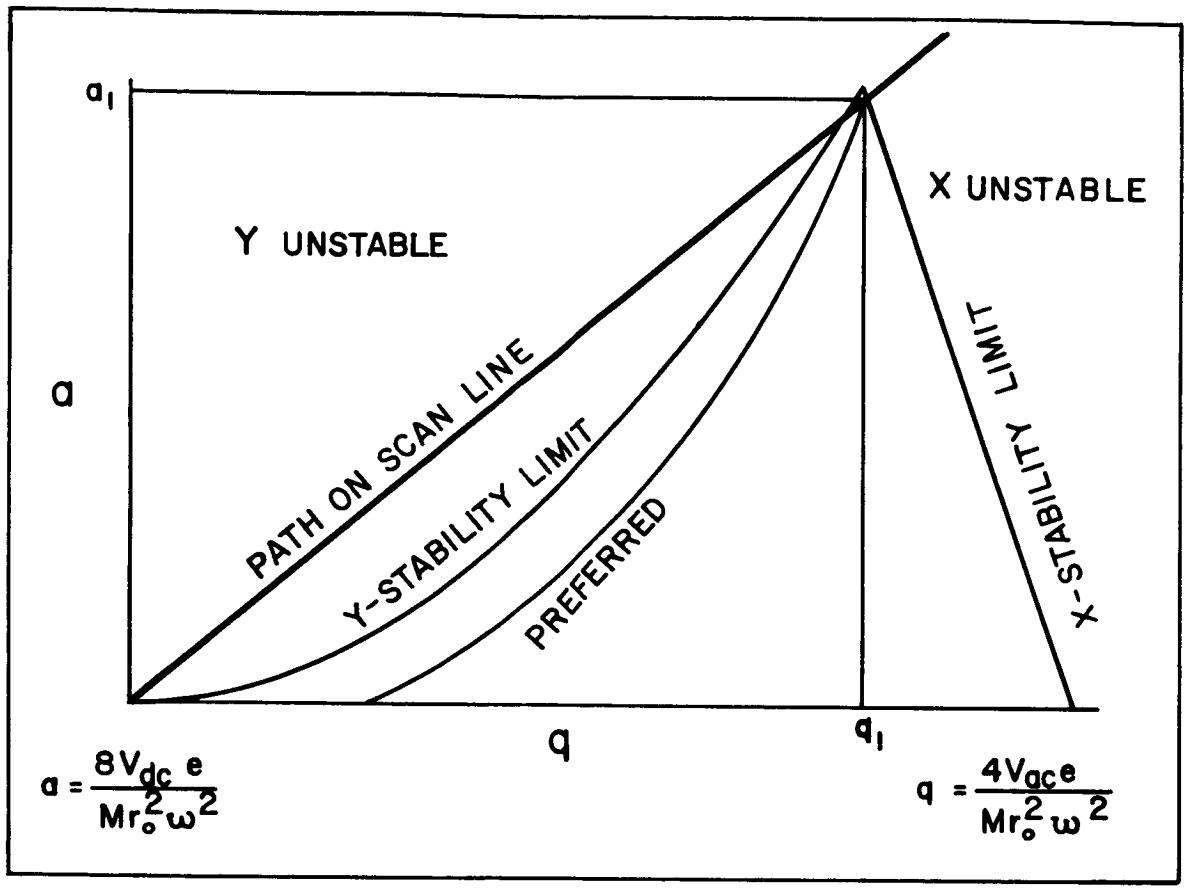

STABILITY DIAGRAM, SHOWING TWO PATHS OF WORKING POINT DURING TRAVERSAL OF FRINGING FIELD.

FIGURE 1

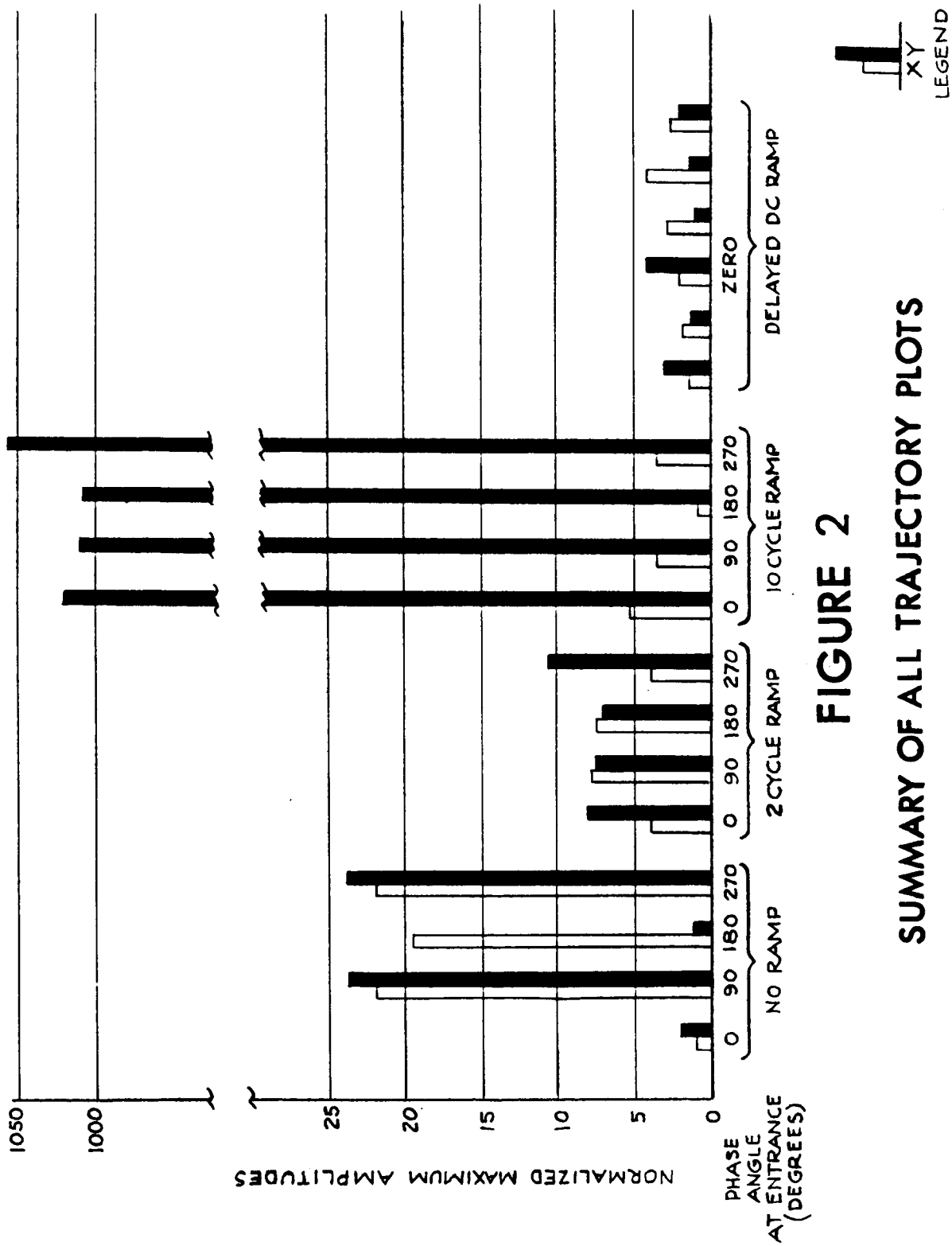

FIGURE 2

SUMMARY OF ALL TRAJECTORY PLOTS

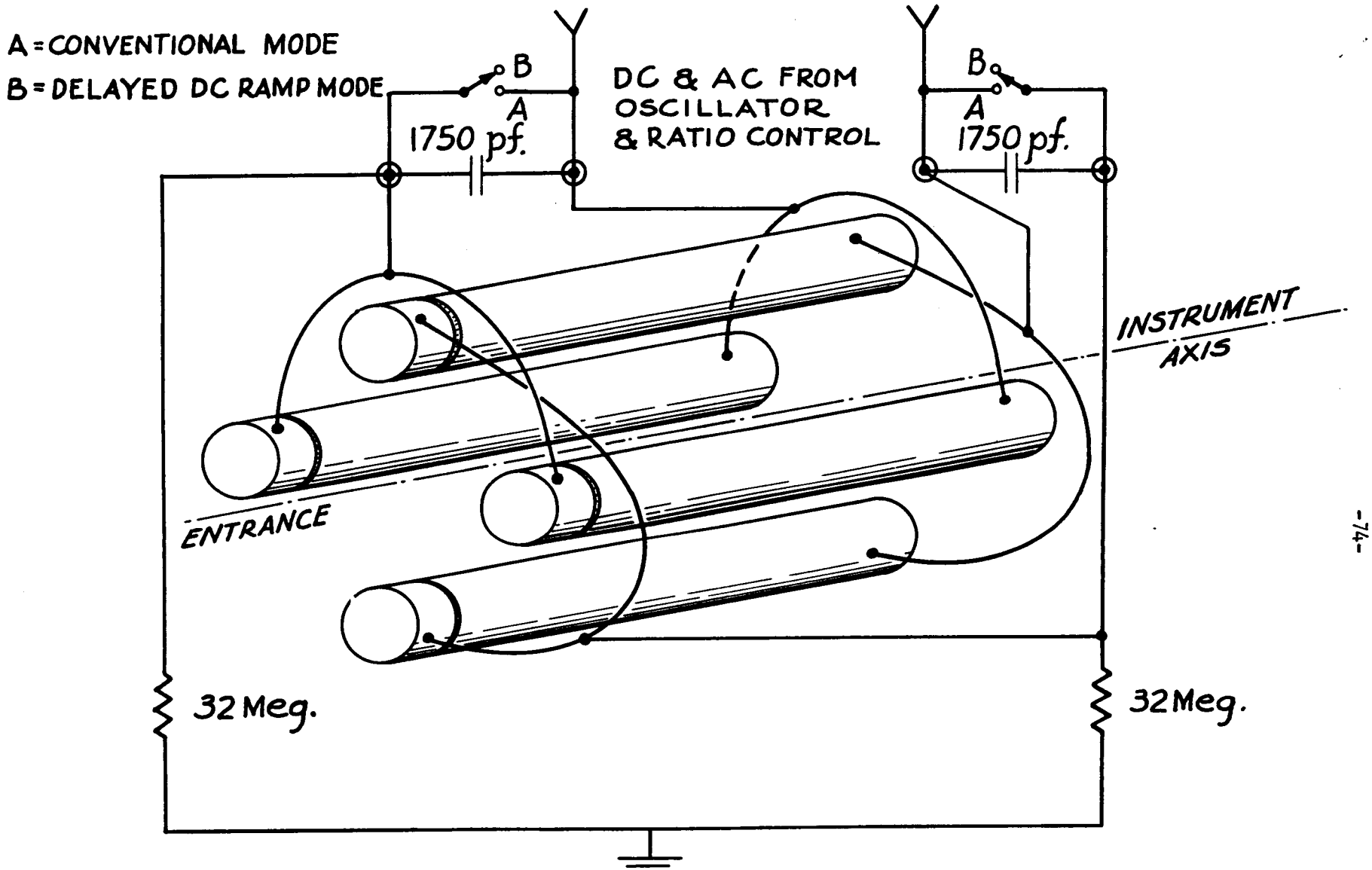

APPARATUS
FIGURE 3

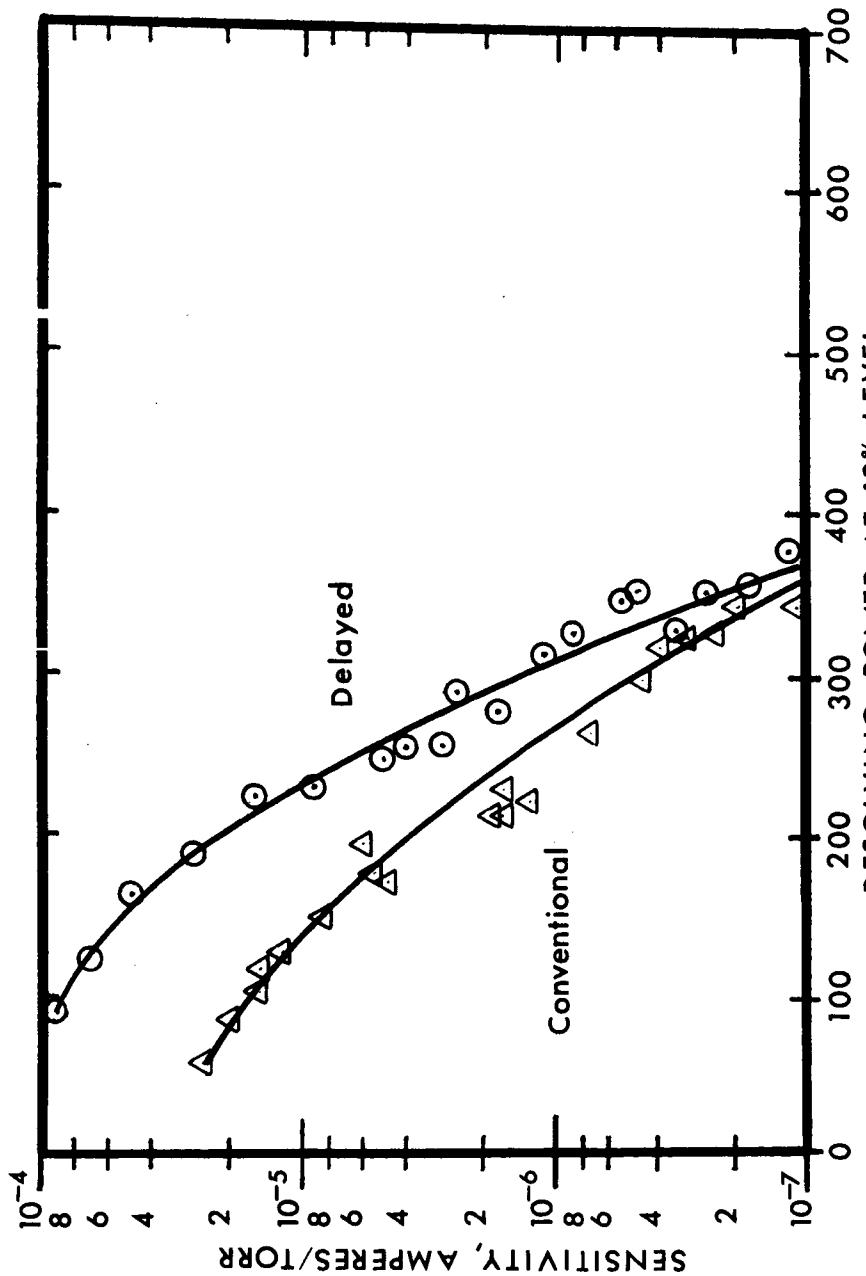

FIGURE 4

SENSITIVITY VS. RESOLVING POWER FOR CONVENTIONAL AND DELAYED MODES WITH 15-VOLT IONS

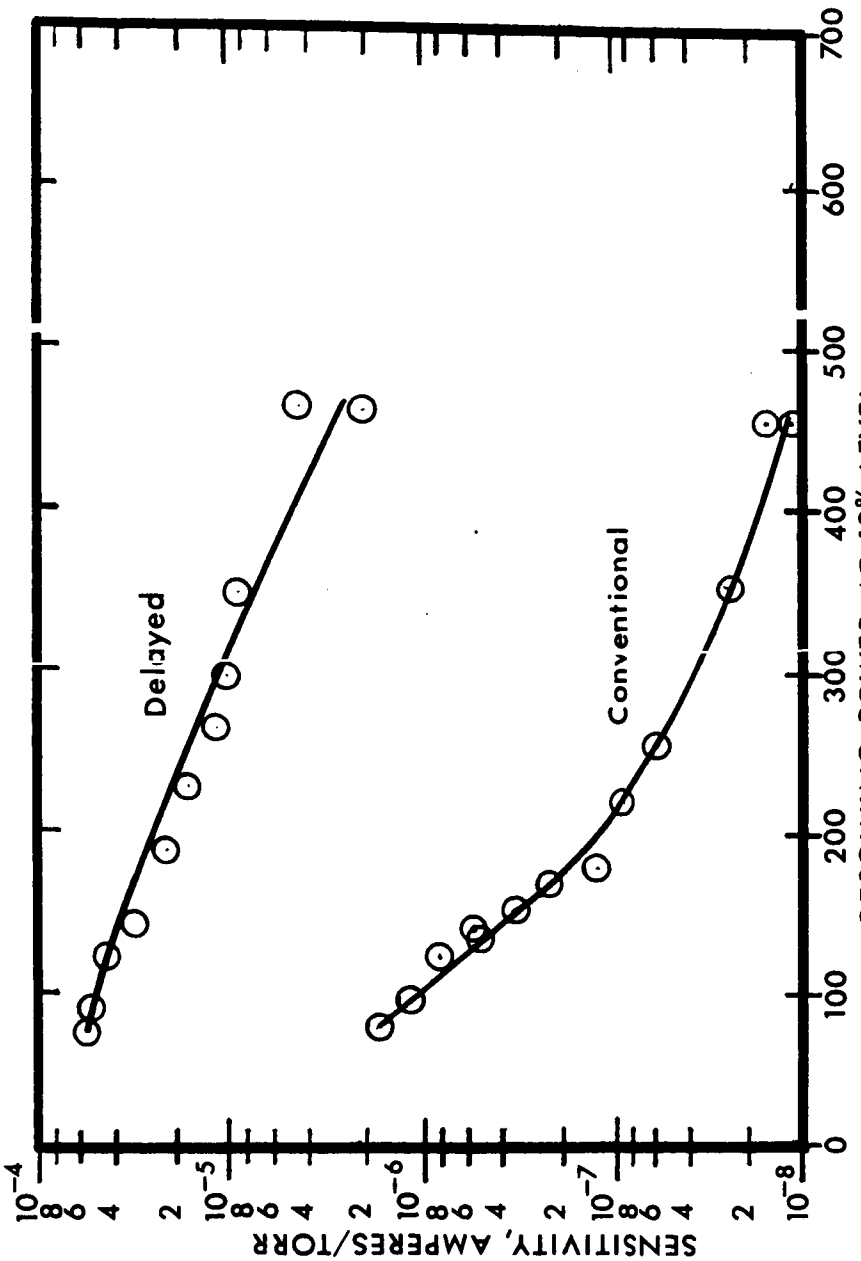

FIGURE 5

SENSITIVITY VS. RESOLVING POWER FOR CONVENTIONAL AND DELAYED MODES WITH 8-VOLT IONS

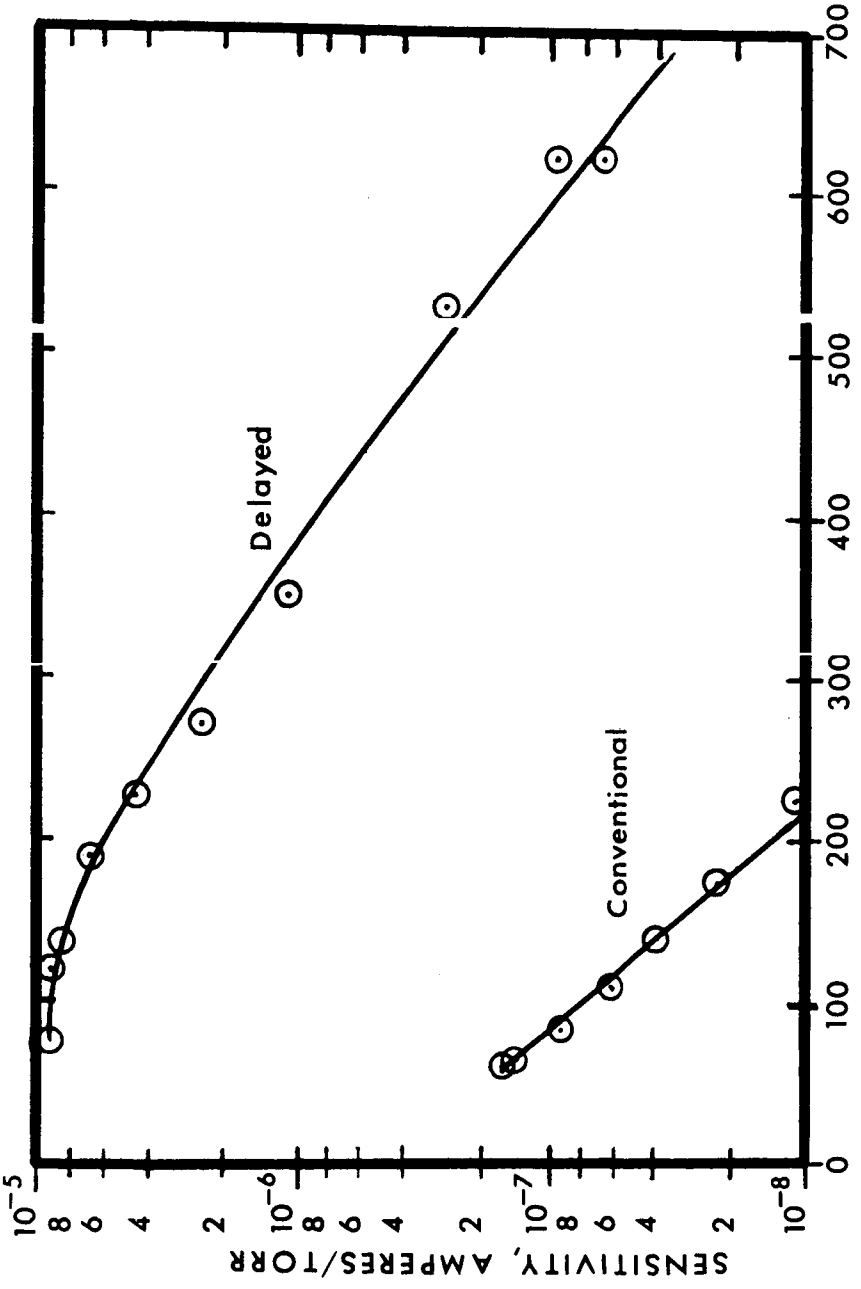

FIGURE 6

SENSITIVITY VS. RESOLVING POWER FOR CONVENTIONAL AND DELAYED MODES WITH 4-VOLT IONS

ACKNOWLEDGEMENTS

It is a great pleasure to acknowledge the support and encouragement given to this activity by Dr. Donald P. Easter (NASA Headquarters) and his associate, Charles E. Giffin (JPL). Walter S. Chamberlin designed the electronic circuitry for the experiments described in Part II of this report. He supervised its assembly and test. Further, he obtained and reduced most of the data presented in this entire report. Fred Pickett designed, fabricated and assembled many of the special components, like the ion sources. Frank Wiens supervised the design, fabrication and assembly of the quadrupole units. Richard C. Gilsdorf made the detailed designs of the hyperbolic field-forming structure, and outlined the method of fabricating the hyperbolic structures. Tom Harris, of Optical Research Associates, did the computer programming and calculations. Alan G. Richards administered the Contract until his retirement. Since that time, Robert F. Cummings has performed this function. Many others at the Bell & Howell Research Center made vital contributions to the successful conclusion of the project. To all we are most grateful.

TABLE I

RADIAL COMPONENT OF VELOCITIES OF IONS AS THEY LEAVE THE QUADRUPOLE

TERMINATION RAMP CONFIGURATIONS				ESCAPE VELOCITY	
Phase $\angle$, °	Fields, % DC	AC	Figures Legend	$100(x/r_o)/\omega t$	$100(y/r_o)/\omega t$
0 to 140	100	100	13, 14, 23	- 5.3	+ 5.1
140 + 4π	0	0	_____ X1, Y1		
0 to 140 + π/2	100	100	13, 14, 23	- 7.8	+ 3.3
140 + 4.5π	0	0	_ _ _ X2, Y2		
0 to 140 + π	100	100	13, 14, 23	- 7.6	+ 3.9
140 + 5π	0	0	- - - X3, Y3		
0 to 140	100	100	15, 16, 24	- 0.17	+ 54
140 + 12π	0	0	_____ X4, Y4		
0 to 140 + π/2	100	100	15, 16, 24	- 4.2	+ 49
140 + 12.5π	0	0	_ _ _ X5, Y5		
0 to 140 + π	100	100	15, 16, 24	- 5.5	+ 50
140 + 13π	0	0	- - - X6, Y6		
0 to 140	100	100	17, 18, 25	+ 2.7	+540
140 + 20π	0	0	_____ X7, Y7		
0 to 140 + π/2	100	100	17, 18, 25	- 1.1	+510
140 + 20.5π	0	0	_ _ _ X8, Y8		
0 to 140 + π	100	100	17, 18, 25	- 4.2	+513
140 + 21π	0	0	- - - X9, Y9		
0 to 140	100	100	19, 20, 26	- 2.9	+ 0.22
140 + 10π	0	100	_____ X10, Y10		
140 + 20π	0	0			
0 to 140 + π/2	100	100	19, 20, 26	- 3.5	- 0.18
140 + 10.5π	0	100	_ _ _ X11, Y11		
140 + 20.5π	0	0			

TABLE I

(Continued)

TERMINATION RAMP CONFIGURATIONS				ESCAPE VELOCITY	
Phase $\angle$, °	Fields, % DC	AC	Figures Legend	$100(x/r_o)/\omega t$	$100(y/r_o)/\omega t$
0 to 140 + π	100	100	19, 20, 26	- 2.9	- 0.17
140 + 11π	0	100	- - - X12, Y12		
140 + 21π	0	0			
0 to 140	100	100	21, 22, 27	- 2.2	2.64
140 + 4π	0	100	____ X13, Y13		
140 + 20π	0	0			
0 to 140 + π/2	100	100	21, 22, 27	+ 0.66	- 3.14
140 + 4.5π	0	100	_ _ _ X14, Y14		
140 + 20.5π	0	0			
0 to 140 + π	100	100	21, 22, 27	+ 3.8	- 2.9
140 + 5π	0	100	- - - X15, Y15		
140 + 21π	0	0			
Approximate maximum velocity of ions in quadrupole				24	12

TABLE II

E_y PERTURBATIONS AT VARIOUS x AND y POSITIONS

y/x	0.1	0.2	0.3	0.4	0.5	0.6	0.7
0.0	-.00000029	-.00000468	-.00002434	-.00008244	- 00022995	-.00058669	-.00143147
0.1	.00000116	.00000556	.0000024.2	-.00002304	-. 00009821	-.00029027	-.00077210
0.2	-.00001176	.00001809	.00005551	.00009946	.00017511	.00034362	.00069667
0.3	-.00009274	-.00001246	.00008132	.00017382	.00032312	.00071885	.00174580
0.4	-.00035969	-.00015287	.00005997	.00017093	.00018380	.00032633	.00116691
0.5	-.00111688	-.00055384	.00003325	.00028714	-. 00001105	-.00076404	-.00141202
0.6	-.00319634	-.00168890	.0000081.2	.00100335	. 00057639	-.00153666	-.00497809
0.7	-.00873912	-.00494287	-.0003801.1	.00298774	. 00346805	.00013517	-.00697810
0.8	-.02284181	-.01385659	-.00260809	.00680168	.01085148	.00753379	-.00342518
0.9	-.05696569	-.03664422	-.01068985	.01239948	.02561574	.02524696	.01102738
1.0	-.13611959	-.09131313	-.03383776	.01846086	.05176245	.05979041	.04338418

TABLE II

(Continued)

y/x	0.8	0.9	1.0
0.0	-.00338361	-.00775858	-.0172697[illegible]1
0.1	-.00195841	-.00476961	-.0111383[illegible]1
0.2	.00132995	.00229549	.00354503
0.3	.00407009	.00879848	.01782870
0.4	.00376013	.00988997	.02255127
0.5	-.00080254	.00298152	.01293319
0.6	-.00872107	-.01108692	-.00977048
0.7	-.01698273	-.02842574	-.0396821[illegible]
0.8	-.02095677	-.04335915	-.0690725[illegible]
0.9	-.01494124	-.04968874	-.09067999
1.0	.00761013	-.04144051	-.0988371[illegible]

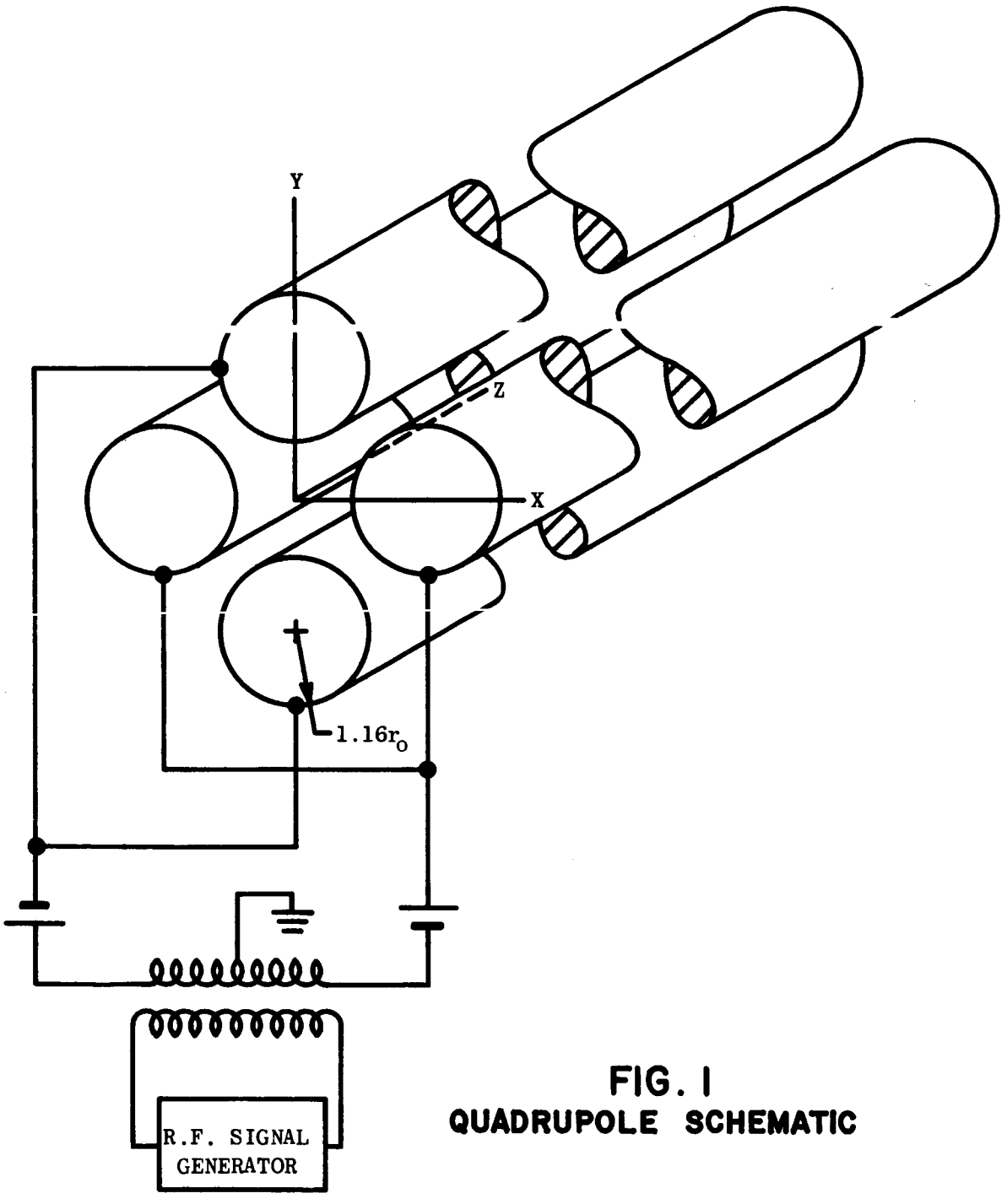

FIG. 1
QUADRUPOLE SCHEMATIC

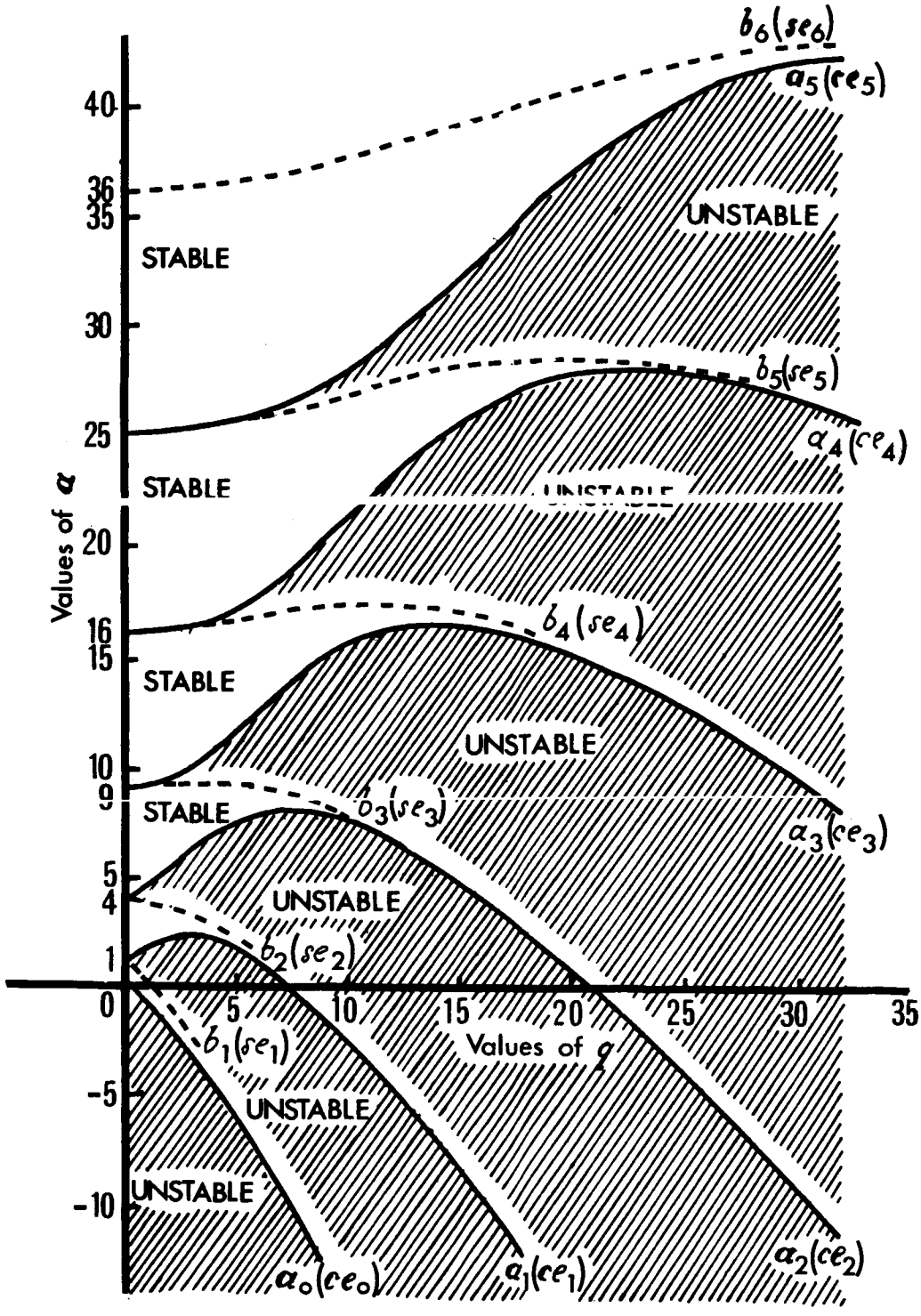

Stability chart for Mathieu functions of integral order. The characteristic curves a_0, b_1, b_2,...divide the plane into regions of stability and instability. The even-order curves are symmetrical, but the odd-order curves are asymmetrical about the a-axis. Nevertheless the diagram is symmetrical about the a-axis.

Fig. 2 - STABILITY CHART

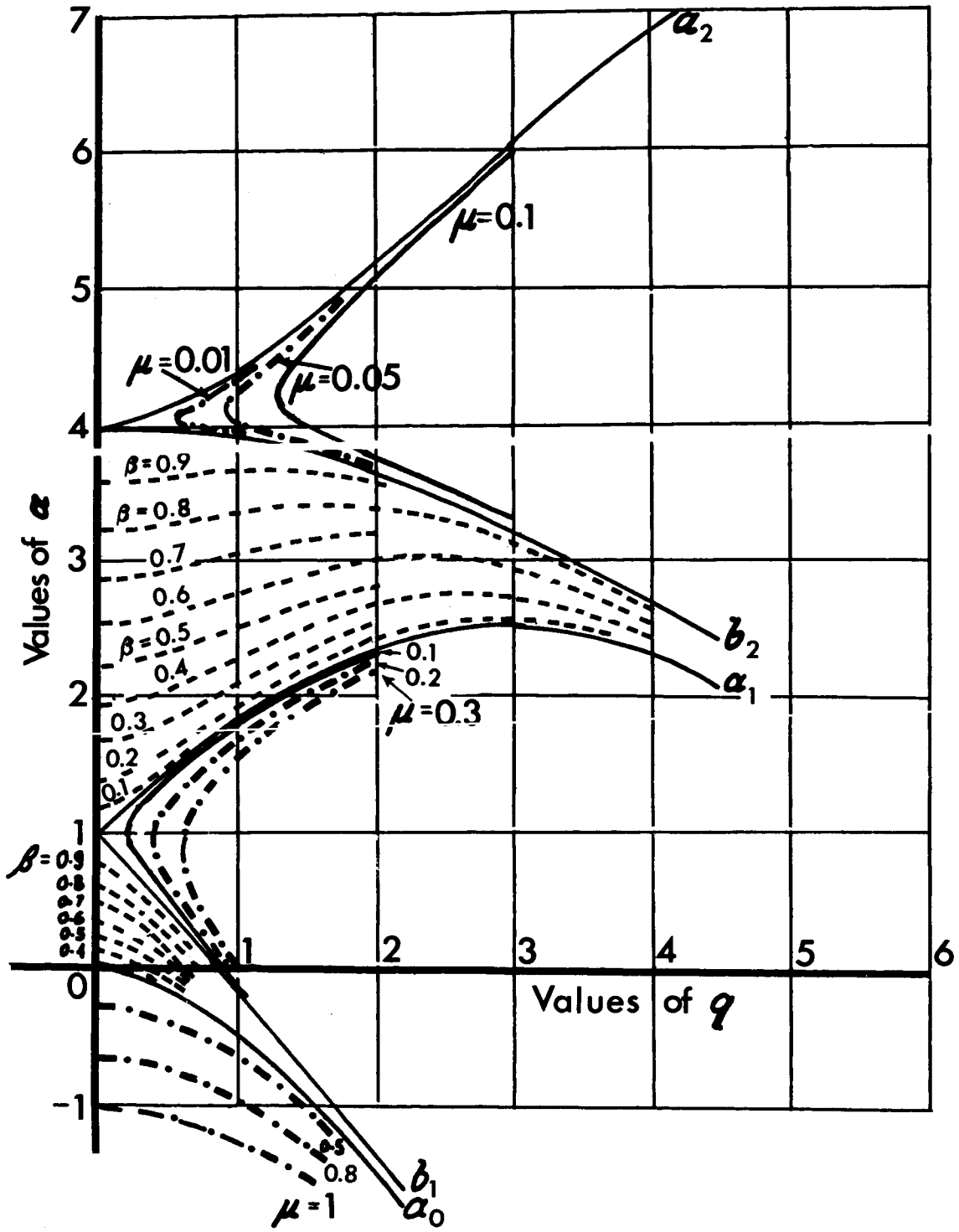

Iso-$\beta\mu$ stability chart for Mathieu functions of fractional order. The iso-β and iso-μ curves are symmetrical about the a-axis.

Fig. 3 - STABILITY CHART

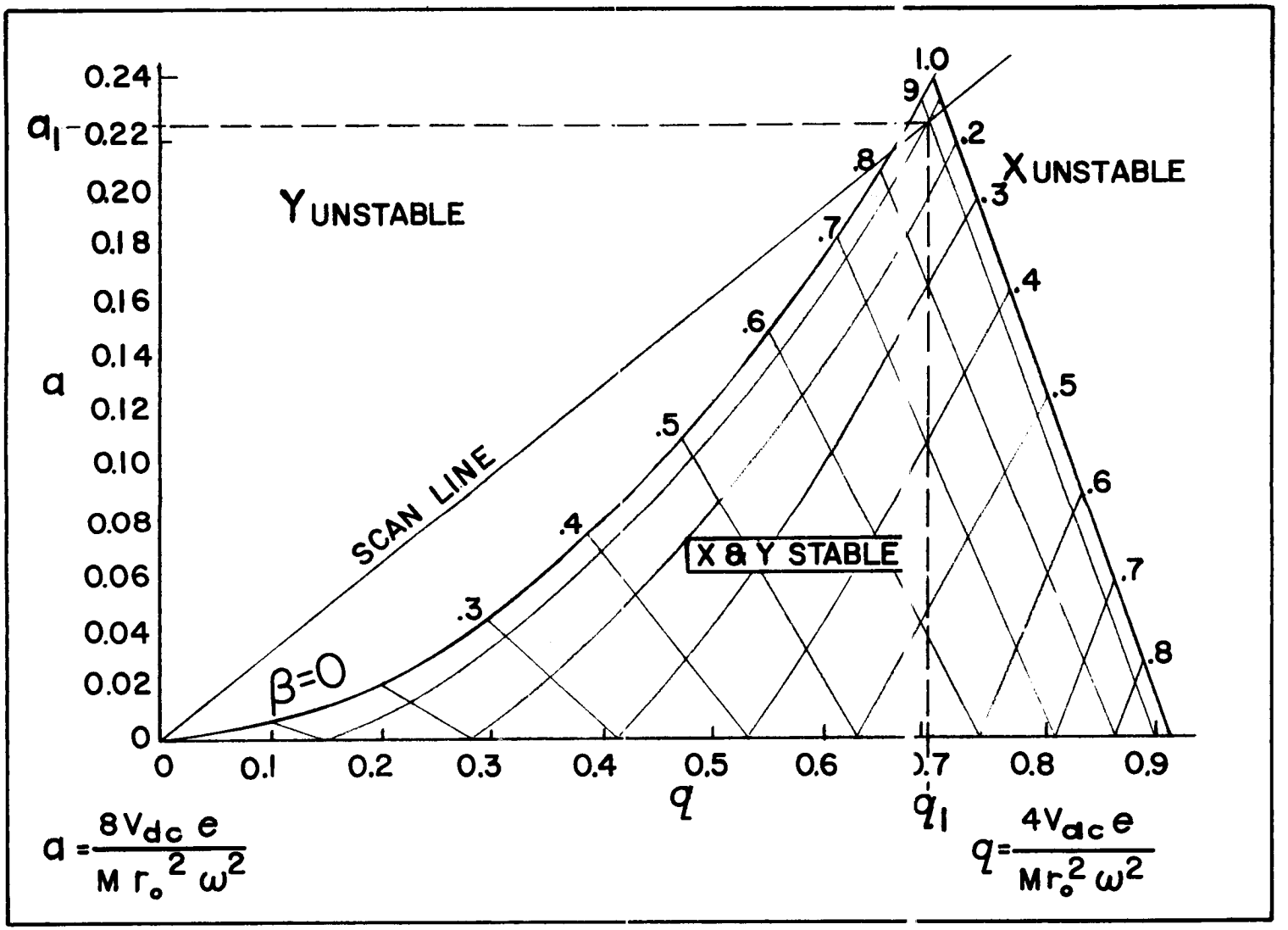

STABILITY DIAGRAM FOR BOTH X & Y

FIGURE 4

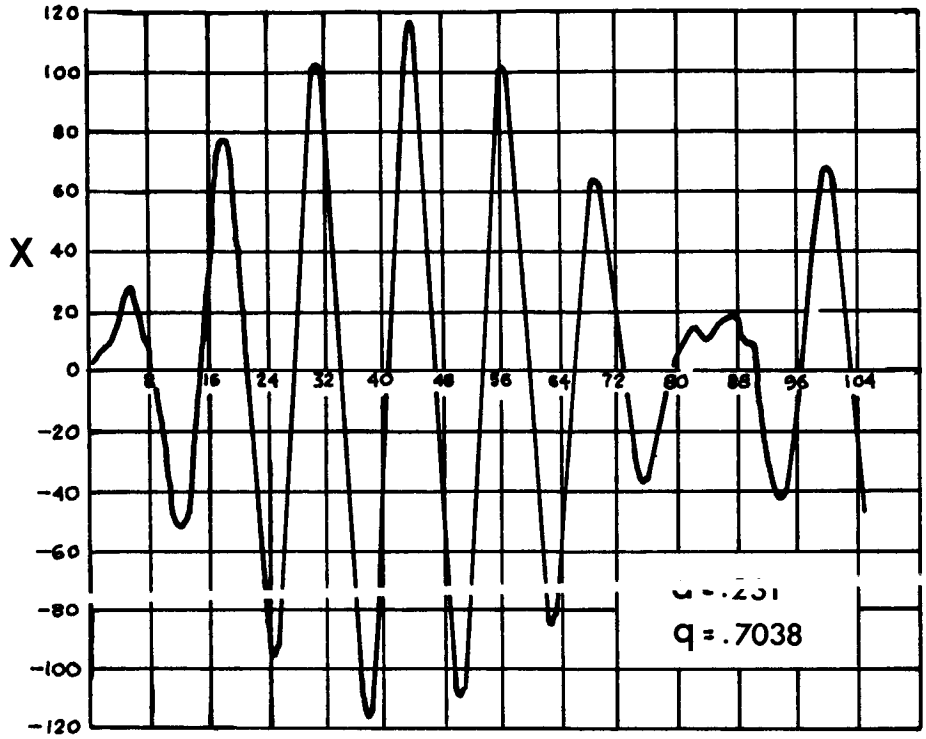

ION TRAJECTORY IN THE X–Z PLANE
FIG. 5

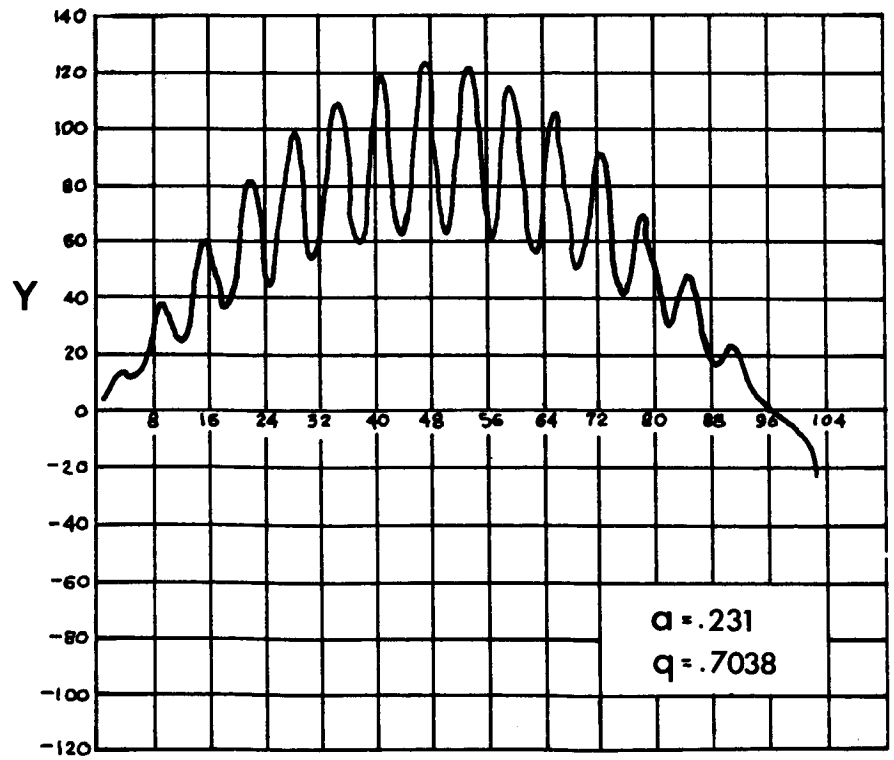

ION TRAJECTORY IN THE Y-Z PLANE
FIG. 6

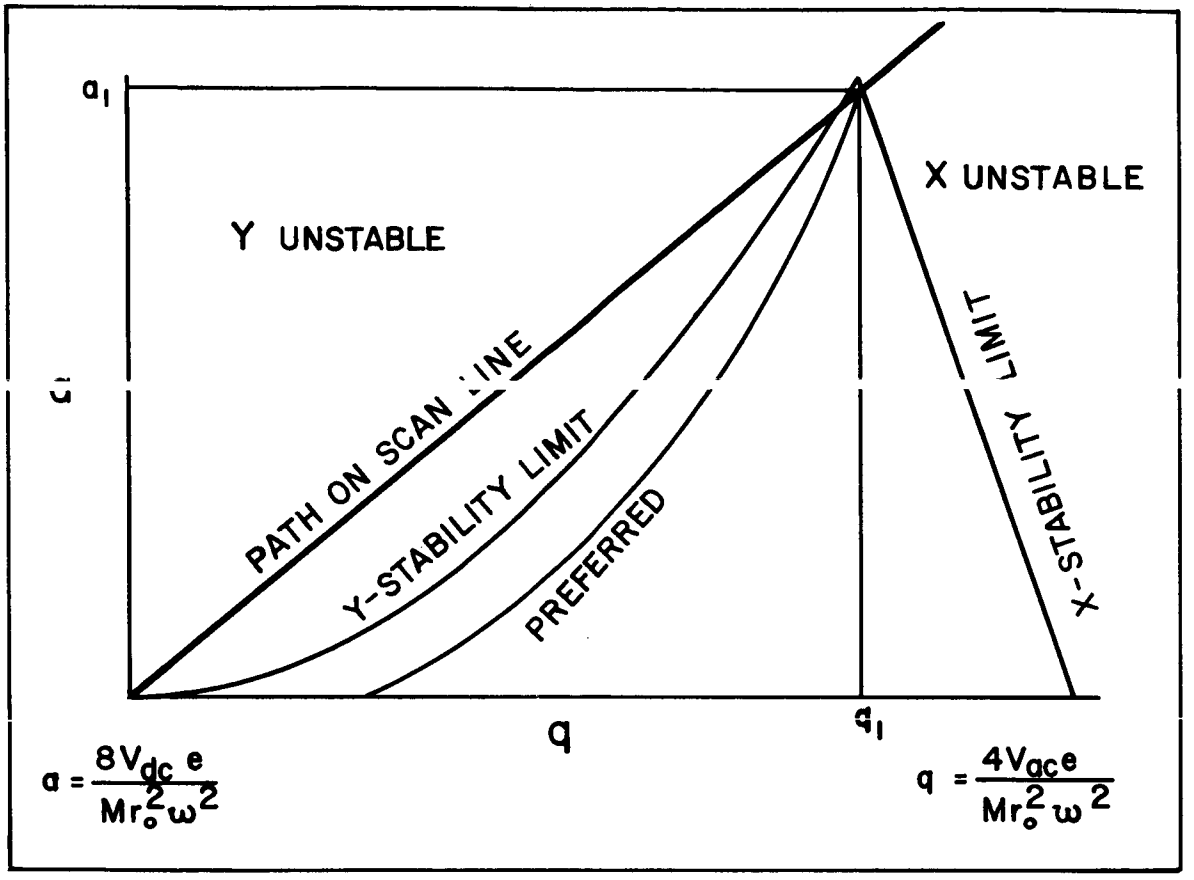

STABILITY DIAGRAM, SHOWING TWO PATHS OF WORKING POINT DURING TRAVERSAL OF FRINGING FIELD.

FIGURE 7

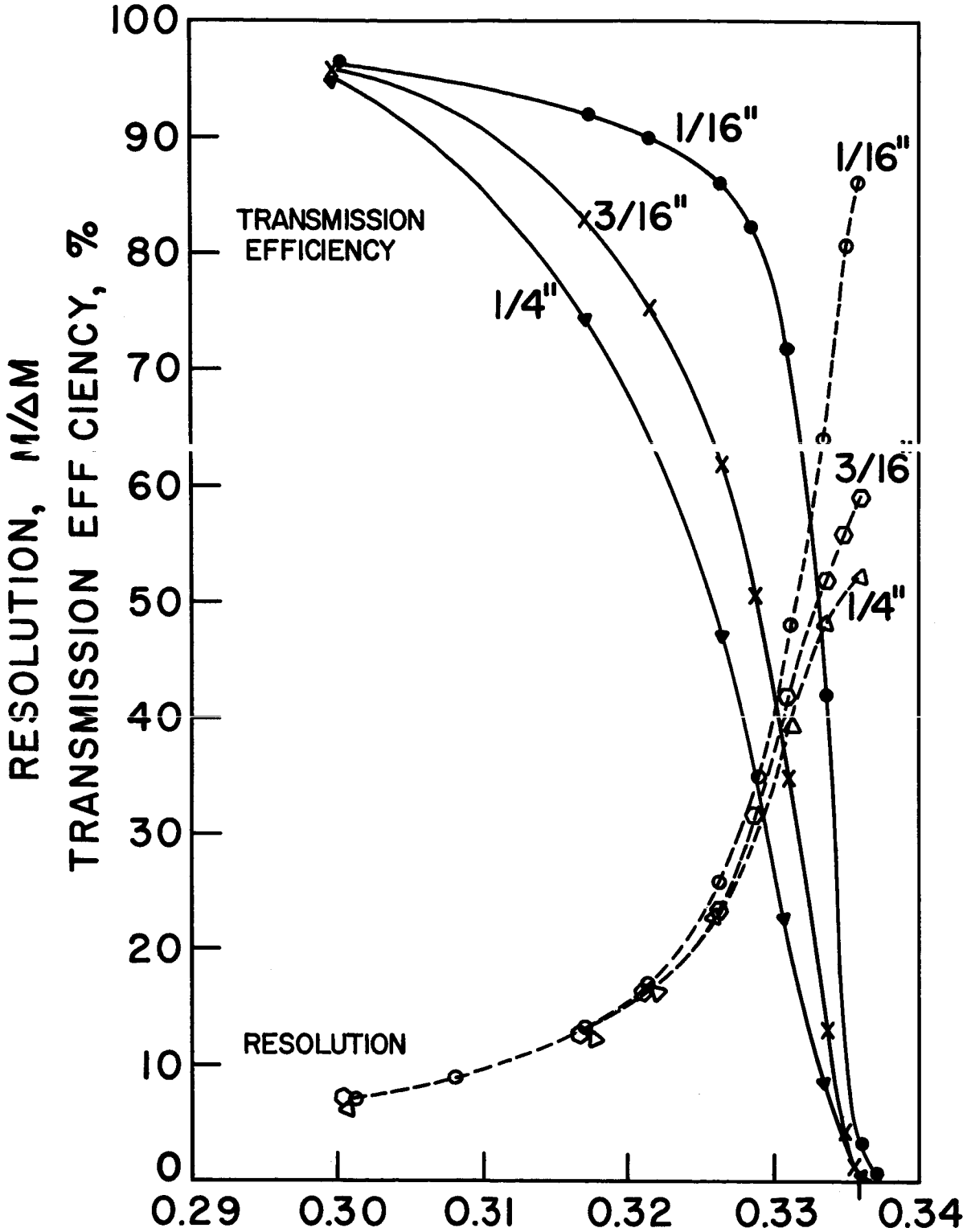
100
90
80
70
60
50
40
30
20
10
0
0.29
0.30
0.31
0.32
0.33
0.34
RESOLUTION, M/ΔM
TRANSMISSION EFFICIENCY, %
TRANSMISSION EFFICIENCY
RESOLUTION
1/16"
3/16"
1/4"
1/16"
3/16"
1/4"
TRANSMISSION EFFICIENCY AND
RESOLUTION AS A FUNCTION OF $\frac{a}{q}$

FIGURE 8

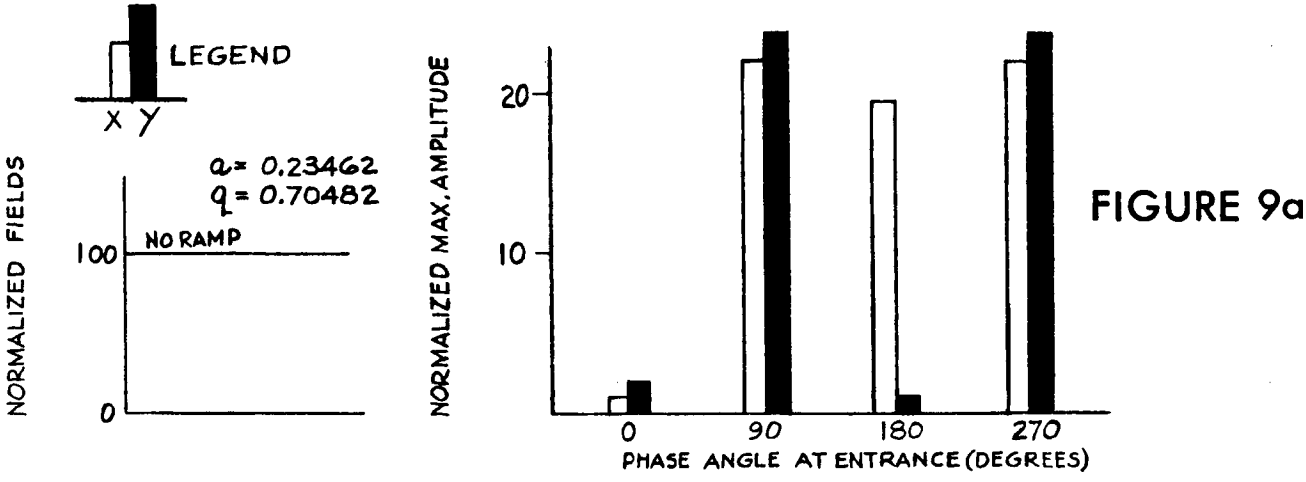

FIGURE 9a

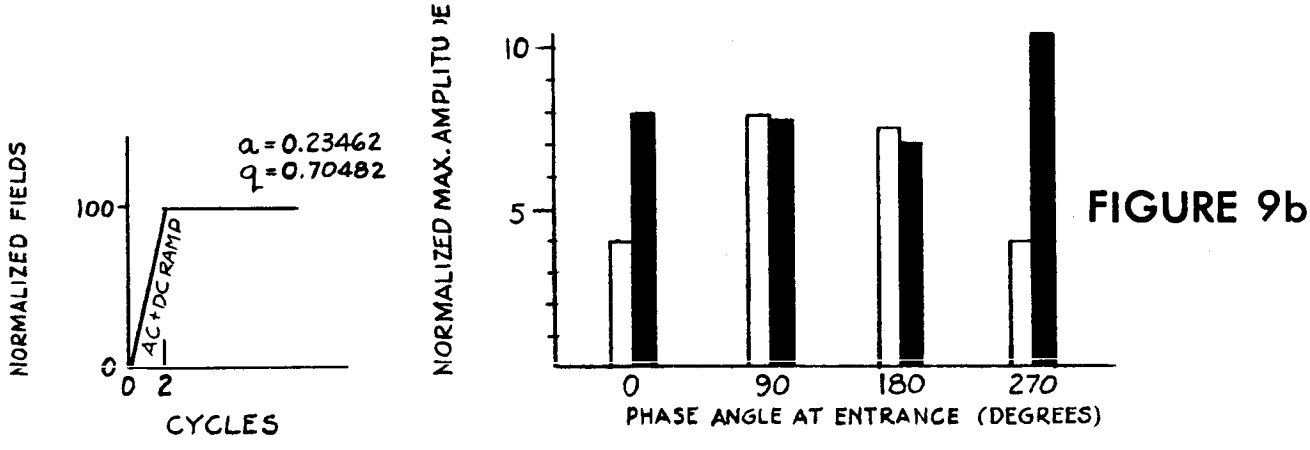

FIGURE 9b

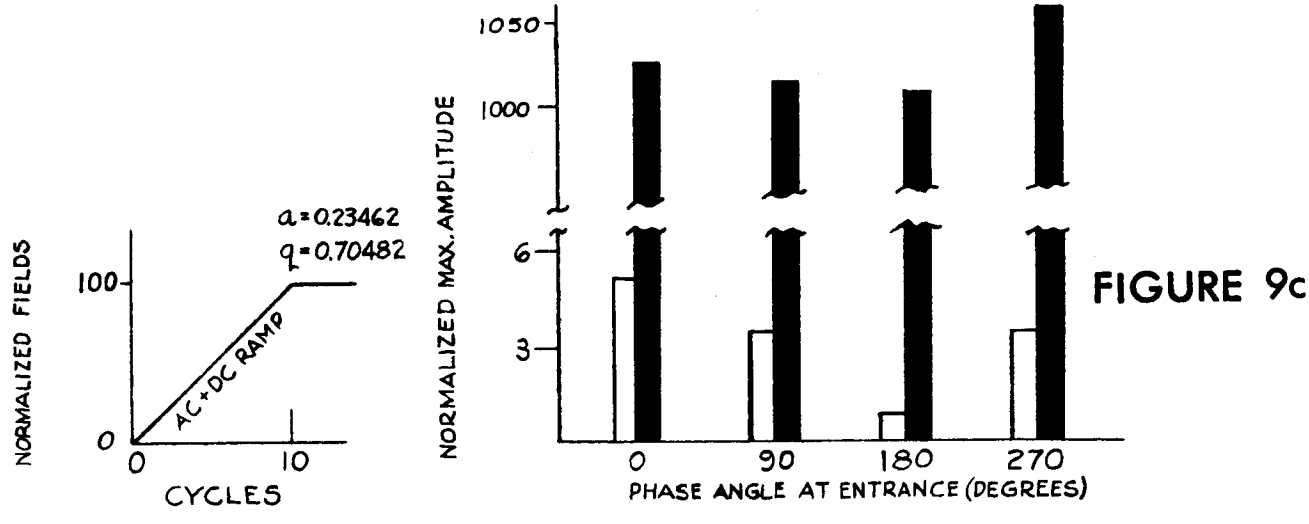

FIGURE 9c

FIGURE 9

SUMMARY OF TRAJECTORY PLOTS WITH COINCIDENT RAMPS

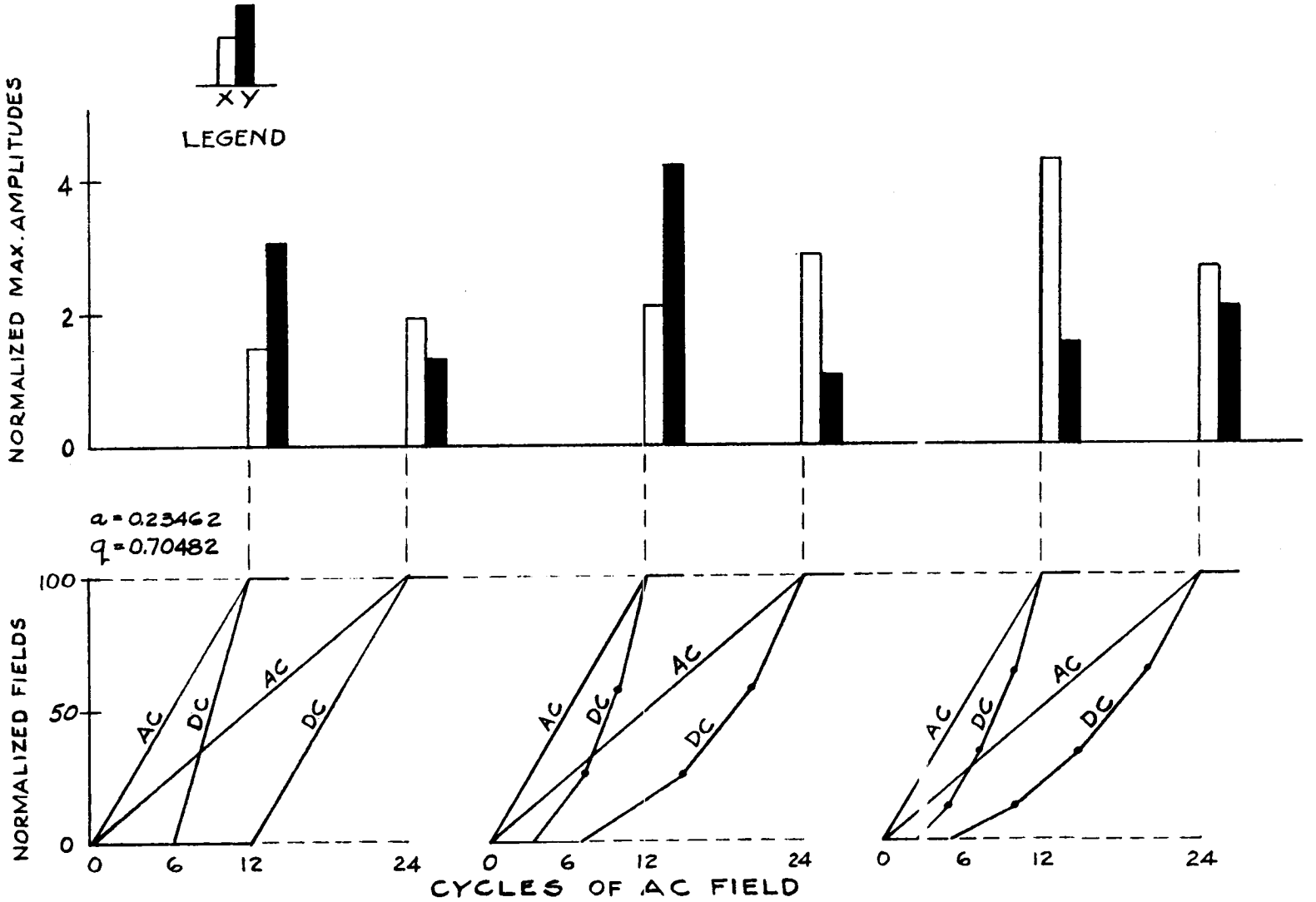

FIGURE 10

SUMMARY OF TRAJECTORY PLOTS WITH DELAYED D.C. RAMPS

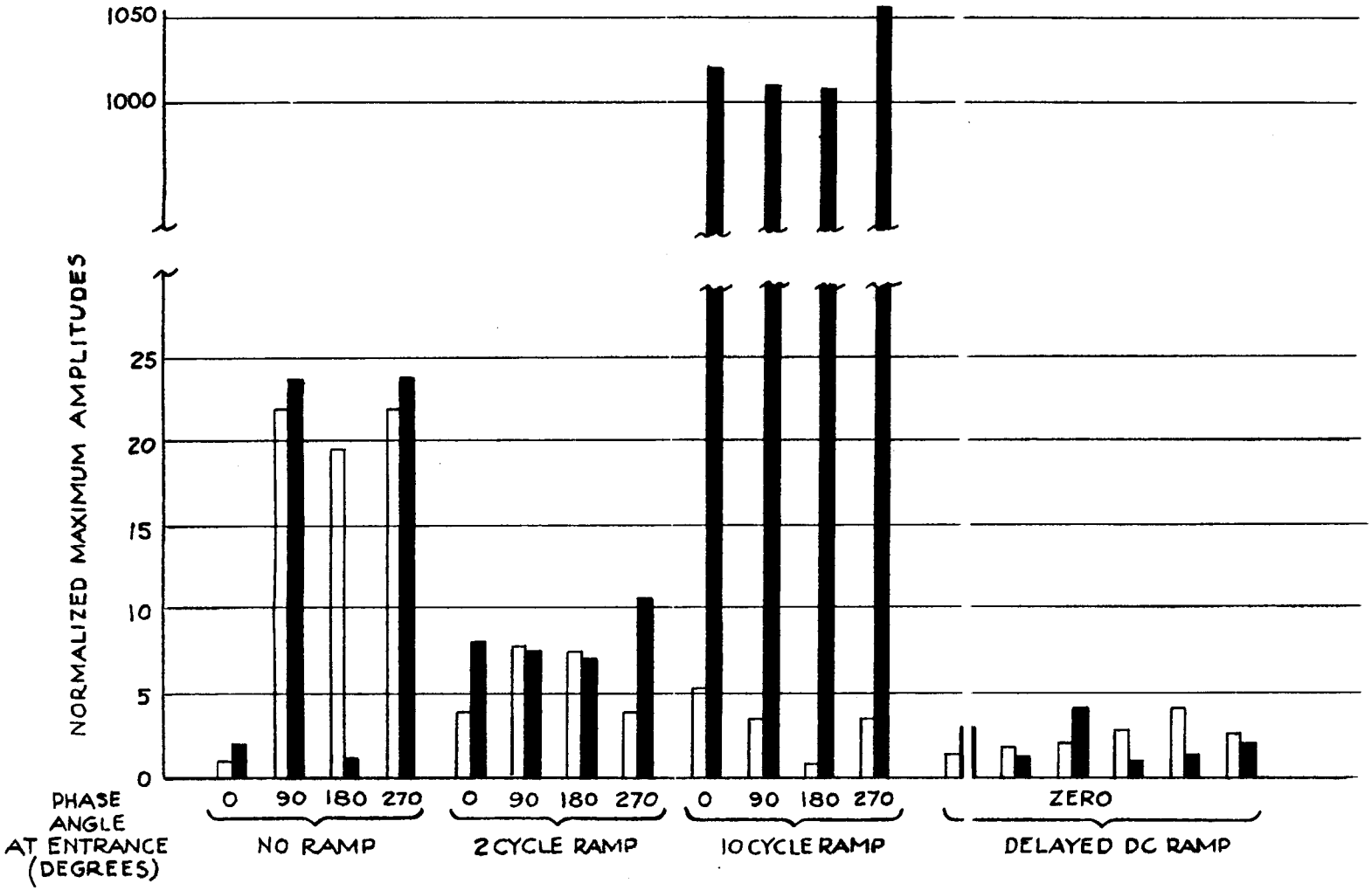

FIGURE 11

SUMMARY OF ALL TRAJECTORY PLOTS

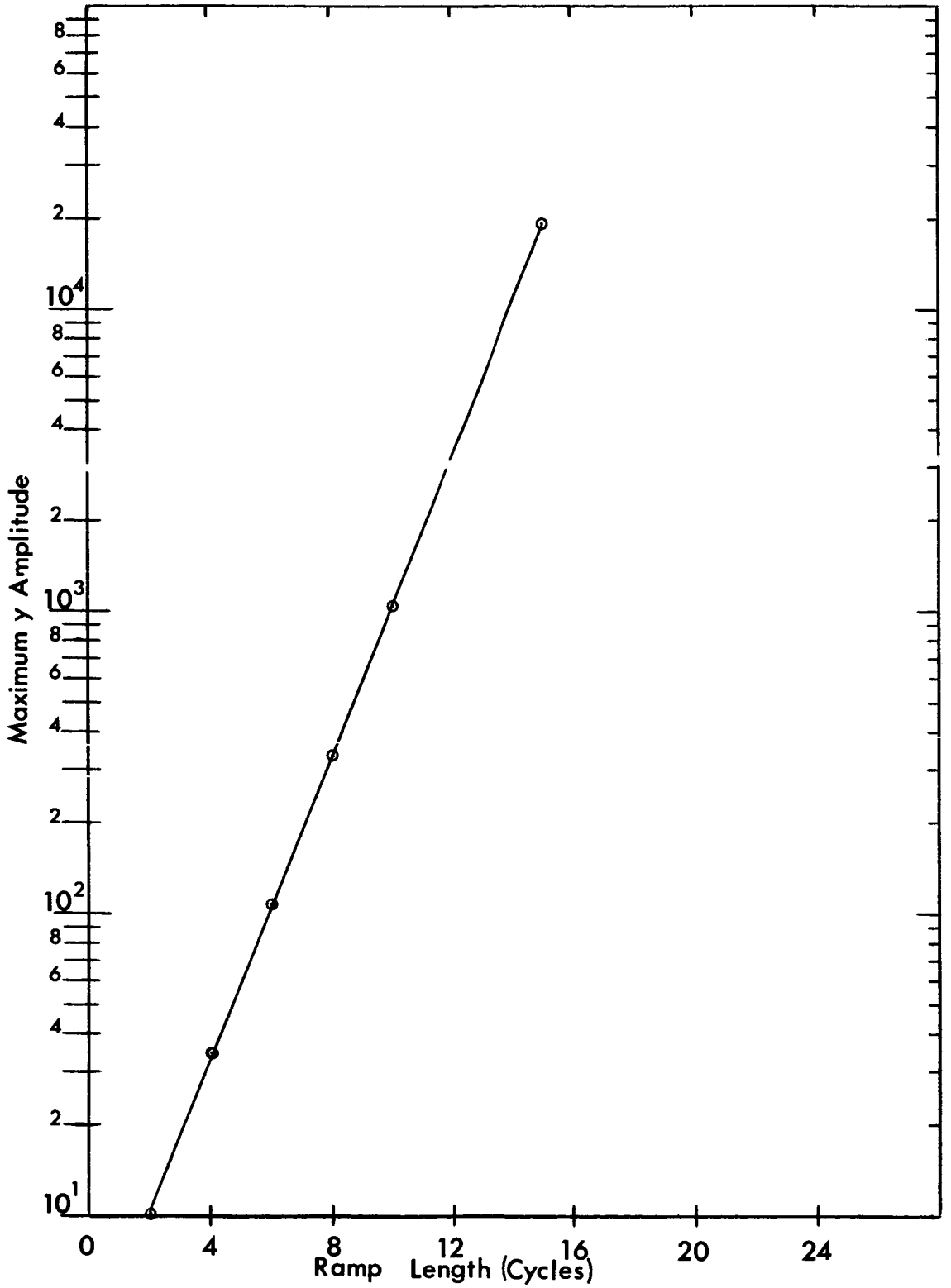

FIGURE 12

MAXIMUM AMPLITUDE OF y-TRAJECTORY AS A FUNCTION OF RAMP LENGTH

$a = 0.23462$; $q = 0.70482$; $m/dm \approx 100$

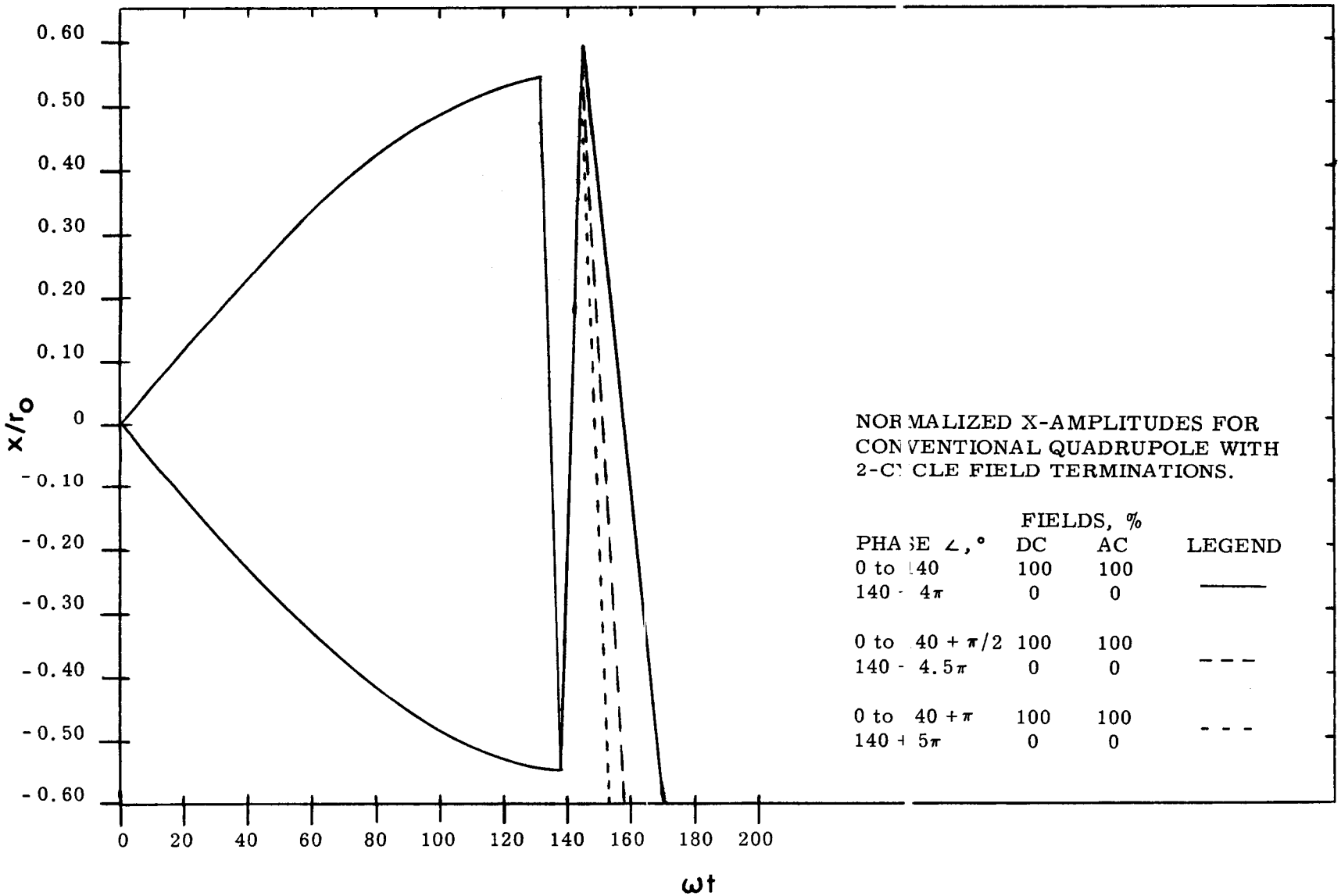
0.60
0.50
0.40
0.30
0.20
0.10
0
-0.10
-0.20
-0.30
-0.40
-0.50
-0.60
x/r_o
0
20
40
60
80
100
120
140
160
180
200
ωt
NORMALIZED X-AMPLITUDES FOR CONVENTIONAL QUADRUPOLE WITH 2-CYCLE FIELD TERMINATIONS.
FIELDS, %
PHASE ∠, °
DC
AC
LEGEND
0 to 140
100
100
140 - 4π
0
0
0 to 140 + π/2
100
100
140 - 4.5π
0
0
0 to 140 + π
100
100
140 + 5π
0
0

FIGURE 13

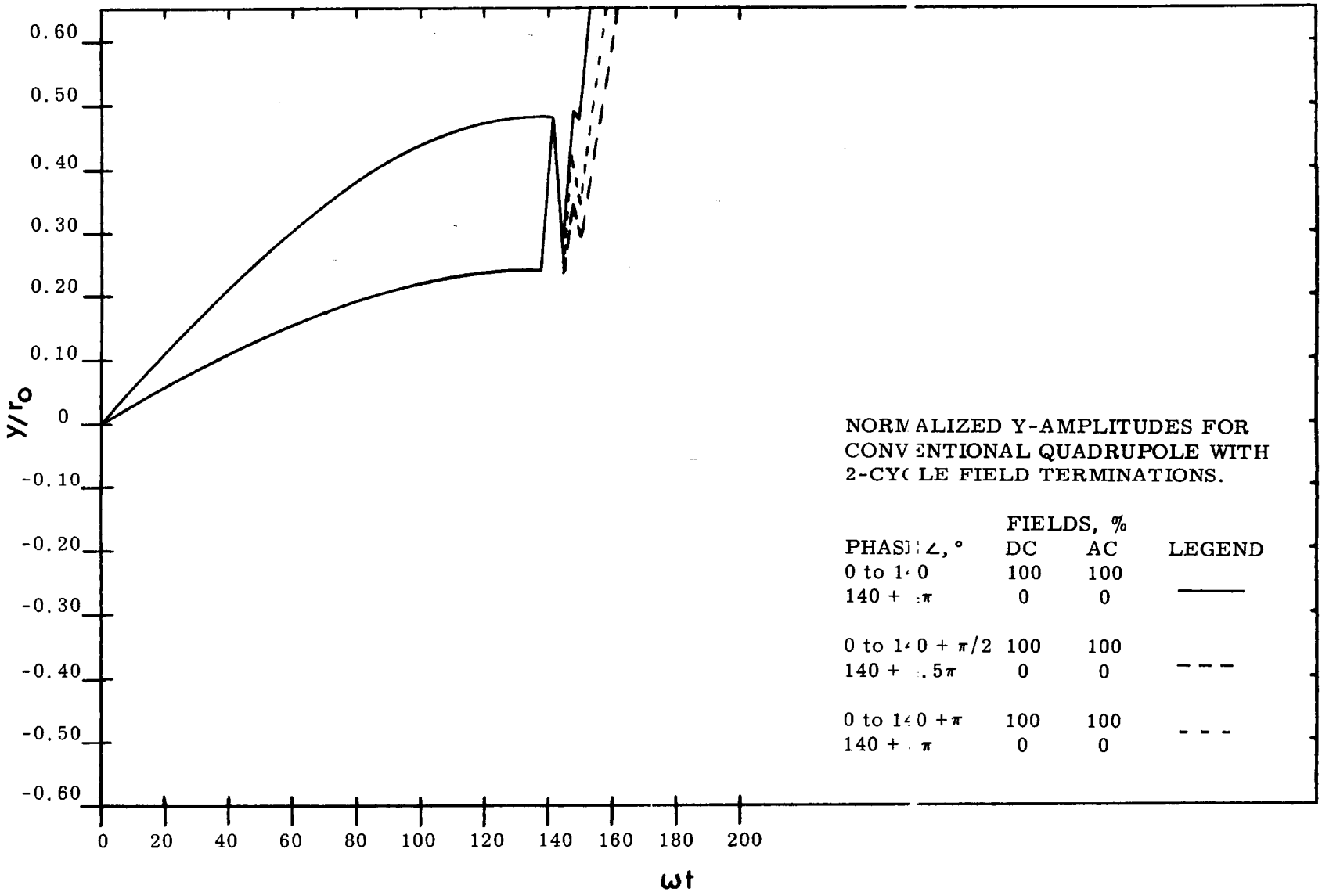
0.60
0.50
0.40
0.30
0.20
0.10
0
-0.10
-0.20
-0.30
-0.40
-0.50
-0.60
y/r_o
0
20
40
60
80
100
120
140
160
180
200
ωt
NORMALIZED Y-AMPLITUDES FOR CONVENTIONAL QUADRUPOLE WITH 2-CYCLE FIELD TERMINATIONS.
PHASE ∠, °
FIELDS, %
DC
AC
LEGEND
0 to 140
100
100
140 + π
0
0
0 to 140 + π/2
100
100
140 + 1.5π
0
0
0 to 140 + π
100
100
140 + 2π
0
0

FIGURE 14

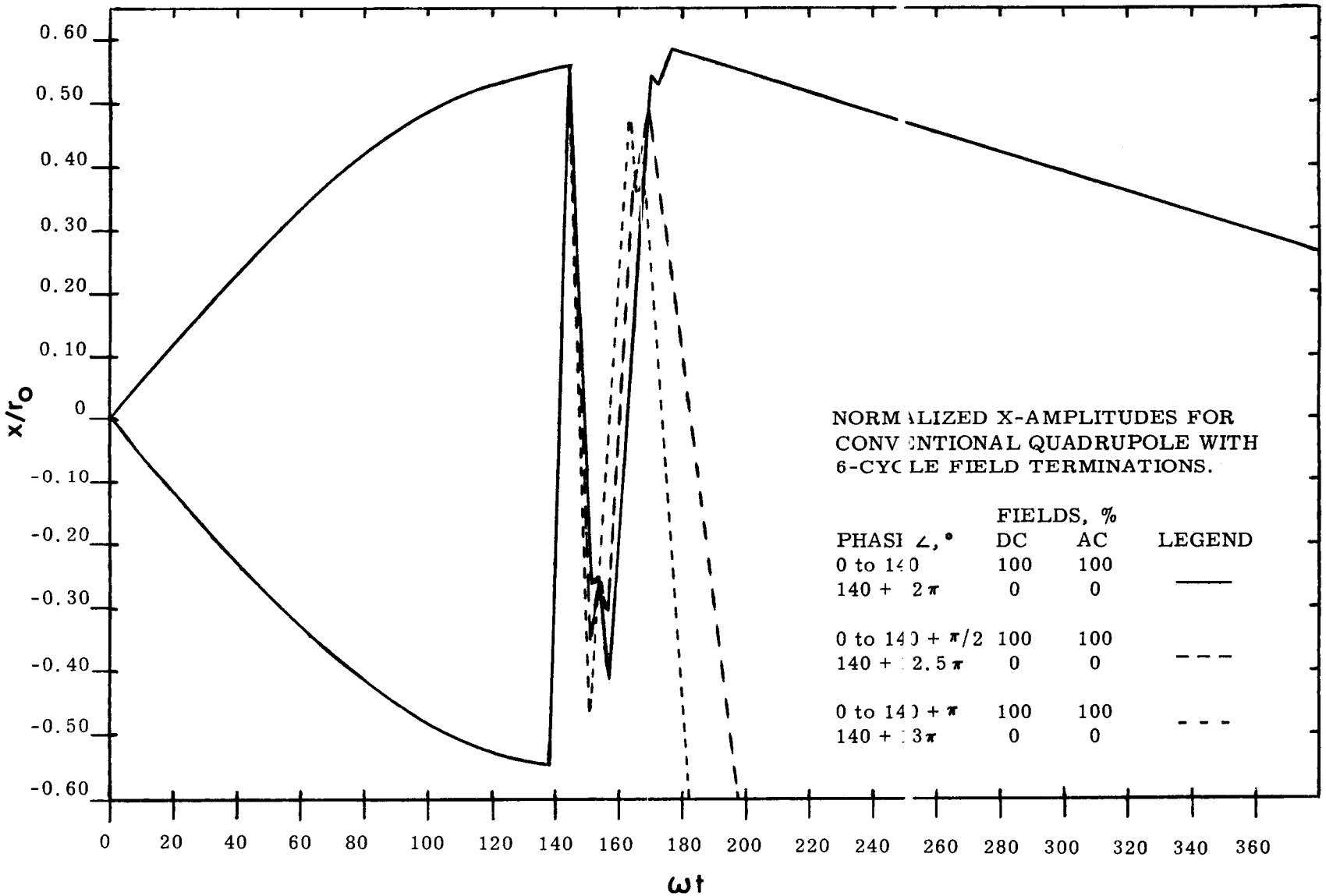
0.60
0.50
0.40
0.30
0.20
0.10
0
-0.10
-0.20
-0.30
-0.40
-0.50
-0.60
x/r_o
0
20
40
60
80
100
120
140
160
180
200
220
240
260
280
300
320
340
360
ωt
NORMALIZED X-AMPLITUDES FOR CONVENTIONAL QUADRUPOLE WITH 6-CYCLE FIELD TERMINATIONS.
PHASE ∠, °
FIELDS, % DC
FIELDS, % AC
LEGEND
0 to 140
100
100
140 + 2π
0
0
0 to 140 + π/2
100
100
140 + 2.5π
0
0
0 to 140 + π
100
100
140 + 3π
0
0

FIGURE 15

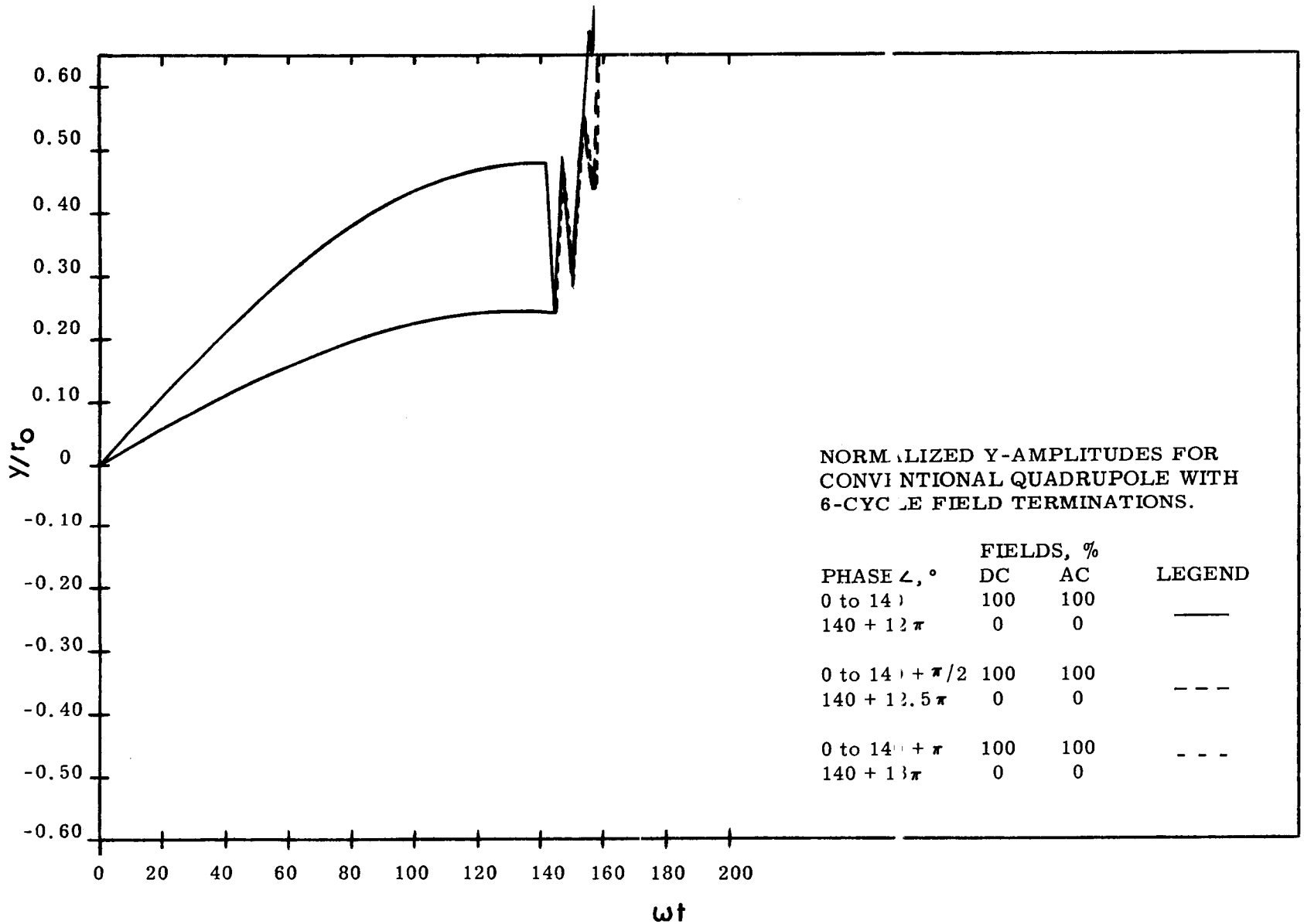
0.60
0.50
0.40
0.30
0.20
0.10
0
-0.10
-0.20
-0.30
-0.40
-0.50
-0.60
y/r_o
0
20
40
60
80
100
120
140
160
180
200
ωt
NORMALIZED Y-AMPLITUDES FOR CONVENTIONAL QUADRUPOLE WITH 6-CYCLE FIELD TERMINATIONS.
PHASE ∠, °
FIELDS, %
DC
AC
LEGEND
0 to 140
100
100
140 + 12π
0
0
0 to 140 + π/2
100
100
140 + 12.5π
0
0
0 to 140 + π
100
100
140 + 13π
0
0

FIGURE 16

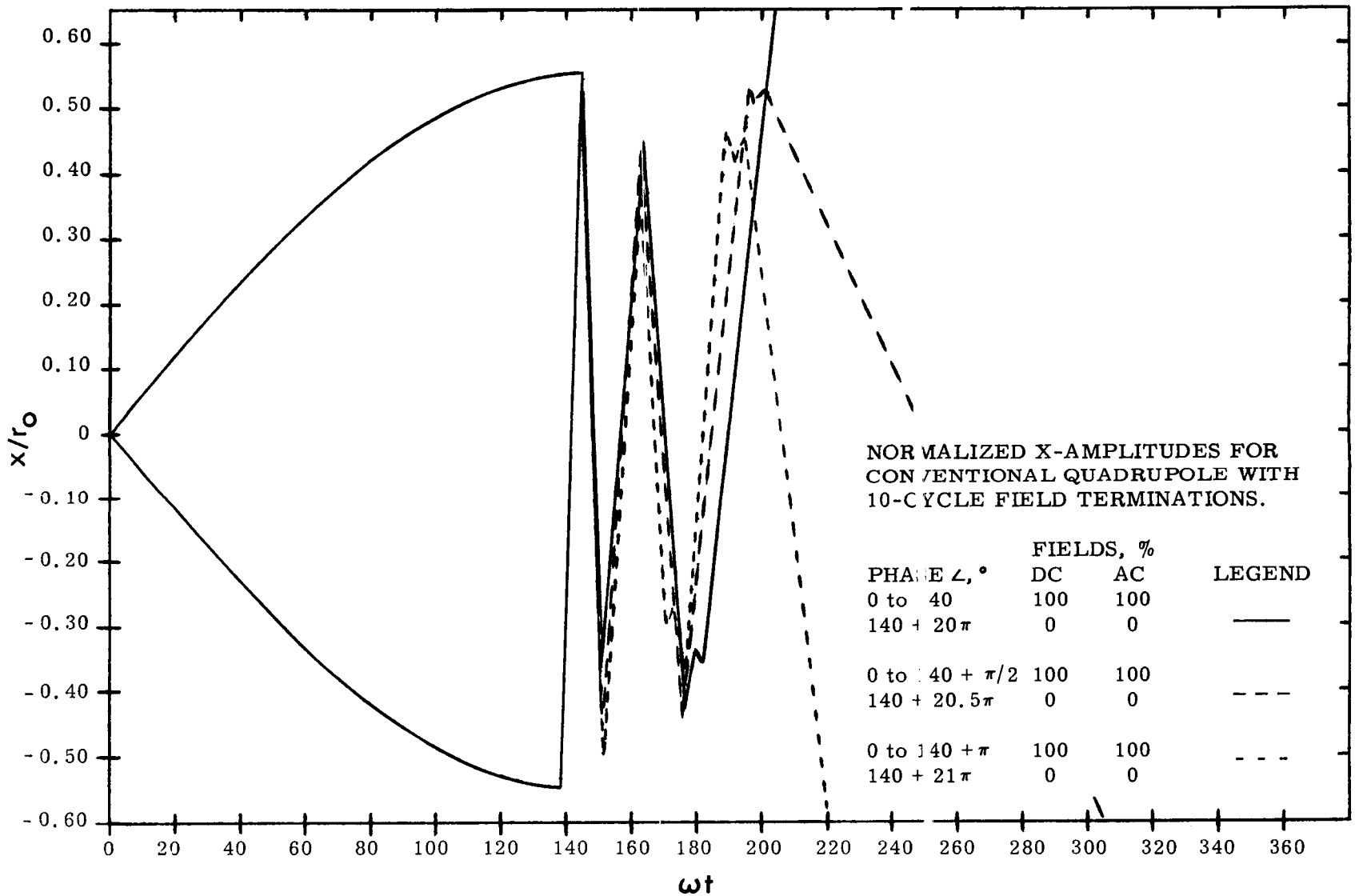
0.60
0.50
0.40
0.30
0.20
0.10
0
- 0.10
- 0.20
- 0.30
- 0.40
- 0.50
- 0.60
x/r_o
0
20
40
60
80
100
120
140
160
180
200
220
240
260
280
300
320
340
360
ωt
NORMALIZED X-AMPLITUDES FOR CONVENTIONAL QUADRUPOLE WITH 10-CYCLE FIELD TERMINATIONS.
FIELDS, %
PHASE ∠, °
DC
AC
LEGEND
0 to 40
100
100
140 + 20π
0
0
0 to 140 + π/2
100
100
140 + 20.5π
0
0
0 to 140 + π
100
100
140 + 21π
0
0

FIGURE 17

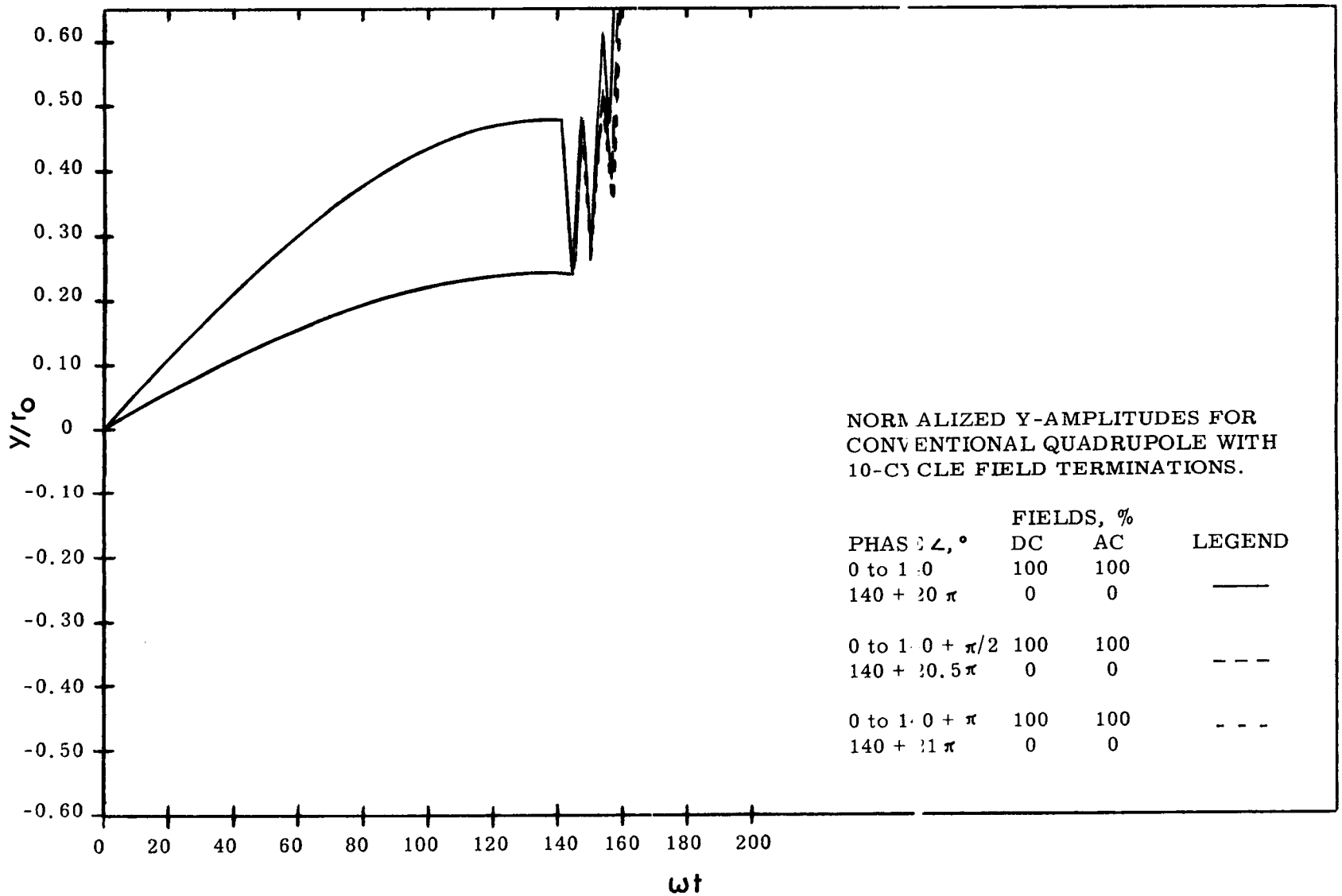
0.60
0.50
0.40
0.30
0.20
0.10
0
-0.10
-0.20
-0.30
-0.40
-0.50
-0.60
y/r₀
0
20
40
60
80
100
120
140
160
180
200
ωt
NORMALIZED Y-AMPLITUDES FOR CONVENTIONAL QUADRUPOLE WITH 10-CYCLE FIELD TERMINATIONS.
PHASE ∠, °
FIELDS, %
DC
AC
LEGEND
0 to 140
100
100
140 + 20 π
0
0
0 to 140 + π/2
100
100
140 + 20.5 π
0
0
0 to 140 + π
100
100
140 + 21 π
0
0

FIGURE 18

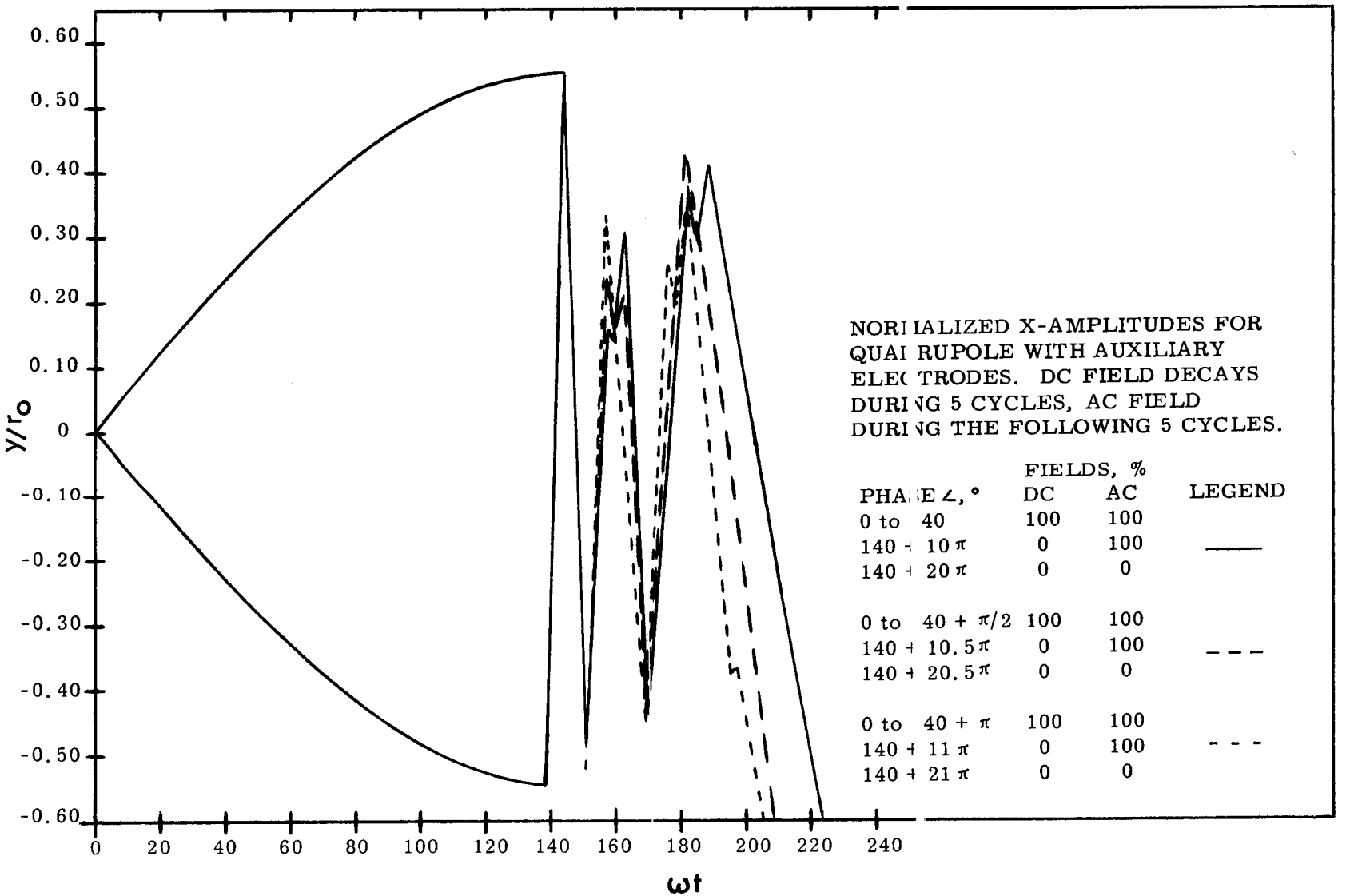
0.60
0.50
0.40
0.30
0.20
0.10
0
-0.10
-0.20
-0.30
-0.40
-0.50
-0.60
y/r_o
0
20
40
60
80
100
120
140
160
180
200
220
240
ωt
NORMALIZED X-AMPLITUDES FOR QUADRUPOLE WITH AUXILIARY ELECTRODES. DC FIELD DECAYS DURING 5 CYCLES, AC FIELD DURING THE FOLLOWING 5 CYCLES.
PHASE ∠, °
FIELDS, %
DC
AC
LEGEND
0 to 40
100
100
140 + 10 π
0
100
140 + 20 π
0
0
0 to 40 + π/2
100
100
140 + 10.5 π
0
100
140 + 20.5 π
0
0
0 to 40 + π
100
100
140 + 11 π
0
100
140 + 21 π
0
0

FIGURE 19

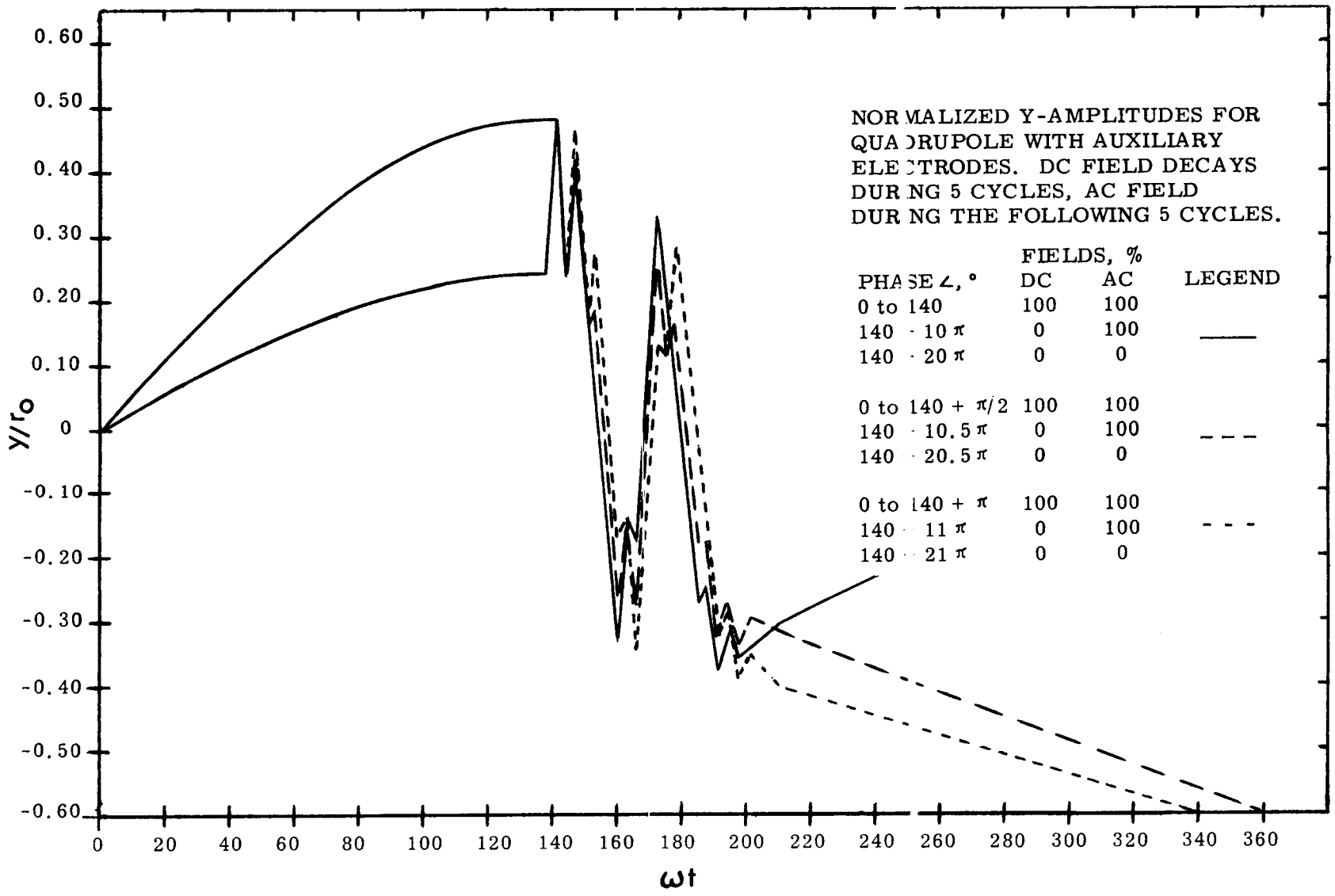
NORMALIZED Y-AMPLITUDES FOR QUADRUPOLE WITH AUXILIARY ELECTRODES. DC FIELD DECAYS DURING 5 CYCLES, AC FIELD DURING THE FOLLOWING 5 CYCLES.
PHASE ∠, °
FIELDS, %
DC
AC
LEGEND
0 to 140
100
100
140 - 10 π
0
100
140 - 20 π
0
0
0 to 140 + π/2
100
100
140 - 10.5 π
0
100
140 - 20.5 π
0
0
0 to 140 + π
100
100
140 - 11 π
0
100
140 - 21 π
0
0
y/r0
0.60
0.50
0.40
0.30
0.20
0.10
0
-0.10
-0.20
-0.30
-0.40
-0.50
-0.60
0
20
40
60
80
100
120
140
160
180
200
220
240
260
280
300
320
340
360
ωt

FIGURE 20

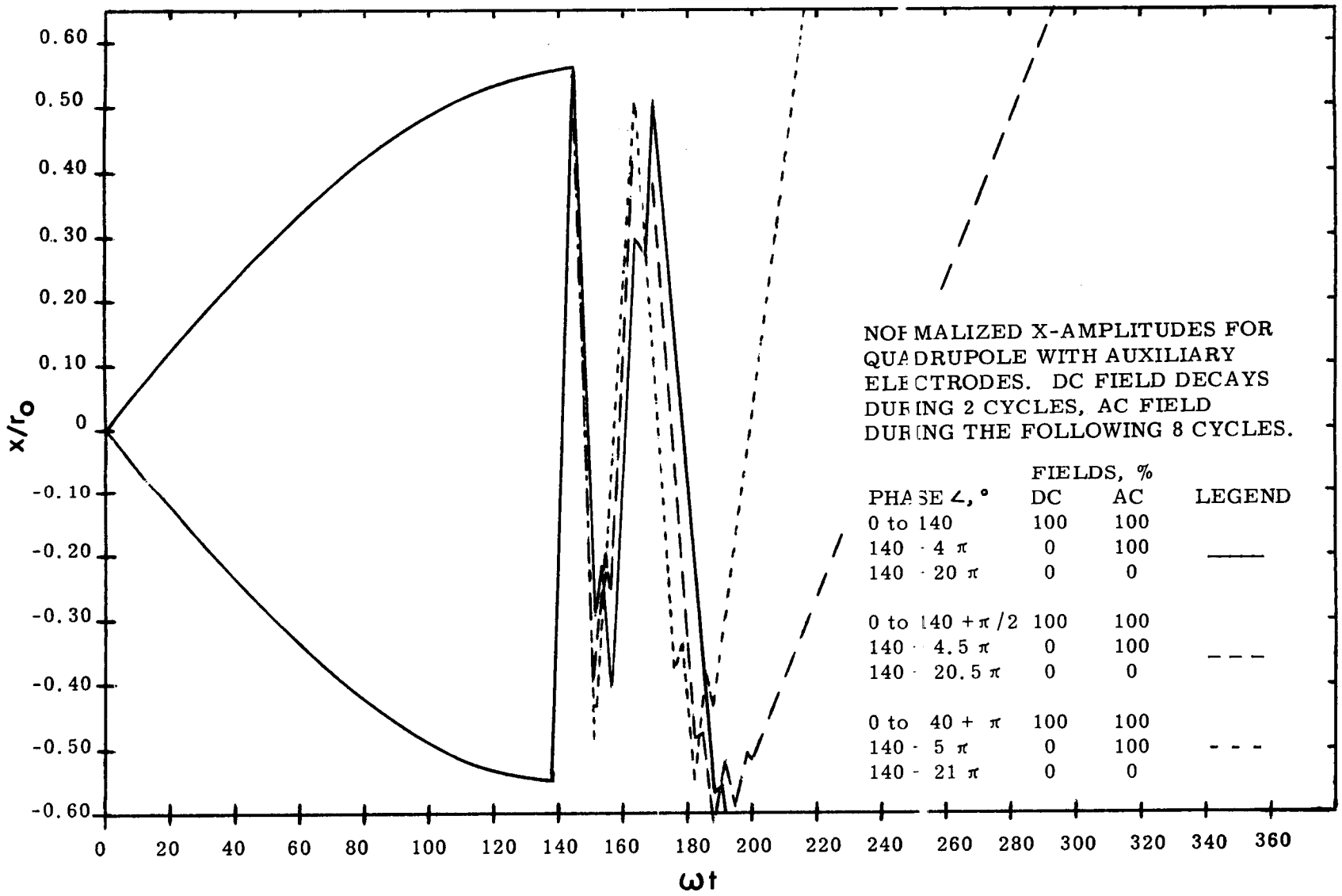
0.60
0.50
0.40
0.30
0.20
0.10
0
-0.10
-0.20
-0.30
-0.40
-0.50
-0.60
x/r_o
0
20
40
60
80
100
120
140
160
180
200
220
240
260
280
300
320
340
360
ωt
NORMALIZED X-AMPLITUDES FOR QUADRUPOLE WITH AUXILIARY ELECTRODES. DC FIELD DECAYS DURING 2 CYCLES, AC FIELD DURING THE FOLLOWING 8 CYCLES.
FIELDS, %
PHASE ∠, °
DC
AC
LEGEND
0 to 140
100
100
140 - 4 π
0
100
140 - 20 π
0
0
0 to 140 + π/2
100
100
140 - 4.5 π
0
100
140 - 20.5 π
0
0
0 to 40 + π
100
100
140 - 5 π
0
100
140 - 21 π
0
0

FIGURE 21

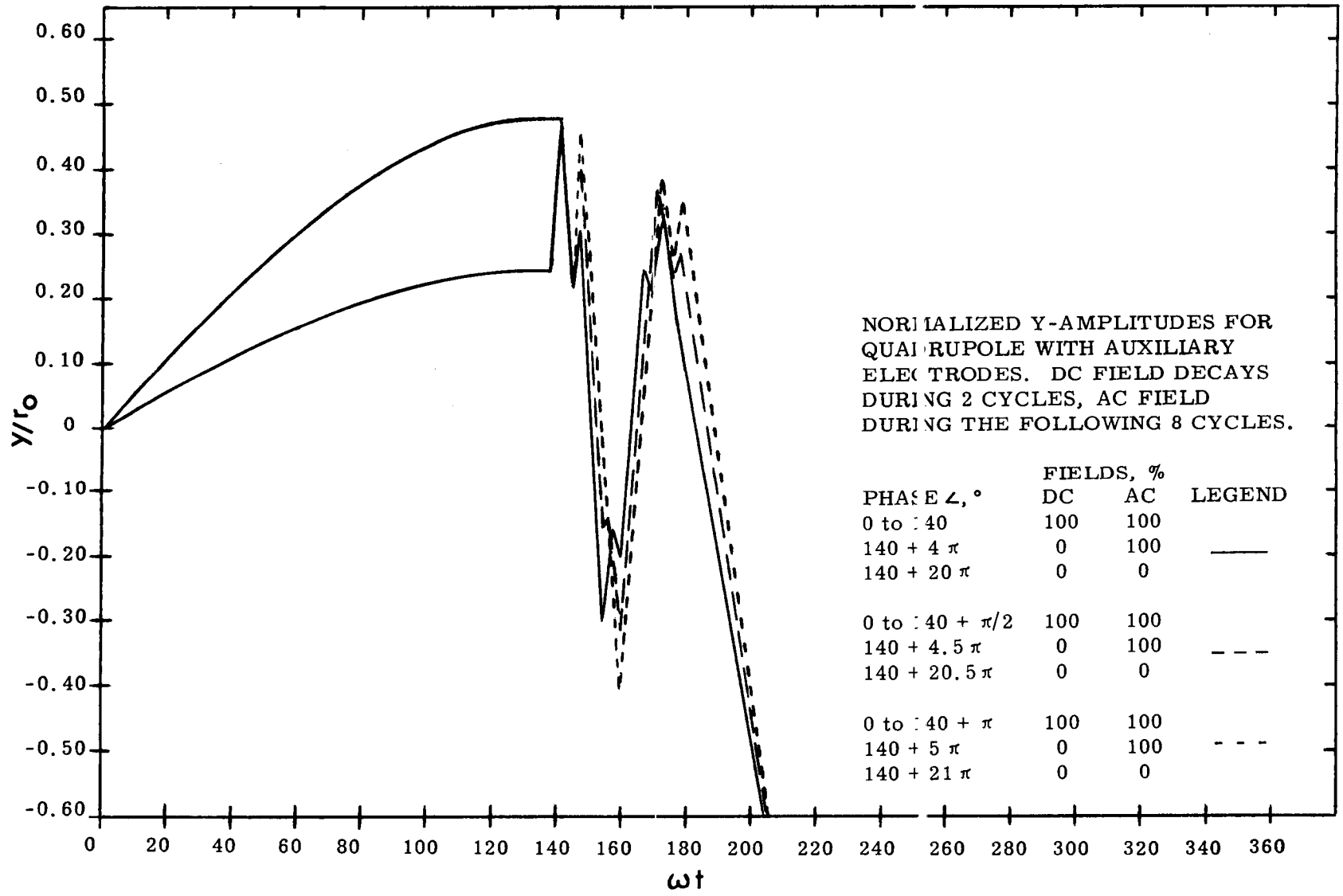
0.60
0.50
0.40
0.30
0.20
0.10
0
-0.10
-0.20
-0.30
-0.40
-0.50
-0.60
y/r_o
0
20
40
60
80
100
120
140
160
180
200
220
240
260
280
300
320
340
360
ωt
NORMALIZED Y-AMPLITUDES FOR QUADRUPOLE WITH AUXILIARY ELECTRODES. DC FIELD DECAYS DURING 2 CYCLES, AC FIELD DURING THE FOLLOWING 8 CYCLES.
PHASE ∠, °
FIELDS, %
DC
AC
LEGEND
0 to 140
100
100
140 + 4 π
0
100
140 + 20 π
0
0
0 to 140 + π/2
100
100
140 + 4.5 π
0
100
140 + 20.5 π
0
0
0 to 140 + π
100
100
140 + 5 π
0
100
140 + 21 π
0
0

FIGURE 22

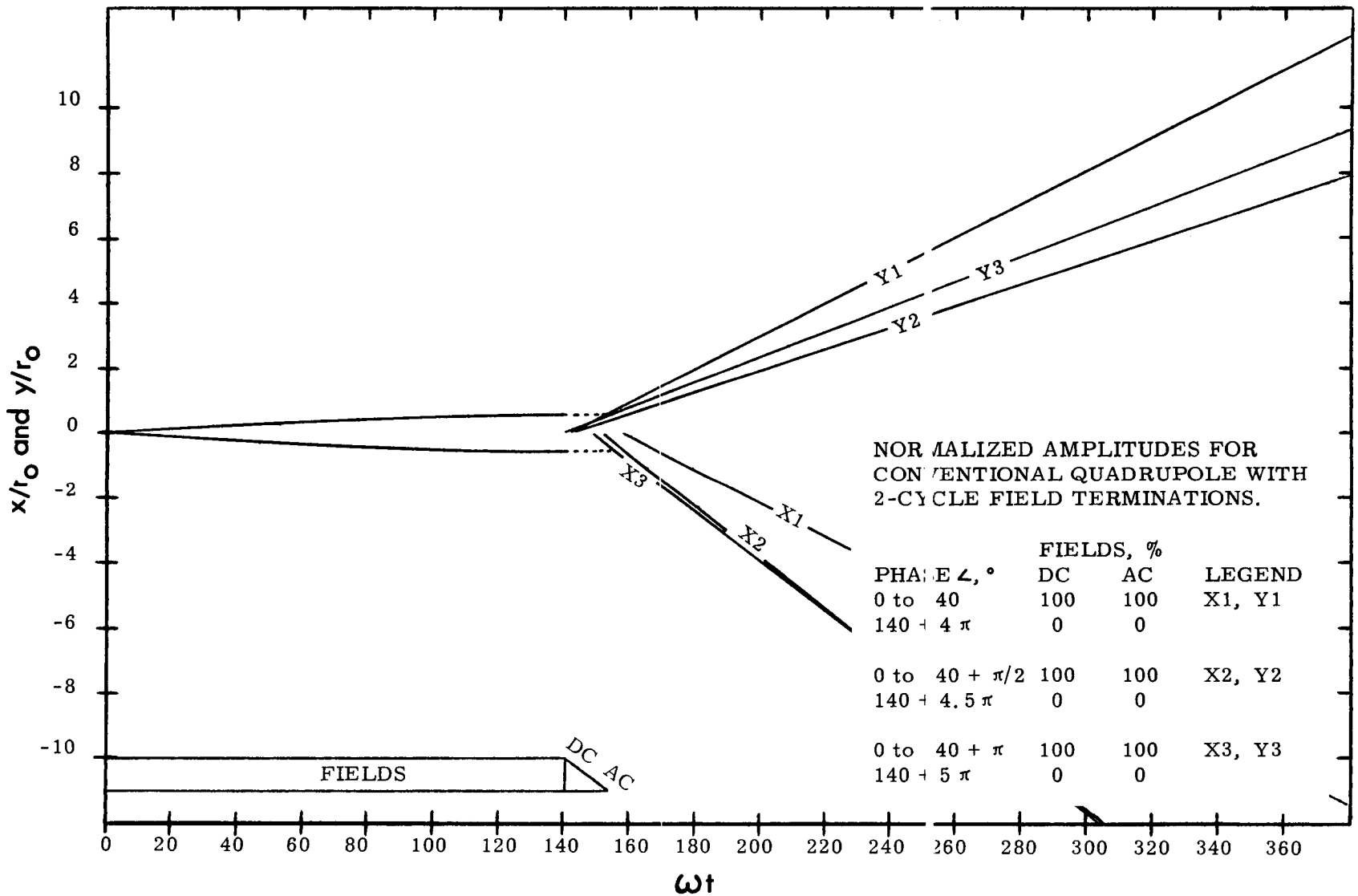
10
8
6
4
2
0
-2
-4
-6
-8
-10
x/r_o and y/r_o
Y1
Y3
Y2
X3
X1
X2
NORMALIZED AMPLITUDES FOR
CONVENTIONAL QUADRUPOLE WITH
2-CYCLE FIELD TERMINATIONS.
FIELDS, %
PHASE ∠, °
DC
AC
LEGEND
0 to 40
100
100
X1, Y1
140 + 4 π
0
0
0 to 40 + π/2
100
100
X2, Y2
140 + 4.5 π
0
0
0 to 40 + π
100
100
X3, Y3
140 + 5 π
0
0
FIELDS
DC
AC
0
20
40
60
80
100
120
140
160
180
200
220
240
260
280
300
320
340
360
ωt

FIGURE 23

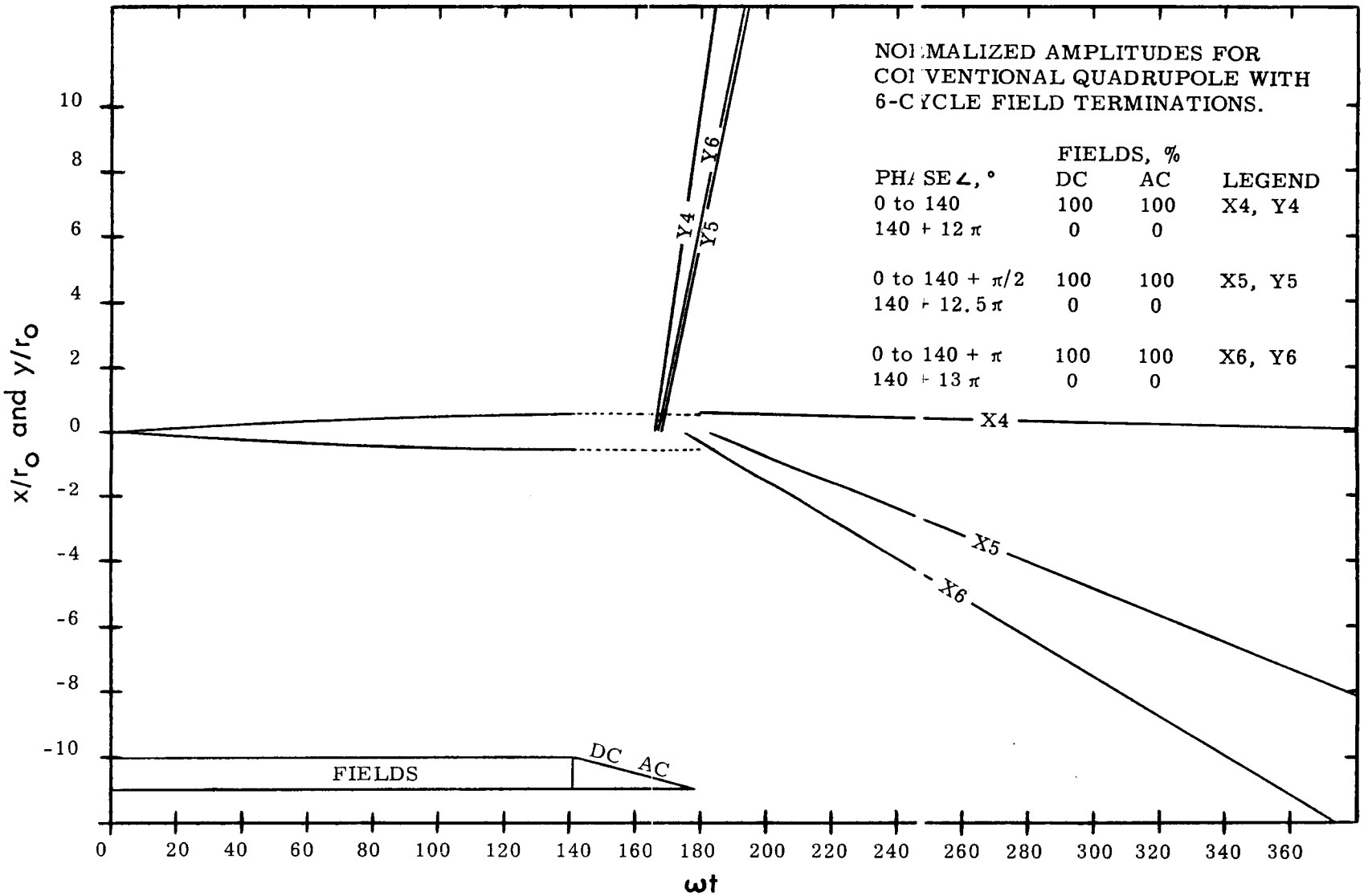
NORMALIZED AMPLITUDES FOR
CONVENTIONAL QUADRUPOLE WITH
6-CYCLE FIELD TERMINATIONS.
FIELDS, %
PHASE ∠, °
DC
AC
LEGEND
0 to 140
100
100
X4, Y4
140 + 12 π
0
0
0 to 140 + π/2
100
100
X5, Y5
140 + 12.5 π
0
0
0 to 140 + π
100
100
X6, Y6
140 + 13 π
0
0
Y4
Y5
Y6
X4
X5
X6
FIELDS
DC
AC
x/r_o and y/r_o
ωt
10
8
6
4
2
0
-2
-4
-6
-8
-10
0
20
40
60
80
100
120
140
160
180
200
220
240
260
280
300
320
340
360

FIGURE 24

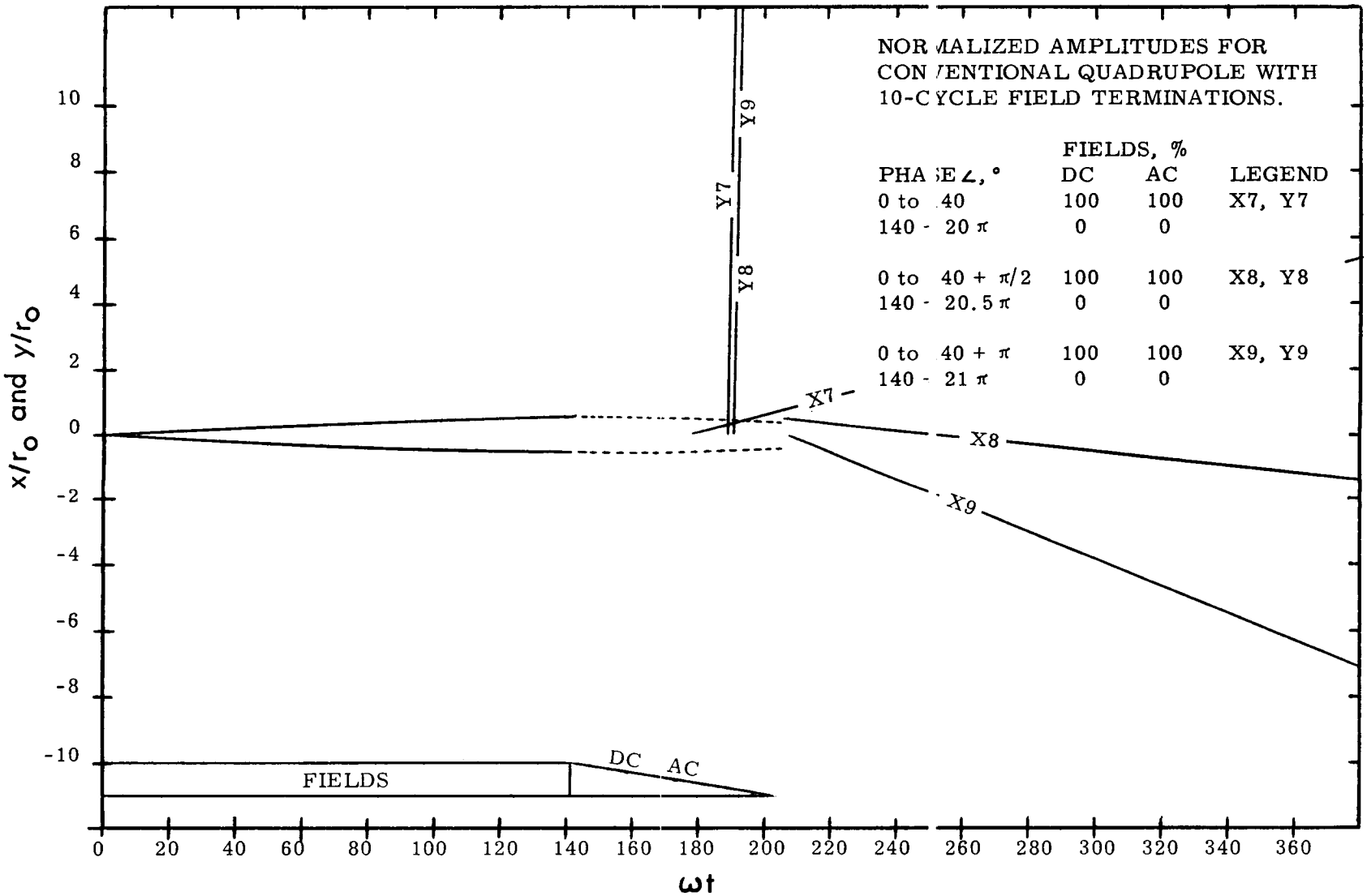
NORMALIZED AMPLITUDES FOR
CONVENTIONAL QUADRUPOLE WITH
10-CYCLE FIELD TERMINATIONS.
FIELDS, %
PHASE ∠, °
DC
AC
LEGEND
0 to 40
100
100
X7, Y7
140 - 20 π
0
0
0 to 40 + π/2
100
100
X8, Y8
140 - 20.5 π
0
0
0 to 40 + π
100
100
X9, Y9
140 - 21 π
0
0
Y9
Y7
Y8
X7
X8
X9
DC
AC
FIELDS
x/r_o and y/r_o
ωt
10
8
6
4
2
0
-2
-4
-6
-8
-10
0
20
40
60
80
100
120
140
160
180
200
220
240
260
280
300
320
340
360

FIGURE 25

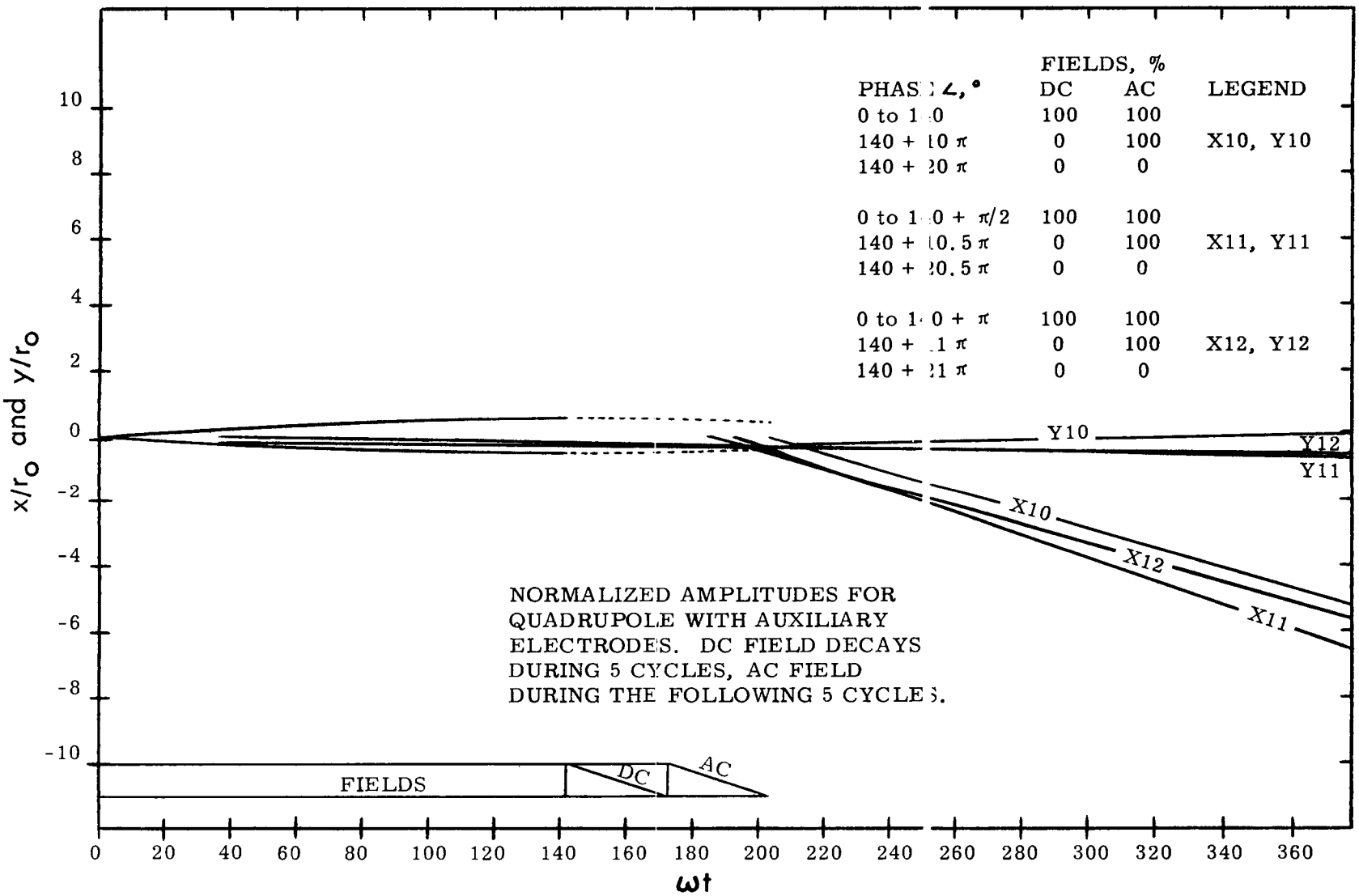
FIELDS, %
PHASE ∠, °
DC
AC
LEGEND
0 to 140
100
100
140 + 10 π
0
100
X10, Y10
140 + 20 π
0
0
0 to 140 + π/2
100
100
140 + 10.5 π
0
100
X11, Y11
140 + 20.5 π
0
0
0 to 140 + π
100
100
140 + 11 π
0
100
X12, Y12
140 + 21 π
0
0
Y10
Y12
Y11
X10
X12
X11
NORMALIZED AMPLITUDES FOR QUADRUPOLE WITH AUXILIARY ELECTRODES. DC FIELD DECAYS DURING 5 CYCLES, AC FIELD DURING THE FOLLOWING 5 CYCLES.
FIELDS
DC
AC
x/r_o and y/r_o
ωt
10
8
6
4
2
0
-2
-4
-6
-8
-10
0
20
40
60
80
100
120
140
160
180
200
220
240
260
280
300
320
340
360

FIGURE 26

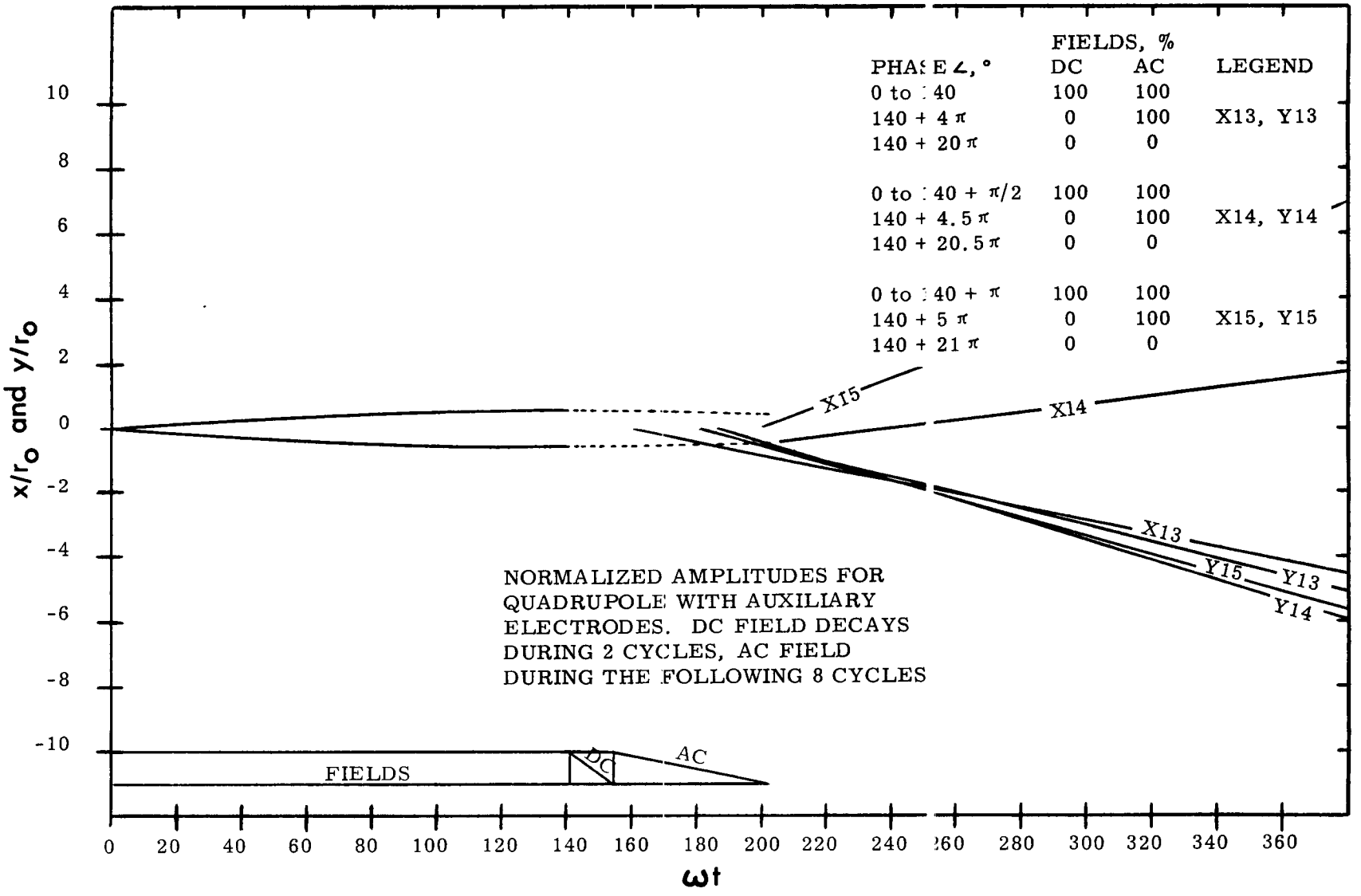
FIELDS, %
PHASE ∠, °
DC
AC
LEGEND
0 to 140
100
100
140 + 4π
0
100
X13, Y13
140 + 20π
0
0
0 to 140 + π/2
100
100
140 + 4.5π
0
100
X14, Y14
140 + 20.5π
0
0
0 to 140 + π
100
100
140 + 5π
0
100
X15, Y15
140 + 21π
0
0
X15
X14
X13
Y15
Y13
Y14
NORMALIZED AMPLITUDES FOR QUADRUPOLE WITH AUXILIARY ELECTRODES. DC FIELD DECAYS DURING 2 CYCLES, AC FIELD DURING THE FOLLOWING 8 CYCLES
FIELDS
DC
AC
x/r0 and y/r0
10
8
6
4
2
0
-2
-4
-6
-8
-10
0
20
40
60
80
100
120
140
160
180
200
220
240
260
280
300
320
340
360
ωt

FIGURE 27

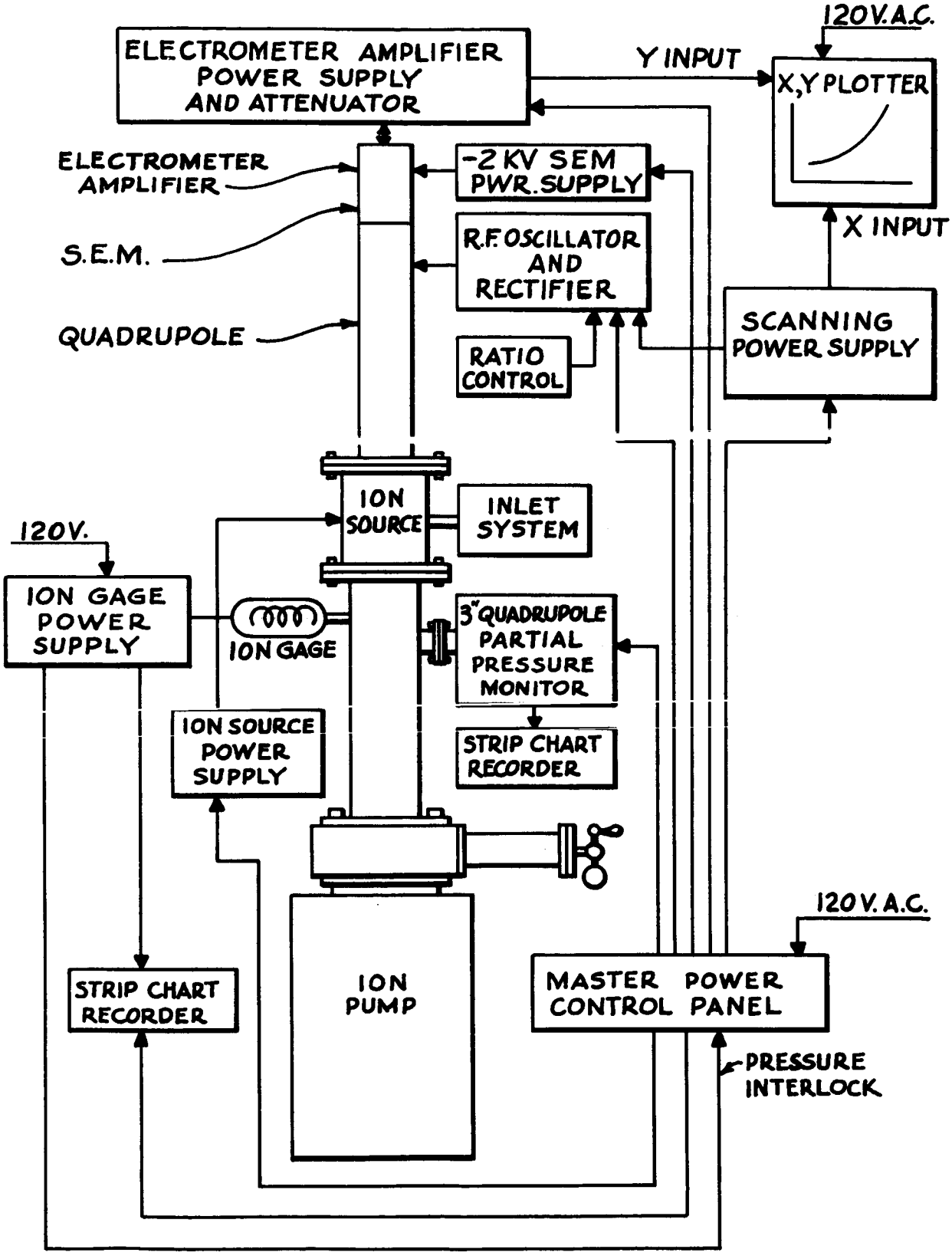

APPARATUS BLOCK DIAGRAM

FIGURE 28

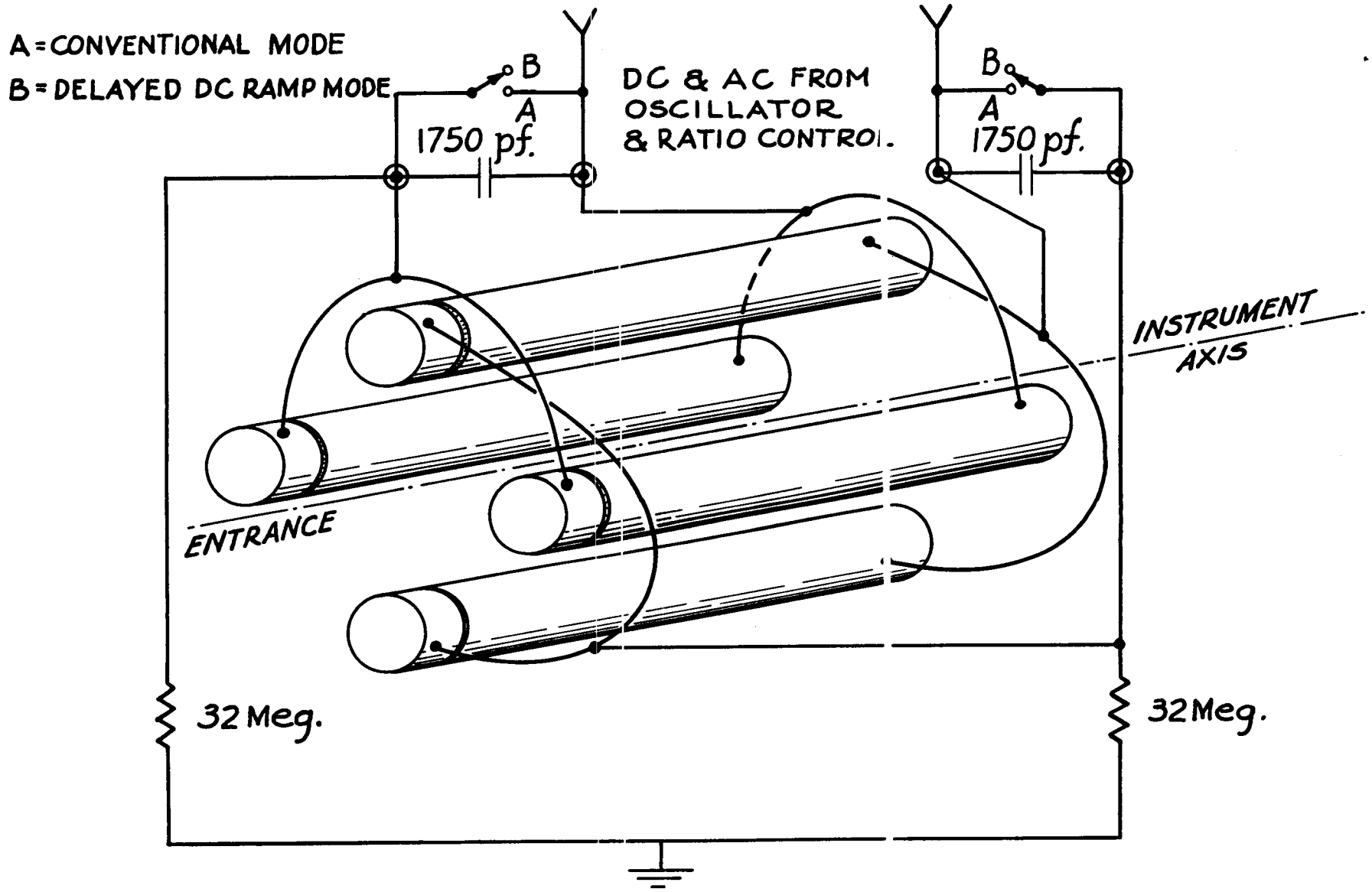

APPARATUS
FIGURE 29

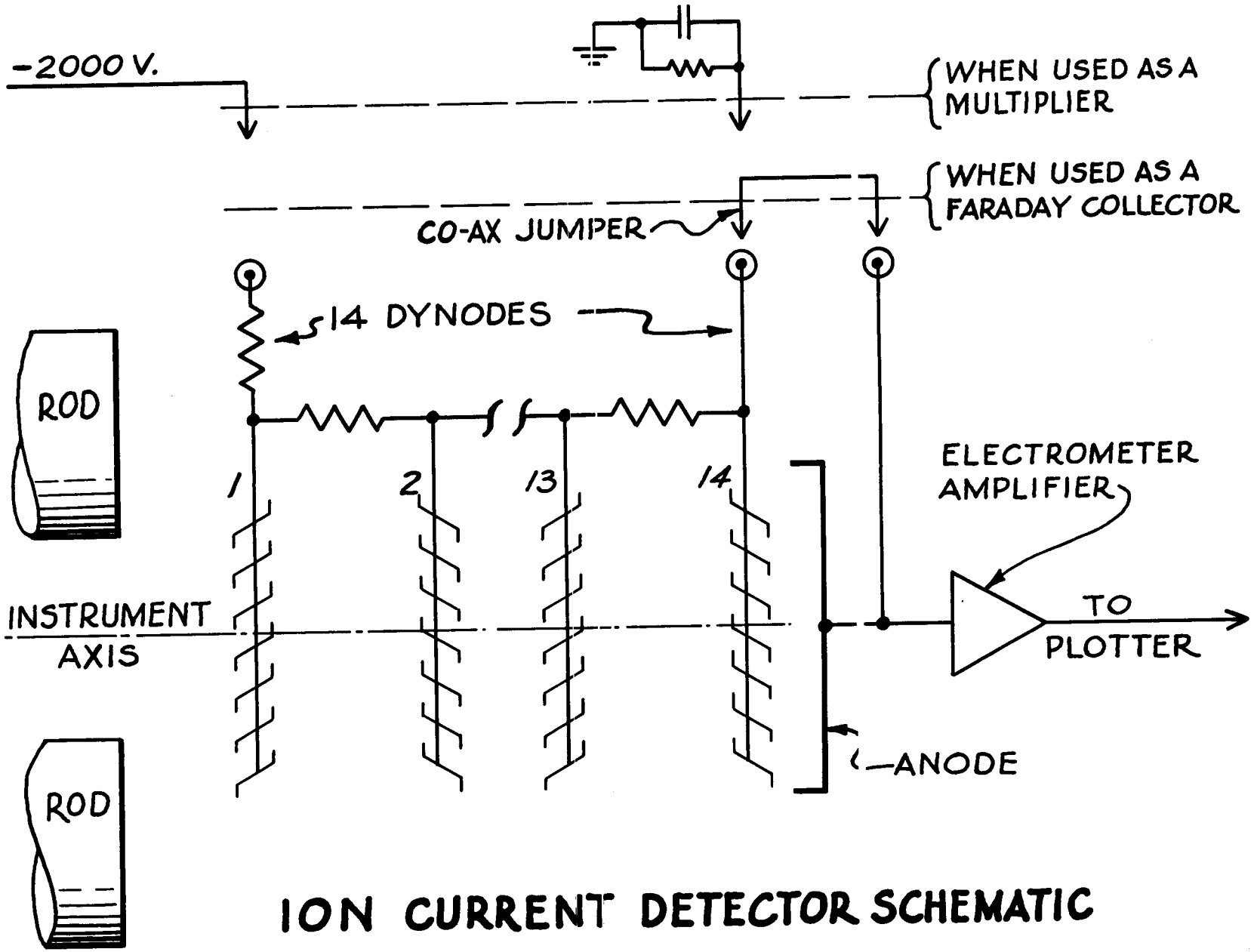

ION CURRENT DETECTOR SCHEMATIC

FIGURE 30

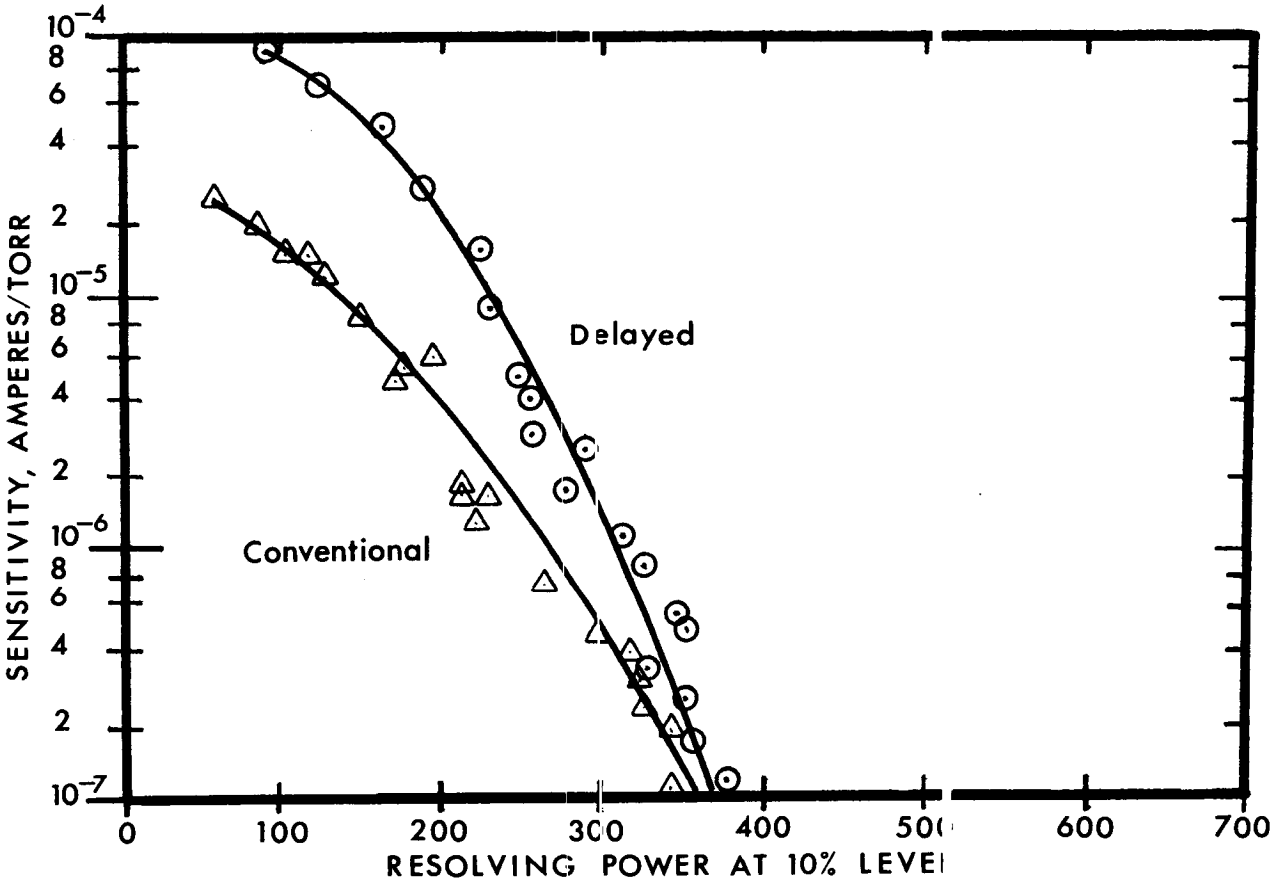

FIGURE 31

SENSITIVITY VS. RESOLVING POWER FOR
CONVENTIONAL AND DELAYED MODES WITH 15-VOLT IONS

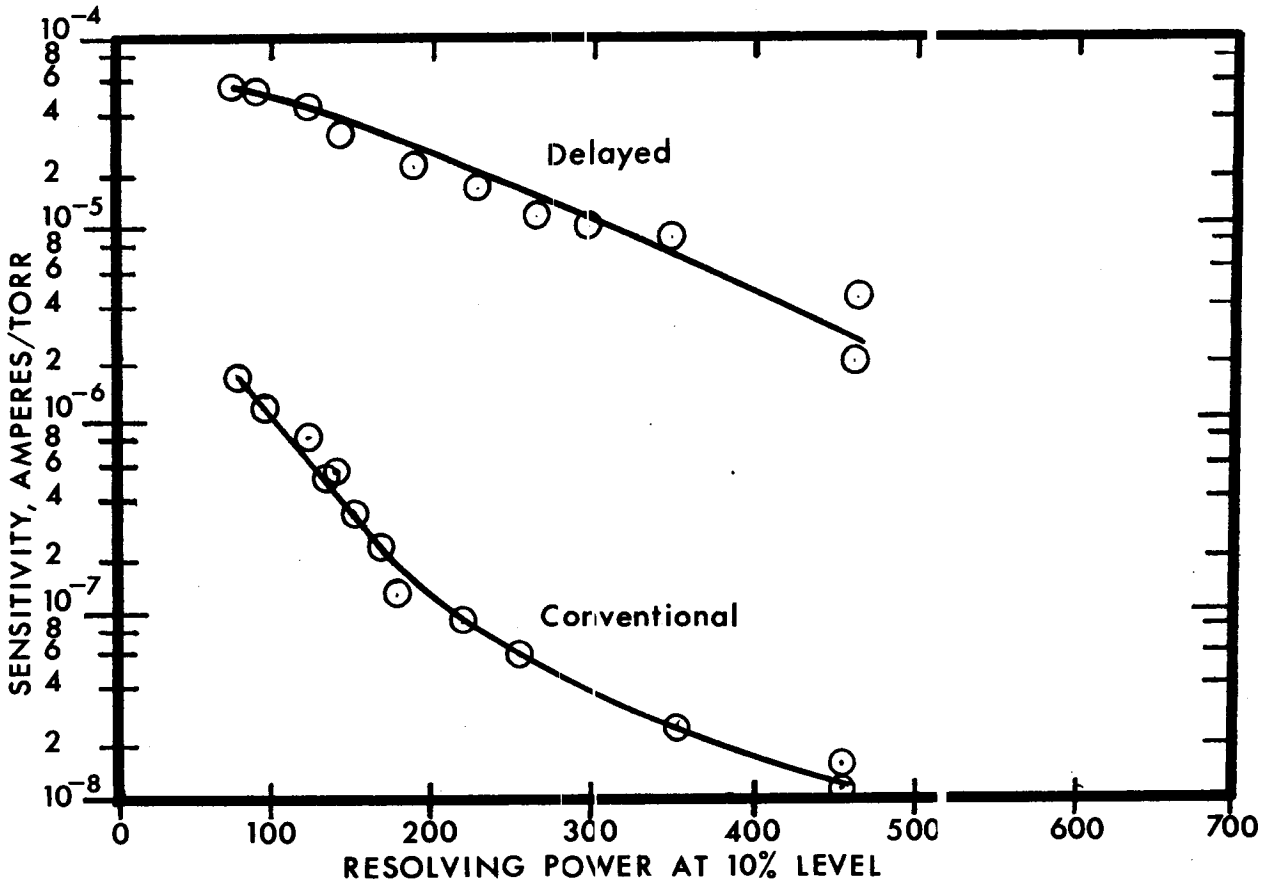

FIGURE 32

SENSITIVITY VS. RESOLVING POWER FOR
CONVENTIONAL AND DELAYED MODES WITH 8-VOLT IONS

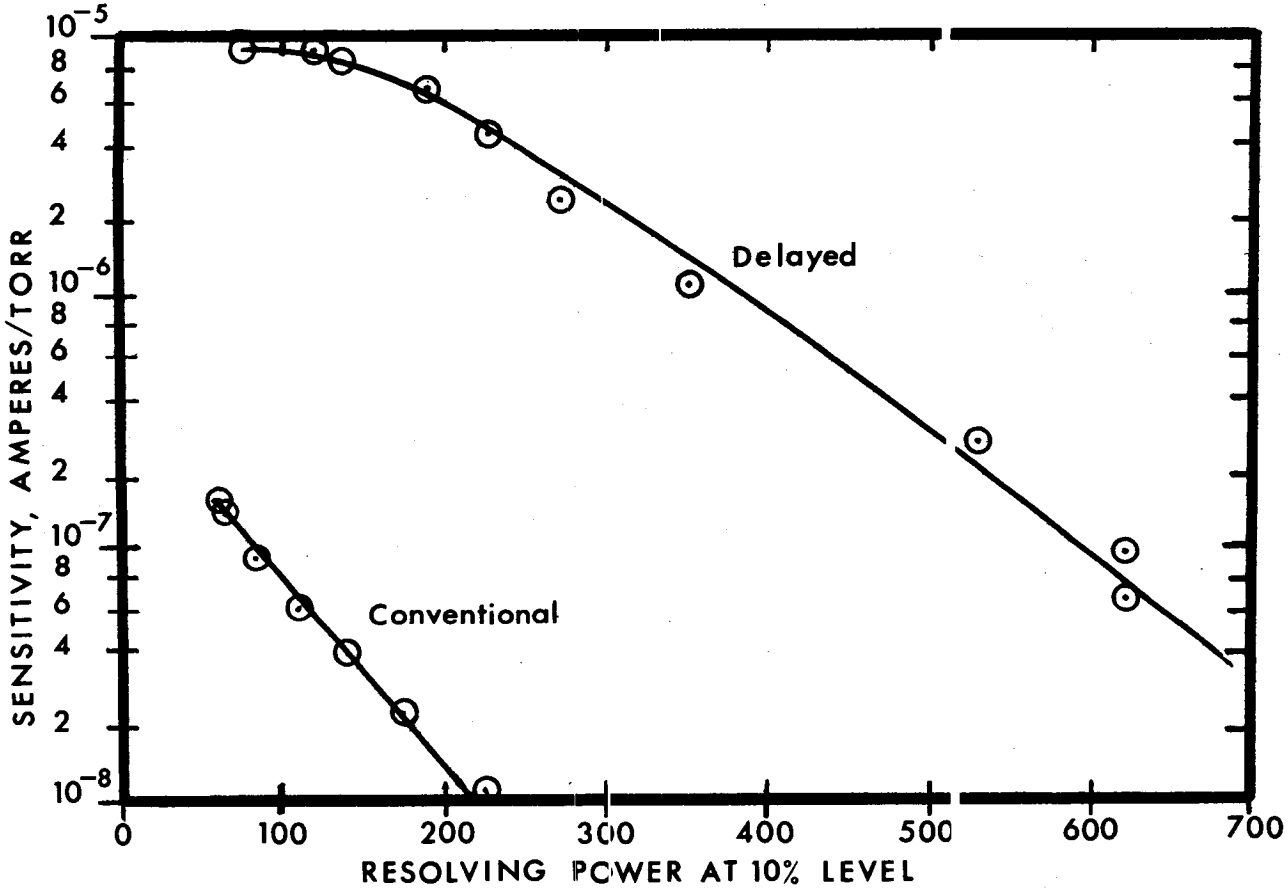

FIGURE 33

SENSITIVITY VS. RESOLVING POWER FOR CONVENTIONAL AND DELAYED MODES WITH 4-VOLT IONS

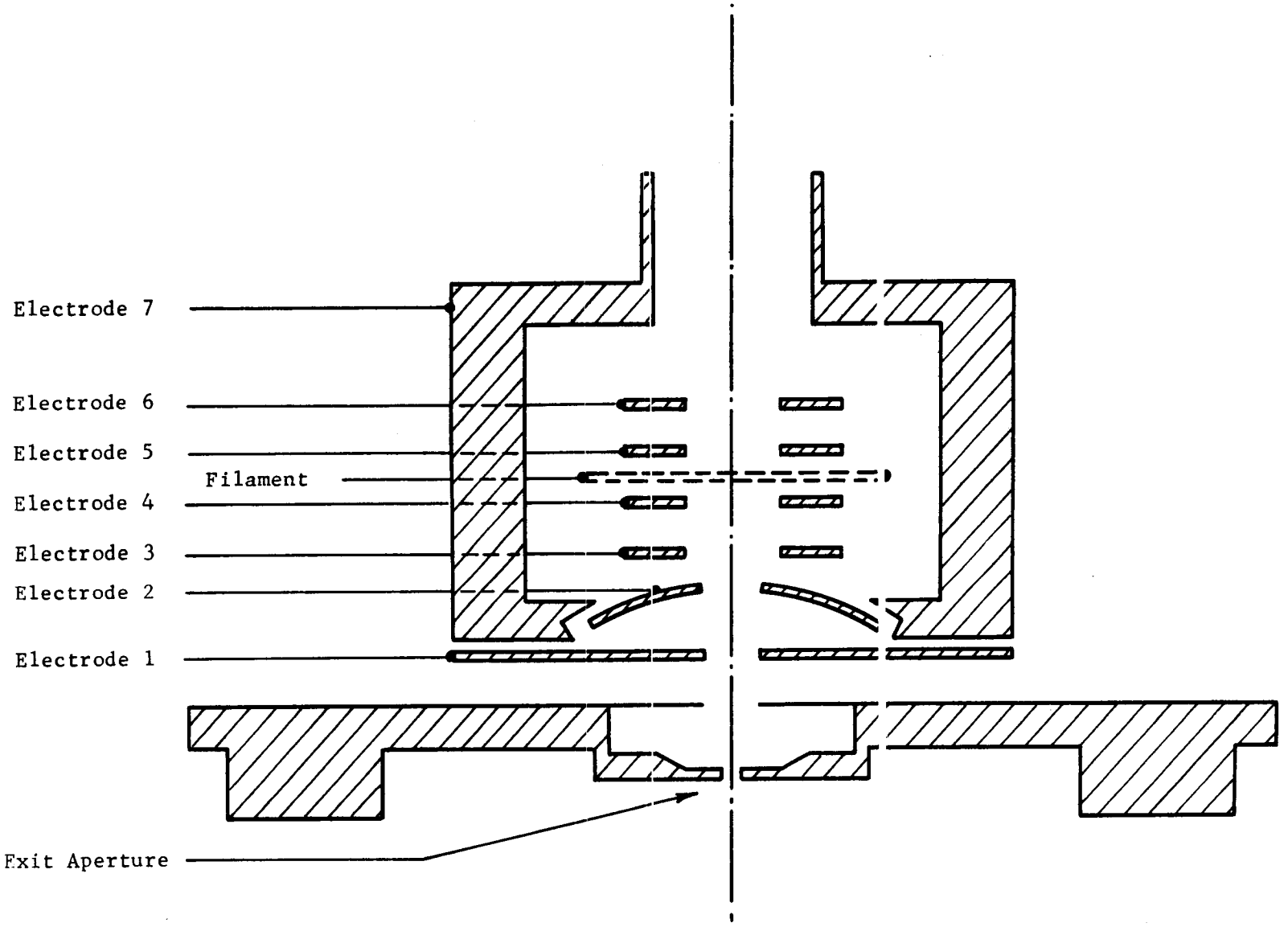

FIGURE 34.

GEOMETRY OF EARLY ION SOURCE

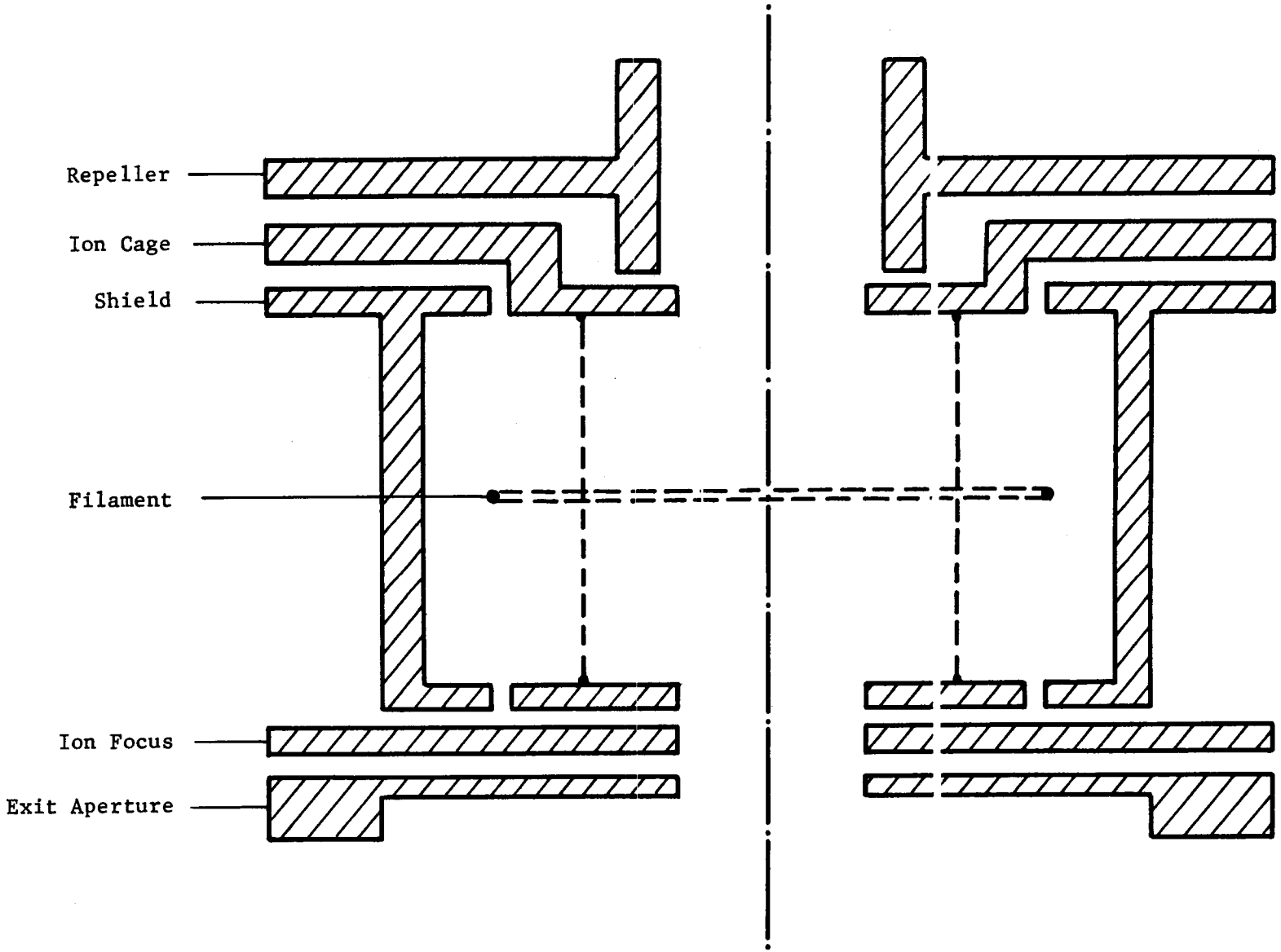

FIGURE 35.

GEOMETRY OF NEW ION SOURCE

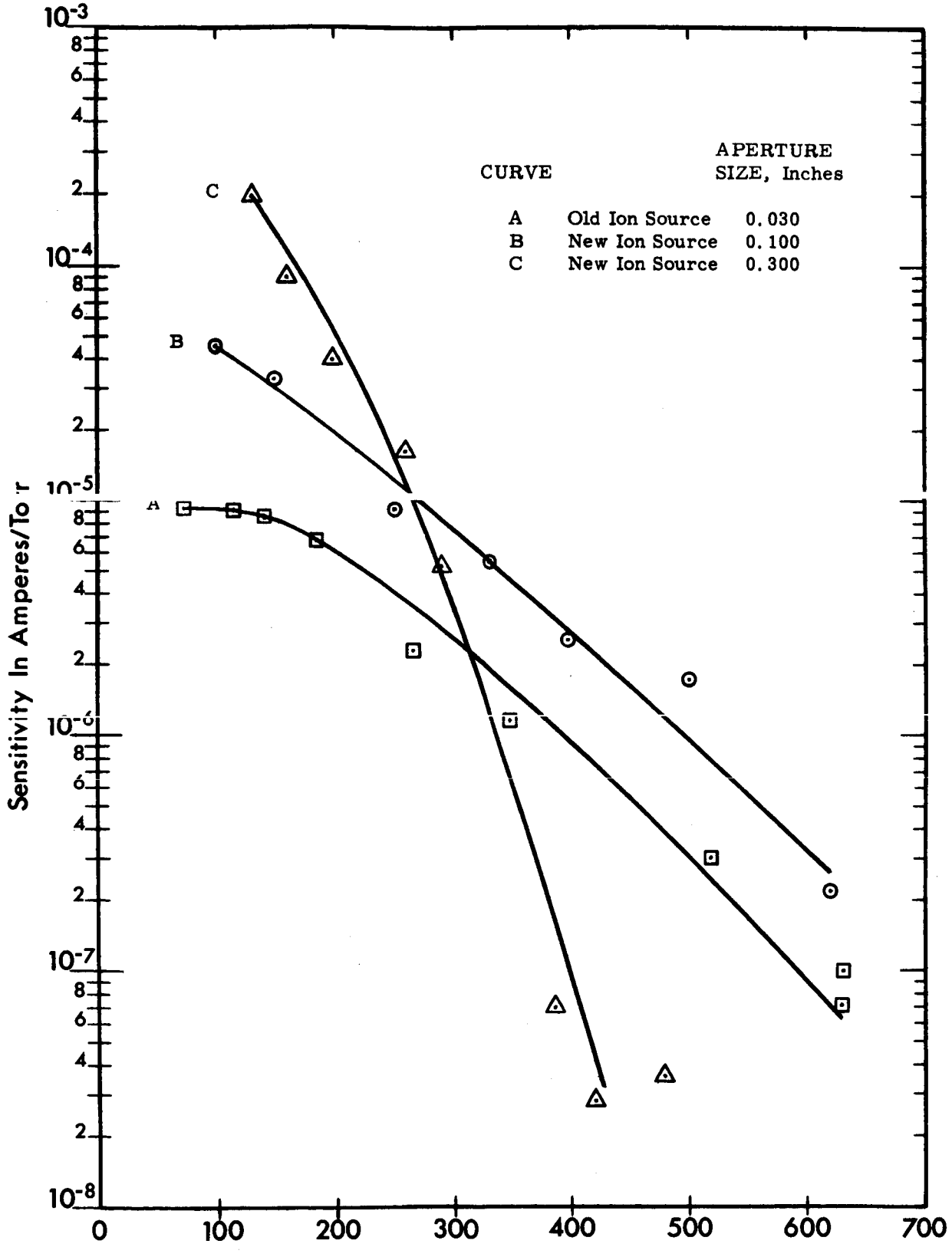

FIGURE 36

OPERATING CHARACTERISTICS OF QUADRUPOLE WITH DIFFERENT ION SOURCE CONFIGURATIONS

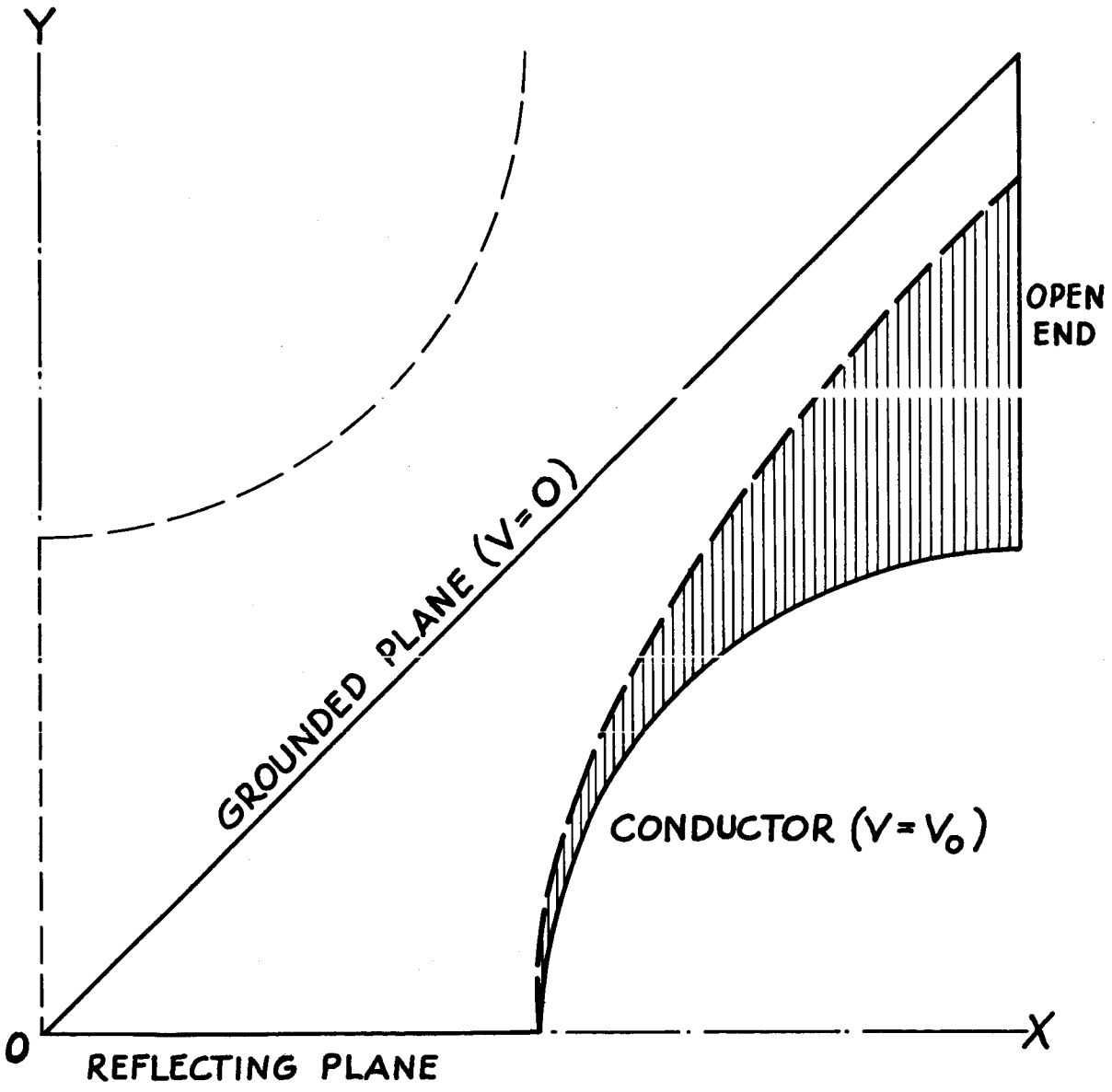

BOUNDARY CONDITIONS FOR
LIEBMANN PROCEDURE

FIGURE 37

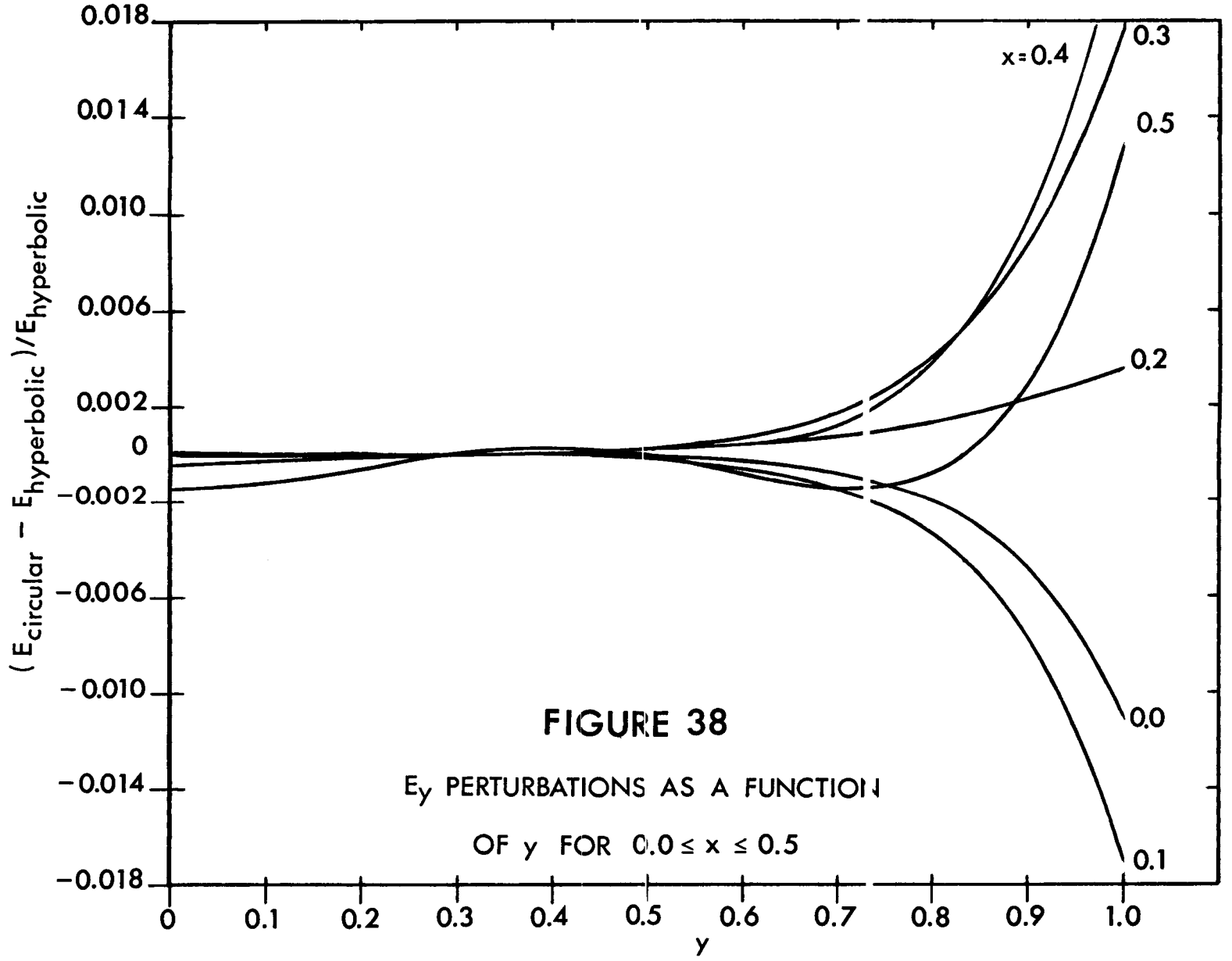

FIGURE 38

E_y PERTURBATIONS AS A FUNCTION OF y FOR $0.0 \leq x \leq 0.5$

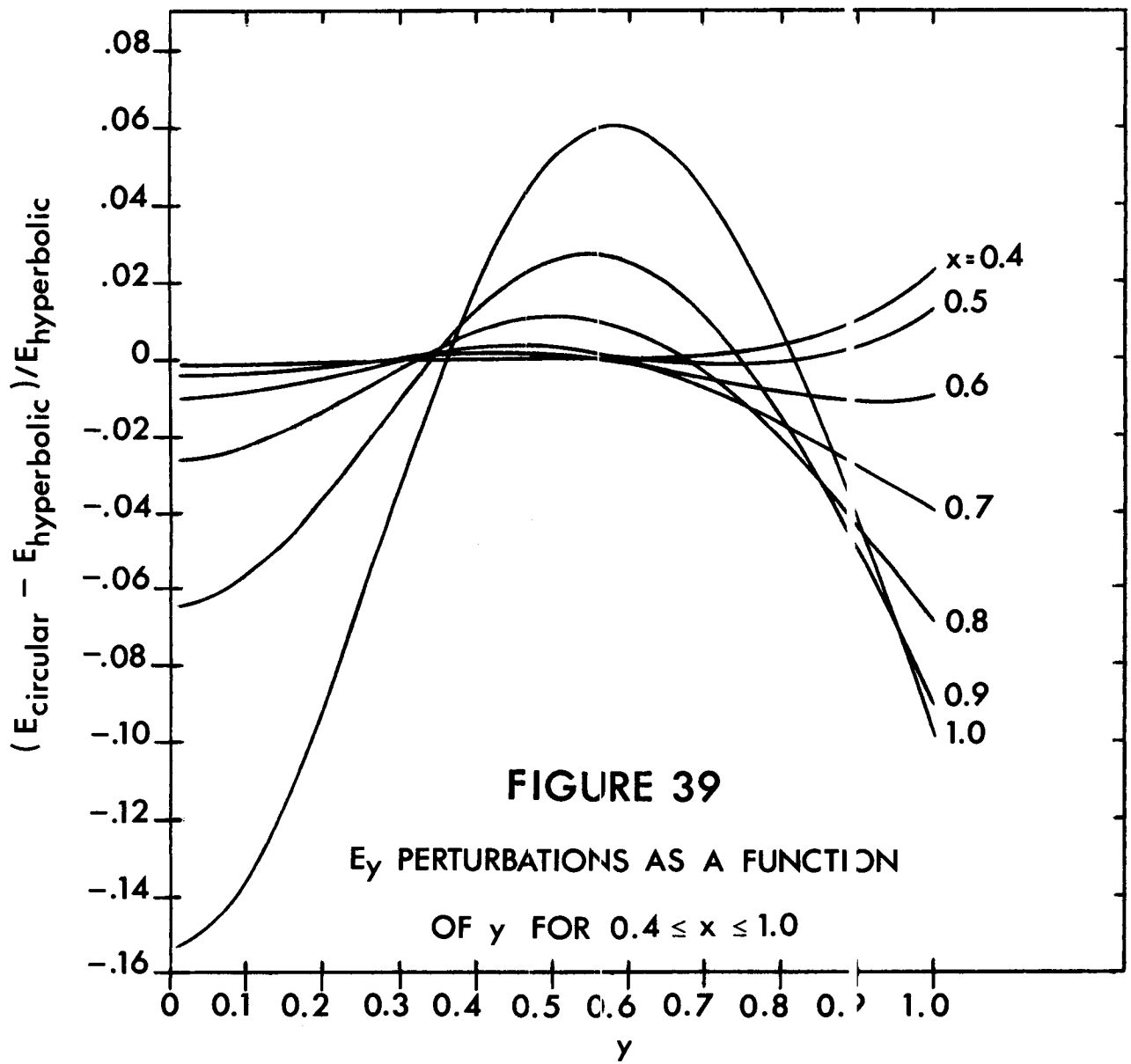

FIGURE 39

E_y PERTURBATIONS AS A FUNCTION OF y FOR $0.4 \leq x \leq 1.0$

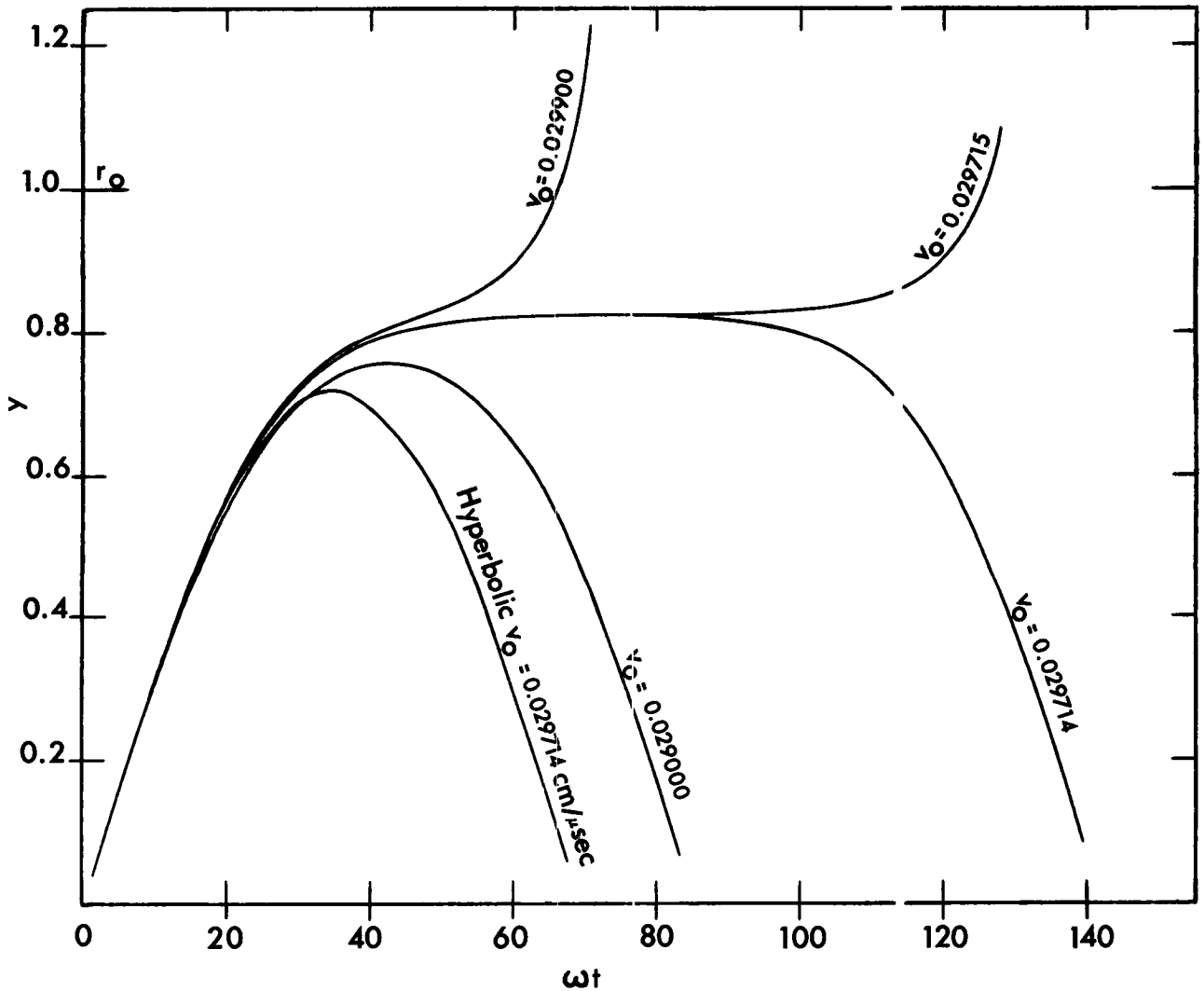

FIGURE 40

y-trajectories for:

x = 0; a = 0.23462; q = 0.70482; m/dm ≈ 100

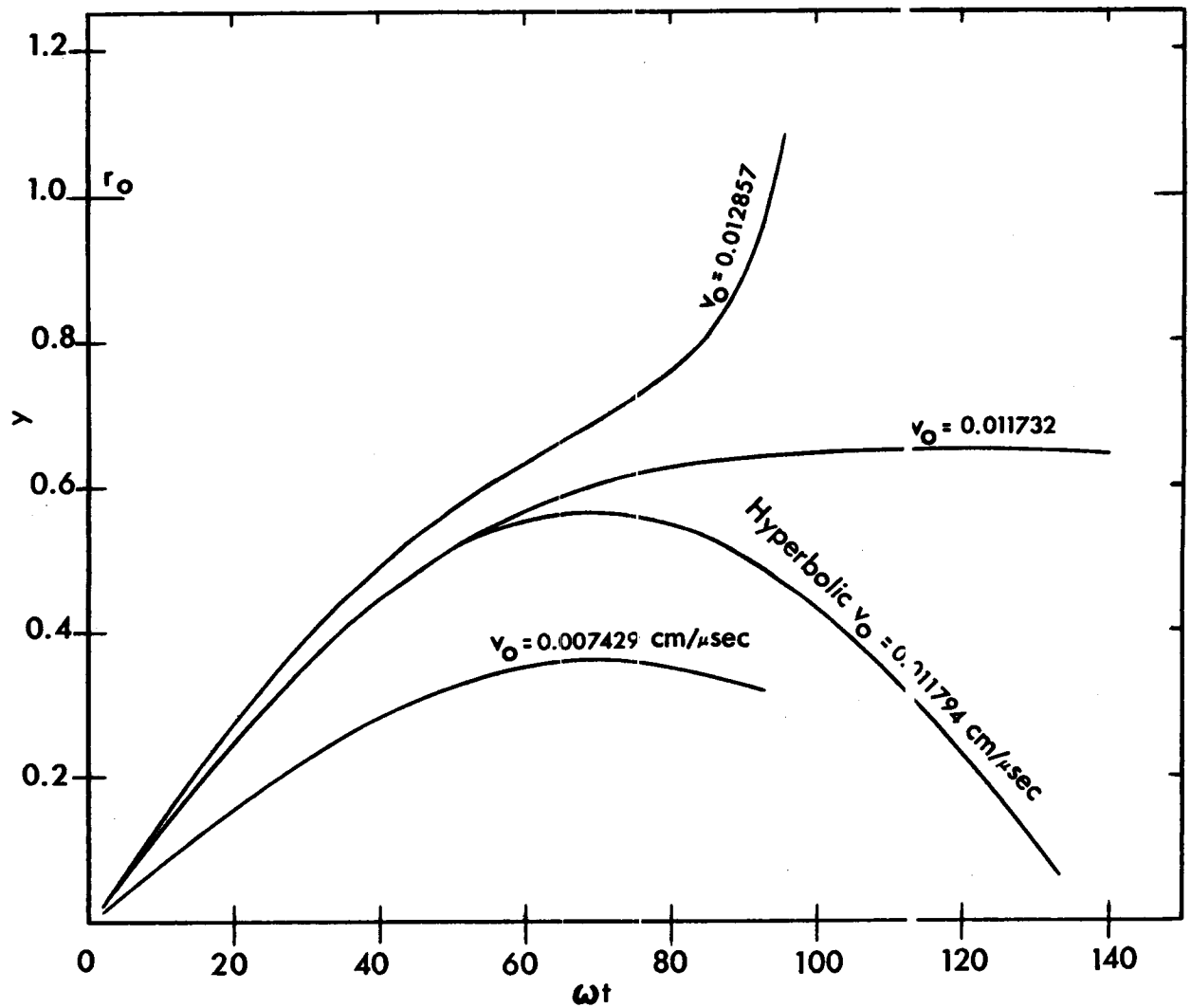

FIGURE 41

y-trajectories for:

x = 0; a = 0.23640; q = 0.70571; m/dm ≈ 400

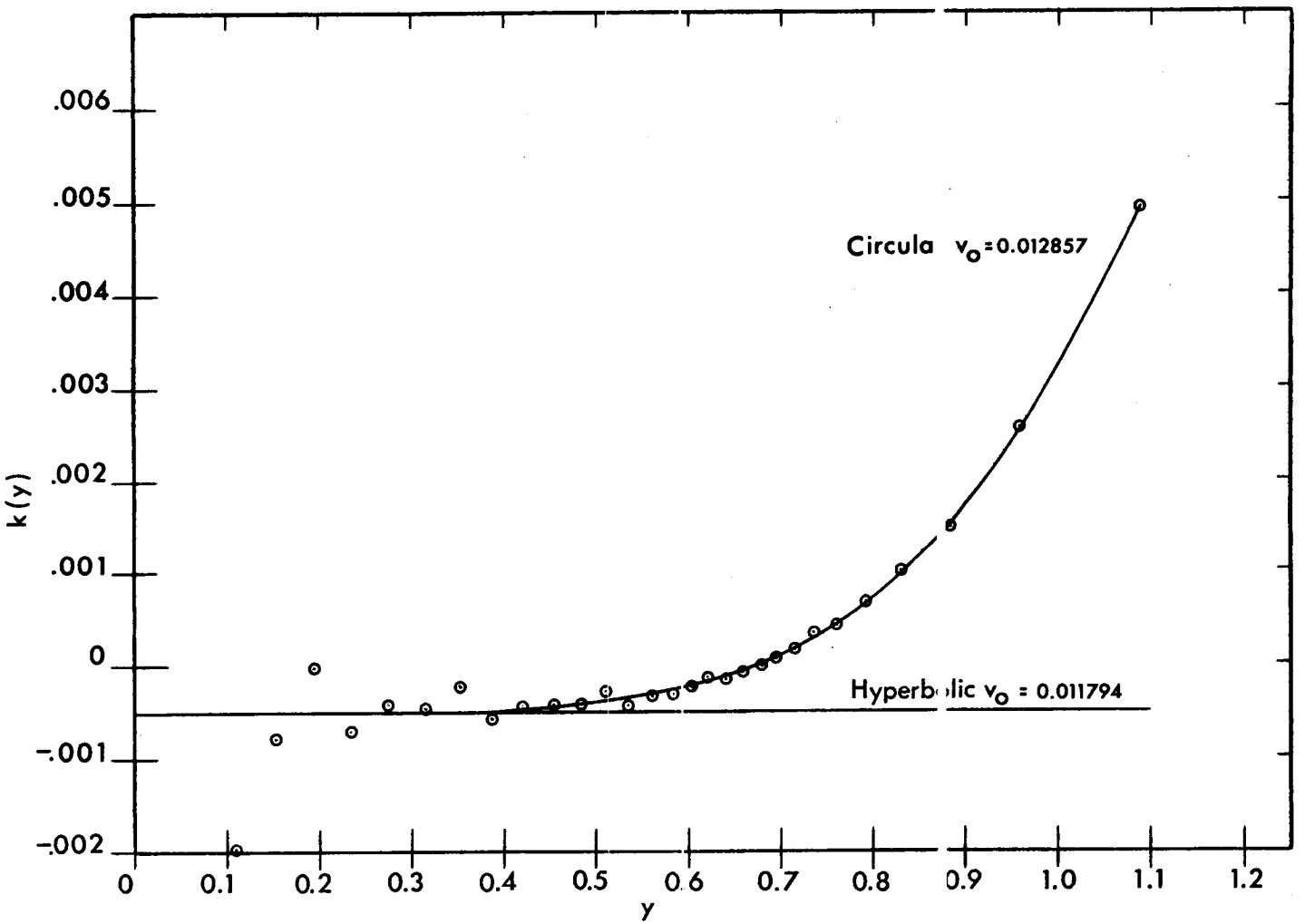

FIGURE 42

k(y) as a function of y for:

x = 0; a = 0.23640; q = 0.70571; m/dm ≈ 400

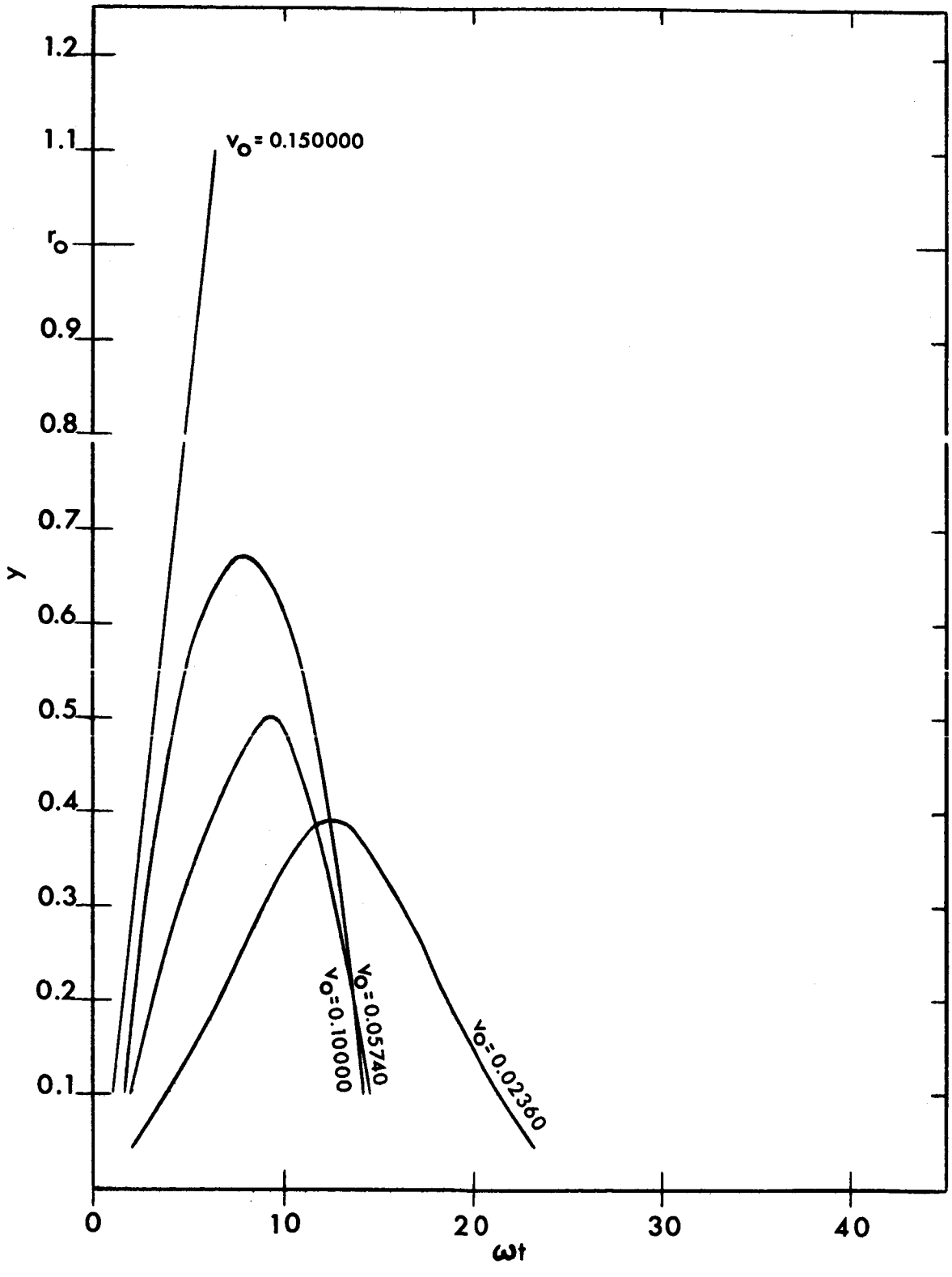

FIGURE 43

y-trajectories for:

$x = r_o$; a = 0.23640; q=0.70571; m/dm ≈ 400

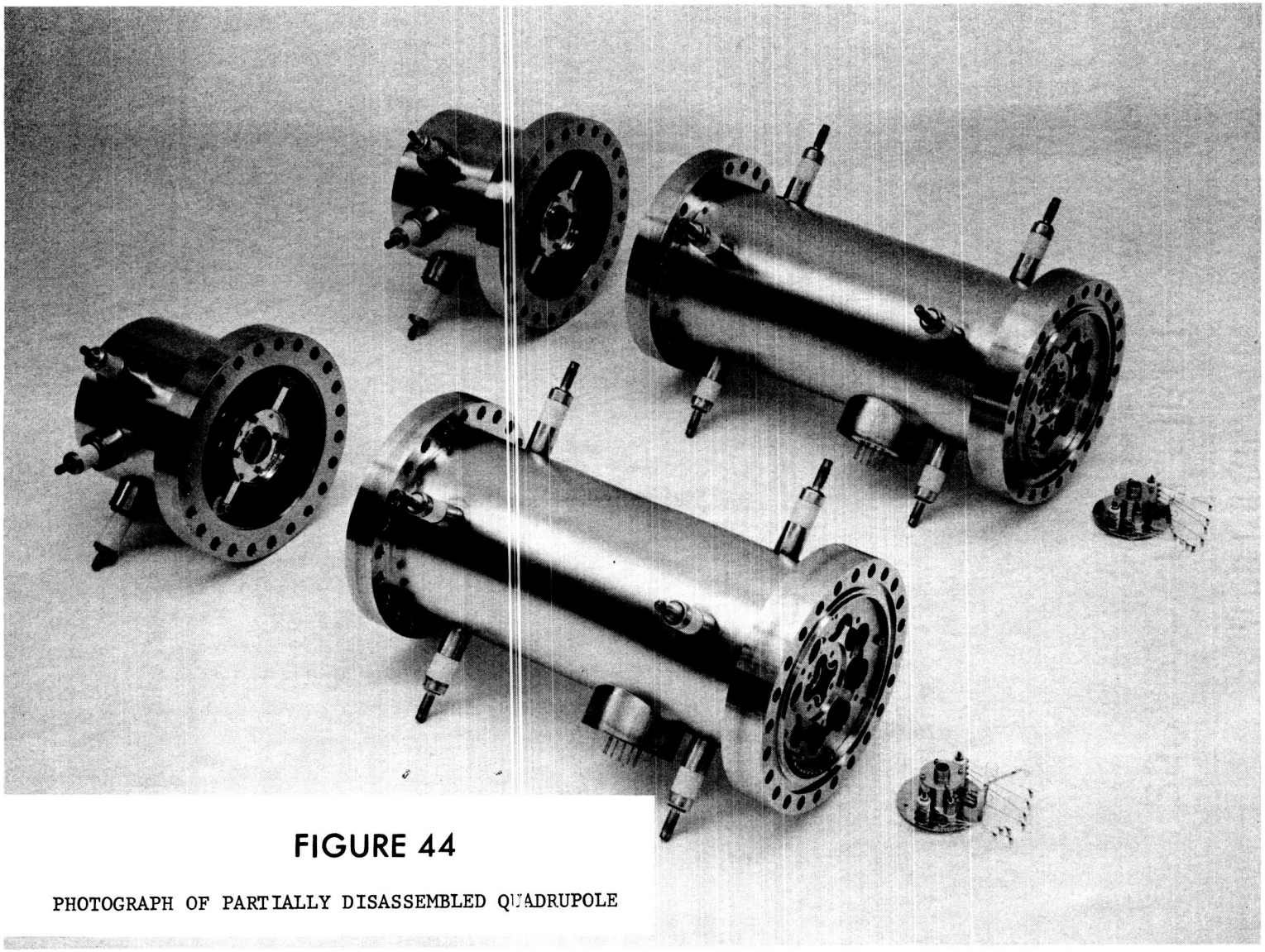

FIGURE 44

PHOTOGRAPH OF PARTIALLY DISASSEMBLED QUADRUPOLE

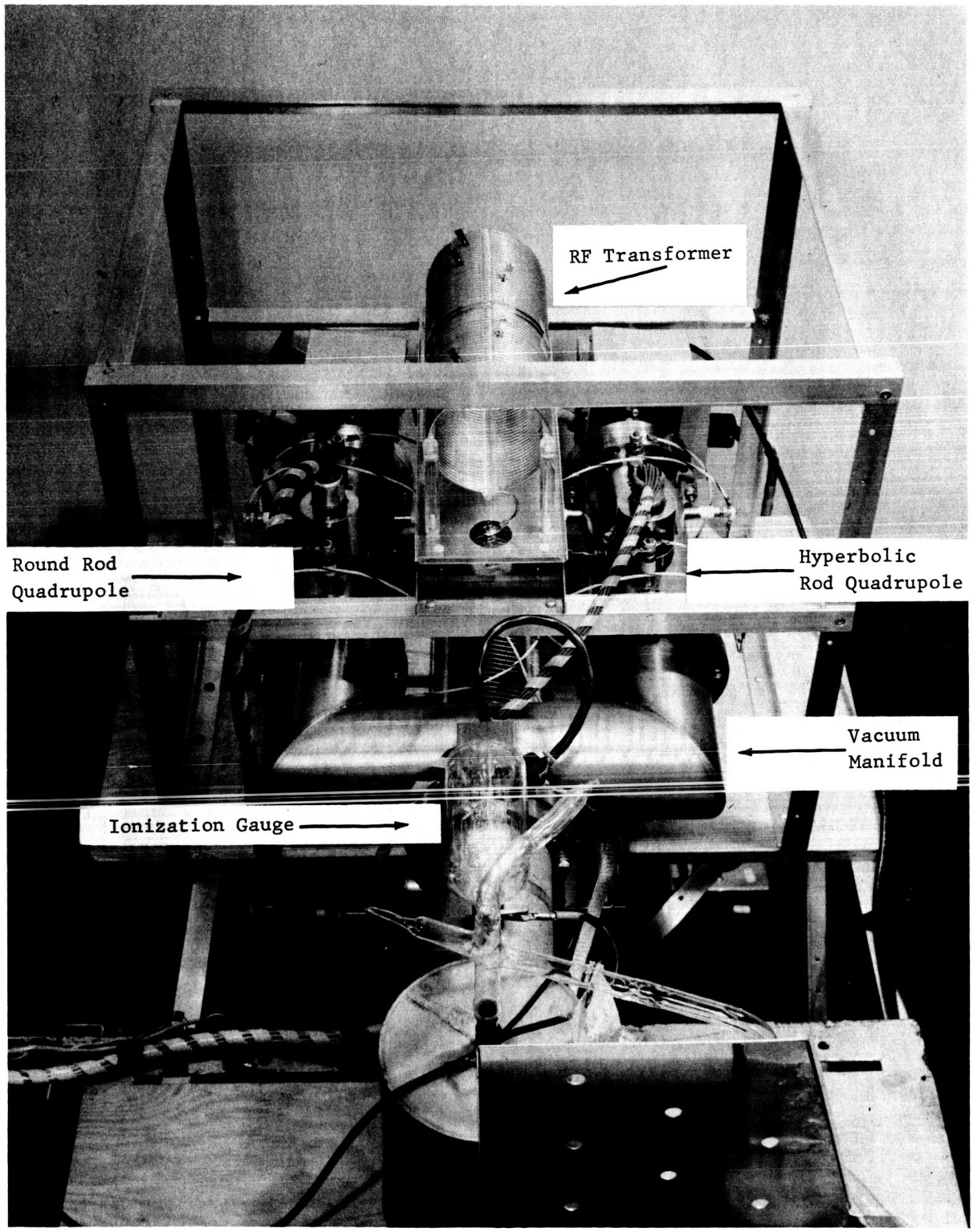

FIGURE 45

VACUUM MANIFOLD ASSEMBLY

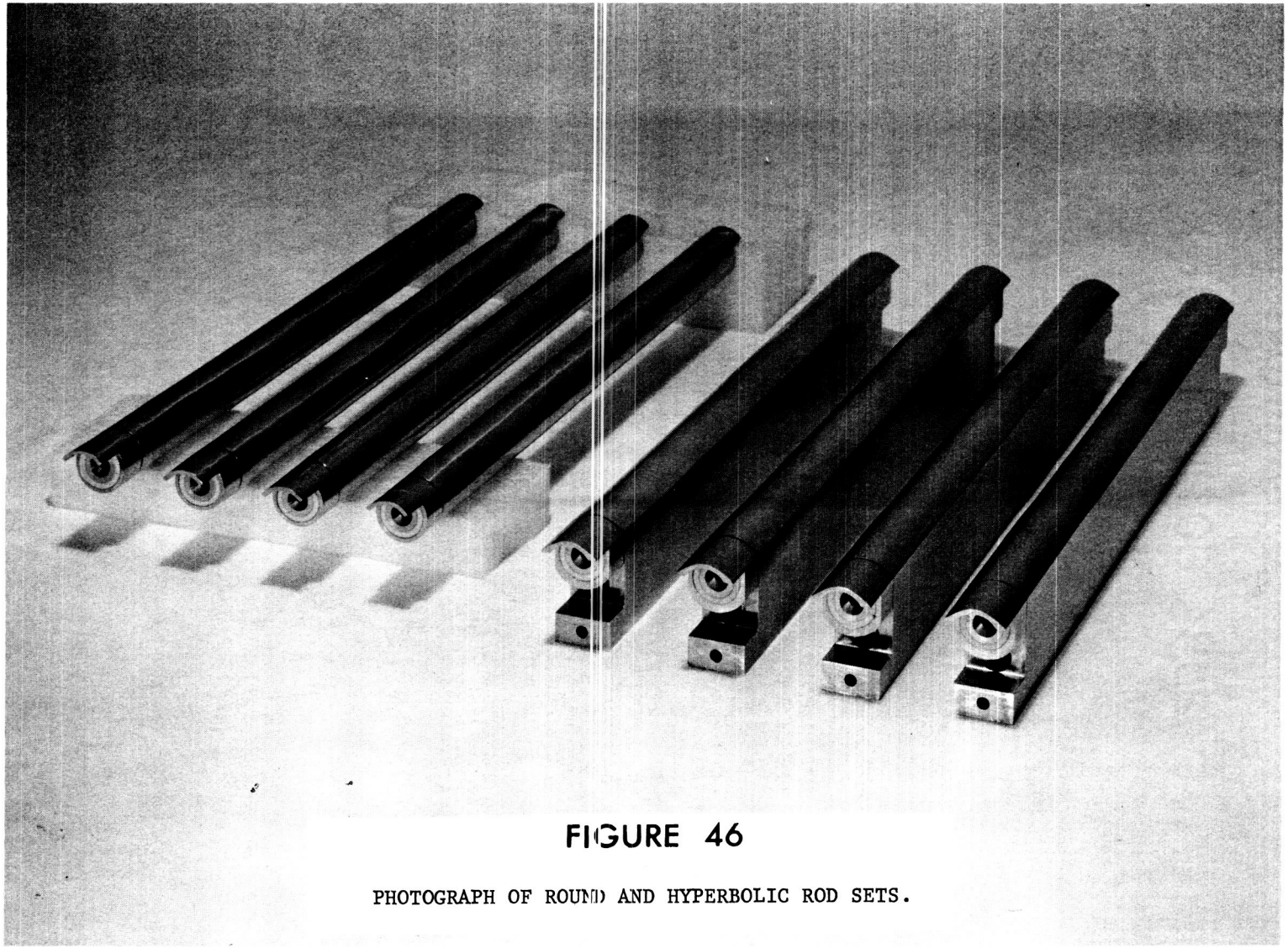

FIGURE 46

PHOTOGRAPH OF ROUND AND HYPERBOLIC ROD SETS.

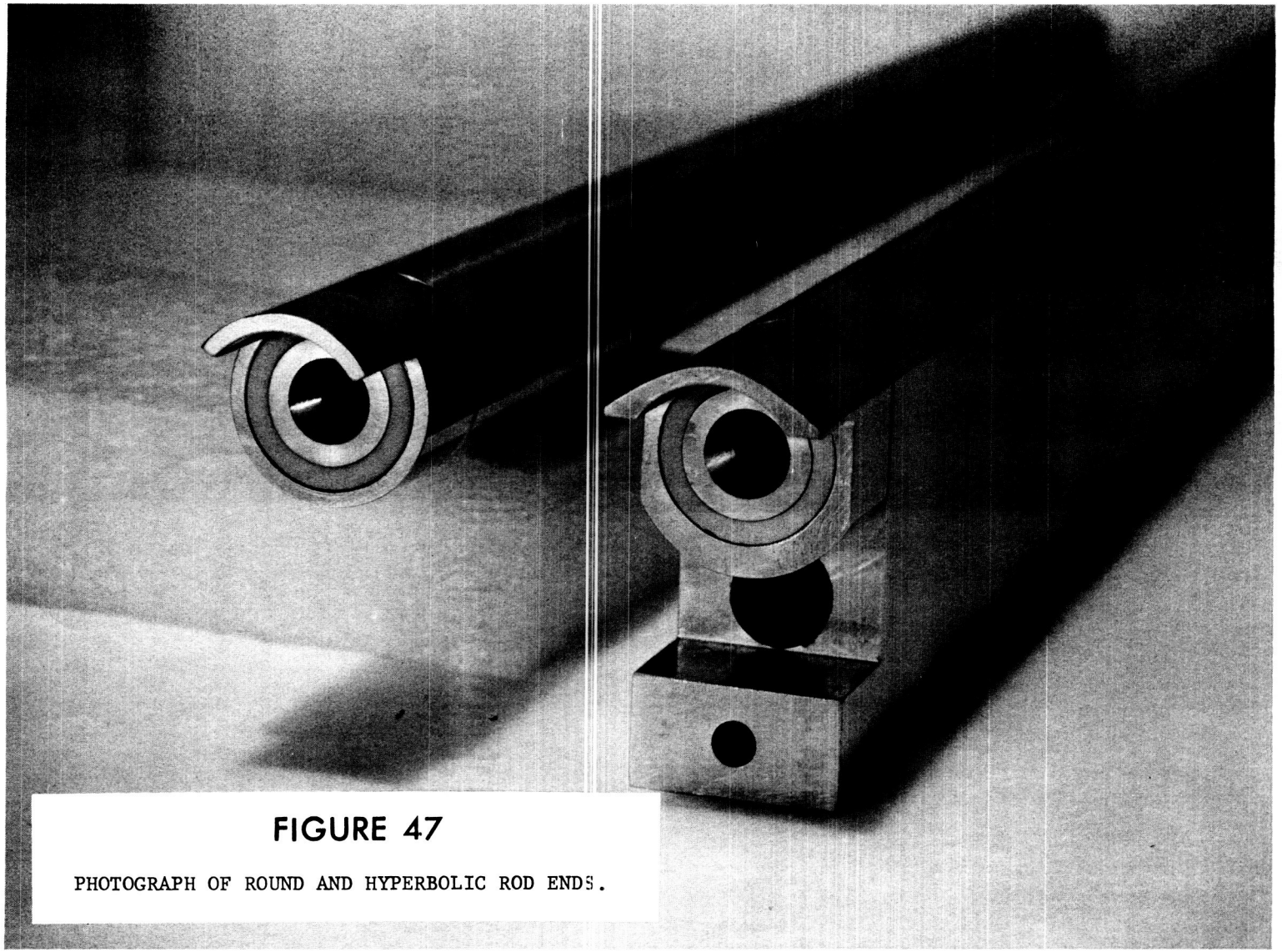

FIGURE 47

PHOTOGRAPH OF ROUND AND HYPERBOLIC ROD ENDS.

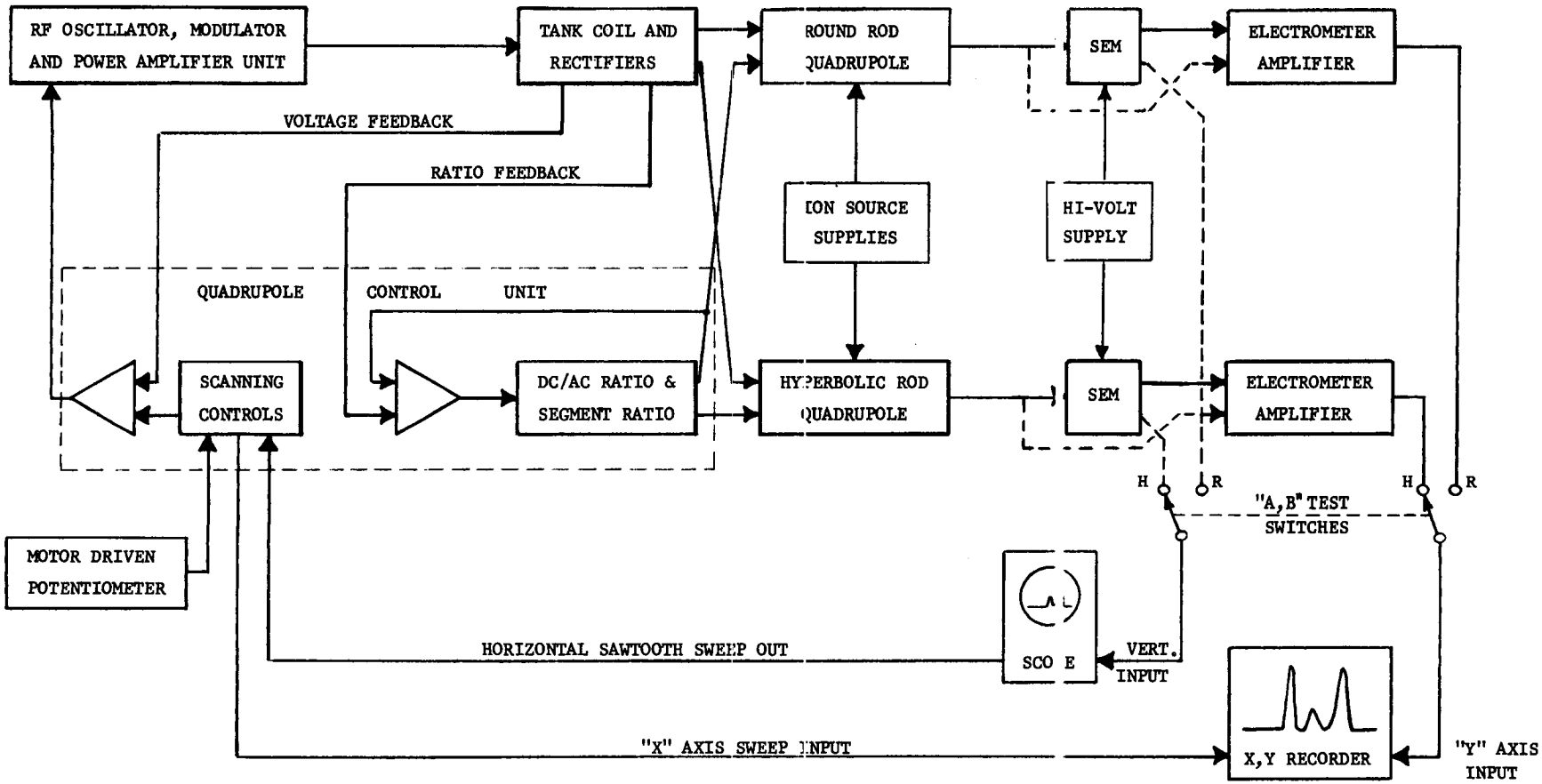

FIGURE 48

BLOCK DIAGRAM OF ELECTRONIC APPARATUS

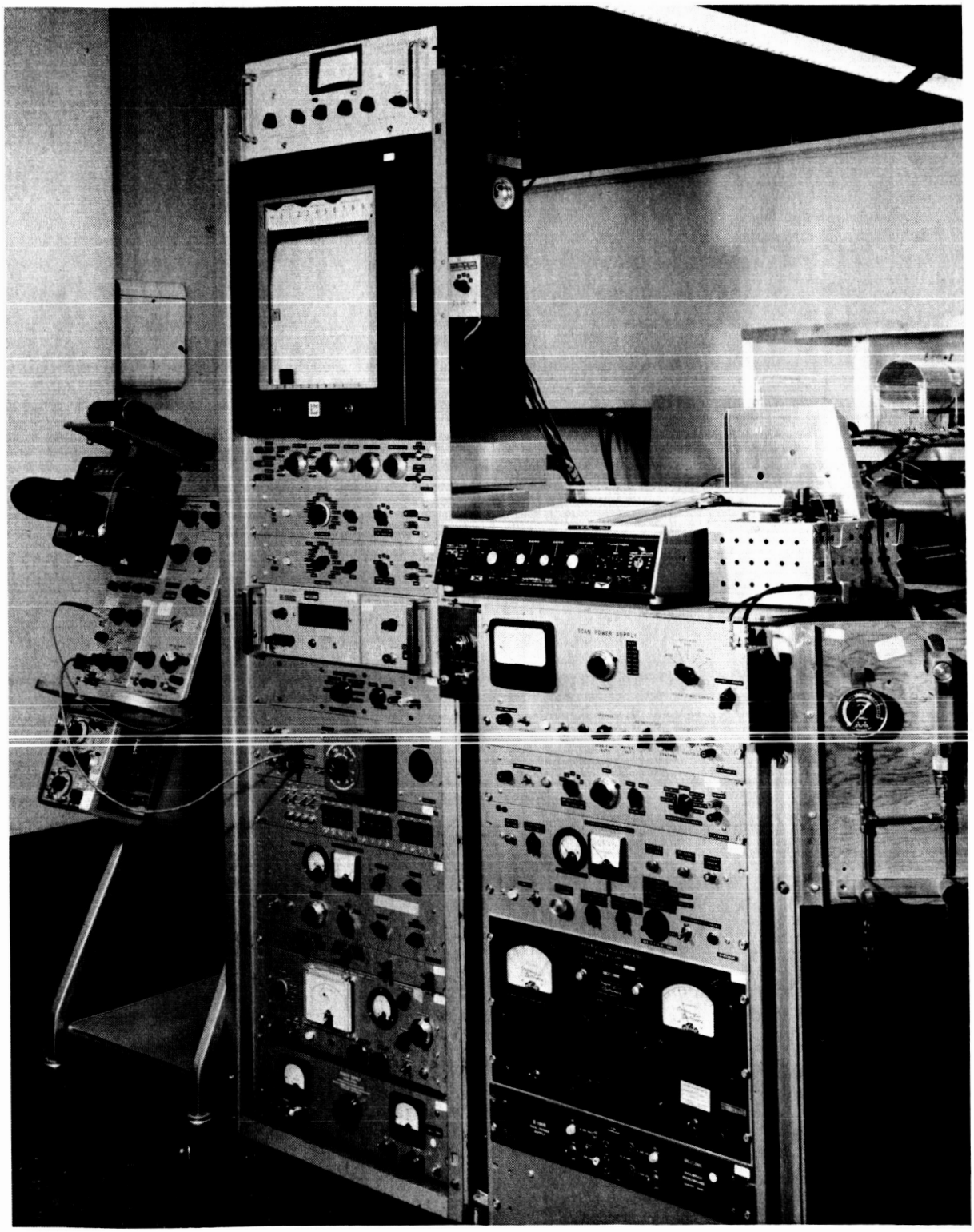

FIGURE 49

ELECTRONIC APPARATUS

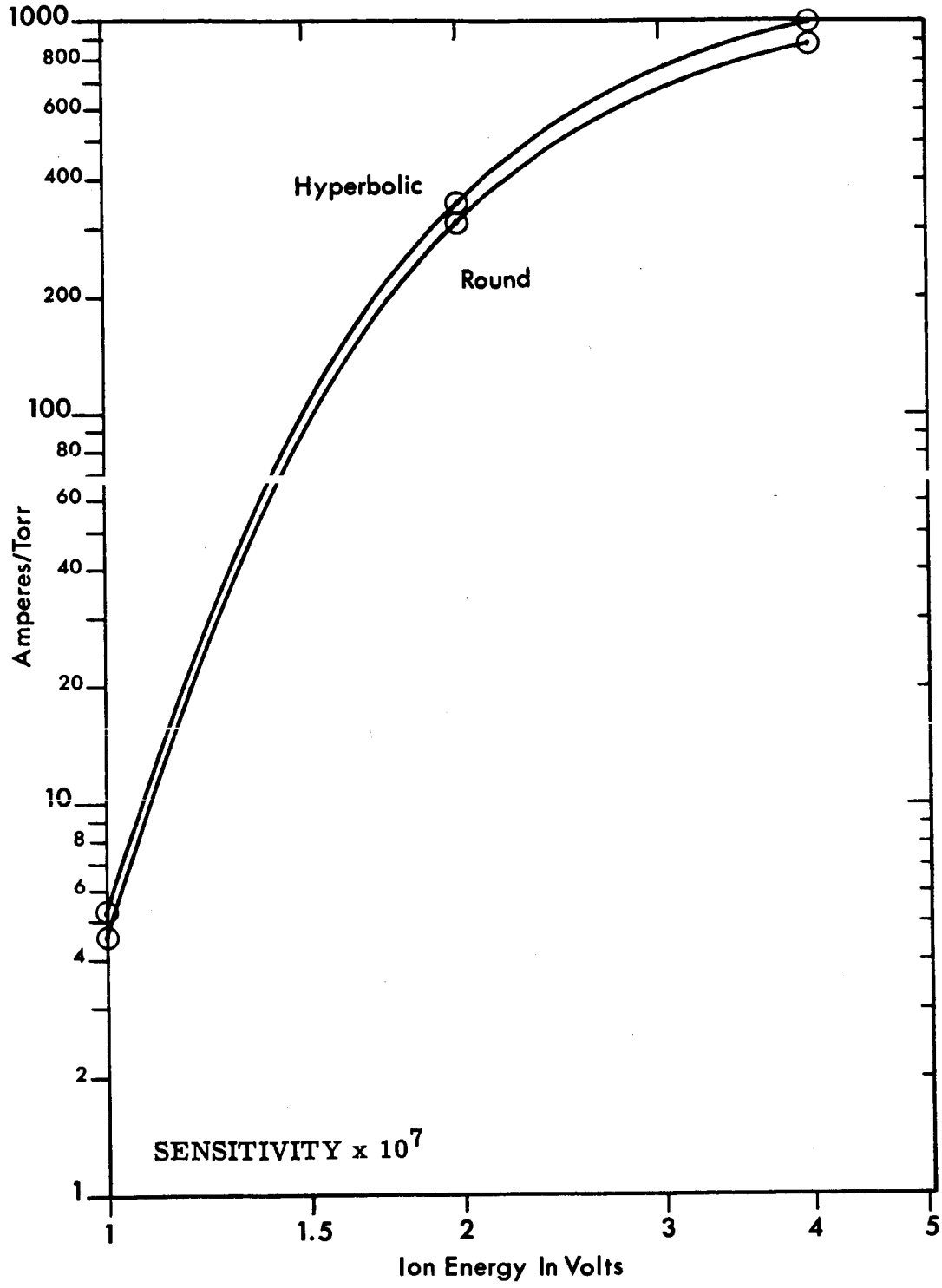

FIGURE 50

SENSITIVITIES OF ION SOURCES FOR THE RESOLVED MASS 84 ISOTOPE OF KRYPTON AS A FUNCTION OF ION ENERGY

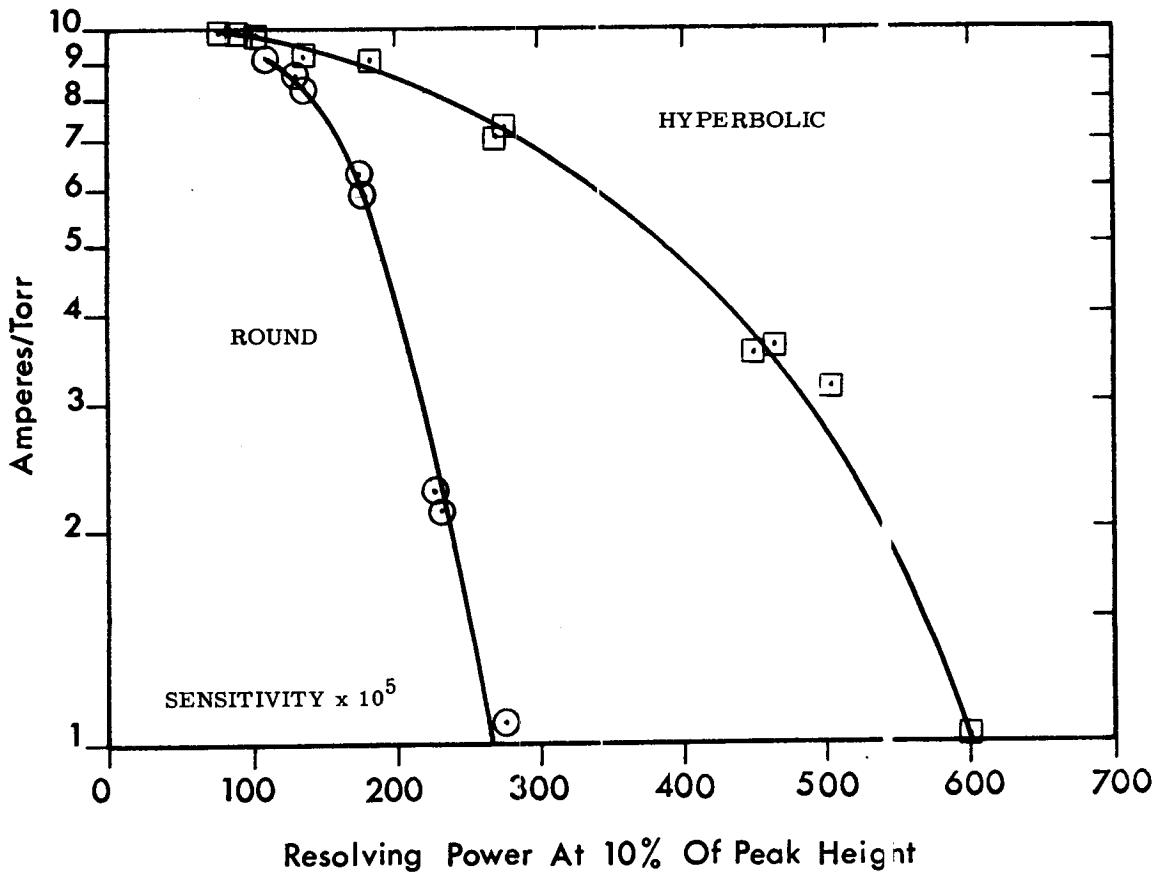

FIGURE 51

SENSITIVITIES OF ROUND AND HYPERBOLIC QUADRUPOLES AS FUNCTIONS OF RESOLVING POWER. EXCITATION FREQUENCY 1.414 MHz; ION ENERGY 4 V; ENTRANCE APERTURE 0.05 INCH

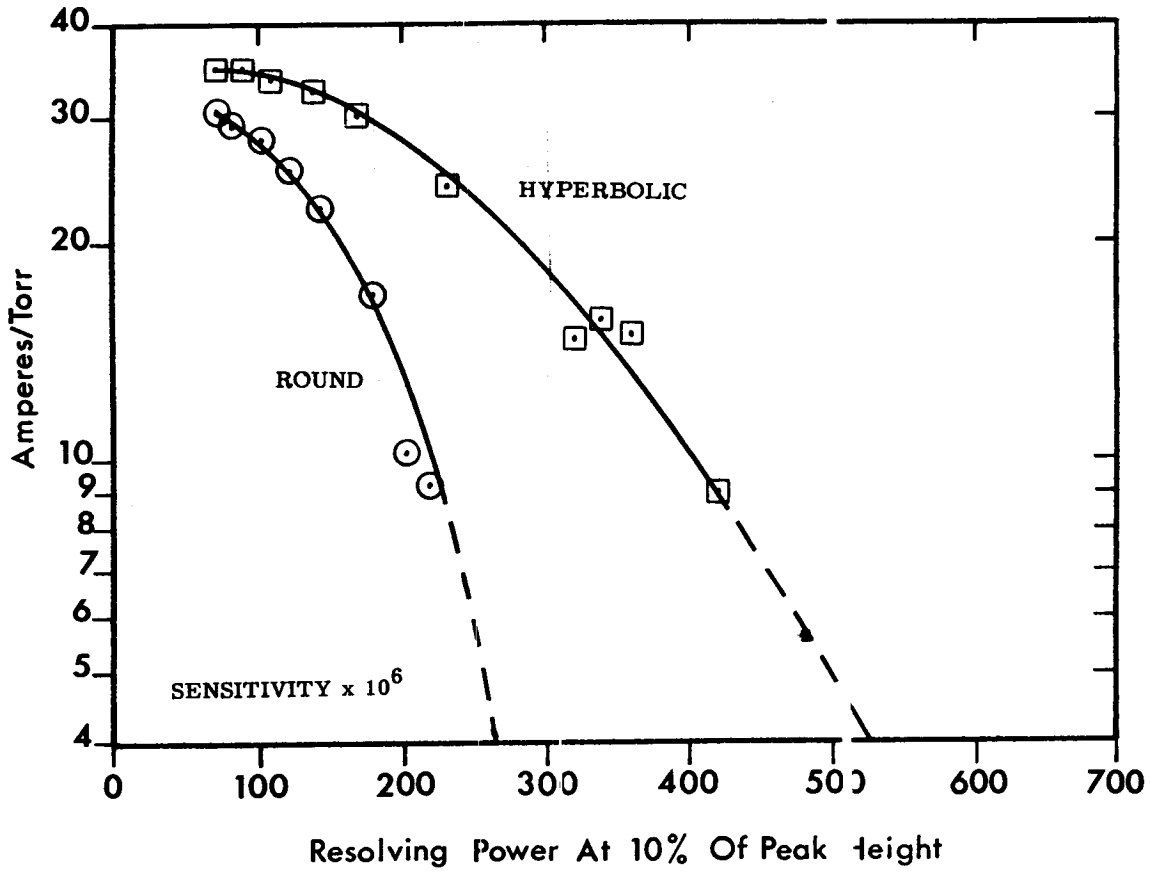

FIGURE 52

SENSITIVITIES OF ROUND AND HYPERBOLIC QUADRUPOLES AS FUNCTIONS OF RESOLVING POWER. EXCITATION FREQUENCY 1.0 MHz; ION ENERGY 2 V; ENTRANCE APERTURE 0.05 INCH

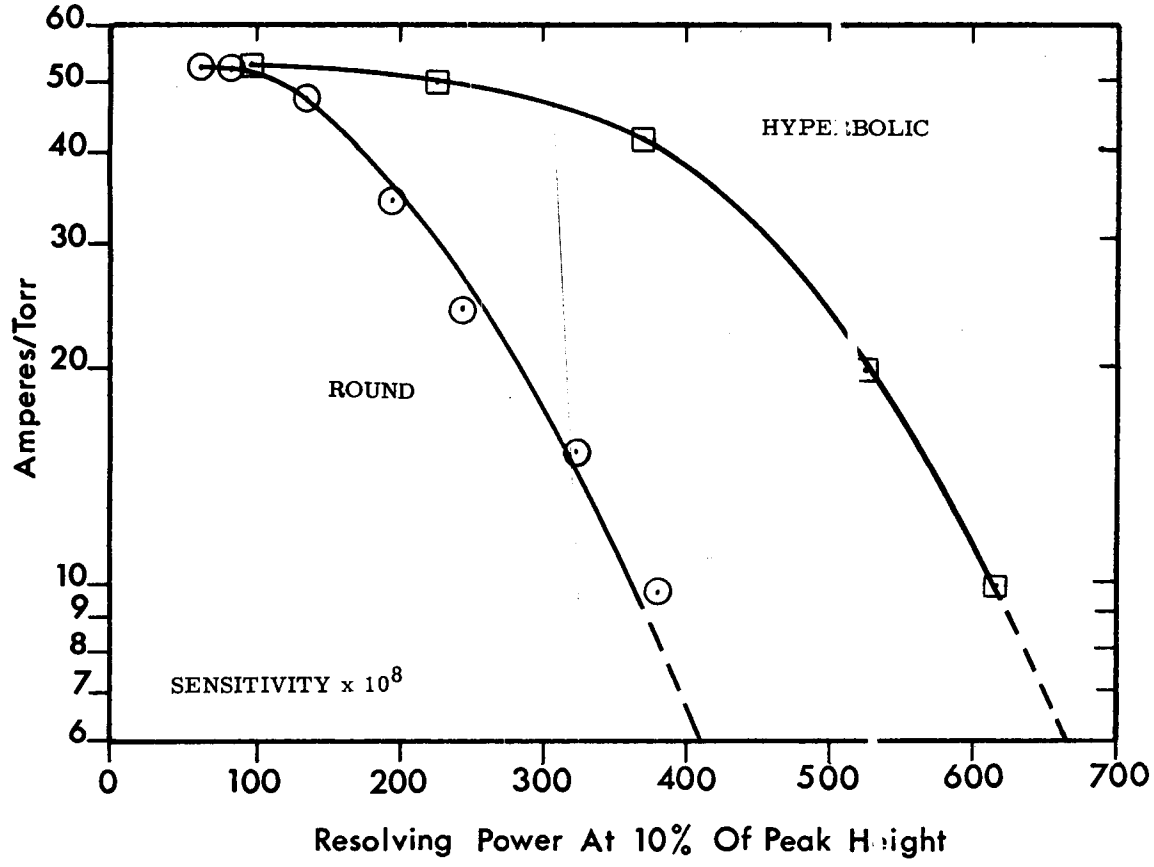

FIGURE 53

SENSITIVITIES OF ROUND AND HYPERBOLIC QUADRUPOLES AS FUNCTIONS OF RESOLVING POWER. EXCITATION FREQUENCY 0.707 MHz; ION ENERGY 1 V; ENTRANCE APERTURE 0.05 INCH

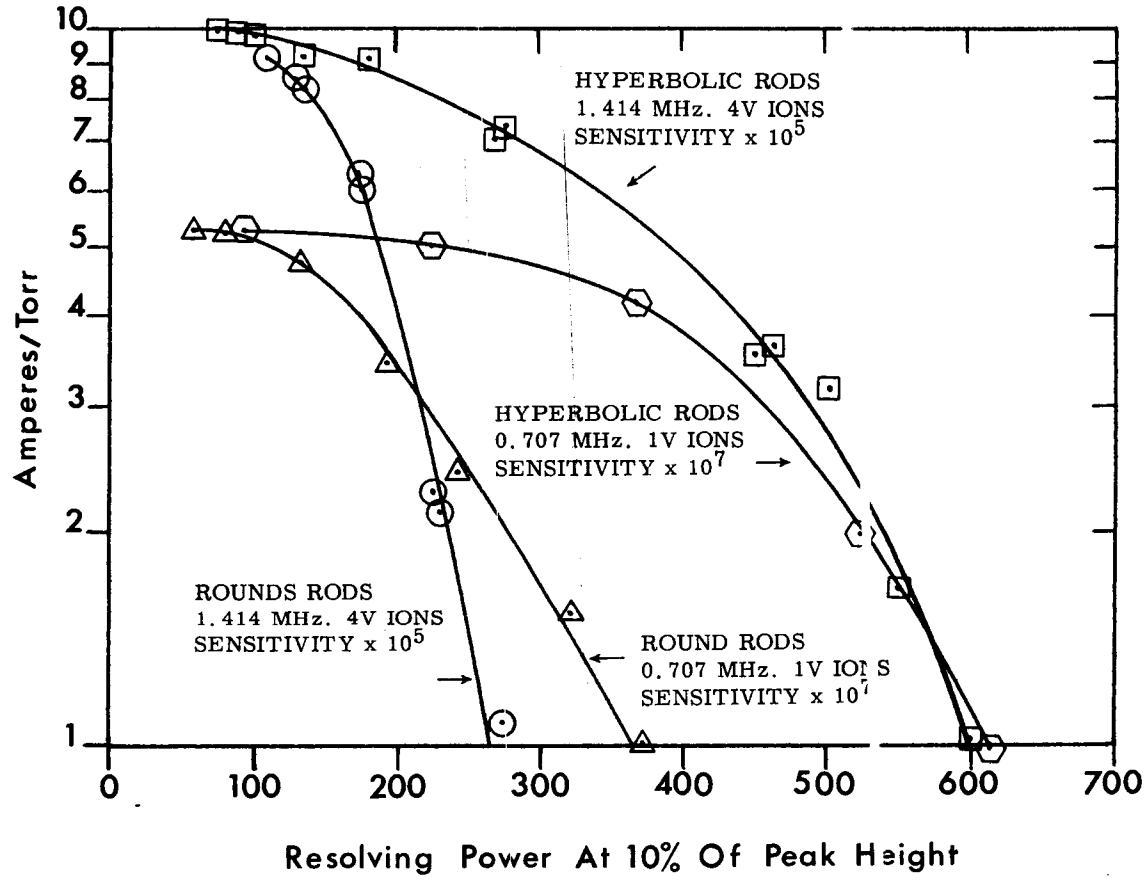

FIGURE 54

SENSITIVITIES OF ROUND AND HYPERBOLIC QUADRUPOLES AS FUNCTIONS OF RESOLVING POWER FOR TWO OPERATING CONDITIONS

ENTRANCE APERTURE 0.05 INCH

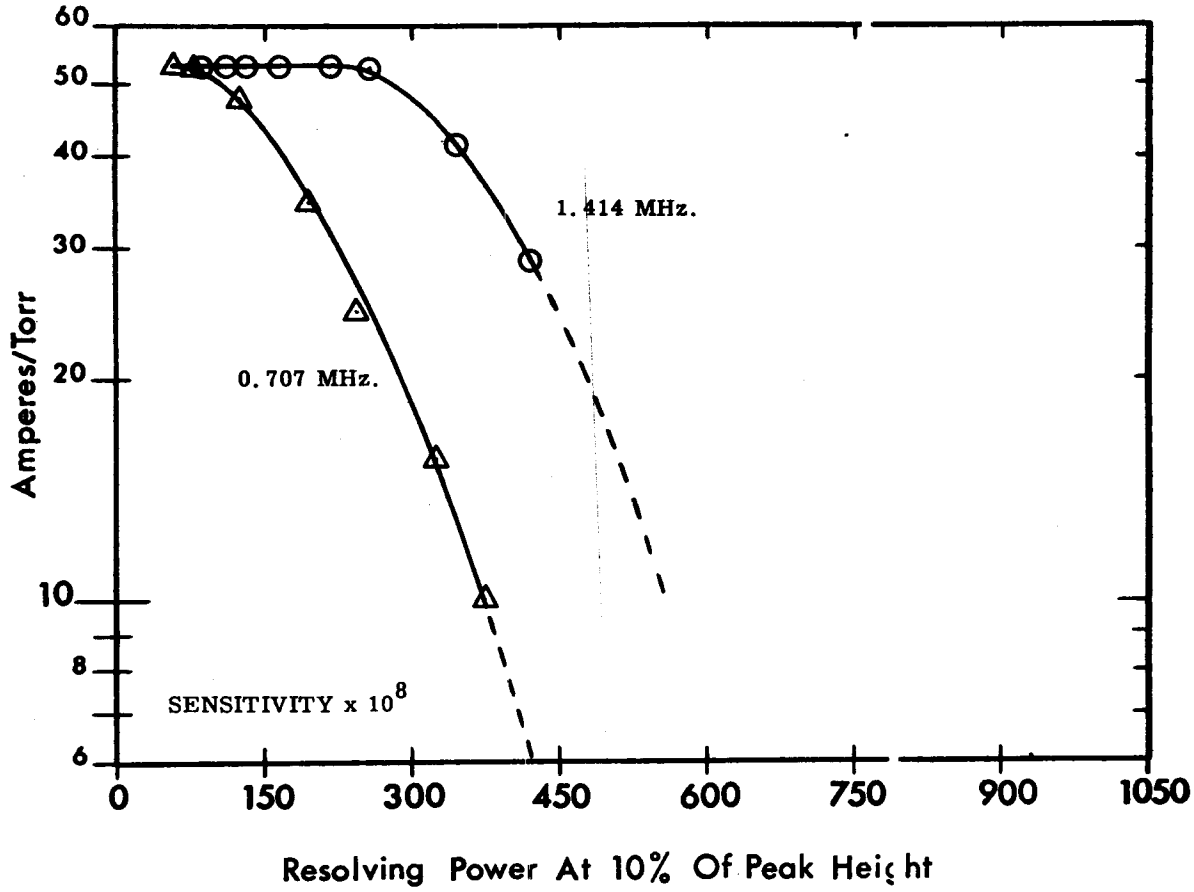

FIGURE 55

SENSITIVITY OF ROUND ROD QUADRUPOLE AS A FUNCTION OF RESOLVING POWER FOR TWO OPERATING FREQUENCIES. ION ENERGY 1 VOLT ENTRANCE APERTURE 0.050 INCH

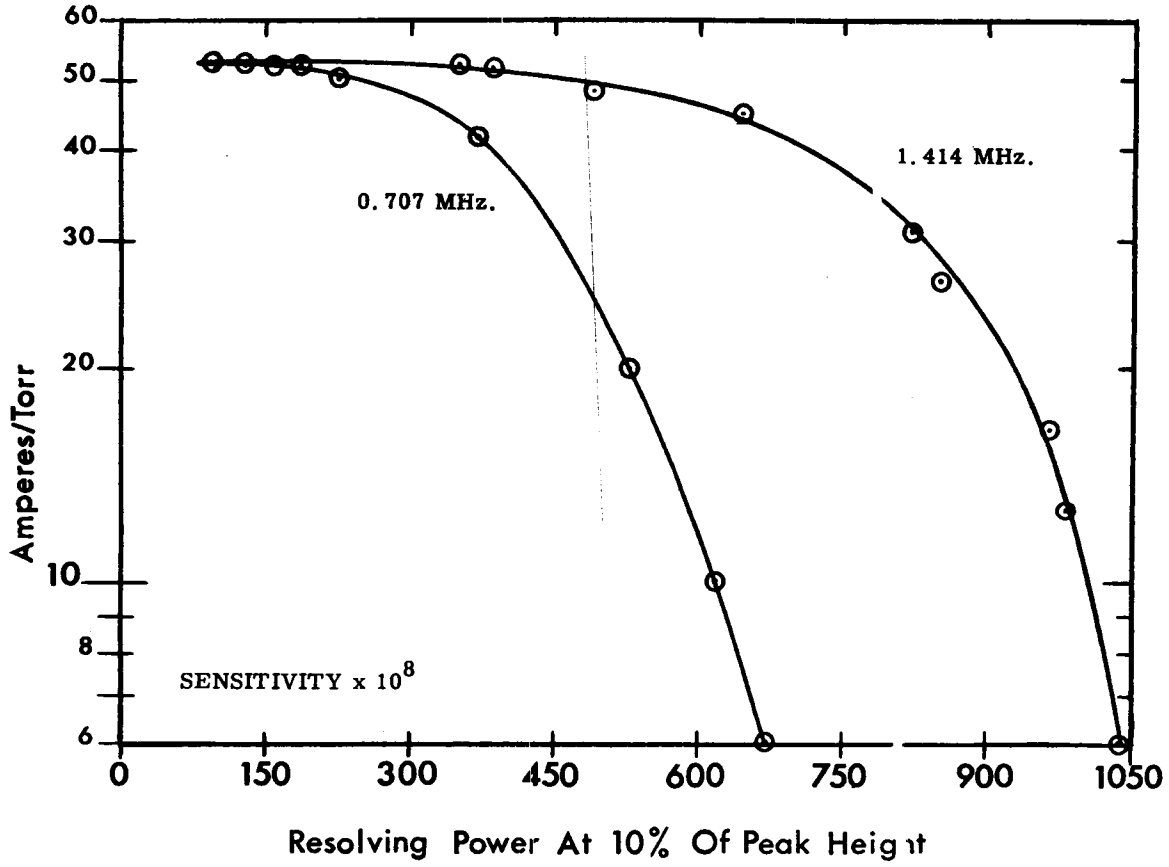

FIGURE 56

SENSITIVITY OF HYPERBOLIC ROD QUADRUPOLE AS A FUNCTION OF RESOLVING POWER FOR TWO OPERATING FREQUENCIES. ION ENERGY 1 V. ENTRANCE APERTURE 0.050 INCH

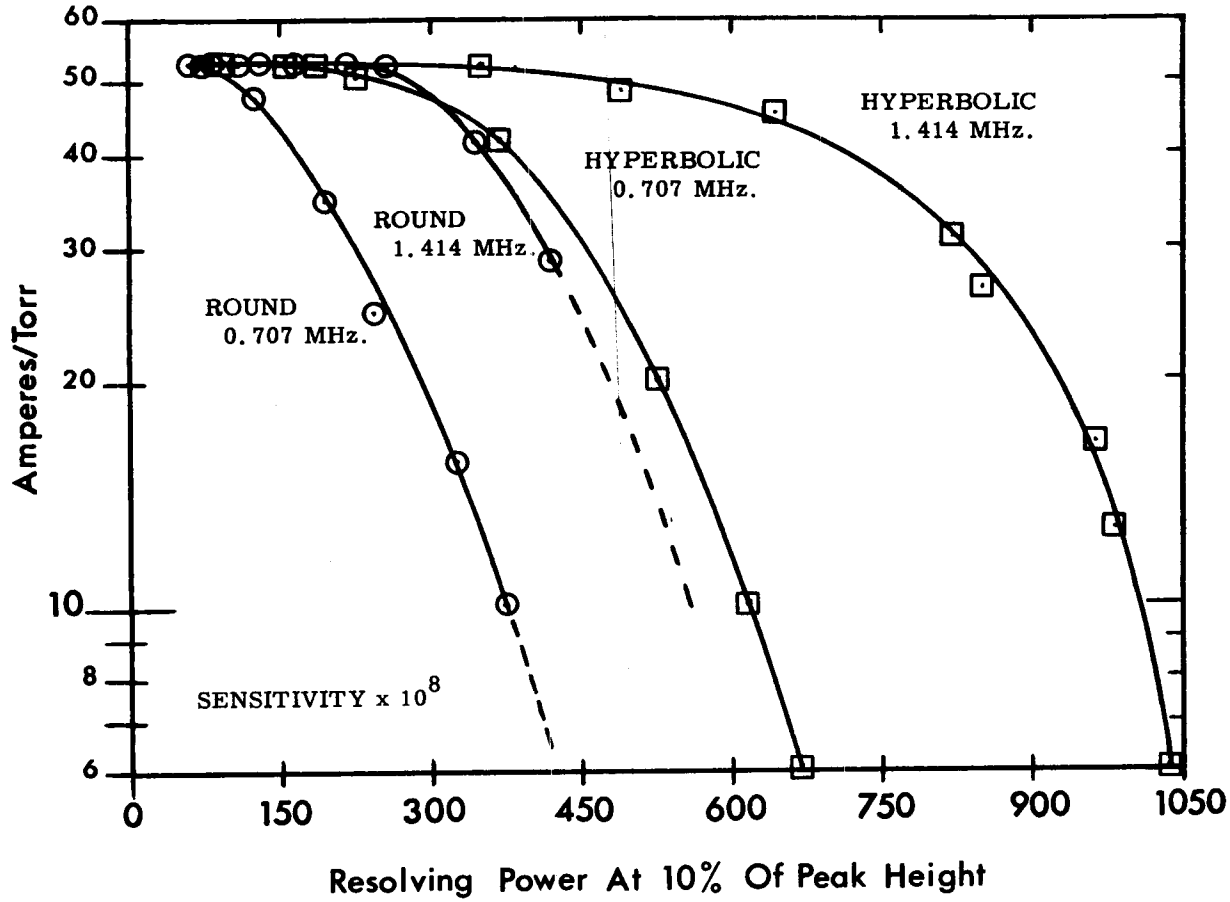

FIGURE 57

SENSITIVITY OF ROUND AND HYPERBOLIC ROD QUADRUPOLES AS A FUNCTION OF RESOLVING POWER FOR TWO OPERATING FREQUENCIES. ION ENERGY 1 V. ENTRANCE APERTURE 0.050 INCH

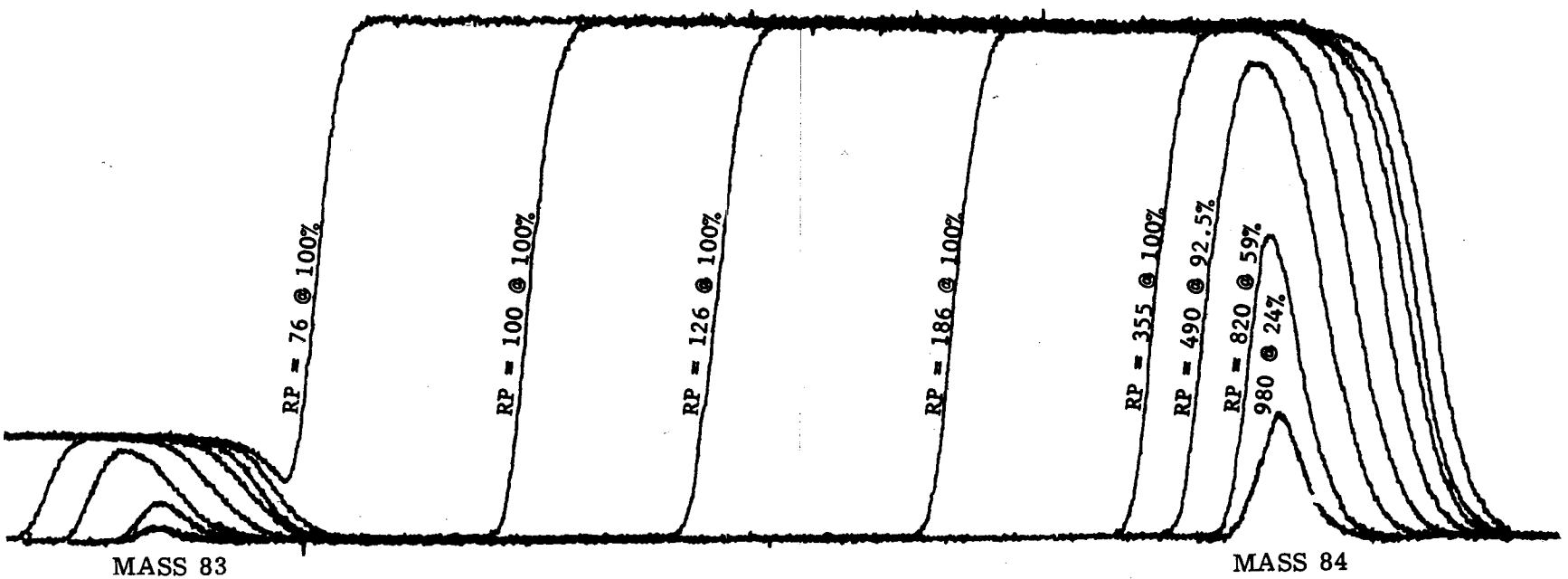

FIGURE 58

MULTIPLE SCANS OF MASS 84 PEAK AT VARIOUS RESOLVING POWERS

EXCITATION FREQUENCY 1.414 MHz.; ION ENERGY 1.0 VOLT
HYPERBOLIC RODS, DELAYED dc MODE OF OPERATION
ENTRANCE APERTURE 0.050 INCH

REFERENCES

[1] Paul, W.; Reinhard, H. P.; and von Zahn, U.: Z. Physik, Vol. 152, 1958, p. 143.

[2] McLachlan: Theory and Application of Mathieu Functions, (Oxford), 1947.

[3] Meixner, J.; and Schafke, F. W.: Mathieusche Funktionen und Spharioid-funktionen. (Berlin), 1954.

[4] Brubaker, W. M.: Auxiliary Electrodes for Quadrupole Mass Filters. U. S. Patent 3,129,327, April 14, 1964.

[5] Brubaker, W. M.; and Tuul, J.: Performance Studies of a Quadrupole Mass Filter. RSI, Vol. 35, Aug. 1964, p. 1007.

APPENDIX

Introduction

The following 36 pages of the Appendix contain the detailed X and Y trajectory plots (Figs. A-1 through A-36). With the exception of a very few drafting errors, these graphs represent an accurate plot of the data printed out in tabular form from the digital computer. Each point on the graph represents a reversal in the corresponding x- or y-component of velocity. Straight lines were drawn from point to point, and no attempt was made to approximate the actual path of the ion between points. In some cases these lines are quite long because, although still modulated by the ac field, the component of velocity does not reverse.

The variations of the ac and dc fields with respect to time are shown on each of the graphs. On the first eight where the ramp is zero, the representation is a straight line at 100% of normal field strength. In all the other graphs, the exact nature of the coincident and delayed ramps is shown with all changes in slope, marked along the top border in cycles of ac field. Both the field characteristic and the ion trajectory are plotted with respect to ωt.

Table A-1, below, shows the figure numbers in the text in which these detailed plots are summarized.

TABLE A-1

Figures in Appendix	Figure in Text
A-1 through A-8	9a
A-9 through A-16	9b
A-17 through A-24	9c
A-25 through A-36	10
A-1 through A-36	11

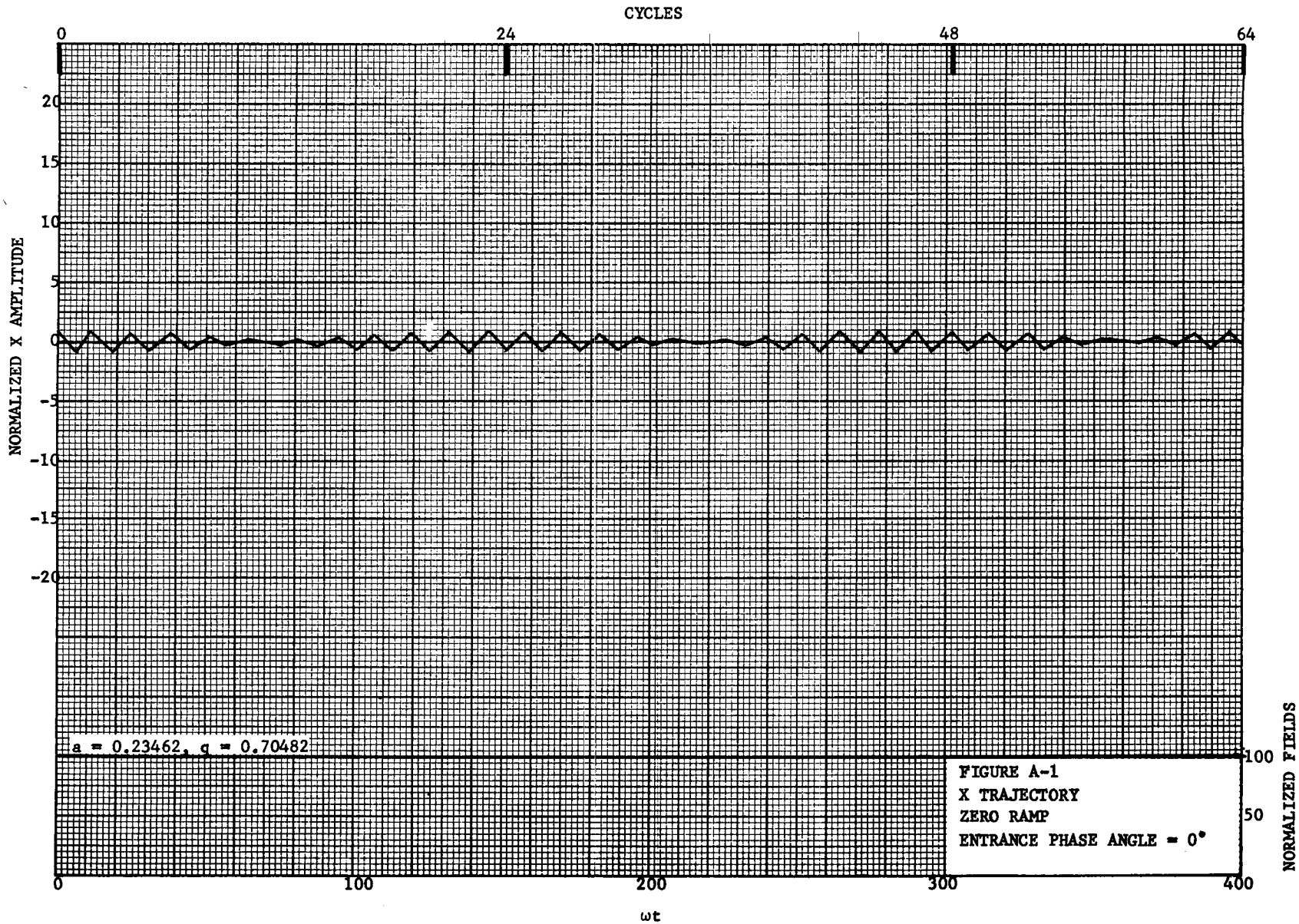

FIGURE A-1
X TRAJECTORY
ZERO RAMP
ENTRANCE PHASE ANGLE = 0°

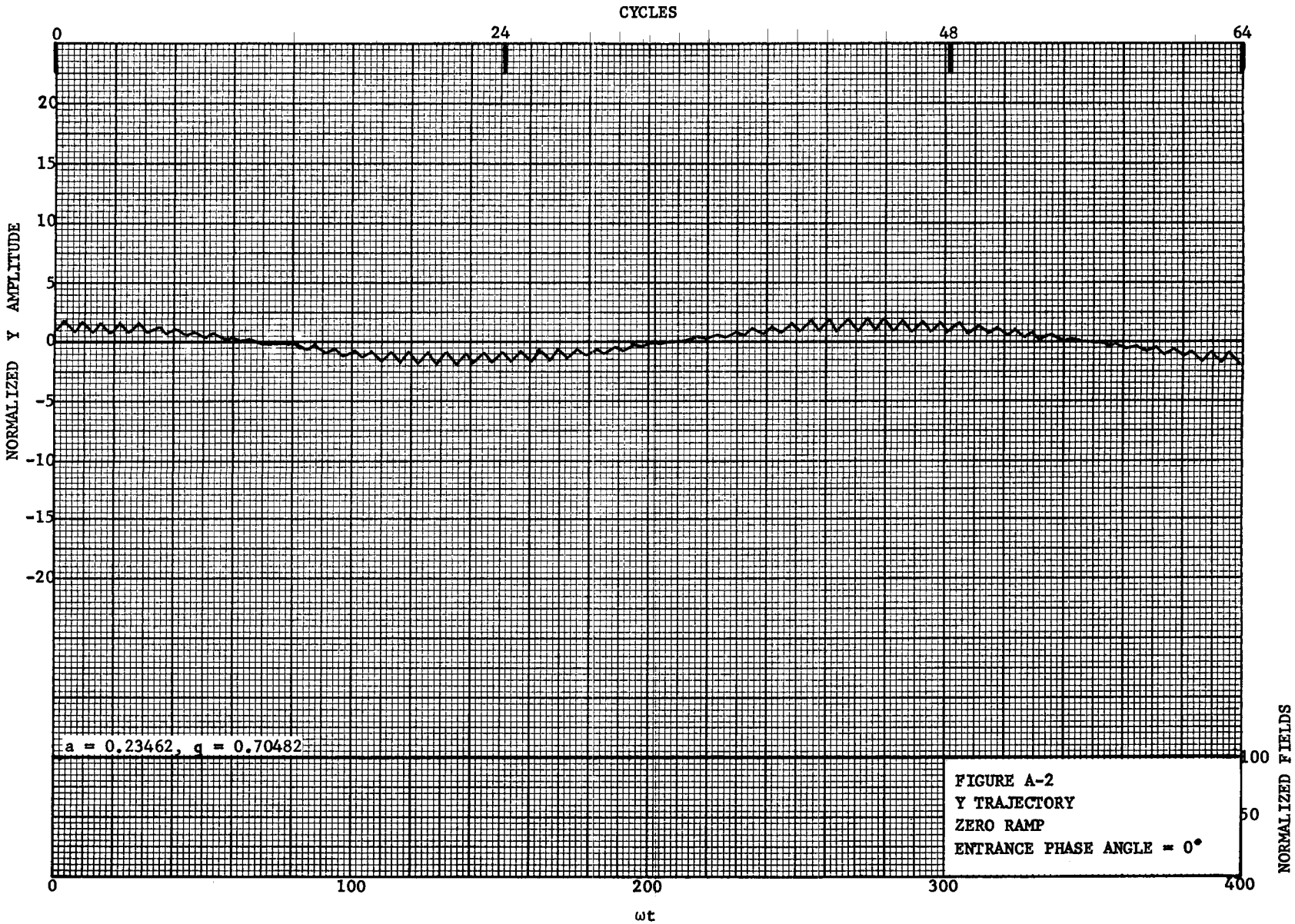
CYCLES
0
24
48
64
20
15
10
5
0
-5
-10
-15
-20
NORMALIZED Y AMPLITUDE
a = 0.23462, q = 0.70482
0
100
200
300
400
ωt
100
50
NORMALIZED FIELDS
FIGURE A-2
Y TRAJECTORY
ZERO RAMP
ENTRANCE PHASE ANGLE = 0°

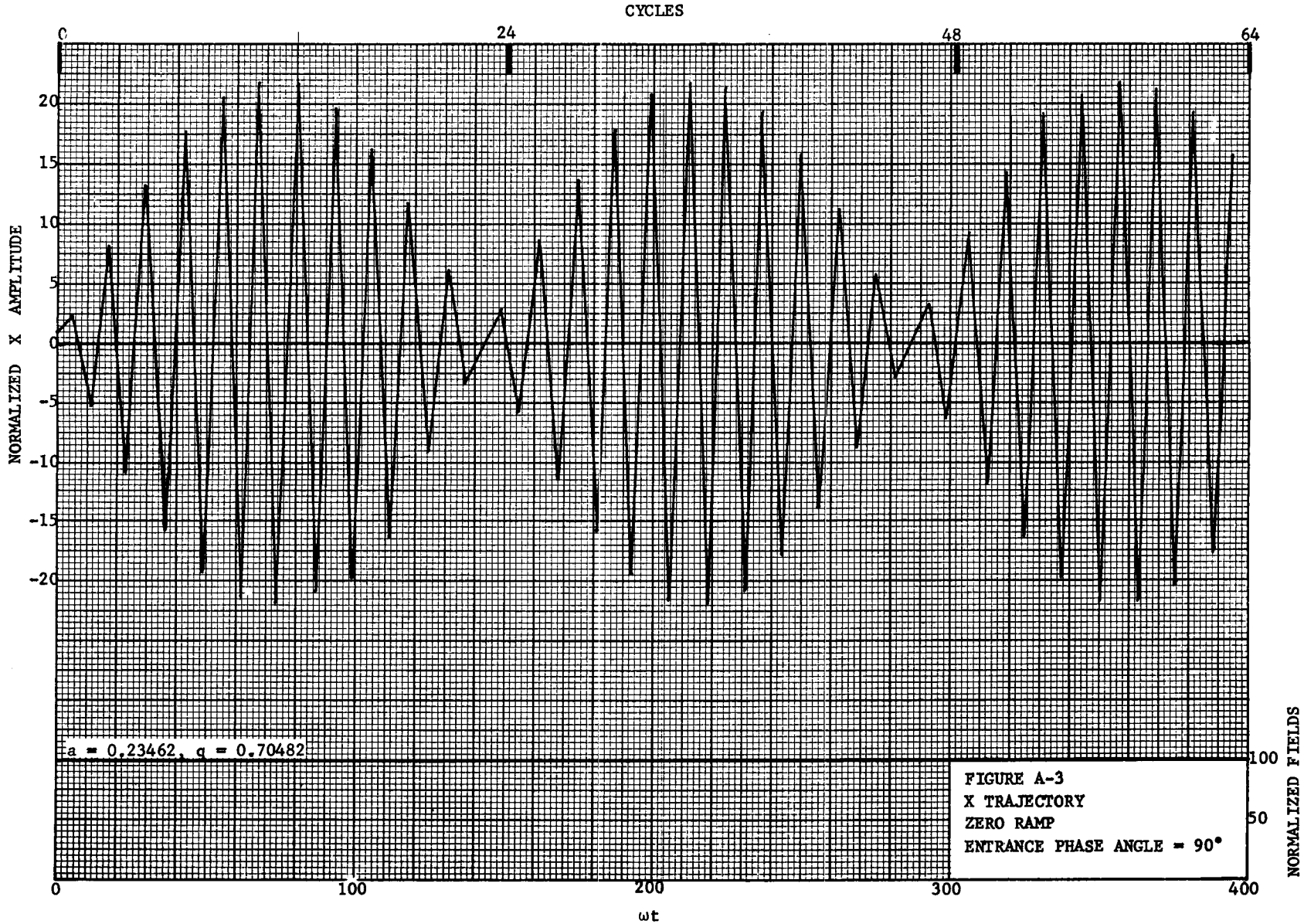

FIGURE A-3
X TRAJECTORY
ZERO RAMP
ENTRANCE PHASE ANGLE = 90°

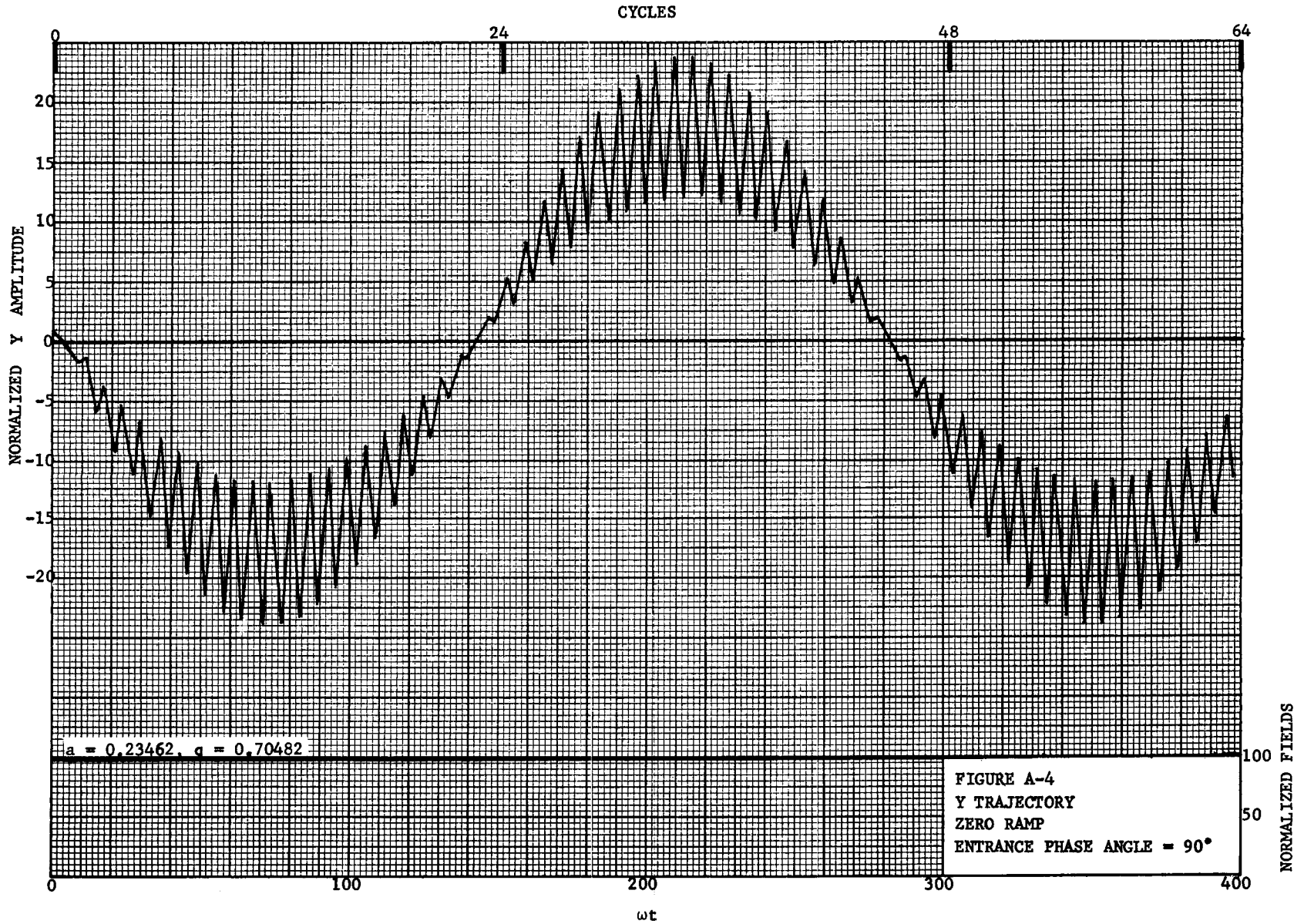

FIGURE A-4
Y TRAJECTORY
ZERO RAMP
ENTRANCE PHASE ANGLE = 90°

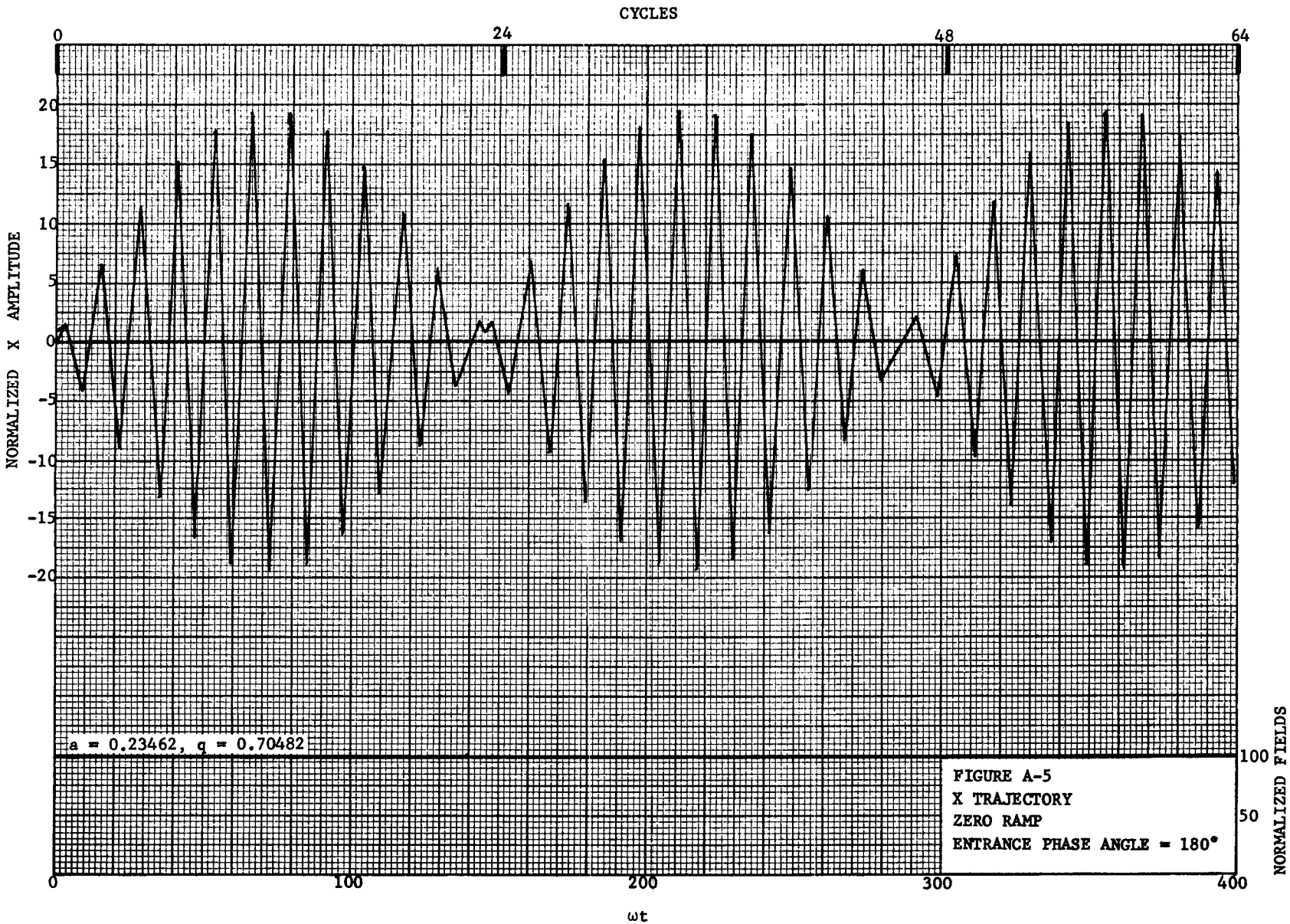

FIGURE A-5
X TRAJECTORY
ZERO RAMP
ENTRANCE PHASE ANGLE = 180°

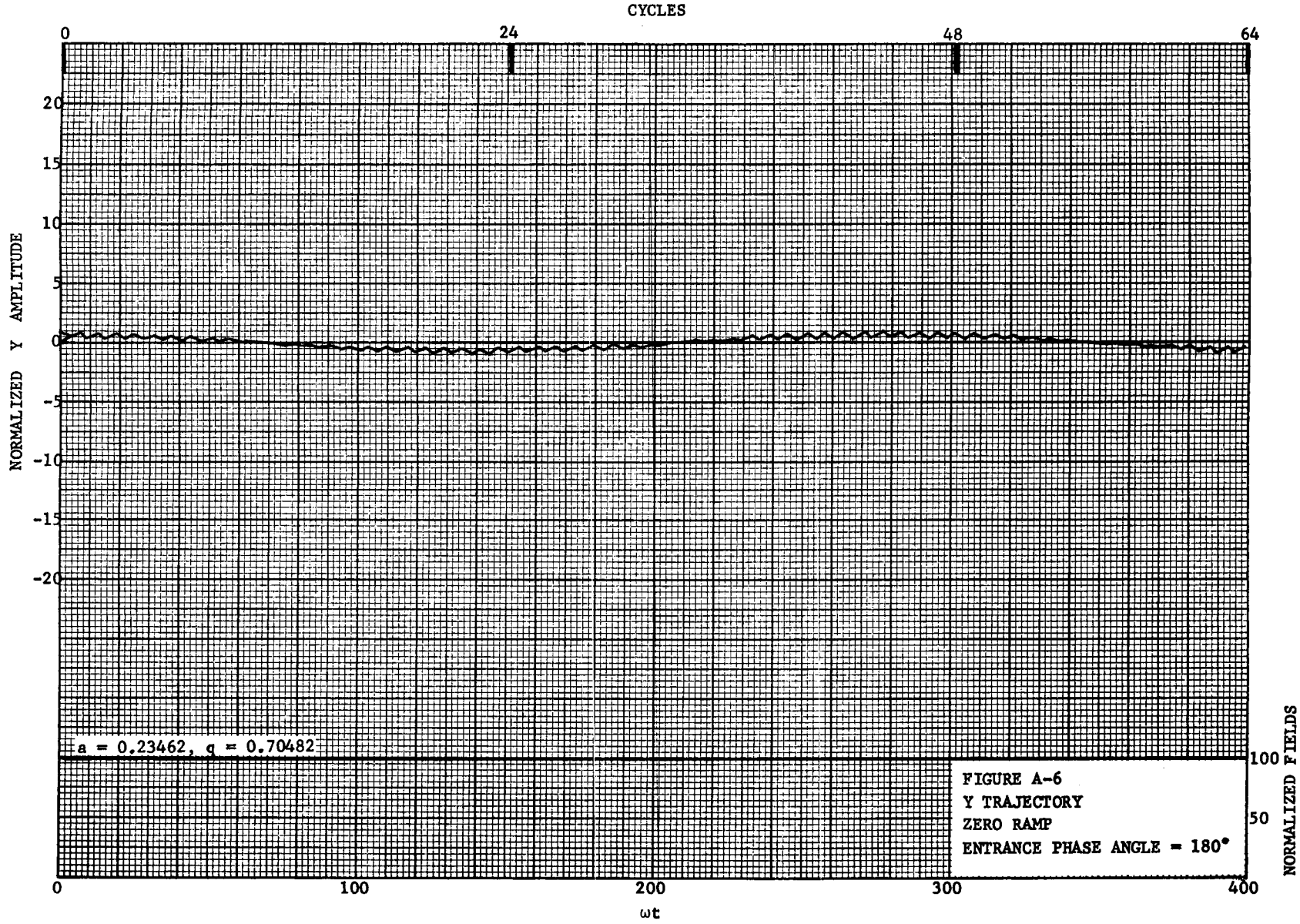
CYCLES
0
24
48
64
20
15
10
5
0
-5
-10
-15
-20
NORMALIZED Y AMPLITUDE
a = 0.23462, q = 0.70482
0
100
200
300
400
ωt
100
50
NORMALIZED FIELDS
FIGURE A-6
Y TRAJECTORY
ZERO RAMP
ENTRANCE PHASE ANGLE = 180°

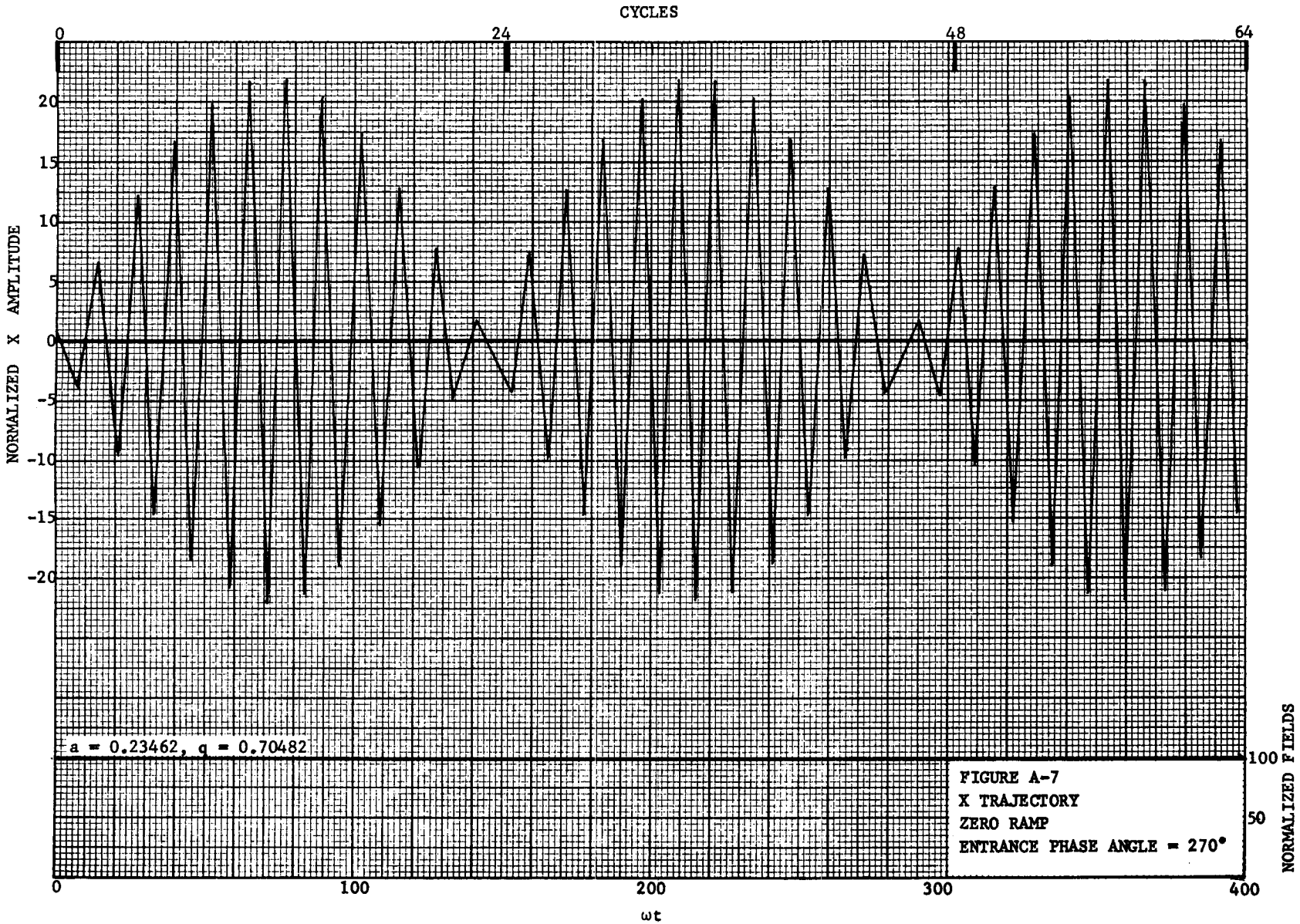

FIGURE A-7
X TRAJECTORY
ZERO RAMP
ENTRANCE PHASE ANGLE = 270°

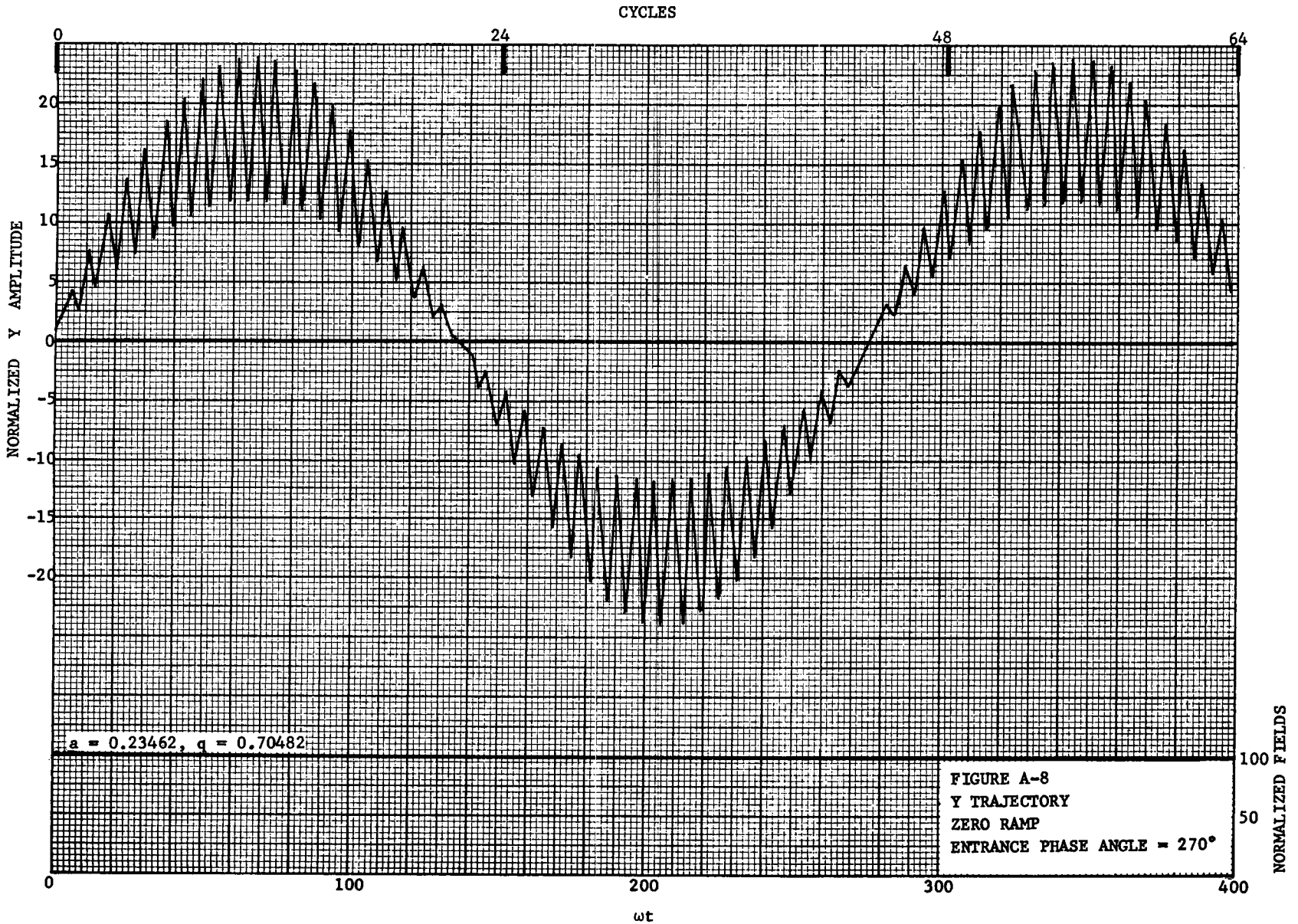

FIGURE A-8
Y TRAJECTORY
ZERO RAMP
ENTRANCE PHASE ANGLE = 270°

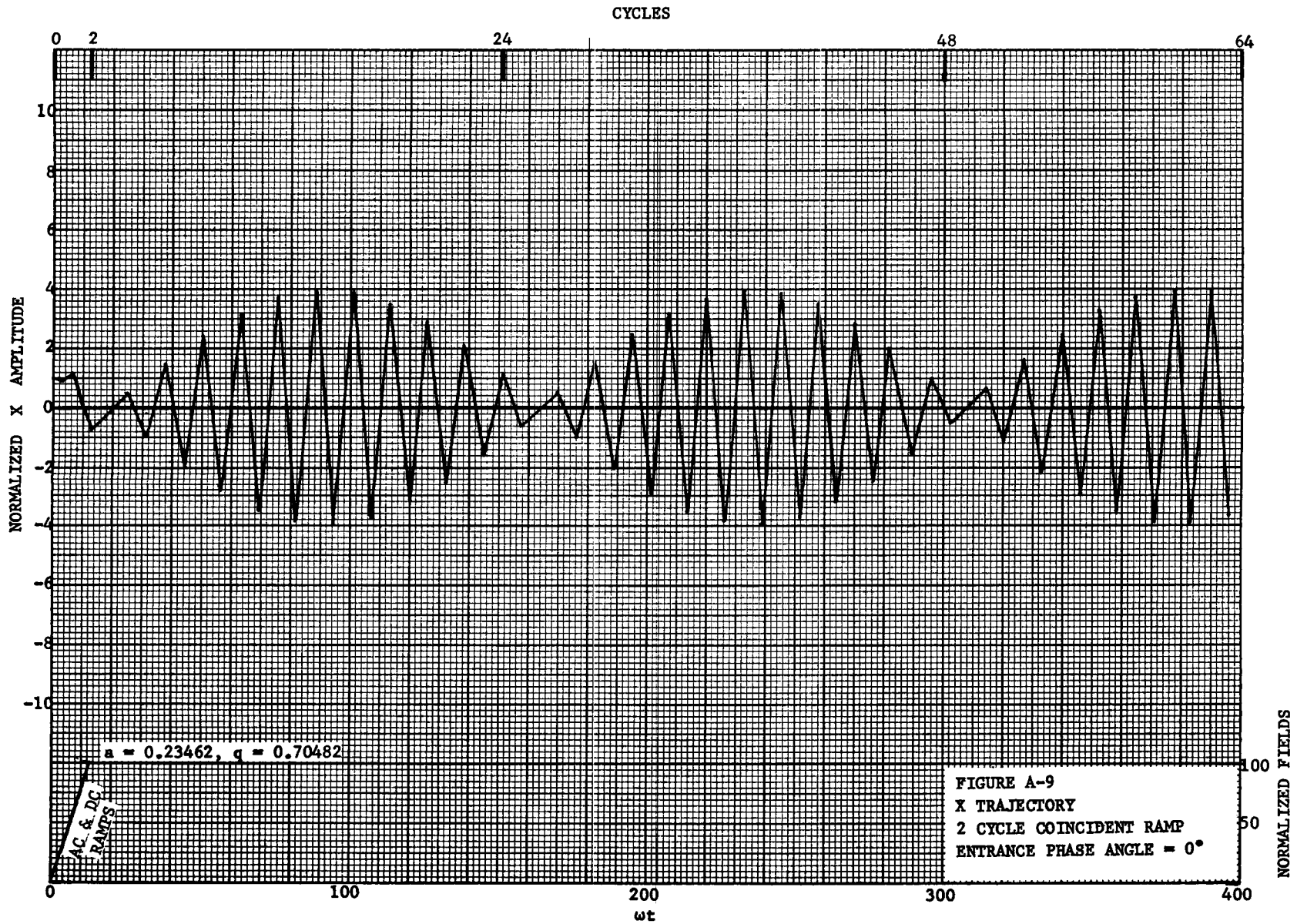

FIGURE A-9
X TRAJECTORY
2 CYCLE COINCIDENT RAMP
ENTRANCE PHASE ANGLE = 0°

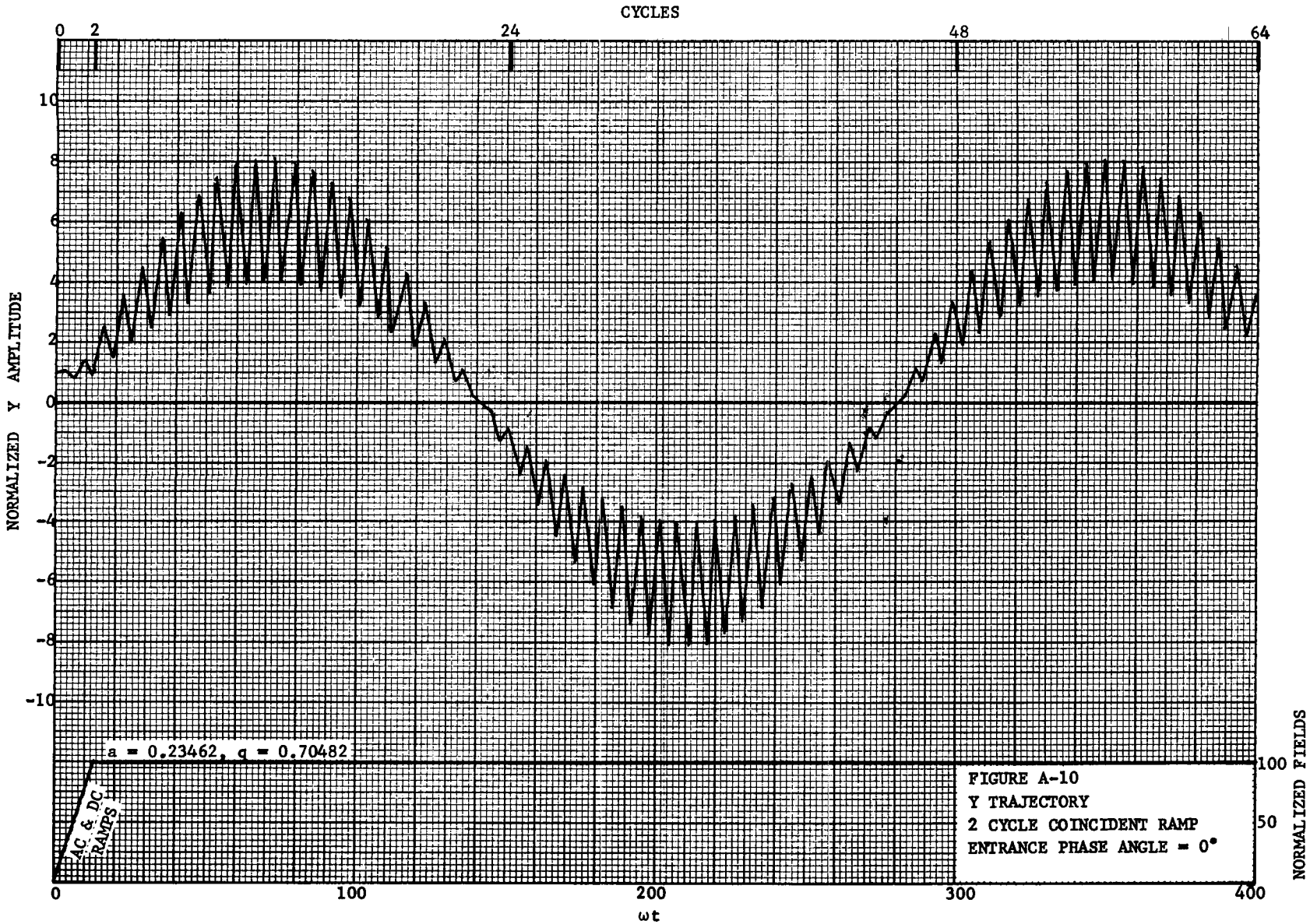

FIGURE A-10
Y TRAJECTORY
2 CYCLE COINCIDENT RAMP
ENTRANCE PHASE ANGLE = 0°

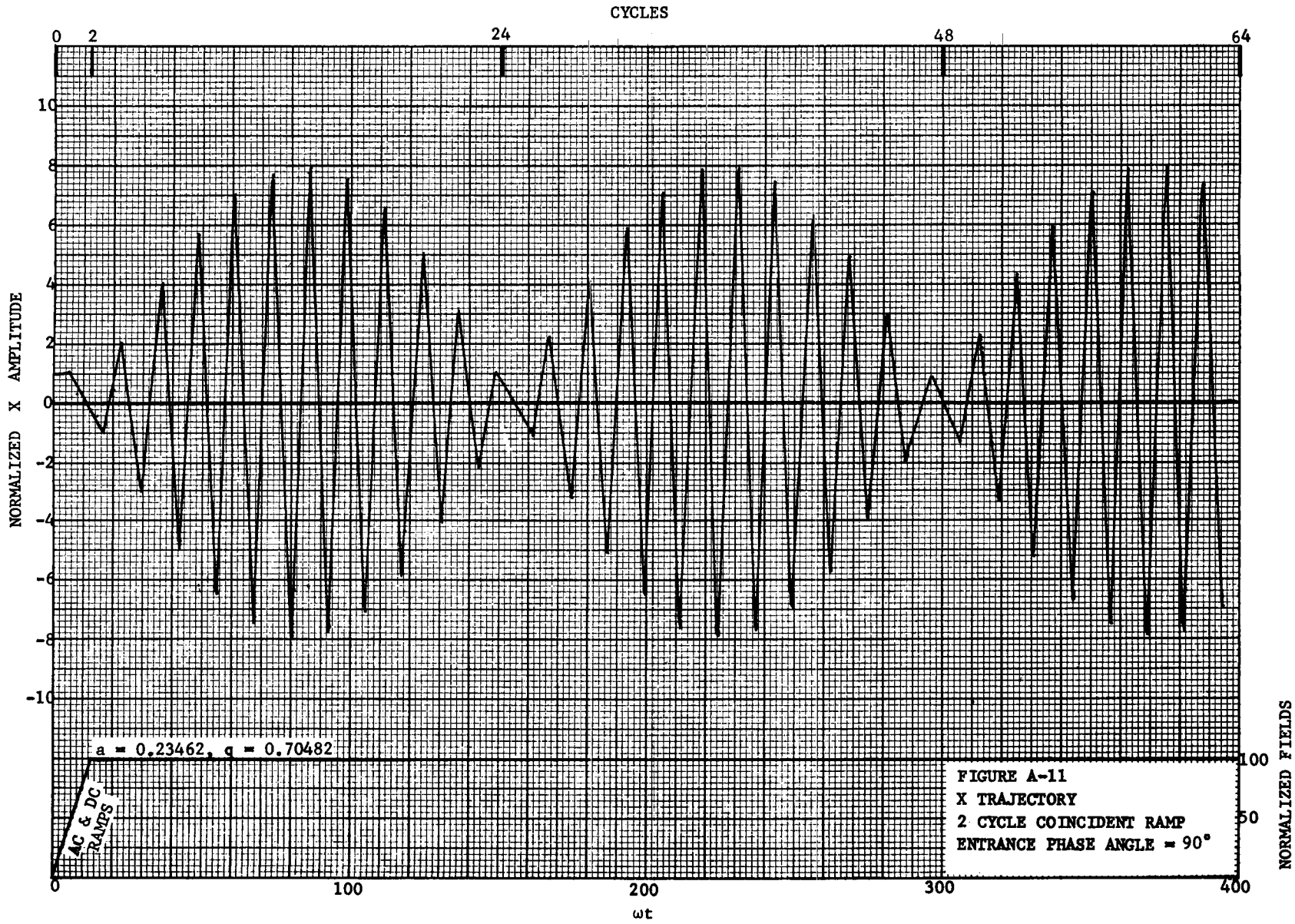

FIGURE A-11
X TRAJECTORY
2 CYCLE COINCIDENT RAMP
ENTRANCE PHASE ANGLE = 90°

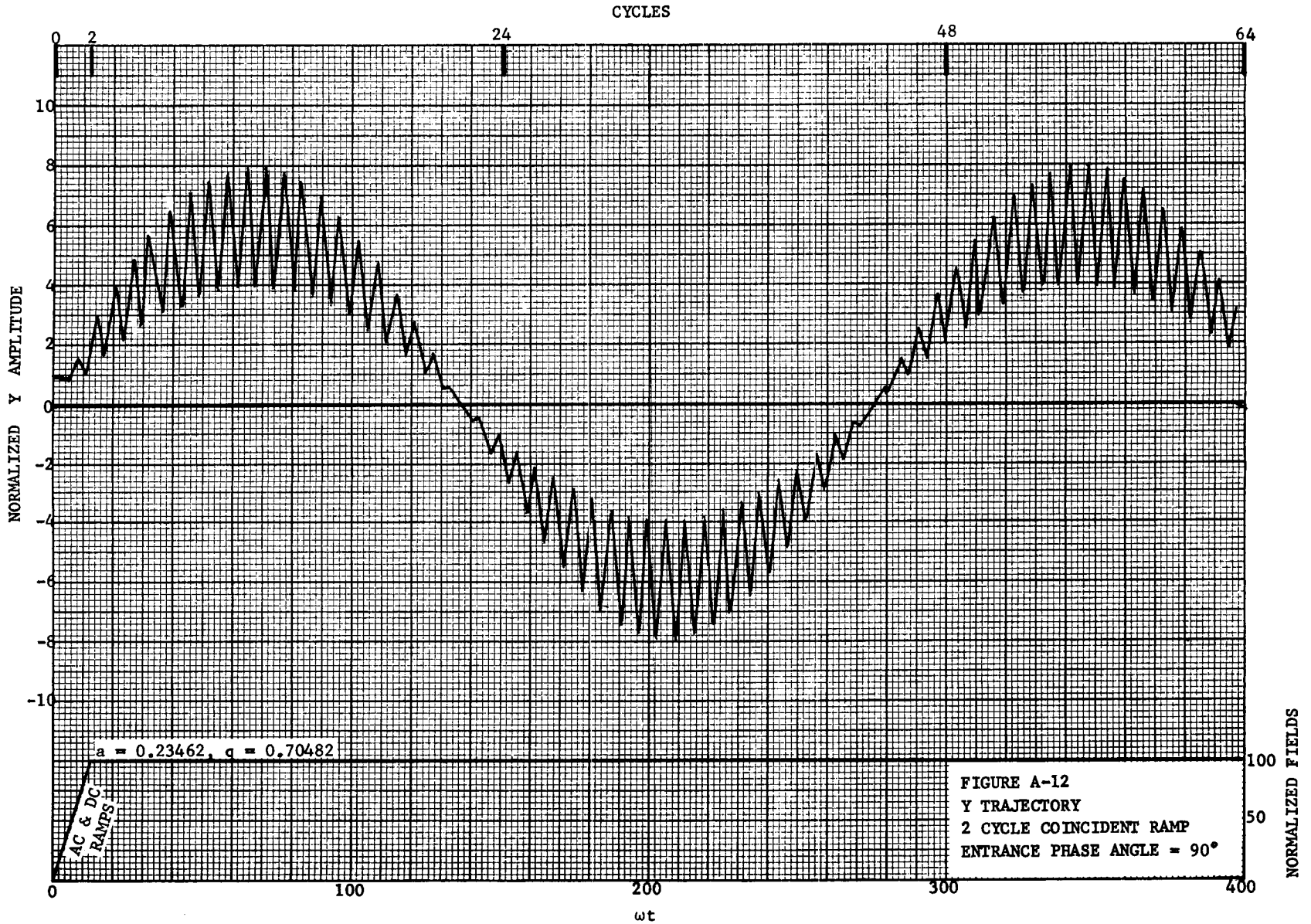

FIGURE A-12
Y TRAJECTORY
2 CYCLE COINCIDENT RAMP
ENTRANCE PHASE ANGLE = 90°

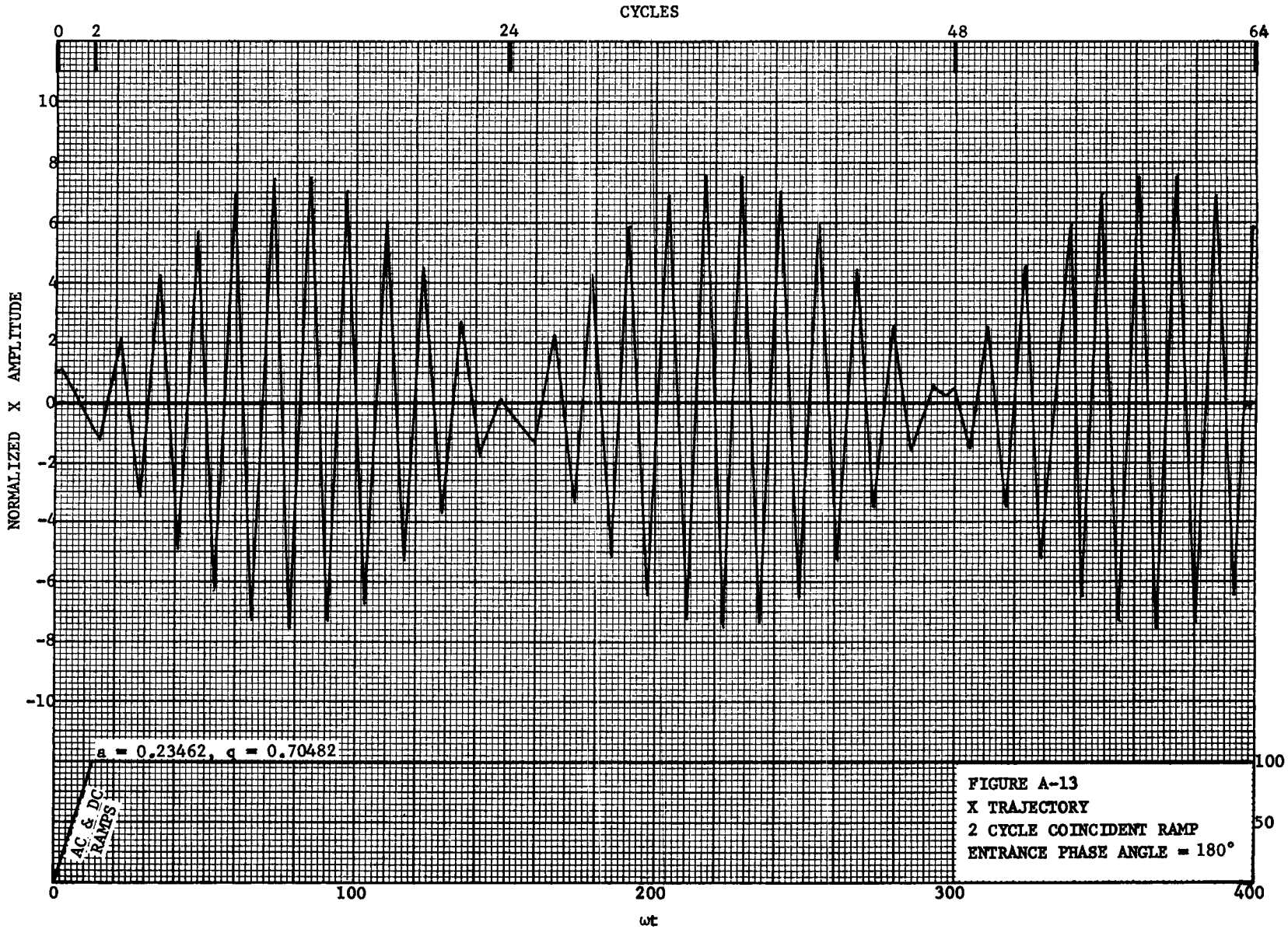

FIGURE A-13
X TRAJECTORY
2 CYCLE COINCIDENT RAMP
ENTRANCE PHASE ANGLE = 180°

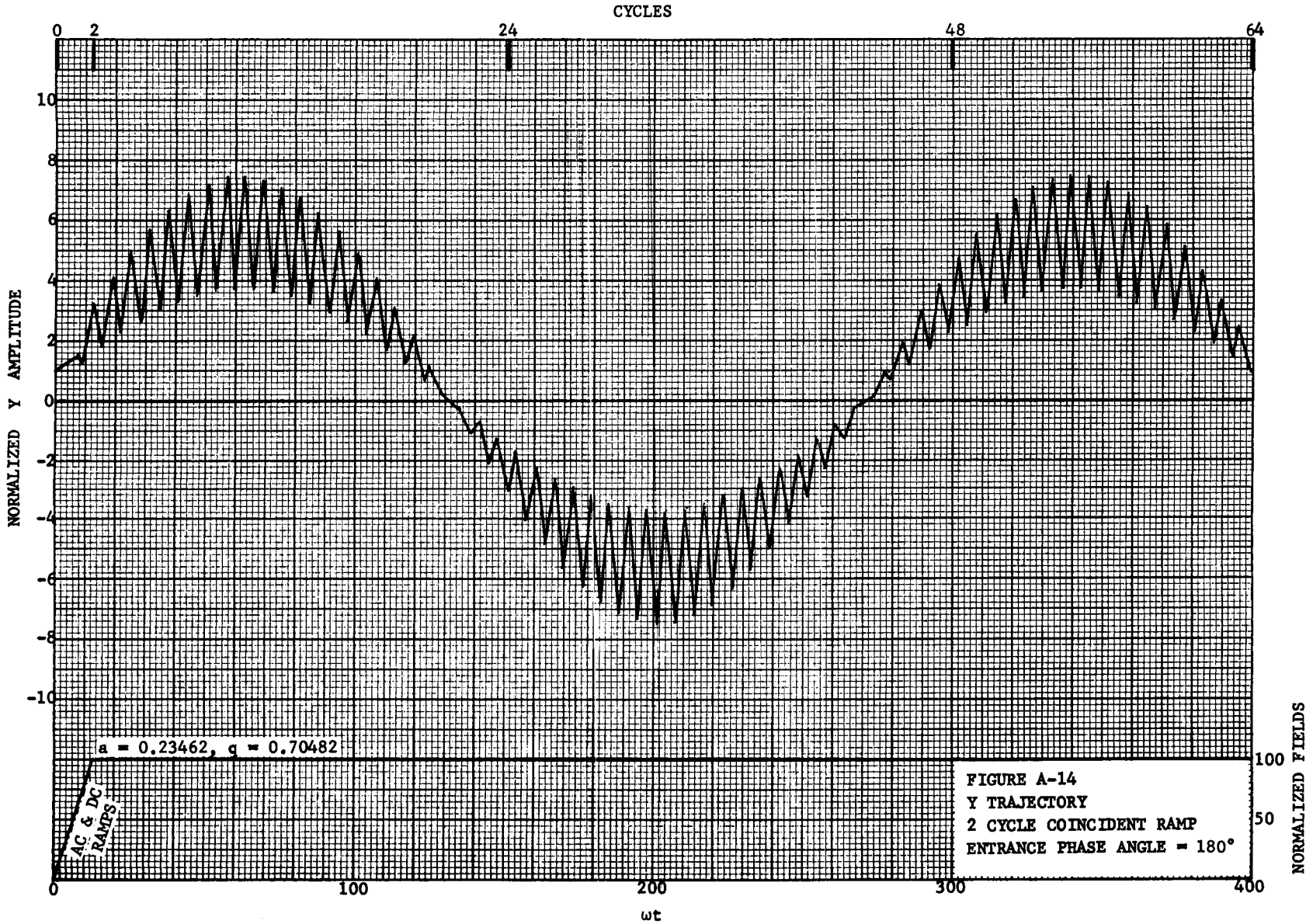

FIGURE A-14
Y TRAJECTORY
2 CYCLE COINCIDENT RAMP
ENTRANCE PHASE ANGLE = 180°

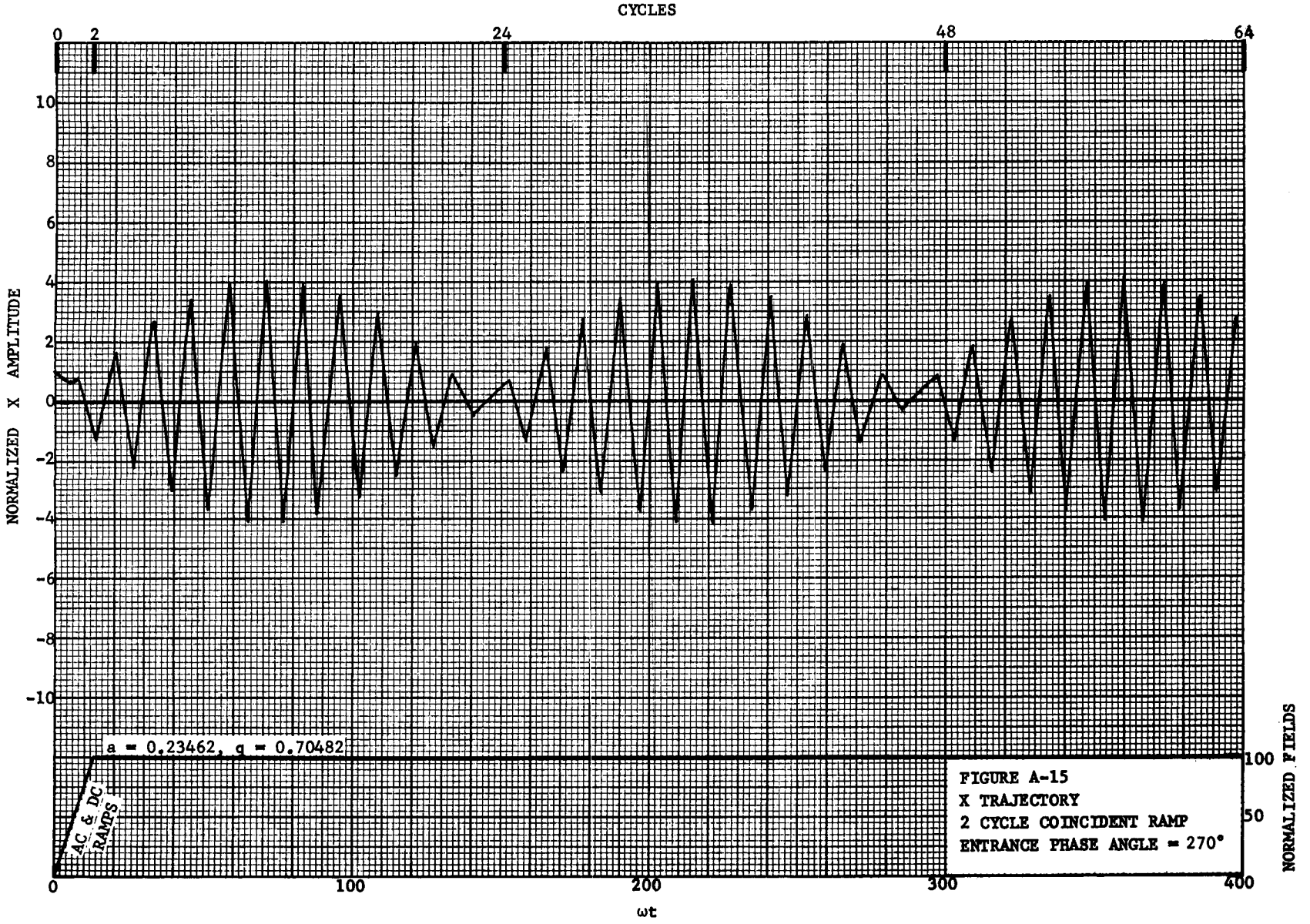

FIGURE A-15
X TRAJECTORY
2 CYCLE COINCIDENT RAMP
ENTRANCE PHASE ANGLE = 270°

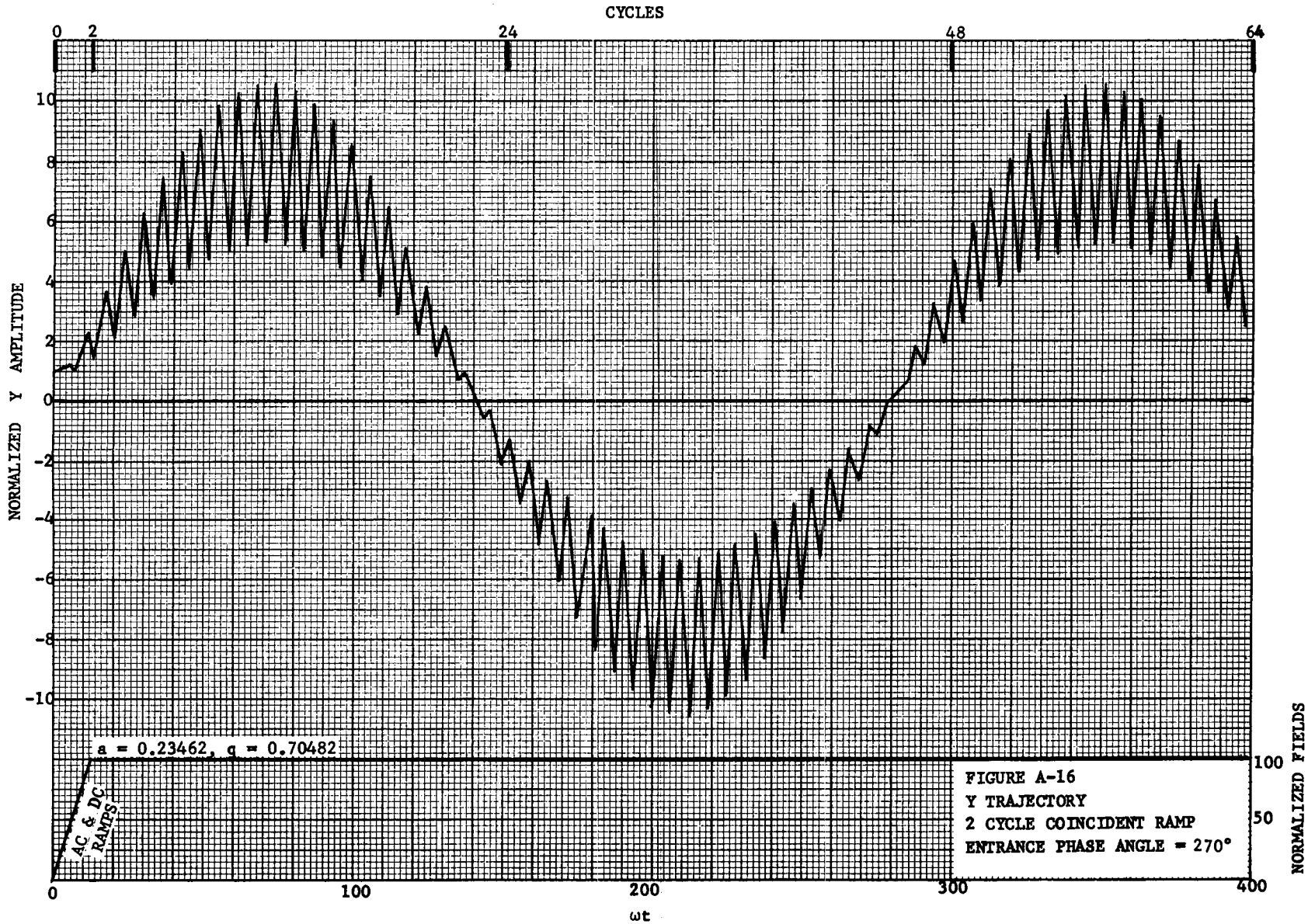

FIGURE A-16
Y TRAJECTORY
2 CYCLE COINCIDENT RAMP
ENTRANCE PHASE ANGLE = 270°

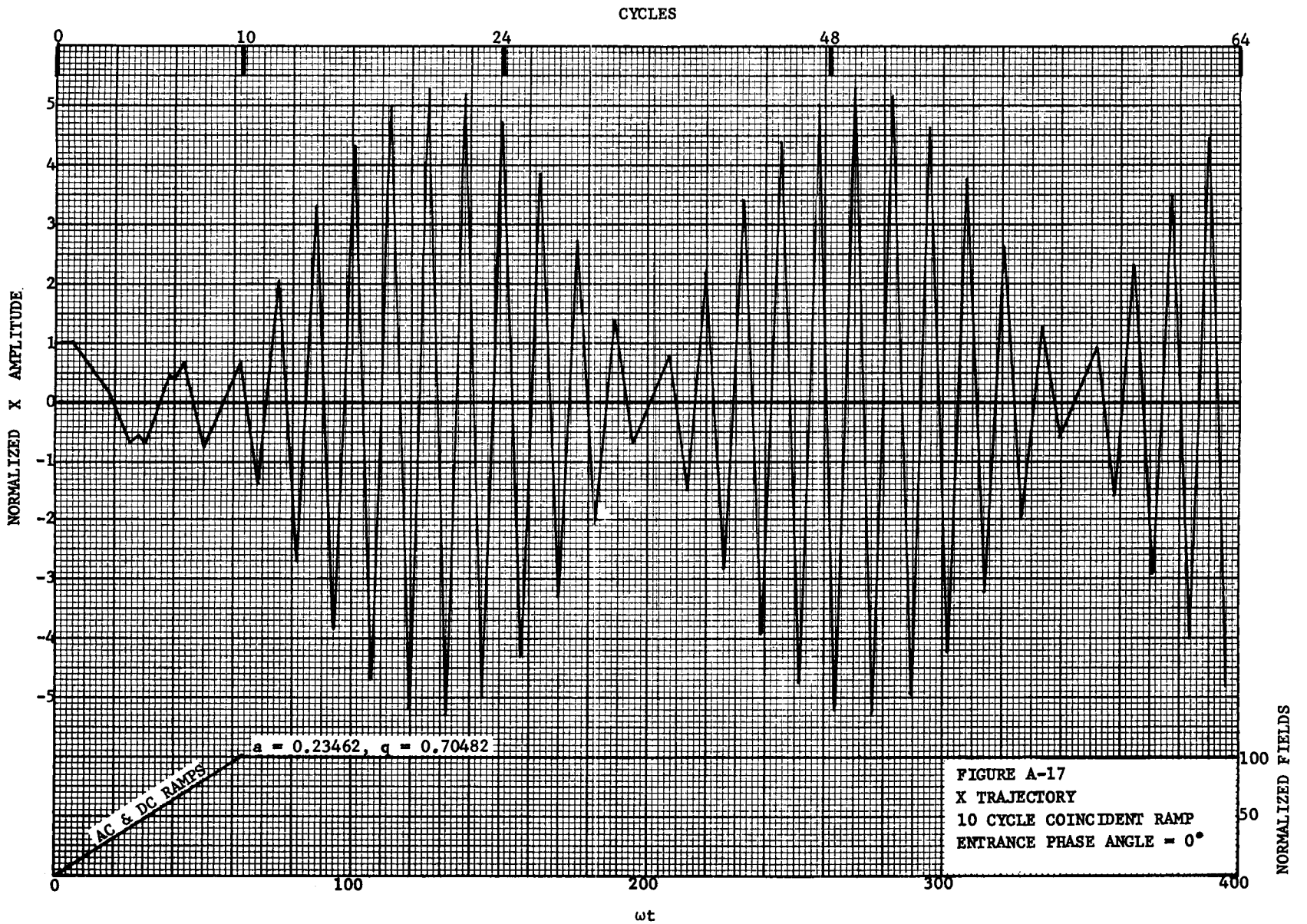

FIGURE A-17
X TRAJECTORY
10 CYCLE COINCIDENT RAMP
ENTRANCE PHASE ANGLE = 0°

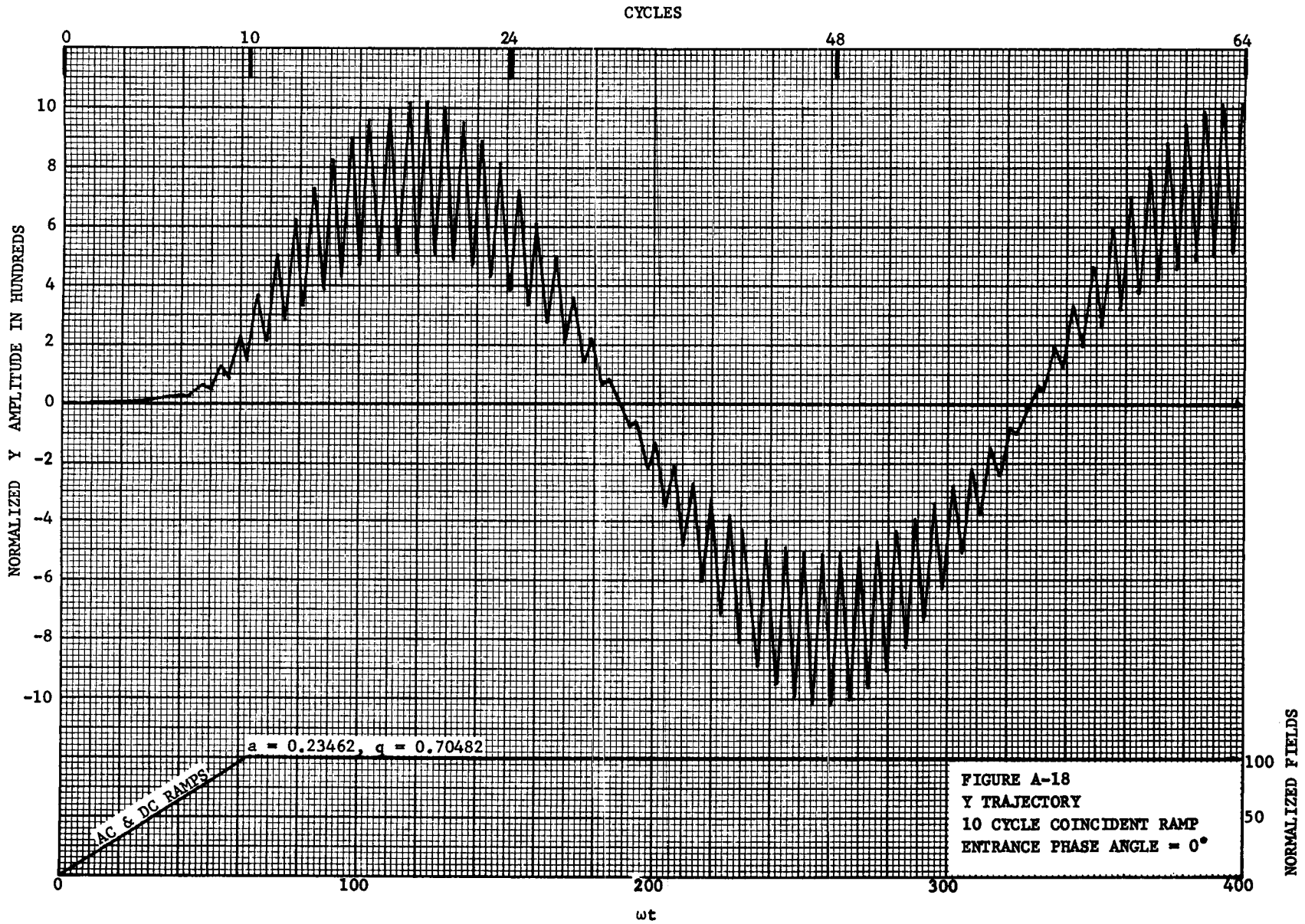

FIGURE A-18
Y TRAJECTORY
10 CYCLE COINCIDENT RAMP
ENTRANCE PHASE ANGLE = 0°

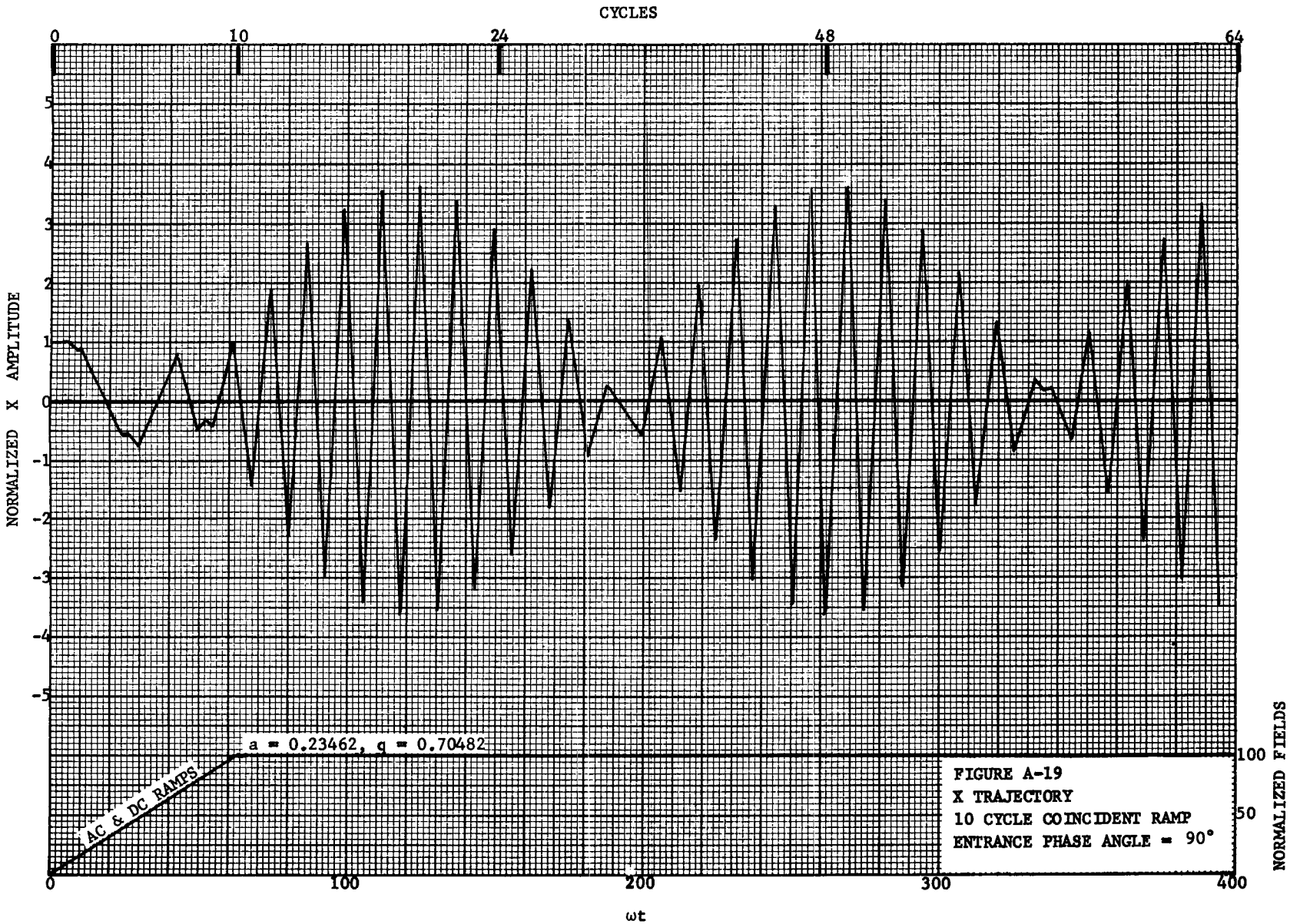
CYCLES
0
10
24
48
64
NORMALIZED X AMPLITUDE
5
4
3
2
1
0
-1
-2
-3
-4
-5
a = 0.23462, q = 0.70482
AC & DC RAMPS
0
100
200
300
400
ωt
100
50
NORMALIZED FIELDS
FIGURE A-19
X TRAJECTORY
10 CYCLE COINCIDENT RAMP
ENTRANCE PHASE ANGLE = 90°

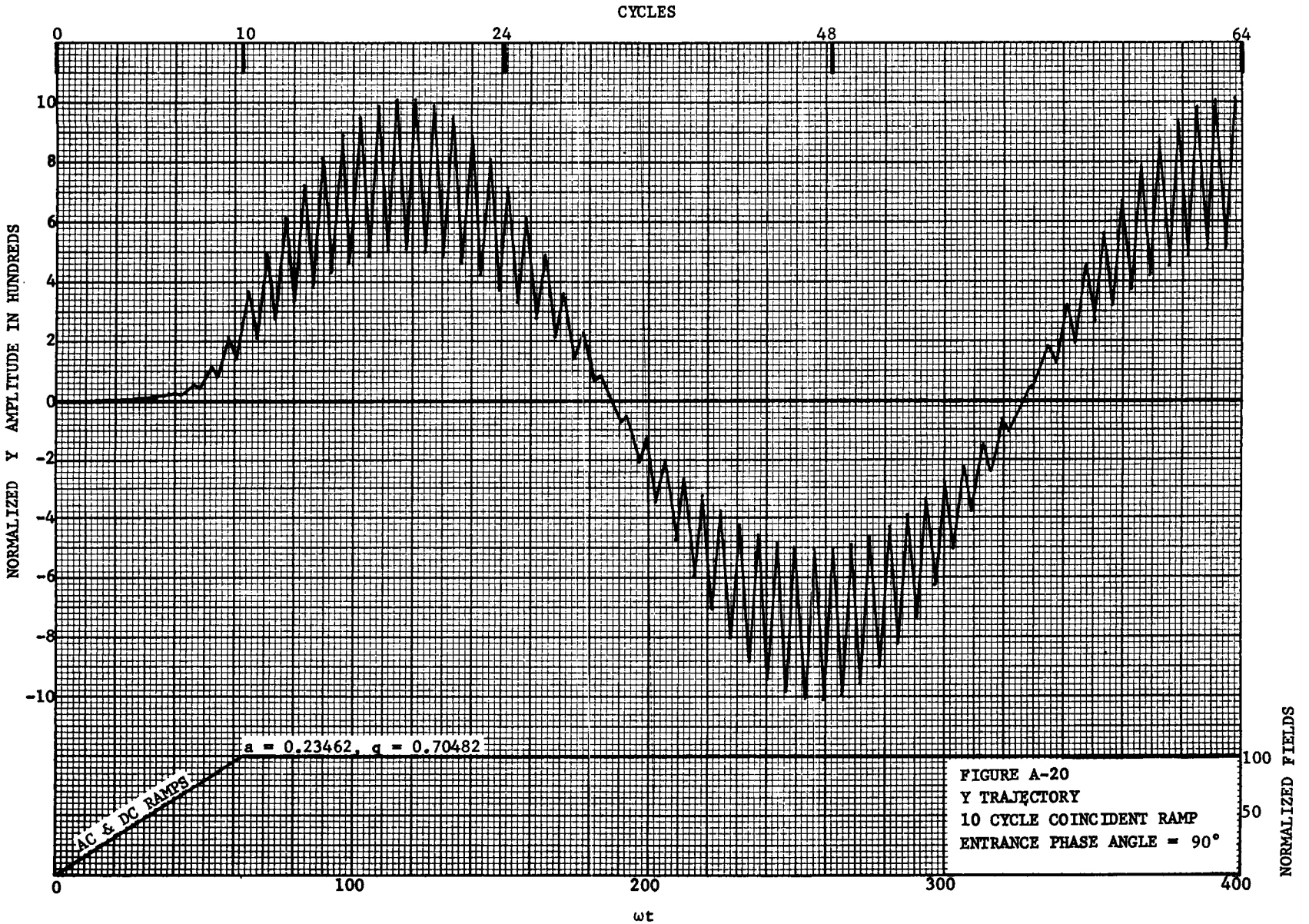

FIGURE A-20
Y TRAJECTORY
10 CYCLE COINCIDENT RAMP
ENTRANCE PHASE ANGLE = 90°

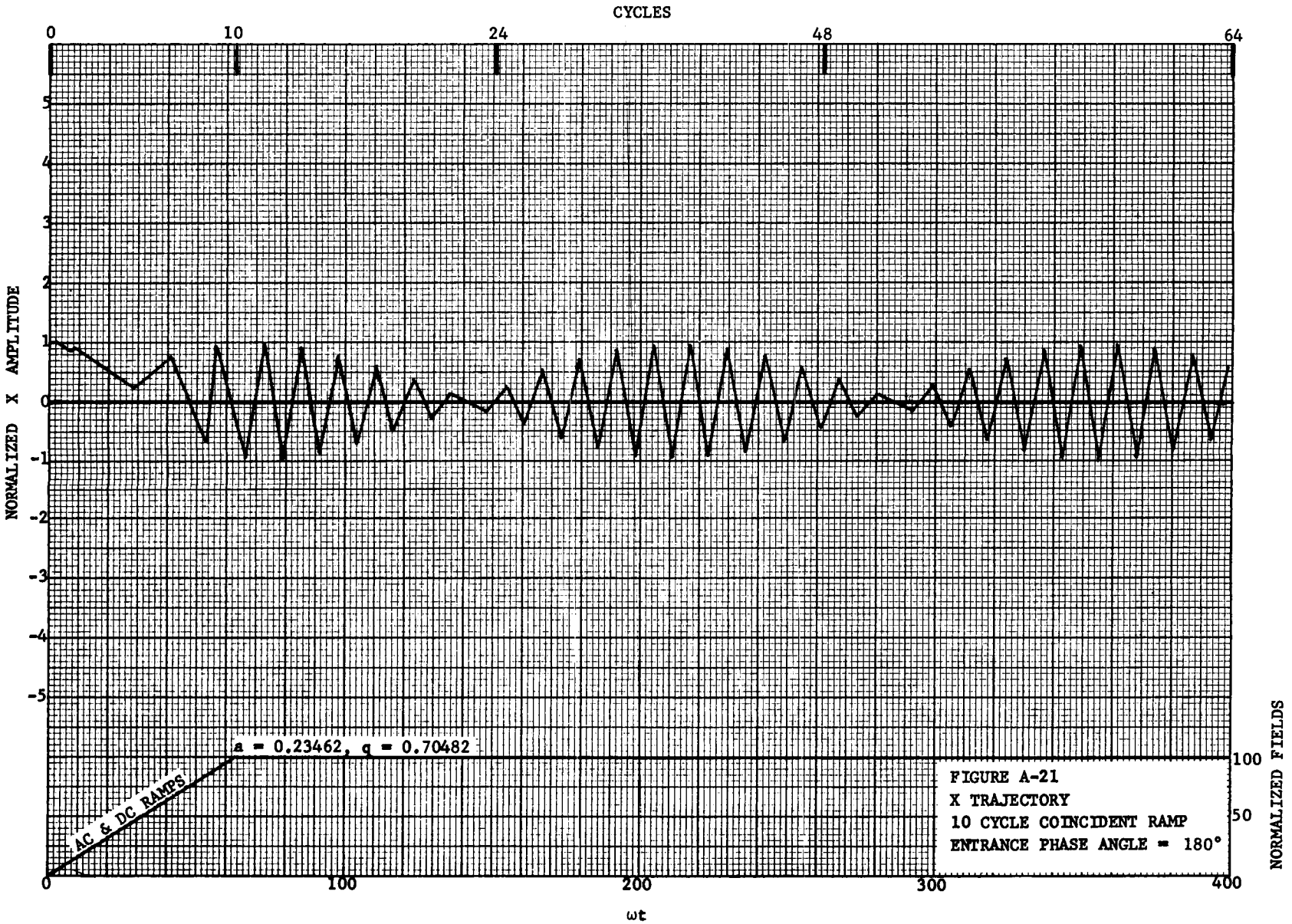
CYCLES
0
10
24
48
64
NORMALIZED X AMPLITUDE
5
4
3
2
1
0
-1
-2
-3
-4
-5
a = 0.23462, q = 0.70482
AC & DC RAMPS
0
100
200
300
400
ωt
100
50
NORMALIZED FIELDS
FIGURE A-21
X TRAJECTORY
10 CYCLE COINCIDENT RAMP
ENTRANCE PHASE ANGLE = 180°

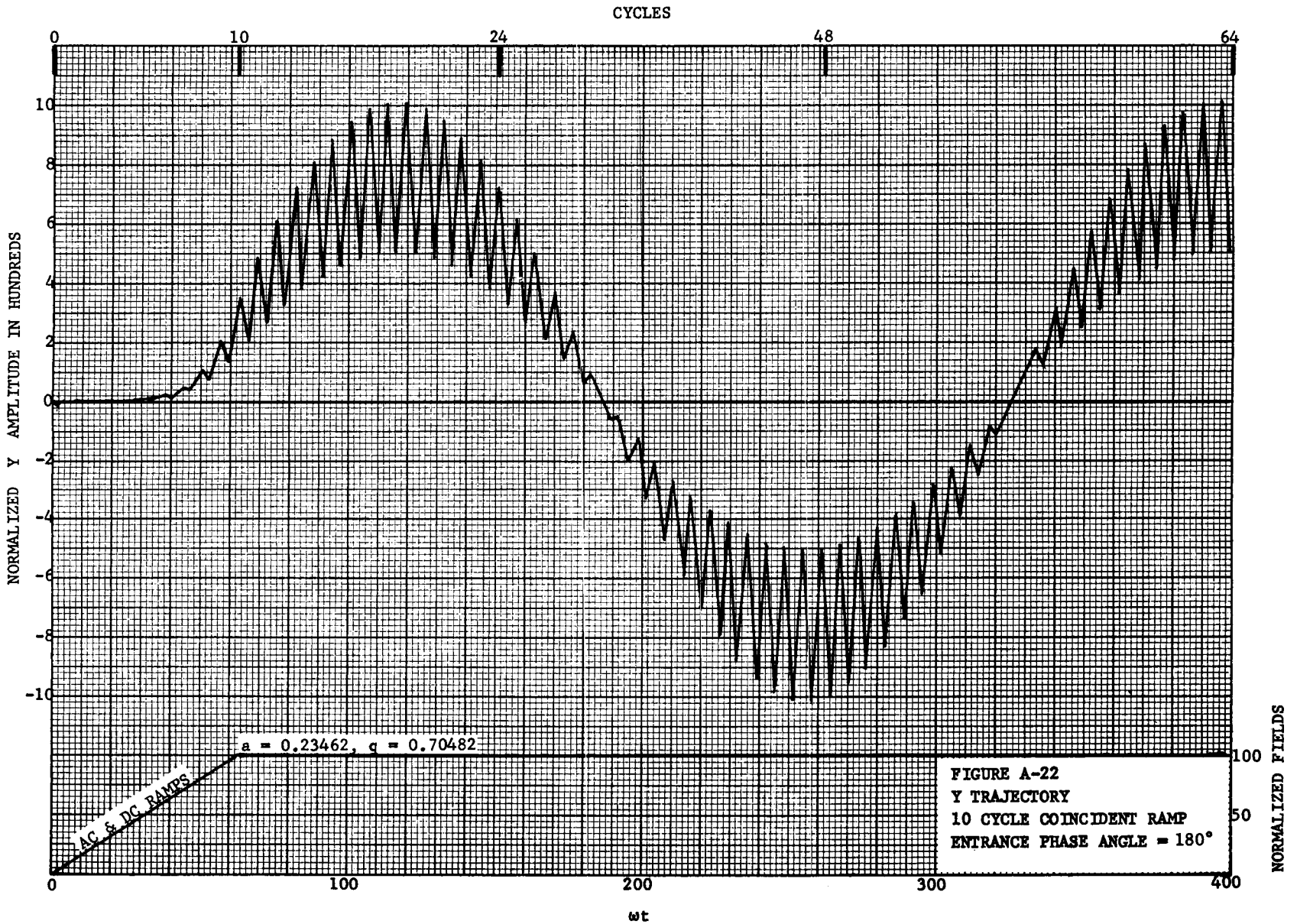

FIGURE A-22
Y TRAJECTORY
10 CYCLE COINCIDENT RAMP
ENTRANCE PHASE ANGLE = 180°

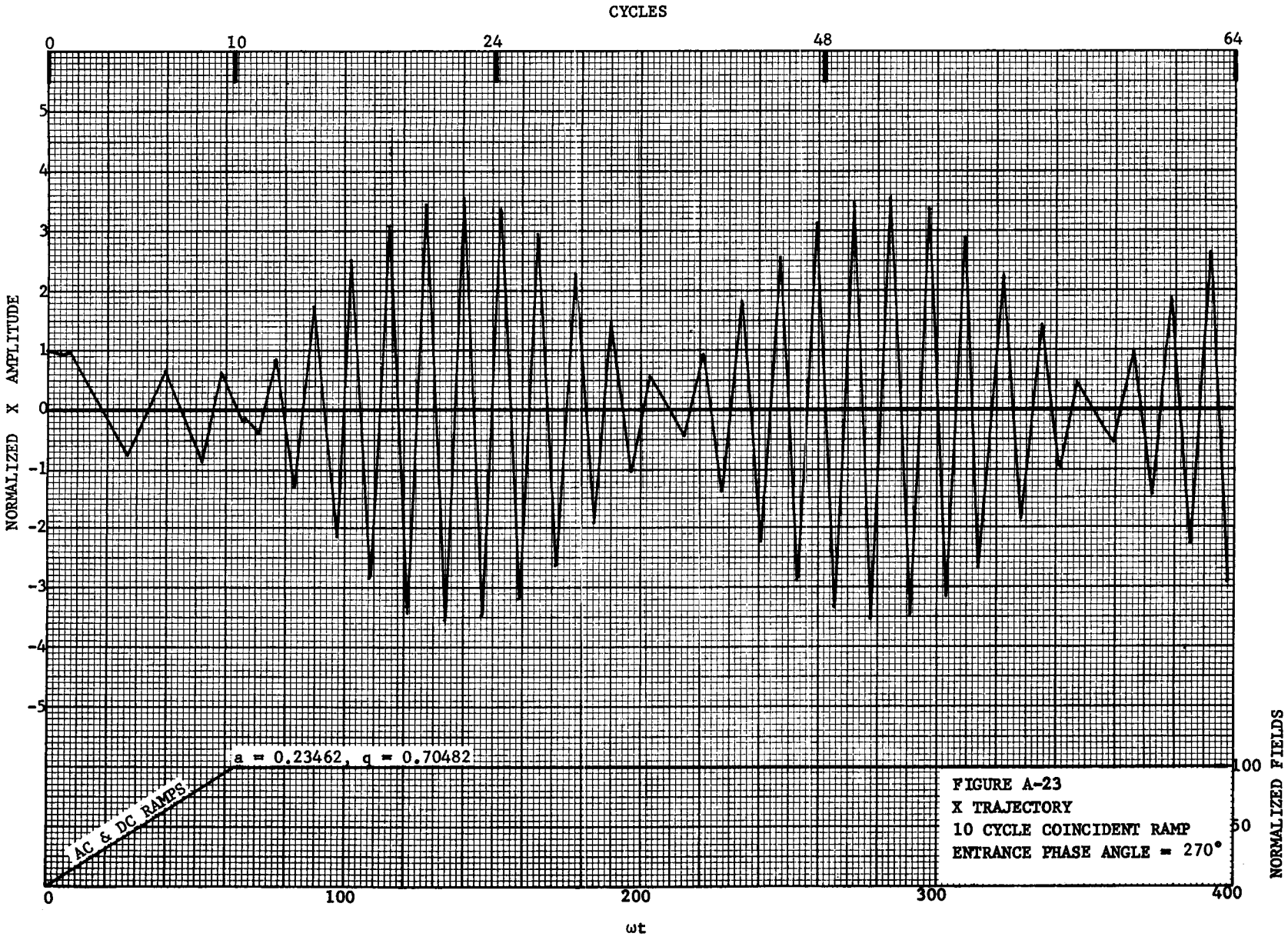

FIGURE A-23
X TRAJECTORY
10 CYCLE COINCIDENT RAMP
ENTRANCE PHASE ANGLE = 270°

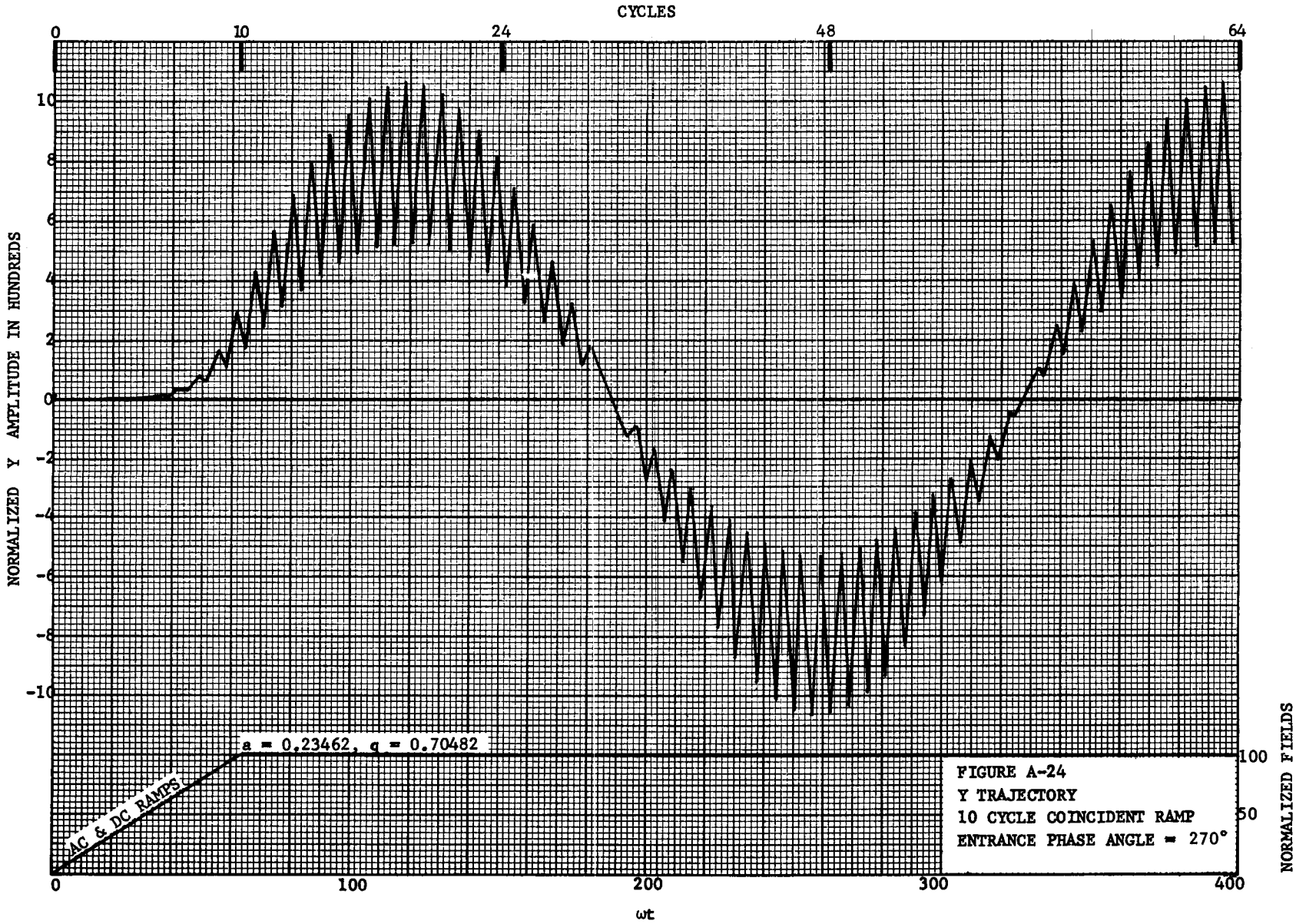

FIGURE A-24
Y TRAJECTORY
10 CYCLE COINCIDENT RAMP
ENTRANCE PHASE ANGLE = 270°

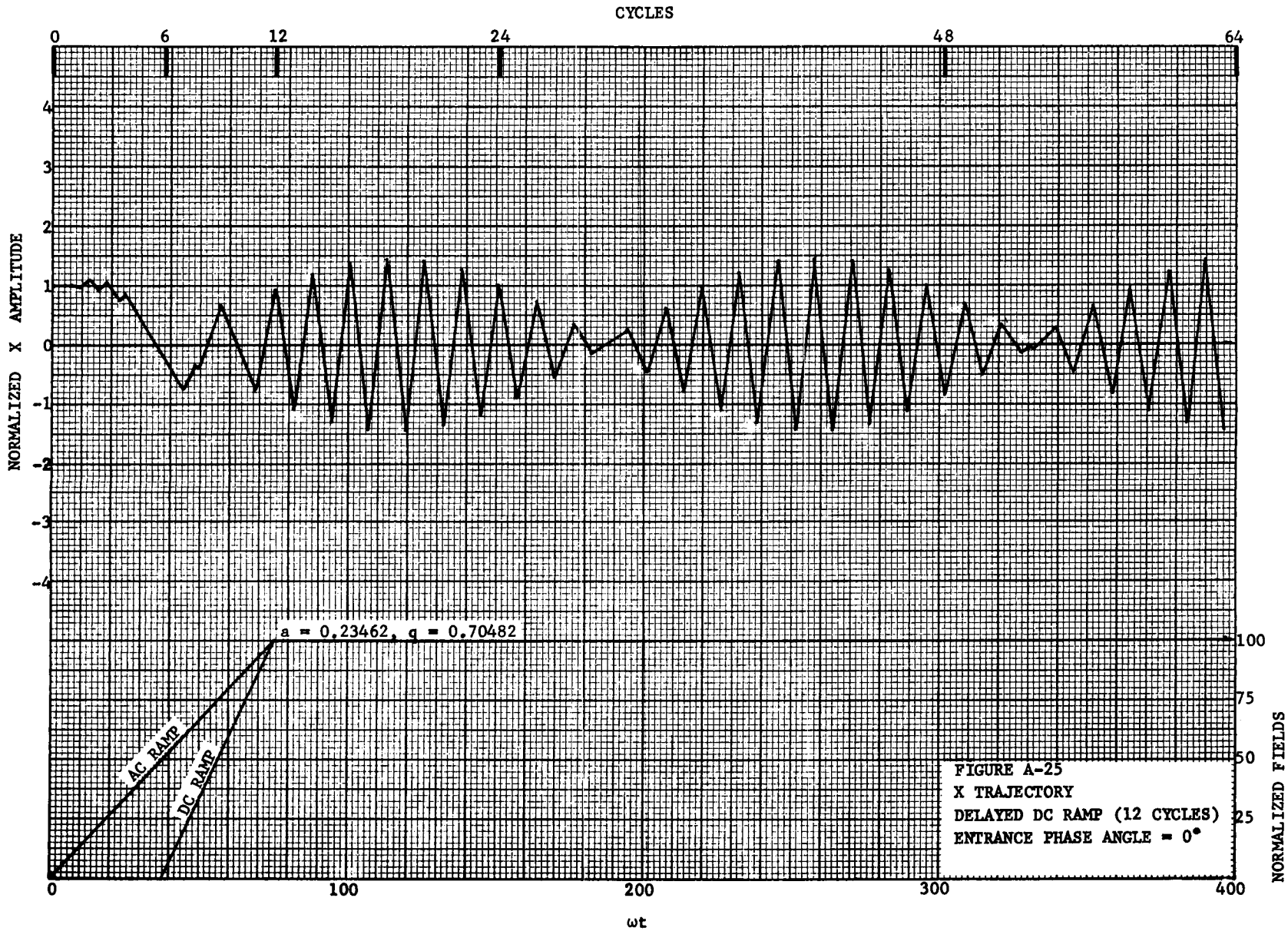

FIGURE A-25
X TRAJECTORY
DELAYED DC RAMP (12 CYCLES)
ENTRANCE PHASE ANGLE = 0°

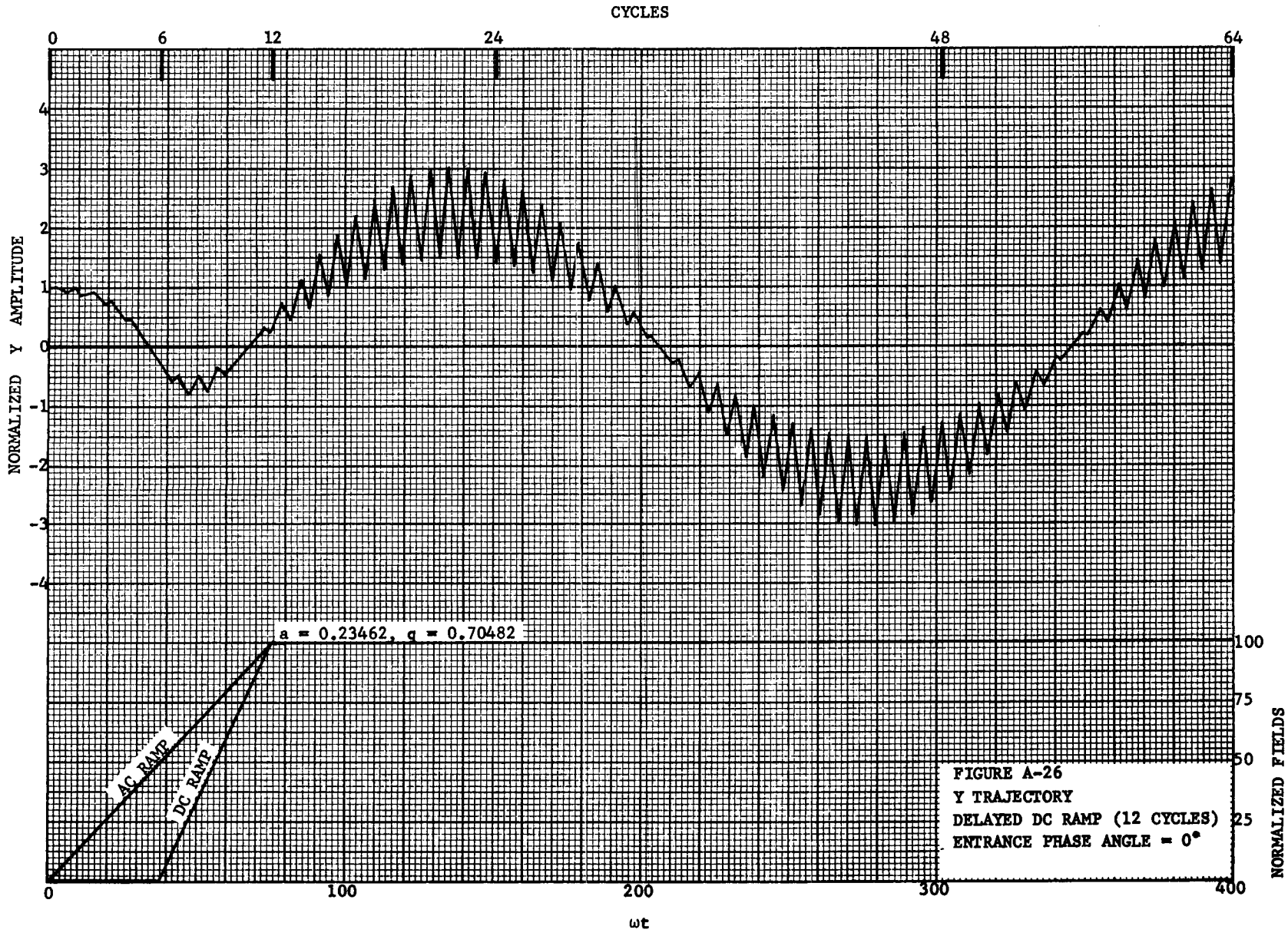

FIGURE A-26
Y TRAJECTORY
DELAYED DC RAMP (12 CYCLES)
ENTRANCE PHASE ANGLE = 0°

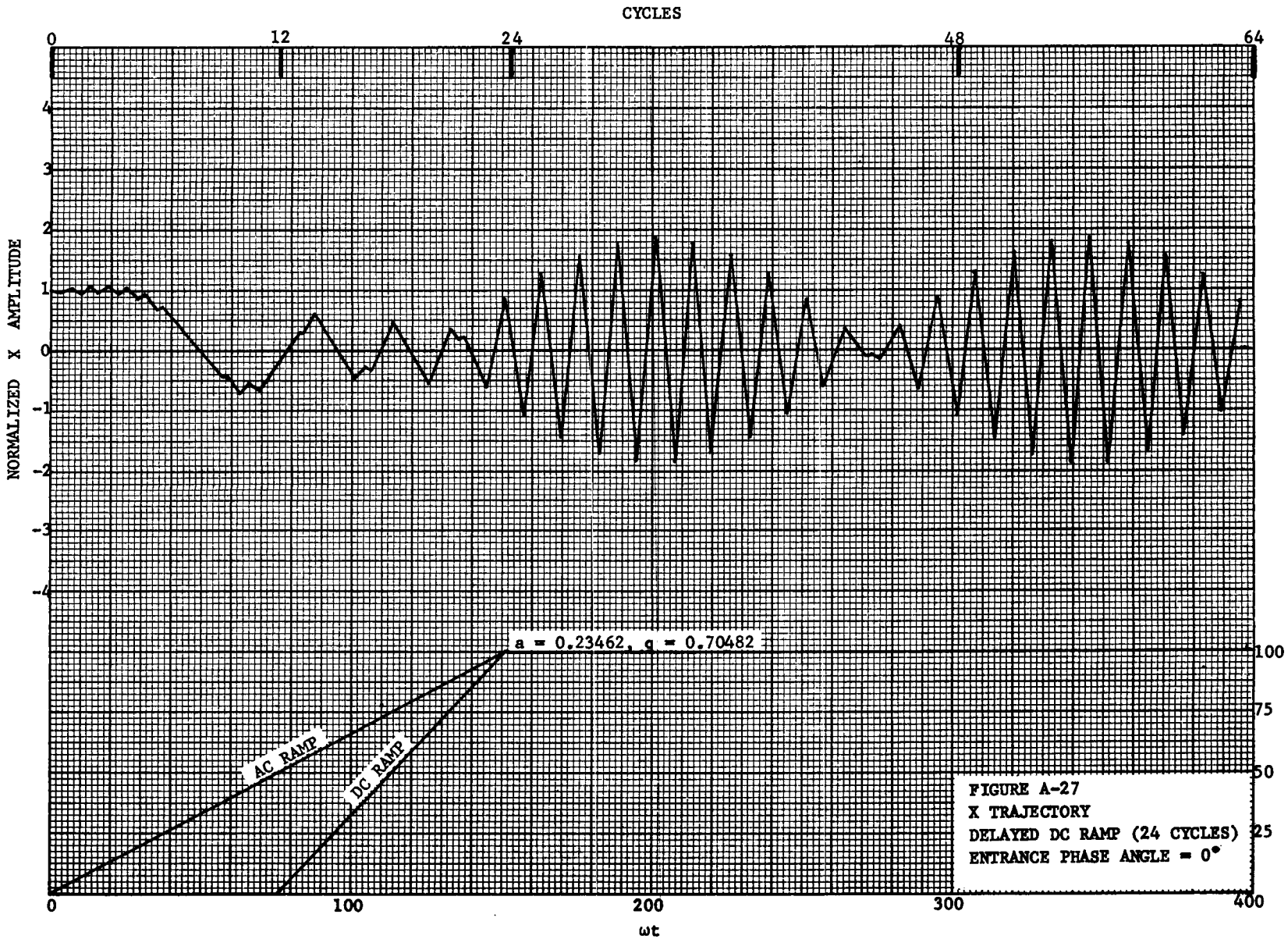

FIGURE A-27
X TRAJECTORY
DELAYED DC RAMP (24 CYCLES)
ENTRANCE PHASE ANGLE = 0°

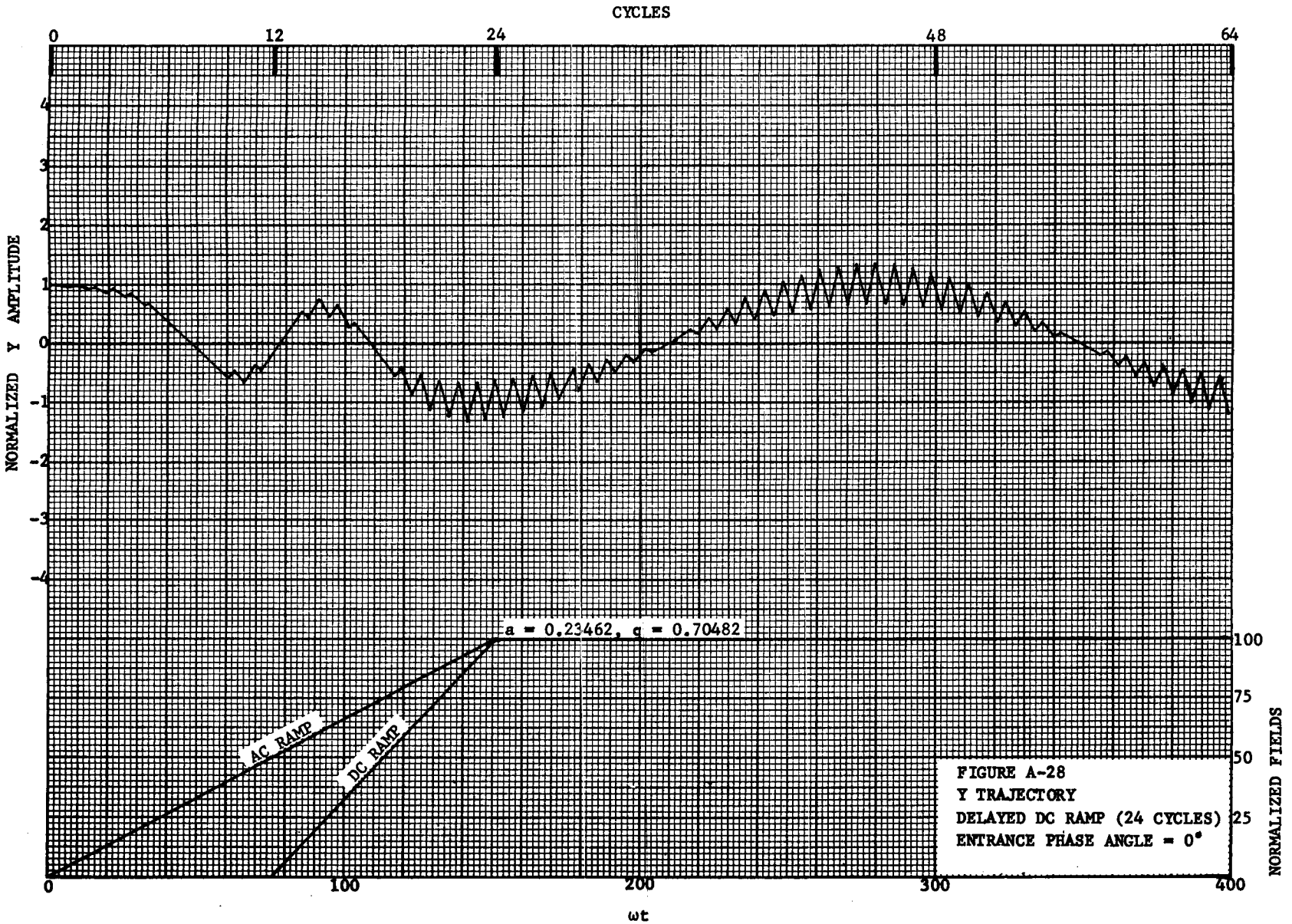

FIGURE A-28
Y TRAJECTORY
DELAYED DC RAMP (24 CYCLES)
ENTRANCE PHASE ANGLE = 0°

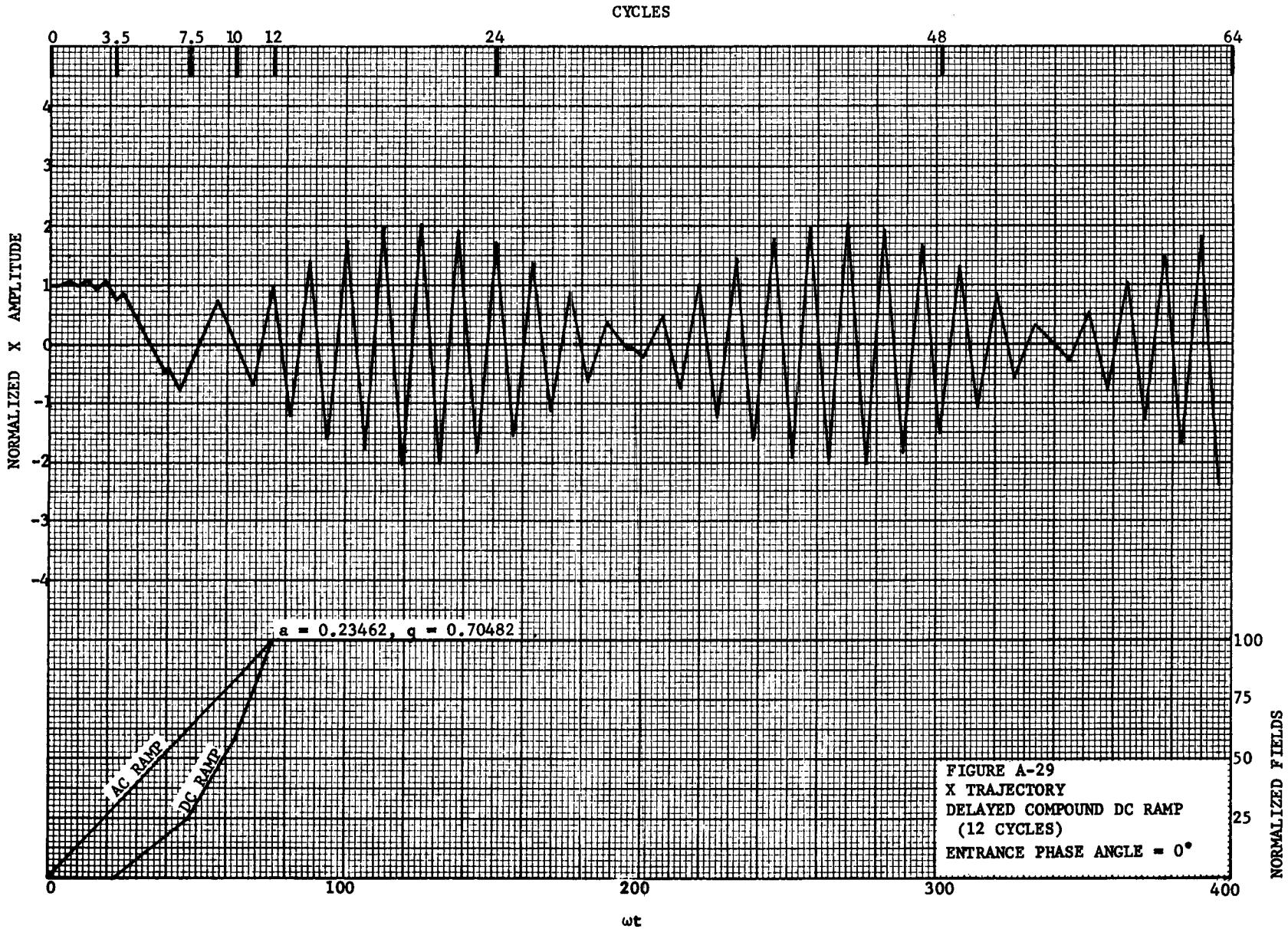

FIGURE A-29
X TRAJECTORY
DELAYED COMPOUND DC RAMP
(12 CYCLES)
ENTRANCE PHASE ANGLE = 0°

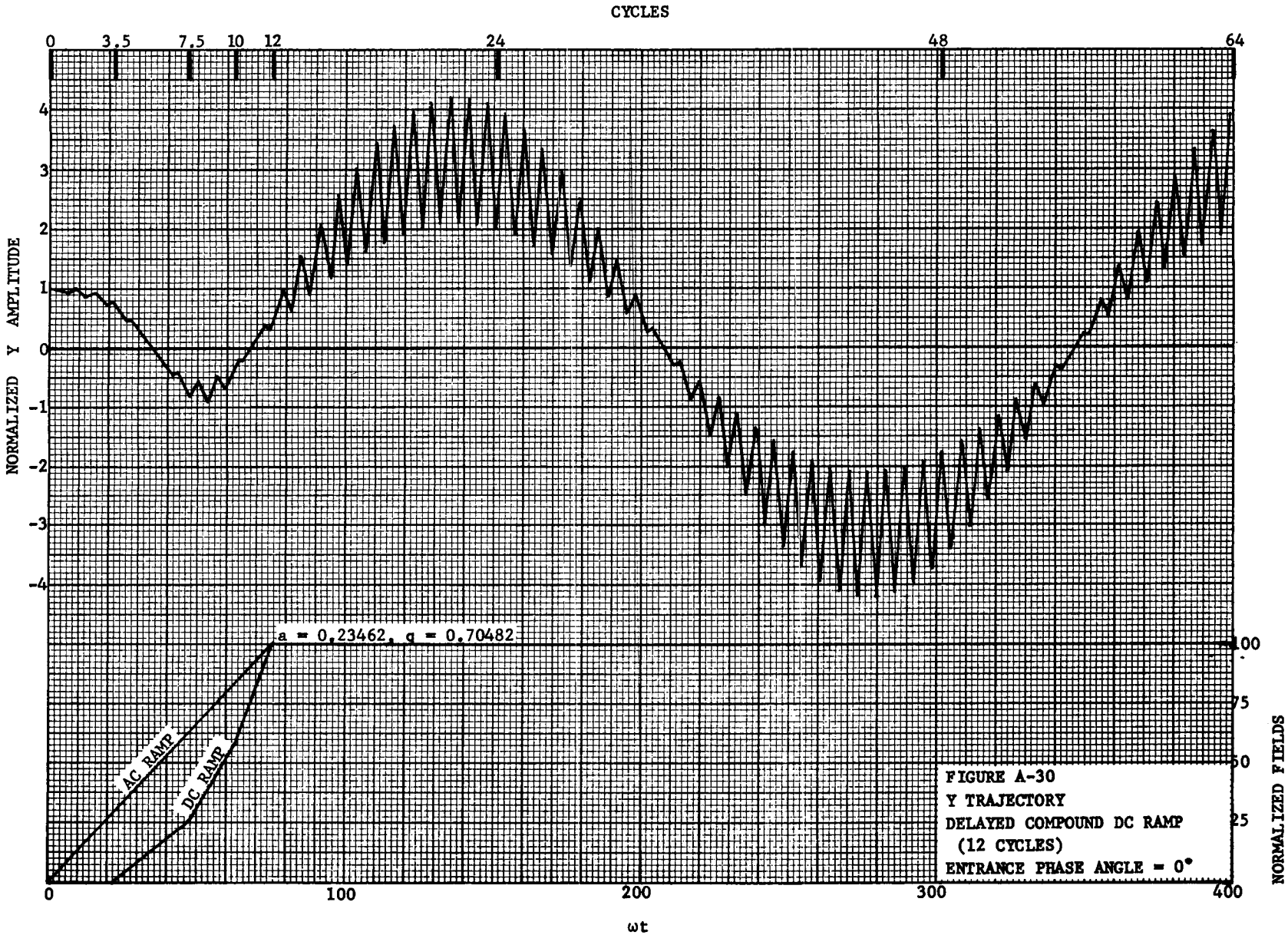

FIGURE A-30
Y TRAJECTORY
DELAYED COMPOUND DC RAMP
(12 CYCLES)
ENTRANCE PHASE ANGLE = 0°

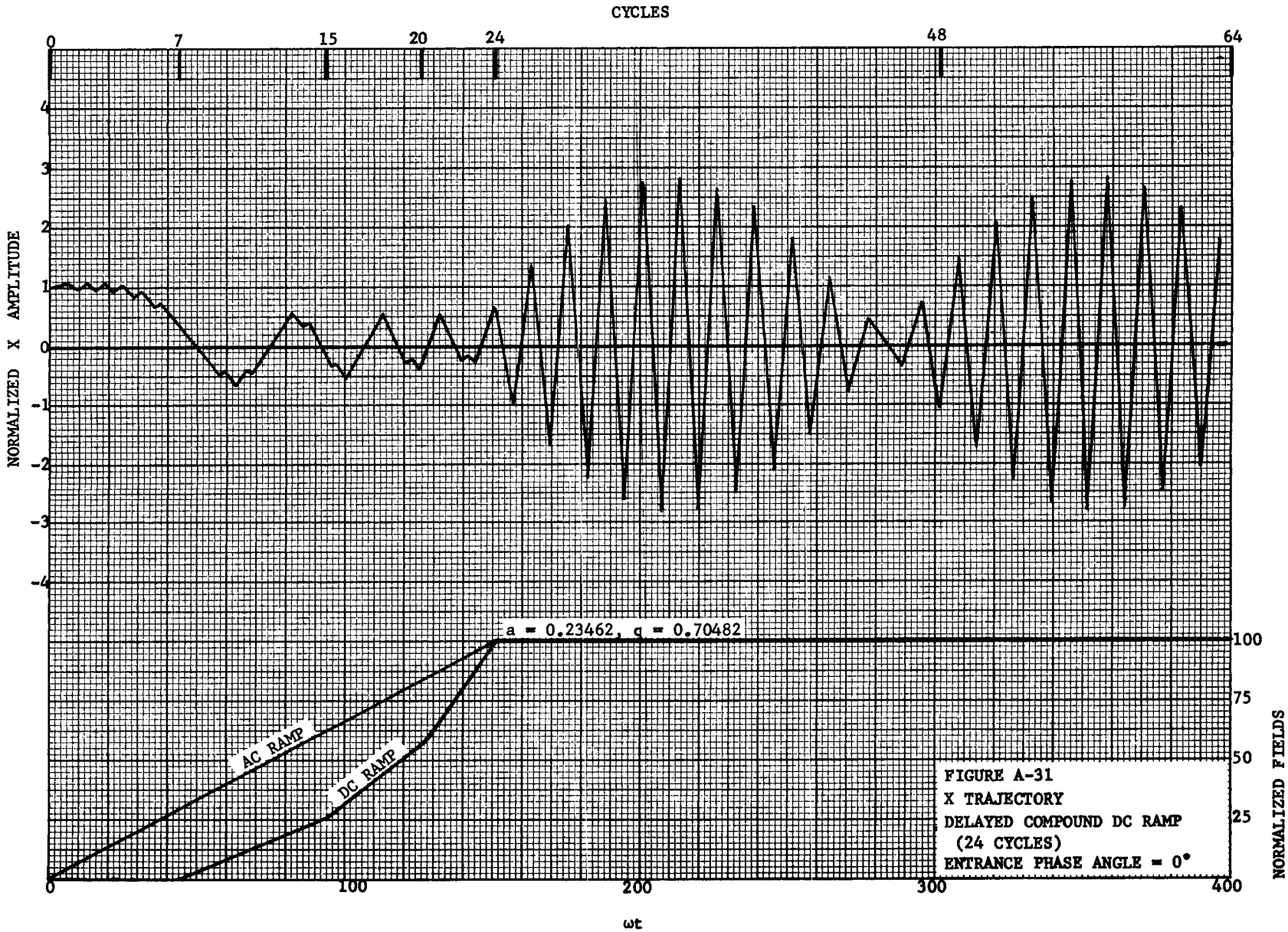
CYCLES
0
7
15
20
24
48
64
NORMALIZED X AMPLITUDE
4
3
2
1
0
-1
-2
-3
-4
a = 0.23462, q = 0.70482
AC RAMP
DC RAMP
100
75
50
25
NORMALIZED FIELDS
0
100
200
300
400
ωt
FIGURE A-31
X TRAJECTORY
DELAYED COMPOUND DC RAMP
(24 CYCLES)
ENTRANCE PHASE ANGLE = 0°

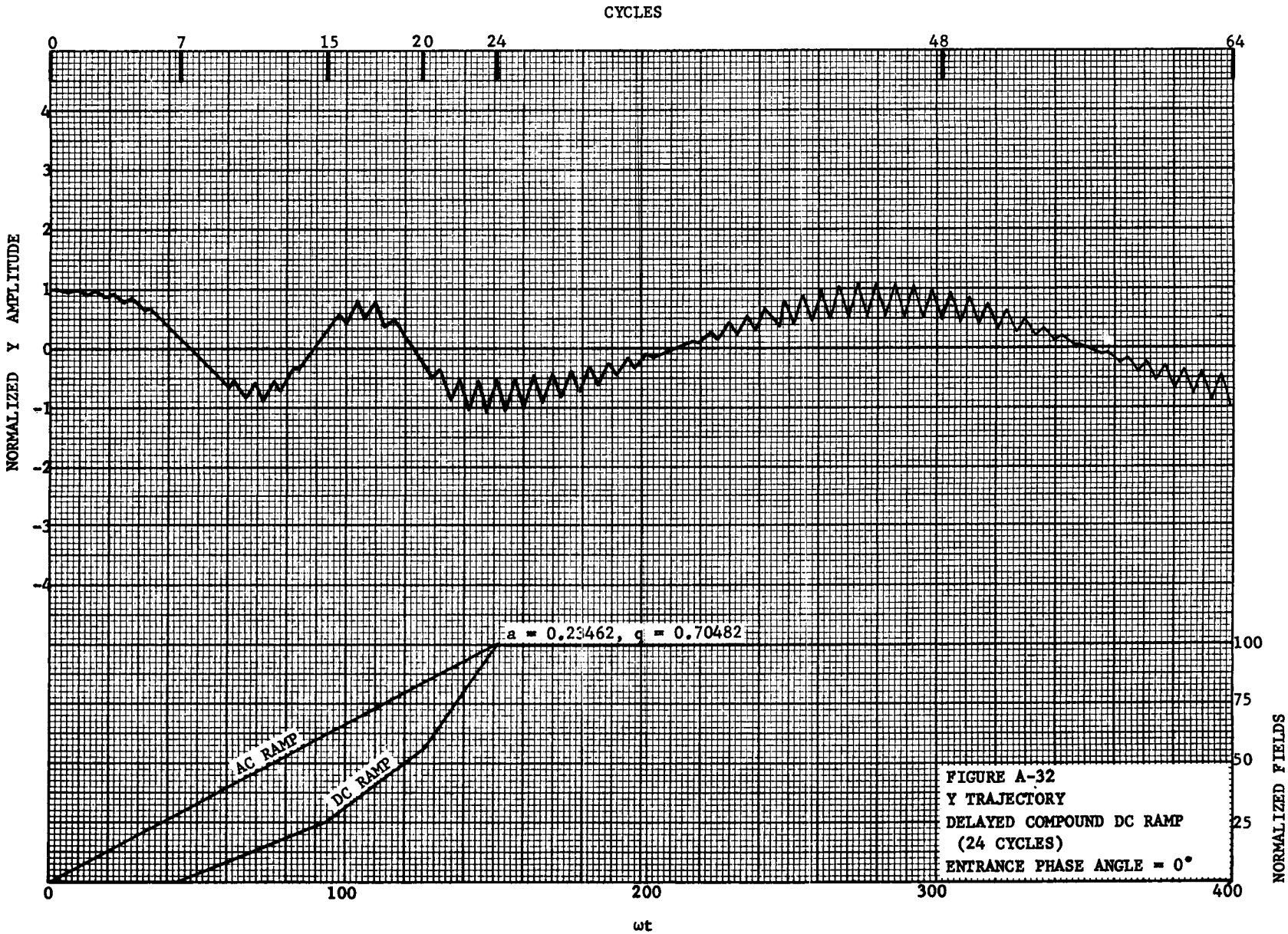

FIGURE A-32
Y TRAJECTORY
DELAYED COMPOUND DC RAMP
(24 CYCLES)
ENTRANCE PHASE ANGLE = 0°

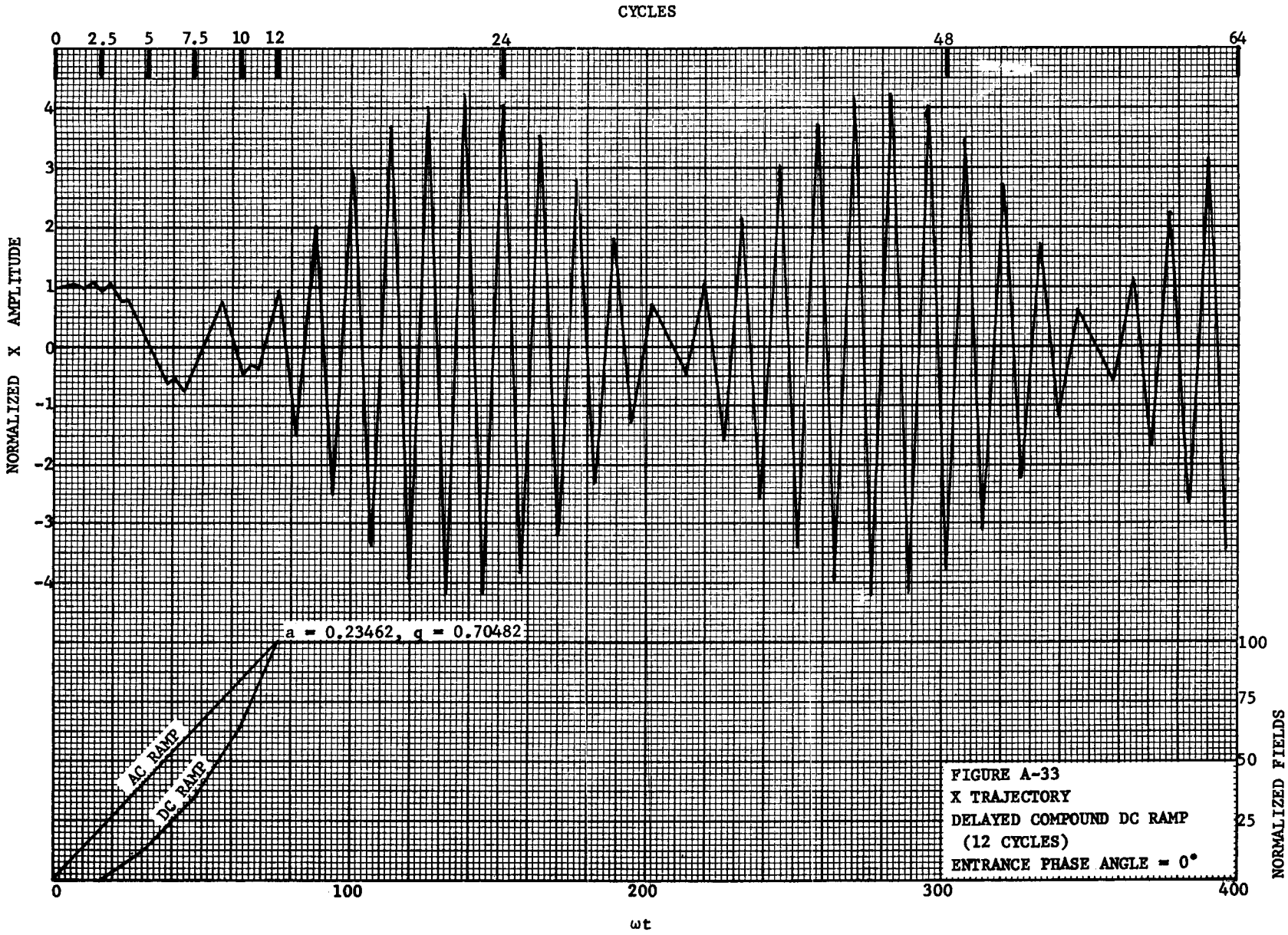
CYCLES
0
2.5
5
7.5
10
12
24
48
64
NORMALIZED X AMPLITUDE
4
3
2
1
0
-1
-2
-3
-4
a = 0.23462, q = 0.70482
AC RAMP
DC RAMP
100
75
50
25
NORMALIZED FIELDS
0
100
200
300
400
ωt
FIGURE A-33
X TRAJECTORY
DELAYED COMPOUND DC RAMP
(12 CYCLES)
ENTRANCE PHASE ANGLE = 0°

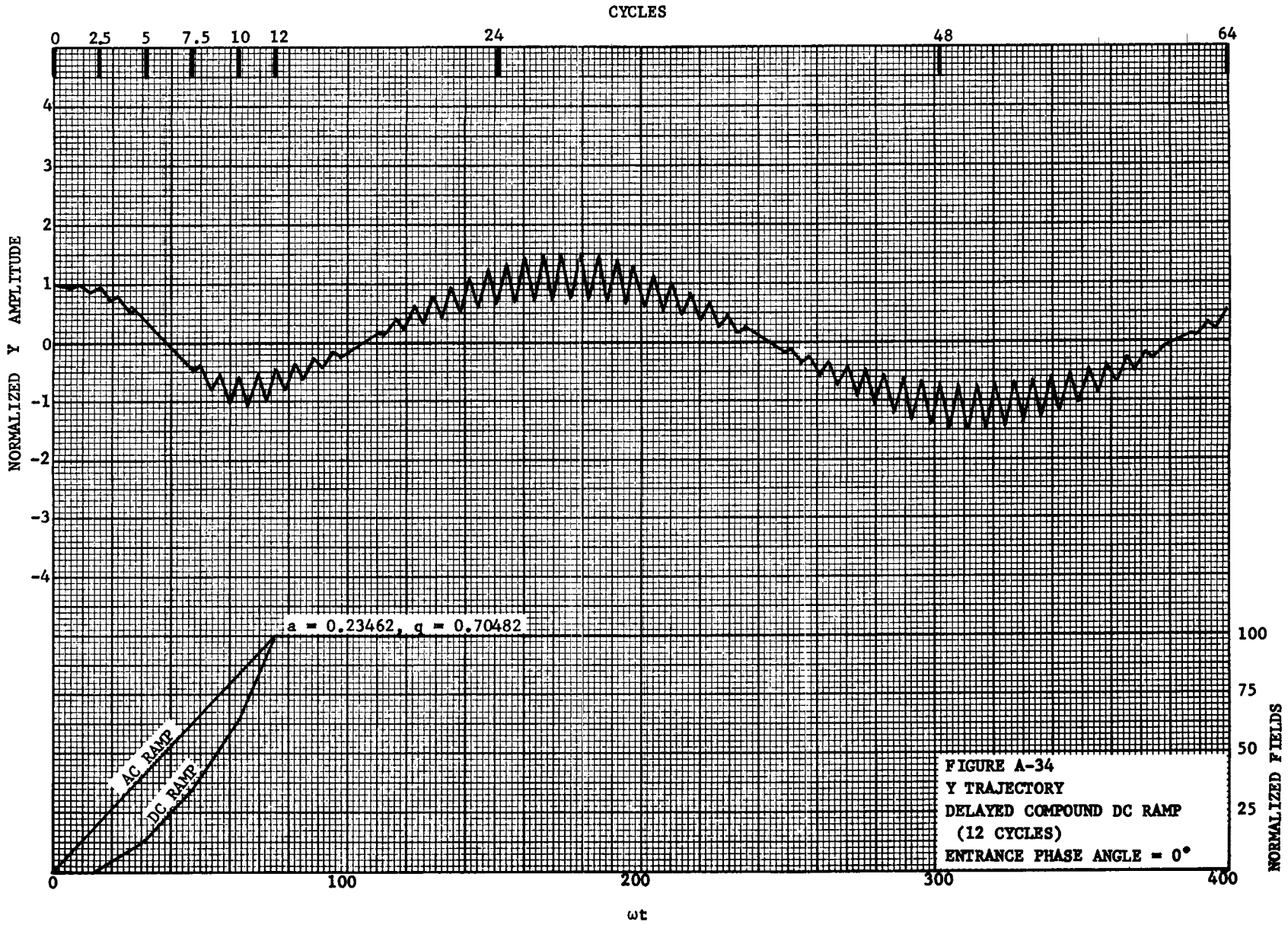

FIGURE A-34
Y TRAJECTORY
DELAYED COMPOUND DC RAMP
(12 CYCLES)
ENTRANCE PHASE ANGLE = 0°

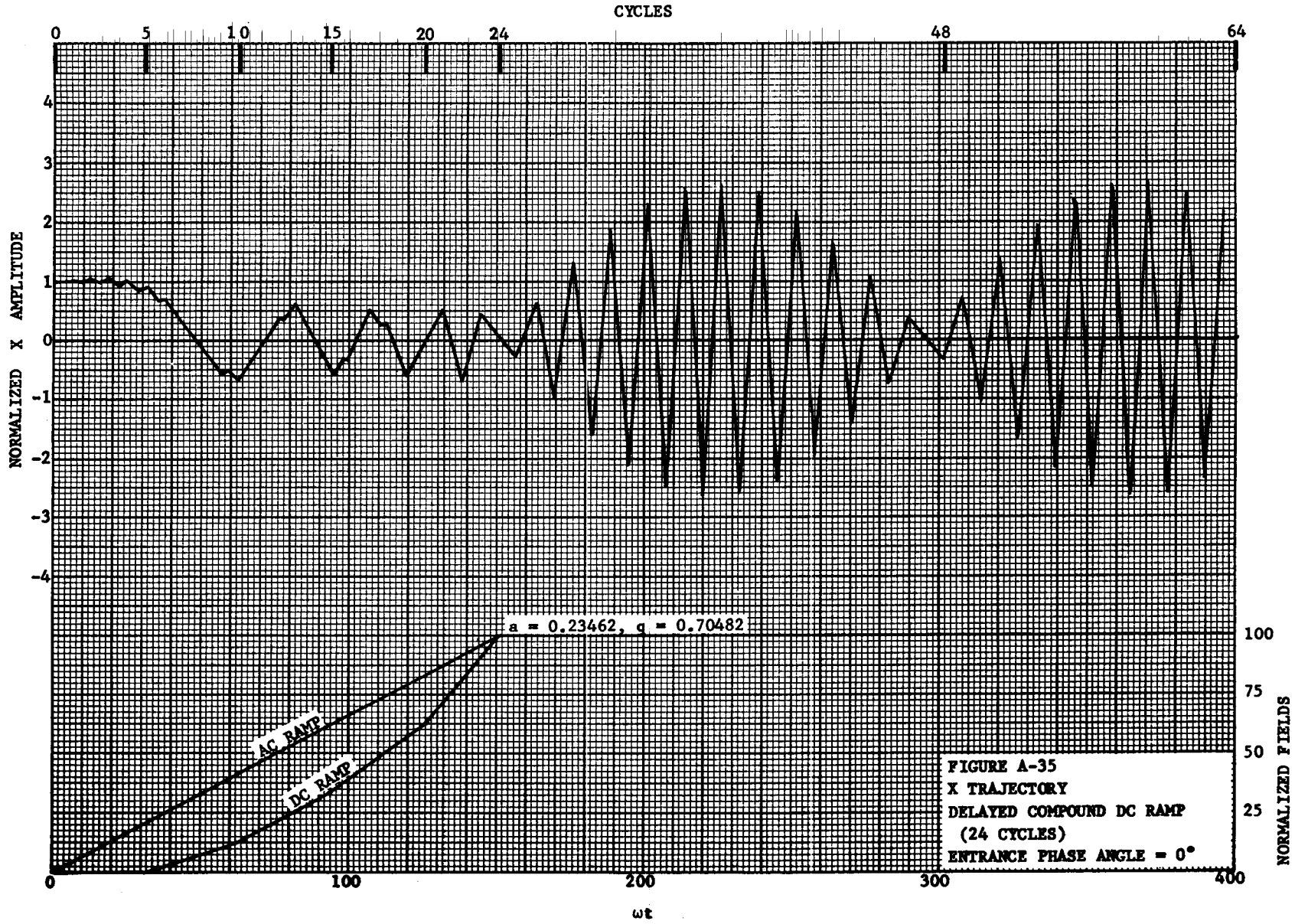
CYCLES
0
5
10
15
20
24
48
64
NORMALIZED X AMPLITUDE
4
3
2
1
0
-1
-2
-3
-4
a = 0.23462, q = 0.70482
AC RAMP
DC RAMP
100
75
50
25
NORMALIZED FIELDS
0
100
200
300
400
ωt
FIGURE A-35
X TRAJECTORY
DELAYED COMPOUND DC RAMP
(24 CYCLES)
ENTRANCE PHASE ANGLE = 0°

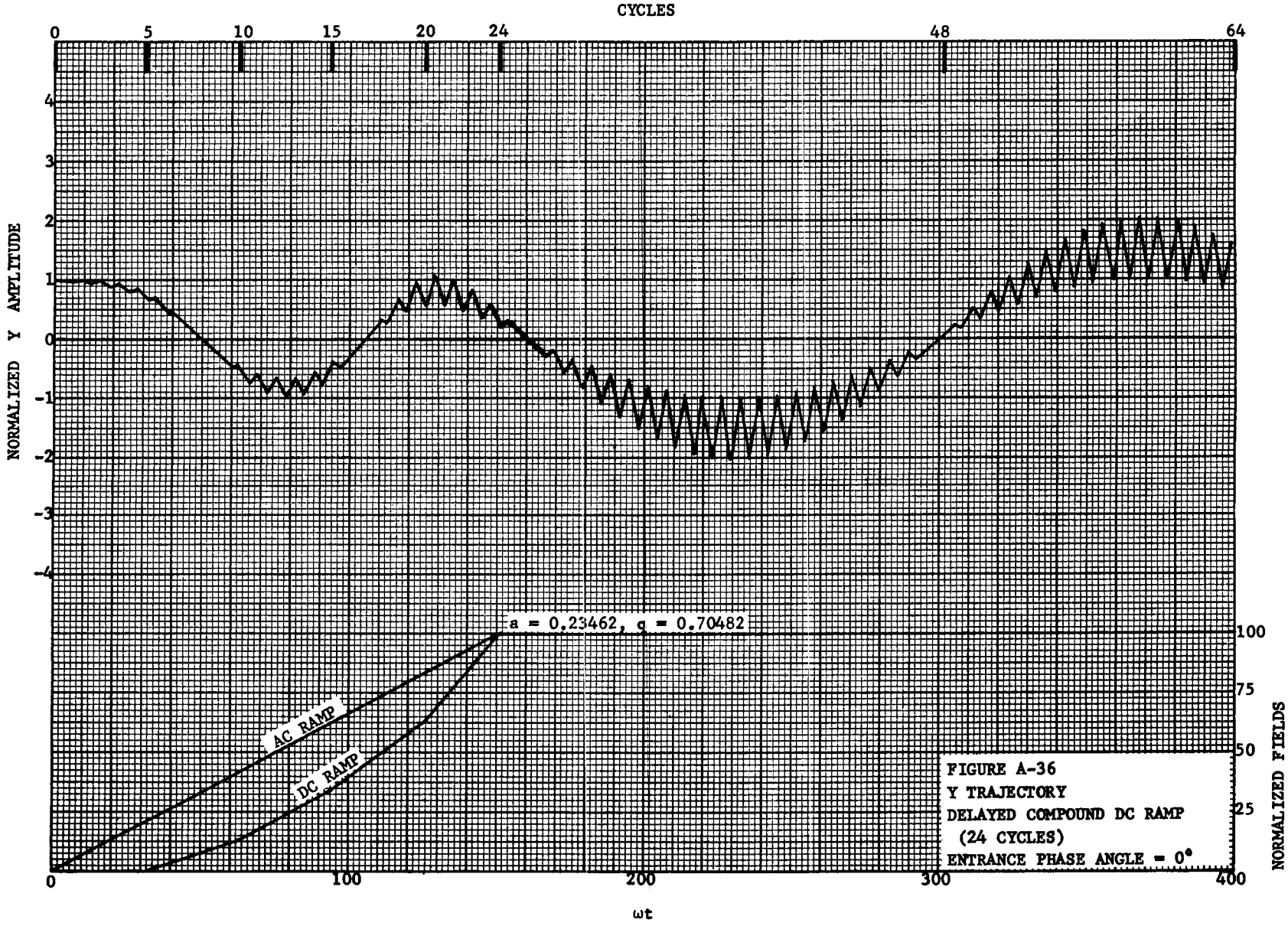

FIGURE A-36
Y TRAJECTORY
DELAYED COMPOUND DC RAMP
(24 CYCLES)
ENTRANCE PHASE ANGLE = 0°